

อุณหพลศาสตร์และจลนศาสตร์ของการแยกเฟส , โครงสร้าง และสมบัติภายใต้แรงดึงของ
พอลิเมอร์ผสมสององค์ประกอบ: พอลิ(เมทริล เมททาคริเลท)/พอลิ(สไตรีน-โค-มาเลอิก แอนไฮไดรด์)

นายพิเชษฐ์ ไรจนพิทยากร

วิทยานิพนธ์นี้เป็นส่วนหนึ่งของการศึกษาตามหลักสูตรปริญญาวิศวกรรมศาสตรดุษฎีบัณฑิต

สาขาวิชาวิศวกรรมเคมี ภาควิชาวิศวกรรมเคมี

คณะวิศวกรรมศาสตร์ จุฬาลงกรณ์มหาวิทยาลัย

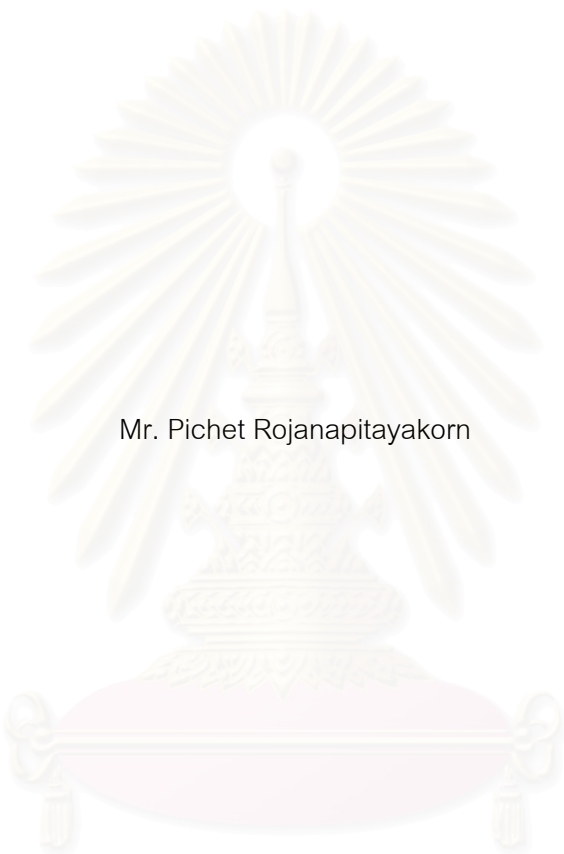
ปีการศึกษา 2543

ISBN 974-13-0183-9

ลิขสิทธิ์ของจุฬาลงกรณ์มหาวิทยาลัย

สถาบันวิทยบริการ
จุฬาลงกรณ์มหาวิทยาลัย

THERMODYNAMICS AND KINETICS OF PHASE SEPARATION, MORPHOLOGIES
AND TENSILE PROPERTIES OF A BINARY POLYMER BLEND:
POLY(METHYL METHACRYLATE)/POLY(STYRENE-CO-MALEIC ANHYDRIDE)



Mr. Pichet Rojanapitayakorn

สถาบันวิทยบริการ

จุฬาลงกรณ์มหาวิทยาลัย

A Dissertation Submitted in Partial Fulfillment of the Requirements
for the Degree of Doctor of Engineering in Chemical Engineering

Department of Chemical Engineering

Faculty of Engineering

Chulalongkorn University

Academic year 2000

ISBN 974-13-0183-9

พิเชษฐ โจรจนพิทยากร : อุณหพลศาสตร์ และจลนศาสตร์ของการแยกเฟส, โครงสร้าง และสมบัติภายใต้แรงดึงของพอลิเมอร์ผสมสององค์ประกอบ: พอลิ(เมทิล เมทาคริเลท)/พอลิ(สไตรีน-โค-มาเลอิก แอนไฮไดรด์) (Thermodynamics and kinetics of phase separation, morphologies and tensile properties of a binary polymer blend: poly(methyl methacrylate)/poly(styrene-co-maleic anhydride). อ.ที่ปรึกษาวิทยานิพนธ์: ผศ.ดร.มล. ศุภกนก ทองใหญ่, อ.ที่ปรึกษาร่วม: ดร. สิริจุฑารัตน์ โควาวิสารัช, 179 หน้า, ISBN 974-13-0183-9

งานวิจัยนี้ได้ทำการศึกษาอุณหพลศาสตร์และจลนศาสตร์ของการแยกเฟส, โครงสร้างและ สมบัติภายใต้แรงดึงของสารผสมระหว่าง พอลิ(สไตรีน-โค-มาเลอิก แอนไฮไดรด์) กับ พอลิ(เมทิล เมทาคริเลท) ที่มีการเติมเซทิล อะคริเลท โคโมโนเมอร์ การศึกษาด้วยเครื่องวัดการกระเจิงแสงแสดงให้เห็นว่า วิธีการผสมมีผลต่อลักษณะการเข้ากันได้ และลักษณะทางจลนศาสตร์ของการแยกเฟส สารผสมที่เตรียมด้วยวิธีการหล่อด้วยสารละลาย (solution casting) ให้เส้นสปินูเดิล (spinodal) และเส้นอุณหภูมิที่เริ่มขุ่น (cloud point) สูงกว่าสารผสมที่เตรียมด้วยวิธีการหลอมผสมด้วยความร้อน (melt mixing) ค่าอัตราการเพิ่มความเข้มของแสงกระเจิง (scattering intensity) ซึ่งได้จากการคำนวณตามทฤษฎีของคานห์และฮิลลาร์ด (Cahn-Hilliard) จะขึ้นกับอุณหภูมิ, วิธีการผสม และความเข้มข้น การศึกษาพฤติกรรมการหน่วง (delay time) พบว่า ลักษณะการหน่วงขึ้นอยู่กับการผสม, ความเข้มข้น, อุณหภูมิ และเลขคลื่นกระเจิง (scattering wave number) ค่าที่ได้จากการทดลองจะคลาดเคลื่อนจากการประมาณด้วยทฤษฎีที่เกี่ยวข้องกับการพันกันของพอลิเมอร์ (entanglement) คาดว่ามีผลเนื่องจากการละบางพจน์ในสมการ หรือ ค่าหน่วงที่วัดได้อาจจะมีความคลาดเคลื่อน จากการทดลองยังพบว่าในช่วงท้ายของการสลายตัวแบบสปินูเดิล ลักษณะการเปลี่ยนความเข้มของแสงกระเจิงที่ผ่านการปรับค่า (normalised scaling function) จะสอดคล้องกับฟังก์ชันสเกลลิง ($\tilde{S}(X)$) ซึ่งใช้ทำนายการเปลี่ยนแปลงของสารผสมนอกช่วงความเข้มข้นวิกฤต เรียกลักษณะการเปลี่ยนแปลงนี้ว่าการเปลี่ยนแปลงแบบกลุ่ม (cluster)

การศึกษาลักษณะของโครงสร้างในชิ้นงานที่ผ่านการดึง (tensile test) ได้พบโครงสร้างที่มีความต่อเนื่องร่วมกัน (co-continuous) ซึ่งสามารถยืนยันการเกิดการสลายตัวแบบสปินูเดิลในชิ้นตัวอย่างดังกล่าว อัตราการเพิ่มขนาดของโครงสร้างที่ได้จากการส่องด้วยกล้องจุลทรรศน์อิเล็กตรอนแบบส่องผ่าน (transmission electron microscopy) จะคลาดเคลื่อนจากค่าที่ได้จากการคำนวณโดยใช้ข้อมูลของเครื่องวัดการกระเจิงแสง คาดว่าน่าจะมีผลจากความหนาของชิ้นงาน และการกระจายความร้อนที่แตกต่างกันของสองวิธี การศึกษาสมบัติทางกลด้วยวิธีการดึงพบว่า ค่าโมดูลัสของยังในพอลิเมอร์ผสมที่แยกเฟสในช่วงต้นของการสลายตัวแบบสปินูเดิลจะสูงกว่าพอลิเมอร์ผสมที่ไม่แยกเฟส คาดว่าการเปลี่ยนแปลงที่เกิดขึ้นจะมีผลมาจากการเปลี่ยนความเข้มข้นขององค์ประกอบ และการจัดเรียงตัวในระดับโมเลกุลของพอลิเมอร์เมื่อได้รับความร้อน ในขณะที่การตรวจสอบด้วยกล้องจุลทรรศน์อิเล็กตรอนแบบส่องผ่าน ไม่พบแนวโน้มของการเปลี่ยนค่าโมดูลัสของยังเนื่องจากการเปลี่ยนแปลงขนาดของเฟส

ภาควิชา	วิศวกรรมเคมี	ลายมือชื่อนิสิต
สาขาวิชา	วิศวกรรมเคมี	ลายมือชื่ออาจารย์ที่ปรึกษา
ปีการศึกษา	2543	ลายมือชื่ออาจารย์ที่ปรึกษาร่วม

#C817785 : MAJOR CHEMICAL ENGINEERING

KEY WORD : polymer blend/ spinodal decomposition/ sample preparation/ delay time/ tensile properties/ morphology

Pichet Rojanapitayakorn : Thermodynamics and kinetics of phase separation, morphologies and tensile properties of a binary polymer blend: poly(methyl methacrylate)/poly(styrene-co-maleic anhydride).

THESIS ADVISOR: Assistant Professor M.L. Supakanok Thongyai, PhD, THESIS CO-ADVISOR: Sirijutaratana Covavisaruch, PhD, 179 pp. ISBN 974-13-0183-9

Thermodynamics and kinetics of phase separation, morphologies and tensile properties were investigated in a blend of poly(styrene-co-maleic anhydride) with a commercial sample of poly(methyl methacrylate) containing ethyl acrylate comonomer. Detailed studies through light scattering showed that sample preparation methods affect the miscibility and kinetics of phase separation. The blends exhibit spinodal and cloud point curves at higher temperatures in the case of solution cast than those from melt mixed samples. The relative values of the Cahn-Hilliard growth rate, $R(q)$, depend on temperature, sample preparation methods and the blend concentration. The delay time behaviour at the onset of phase separation was observed. It was found that sample preparation method, composition, temperature and scattering wave number have an influence on delay time. Comparisons of the experimental data with recent theoretical developments for entangled polymer blends show a discrepancy, this might be attributed to the omission of some terms in those theories or that the origin of the apparent delay time lies elsewhere. In the late stage of spinodal decomposition, the normalised scaling function profiles of 20/80 and 40/60 SMA/PMMAe blends are in good agreement with the conventional universal scaling function ($\tilde{S}(X)$) for off-critical mixture, called the cluster profile.

Detailed studies on morphology of the tensile tested specimens manifest that the co-continuous structure were found, indicating that the blends undergo spinodal decomposition. The comparison of droplet size growth rate approximated from light scattering data with the direct measurement from TEM showed a discrepancy. This is suggested to be the result of heat variation due to different sample thickness and heat transfer during measurement. The analysis of the morphological development of two compositions and two phase separation temperatures as a function of reduced time showed a master curve. The Young's modulus appear to be superior for the blends, which were phase separated inside the early stage of spinodal decomposition. This might be the result of the change in composition and molecular re-arrangement, while the change in phase separating domains as observed by TEM did not clearly manifest any effects on Young's modulus.

Department Chemical Engineering

Student's signature

Field of study Chemical Engineering

Advisor's signature

Academic year 2000

Co-advisor's signature

Acknowledgement

The author would like to express his sincere gratitude to Assistant Professor ML. Supakanok Thongyai, who supervised and encouraged him throughout this course, to Dr. Sirijutaratana Covavisaruch for her kindly advice and invaluable discussion. The author also gratefully acknowledges Professor Julia Higgins for her guidance and constructive advice during his experiment in the UK, to Dr. Nigel Clarke for the collaboration and useful discussion.

Financial supports from the British council and The National Science Technology and Development Agency (NSTDA) are grateful acknowledged. Financial support for the overseas conferences from the graduate school is also appreciated.

The author would like to thank ICI(UK) and DSM(The Netherlands) for their contribution of PMMAe and SMA.

The author wishes to thank the staffs of STREC for their help with experiments. It is his honour to receive a first priority during his experiments. He also would like to thank all member of the polymer group at Imperial College (UK) particular Sarah, Chatchai, Joao, Branko, Dimitra, Tony, Herve, Simon and everyone whose name may not be mentioned here. It is really a great opportunity to practice and carry out experiments at such a friendly and good working atmosphere there. He would like to extend his grateful thank to all members of the polymer group at Chulalongkorn university as well, who always build up such a joyful ambience in the lab and bring up such an interesting subject to discuss. Thank to Lek as well for her incessant support and encouragement.

Finally, his greatest thank should go to his family especially his parents, who always support and understand him not only today but also tomorrow.

Contents

	PAGE
ABSTRACT (IN THAI)	iv
ABSTRACT (IN ENGLISH)	v
ACKNOWLEDGEMENTS.....	vi
CONTENTS.....	vii
LIST OF FIGURES.....	xii
LIST OF TABLES.....	xvii
NOMENCLATURE.....	xix
CHAPTER 1	
INTRODUCTION.....	1
1.1 The methods of blending.....	2
1.2 Methods of study miscibility and phase separation phenomena.....	3
1.2.1 T_g study.....	3
1.2.2 Scattering study.....	4
1.2.3 Morphology study.....	4
1.2.4 Infrared spectroscopy.....	5
1.3 Literature reviews.....	5
1.4 Scope of work.....	8
1.5 Organisation of thesis	9
CHAPTER 2	
THERMODYNAMICS OF POLYMER BLENDS.....	10
2.1 General principles for polymer-polymer miscibility.....	11
2.2 The mechanism of phase separation.....	13
2.2.1 Nucleation and growth.....	16
2.2.2 Spinodal decomposition.....	18
2.3 The statistical thermodynamics of polymer systems.....	19
2.3.1 The general principle of statistical thermodynamics.....	20
2.3.2 The Flory-Huggins approach.....	21

Contents (continued)

	PAGE
2.3.3 The Flory equation of state approach.....	24
2.3.4 Other thermodynamic approach.....	30
2.3.4.1 Cell-hole model.....	30
2.3.4.2 Sanchez and Lacombe's equation of state.....	30
2.3.4.3 Polymer reference interaction site model.....	31
2.3.4.4 Lattice cluster model.....	31
2.4 The solubility parameter mixing approach.....	32
2.5 Conclusions.....	33
CHAPTER 3	
KINETICS OF PHASE SEPARATION IN POLYMER BLENDS.....	35
3.1 Nucleation and growth.....	37
3.1.1 Classical nucleation theory.....	37
3.1.2 Density function theory.....	39
3.1.3 Diffuse interface theory.....	40
3.2 Spinodal decomposition.....	40
3.2.1 The Cahn-Hilliard linearised theory.....	40
3.2.2 Shortcomings of the Cahn-Hilliard linearised theory.....	43
3.2.3 The Cahn-Hilliard-Cook theory.....	46
3.2.4 The nonlinear theory.....	47
3.2.5 The Flory-Huggins-de Gennes theory.....	48
3.2.6 Viscoelastic effects and kinetics of phase separation.....	52
3.2.7 The scaling theories.....	54
3.2.7.1 The evaporation-condensation process.....	54
3.2.7.2 The diffusion-reaction process.....	55
3.2.7.3. Furukawa's approach.....	55
3.3 Conclusions.....	57

Contents (continued)

	PAGE
CHAPTER 4	
MATERIALS AND EXPERIMENTAL TECHNIQUES.....	59
4.1 Material characteristics.....	59
4.2 Sample preparations.....	62
4.2.1 Solution casting.....	62
4.2.2 Melt mixing.....	63
4.2.2.1 Twin screw extruder.....	64
4.3 Experimental techniques.....	65
4.3.1 Differential scanning calorimeter.....	65
4.3.2 Fourier transform infrared spectroscopy.....	66
4.3.3 Gel permeation chromatography.....	67
4.3.4 Light scattering.....	69
4.3.5 Scanning electron microcopy.....	71
4.3.6 Transmission electron microscopy.....	72
4.3.7 Tensile measurement.....	72
CHAPTER 5	
MISCIBILITY AND KINETICS OF PHASE SEPARATION OF SMA/PMMAe	
BLENDS.....	75
5.1 Phase boundary investigations.....	76
5.1.1 Cloud point determination.....	76
5.1.2 Spinodal determination.....	79
5.2 Effects of sample preparation on miscibility.....	81
5.3 Sample preparation dependence on kinetics of phase separation.....	84
5.3.1 The Cahn-Hilliard growth rate ($R(q)$).....	84
5.3.2 The growth rate of spinodal decomposition between intermediate and late stages.....	88
5.4 The validity of Cahn-Hilliard theory.....	93

Contents (continued)

	PAGE
5.4.1 The maximum scattering wave number (q_m).....	94
5.4.2 The maximum Cahn-Hilliard growth rate ($R(q_m)$).....	95
5.5 The scattering analysis for the intermediate and late stages of spinodal decomposition.....	96
5.5.1 The analysis of scaling function $F(X)$	96
5.5.2 Comparison with theoretical scaling structure function.....	100
5.6 Delay time discussion.....	106
5.6.1 Effect of scattering wave number.....	107
5.6.2 Effect of composition.....	107
5.6.3 Effect of sample preparation.....	109
5.6.4 Theoretical approach.....	111
5.7 Conclusions.....	113
CHAPTER 6	
MECHANICAL PROPERTIES AND MORPHOLOGIES OF SMA/PMMAE	
BLENDS	116
6.1 Mechanical properties	116
6.1.1 A principle of linear viscoelastic behaviour of amorphous polymers	116
6.1.2 Stress-strain measurement	118
6.1.3 Breaking phenomena	119
6.1.4 Results and discussion	121
6.1.4.1 Tensile test	121
6.2 Morphology	130
6.2.1 Morphology of homogeneous polymer blends	130
6.2.2 Morphology of heterogeneous polymer blends	130
6.2.3 Electron microscopy results	131
6.2.3.1 The fracture of polymers.....	131

Contents (continued)

	PAGE
6.2.3.2 Morphological development via spinodal decomposition	136
6.3 Conclusions	146
 CHAPTER 7	
CONCLUSIONS AND RECOMMENDATIONS	148
7.1 Conclusions	148
7.2 Recommendations	150
7.2.1 Effects of sample preparation on kinetics of phase separation .	150
7.2.2 Delay time behaviour	150
7.2.3 Mechanical properties	151
7.2.4 Morphology	152
REFERENCES	153
APPENDICES	162
CURRICULUM VITAE	179

สถาบันวิทยบริการ
จุฬาลงกรณ์มหาวิทยาลัย

List of figures

FIGURE		PAGE
1.1	Schematic diagram illustrates three types of properties of polymer blend ...	2
1.2	Approximate ranges of experimental techniques to study blend morphology of (1) interatomic; (2) molecular, spherulites; (3) filler aggregates, compatibilised blends; (4) reinforcements, noncompatible blends; (5) void.....	5
1.3	The schematic diagram of work.....	9
2.1	Plots of Gibbs free energy of mixing as a function of composition for a binary mixture exhibiting three types of mixing behaviour; immiscibility (A), complete miscibility (B) and partial miscibility (C)	11
2.2	Schematic of liquid-liquid temperature-composition phase diagrams. Shade areas represent the temperature-compositon regimes of a solution instability where phase separation occurs.....	13
2.3	Schematic illustration of the relationship between phase diagram and the free energy of mixing.....	14
2.4	Schematic illustration of the free energy-composition diagrams: (A) unstable region, (B) metastable region.....	15
2.5	Schematic illustration of a phase separation by the nucleation and growth mechanism.....	17
2.6	Schematic illustration of phase separation by the spinodal mechanism	18
2.7	A schematic illustration of an example of a possible arrangement in a polymer chain, each contain six segments of molecules.....	21
3.1	Schematic diagrams show the concentration fluctuation in the early (a), intermediate (b) and late stage of spinodal decomposition (c).....	35
3.2	Free successive situations for a reptation chain.....	52
4.1	The chemical structure of poly(methyl methacrylate) (PMMA).....	59
4.2	The chemical structure of poly(styrene-co-maleic anhydride)(SMA).....	60
4.3	Illustration of a plasticating extruder.....	64
4.4	A schematic diagram of differential scanning calorimeter.....	65

List of figures (continued)

FIGURE	PAGE
4.5 A schematic of an FTIR spectrometer.....	66
4.6 A schematic illustrates shows that numbers of processing cycles do not cause molar mass fraction in melt mixed of polymer blends.....	68
4.7 A schematic diagram of light scattering equipment.....	69
4.8 A plot of intensity against temperature for melt mixed SMA/PMMA blend at 0.3 °C/min.....	70
4.9 A photographic illustration of SEM model JSM-6400.....	71
4.10 A photographic illustration of LLOYD model 2000R.....	73
5.1 Dependence of heating rate on the observed cloud point temperature of solution cast SMA/PMMAe blends at various compositions.....	77
5.2 The plot of angular dependence 20/80 melt mixed SMA/PMMAe blends at the heating rate of 0.1 °C/min.....	78
5.3 A plot of ln(intensity) against time for melt mixed SMA/PMMAe blends (20/80), obtained from a temperature jump experiment at 205 °C.....	79
5.4 Plot of $R(q)/q^2$ against q^2 for melt mixed (40/60) SMA/PMMAe blends obtained from different jump temperatures.....	80
5.5 Phase diagrams of SMA/PMMAe blends prepared by solution cast and melt mixed methods.....	81
5.6 The comparison of phenyl bands of 20/80 SMA/PMMAe blends prepared by two sample preparation methods	82
5.7 Plots of glass transition of SMA/PMMAe blends	83
5.8 Effects of preparation method on $R(q)$ for SMA/PMMAe (10/90) blends, obtained from temperature jump experiments at 220 °C.....	85
5.9 Effects of preparation method on $R(q)$ for SMA/PMMAe (20/80) blends, obtained from temperature jump experiments at 210 °C.....	86
5.10 Effects of preparation method on $R(q)$ for SMA/PMMAe (30/70) blends, obtained from temperature jump experiments at 210 °C.....	86
5.11 Effects of preparation method on $R(q)$ for SMA/PMMAe (40/60) blends, obtained from temperature jump experiments at 210 °C.....	87

List of figures (continued)

FIGURE	PAGE
5.12 Effects of preparation method on $R(q)$ for SMA/PMMAe (40/60) blends, obtained from temperature jump experiments at 220 °C.....	87
5.13 Time-change of q_m and I_m as observed by light scattering for solution cast and melt mixed 20/80 SMA/PMMAe blends at the temperature jump of 210 °C	89
5.14 Time-change of q_m and I_m as observed by light scattering for solution cast and melt mixed 40/60 SMA/PMMAe blends at the temperature jump of 210 °C.....	90
5.15 Plots of reduced time and the reduced maximum scattering wave number for SMA/PMMAe blends at different compositions and preparation methods obtained from a temperature jump experiment of 210 °C	92
5.16 Plots of reduced time and the reduced maximum scattered intensity for SMA/PMMAe blends at different compositions and preparation methods obtained from a temperature jump experimngnet of 210 °C	93
5.17 Comparison of q_m from direct observation and calculation from Cahn-Hilliard theory for solution cast SMA/PMMAe (30/70) blends.....	94
5.18 Comparisons of the maximum growth rate $R(q_m)$ from direct observation and calculation from the Cahn-Hilliard theory for SMA/PMMAe (40/60) blends.....	96
5.19 Time evolution of the scaling function $F(X)$ for a melt mixed 20/80 SMA/PMMAe, quenched to 210 °C.....	98
5.20 Time evolution of the scaling function $F(X)$ for a melt mixed 20/80 SMA/PMMAe, quenched to 220 °C.....	99
5.21 Time evolution of the scaling function $F(X)$ for a solution cast 20/80 SMA/PMMAe, quenched to 220 °C.....	99
5.22 Time evolution of the scaling function $F(X)$ for a solution cast 40/60 SMA/PMMAe, quenched to 220 °C.....	100

List of figures (continued)

FIGURE	PAGE
5.23	Time evolution plots of normalised scaling function $\tilde{F}(x)$ based on the profile for percolation regime for 20/80 melt mixed SMA/PMMAe blend at the jump temperature of 210 °C 102
5.24	Time evolution plots of normalised scaling function $\tilde{F}(x)$ based on the profile for cluster regime for 20/80 melt mixed SMA/PMMAe blend at the jump temperature of 210 °C 103
5.25	Time evolution plots of normalised scaling function $\tilde{F}(x)$ based on the profile for deep-quench experiment for 20/80 melt mixed SMA/PMMAe blend at the jump temperature of 210 °C 103
5.26	Time evolution plots of normalised scaling function $\tilde{F}(x)$ based on the profile for cluster regime for 20/80 melt mixed SMA/PMMAe blend at the jump temperature of 220 °C 104
5.27	Time evolution plots of normalised scaling function $\tilde{F}(x)$ based on the profile for cluster regime for 40/60 melt mixed SMA/PMMAe blend at the jump temperature of 210 °C 105
5.28	Time evolution plots of normalised scaling function $\tilde{F}(x)$ based on the profile for cluster regime for 40/60 melt mixed SMA/PMMAe blend at the jump temperature of 220 °C 105
5.29	A typical plot of intensity against time and q for melt mixed (40/60) SMA/PMMAe blends, obtained from a temperature jump experiment at 210 °C 106
5.30	A plot of delay time against q for melt mixed SMA/PMMAe (40/60) blend, from a temperature jump experiment at 205 °C 107
5.31	Plots of delay time against quench depth for solution cast SMA/PMMAe blends at different compositions..... 108
5.32	Plots of delay time against quench depth for melt mixed SMA/PMMAe blends at different compositions..... 109

List of figures (continued)

FIGURE	PAGE
5.33 Plots illustrate the effect of sample preparation method on delay time for 30/70 SMA/PMMAe blends.....	110
5.34 Plots illustrate the effect of sample preparation method on delay time for 20/80 SMA/PMMAe blends.....	110
5.35 Plots of $\tau_d \times R(q)$ against q for 30/70 SMA/PMMAe blends.....	113
6.1 Tensile stressing of a bar.....	117
6.2 Typical stress-strain curves.....	118
6.3 The Dugdale plastic zone model for a craze.....	120
6.4 A schematic diagram shows craze formation by the mechanism of meniscus instability.....	121
6.5 Stress-strain curves of PMMAe and 20/80 SMA/PMMAe blends, which are miscible and phase separated at 210 °C at different stages of SD.....	122
6.6 A comparison of (a) tensile strength at break, (b) Young's modulus and (c) elongation at break for 20/80 SMA/PMMAe blends, which are miscible and phase separated at different times and temperatures.....	124
6.7 Stress-strain curves of PMMAe and 40/60 SMA/PMMAe blends, which are miscible and phase separated at 210 °C at different stages of SD.....	126
6.8 A comparison of (a) tensile strength at break, (b) Young's modulus and (c) elongation at break for 40/60 SMA/PMMAe blends, which are miscible and phase separated at different times and temperatures.....	128
6.9 GPC results of melt mixed 40/60 SMA/PMMAe blends prepared at different phase separation times and temperatures.....	130
6.10 A scanning electron micrograph picture of SMA.....	132
6.11 A scanning electron micrograph picture of PMMAe.....	133
6.12 A scanning electron micrograph picture at high magnification of SMA.....	134
6.13 A scanning electron micrograph picture of a fracture of tensile tested specimen for a miscible 40/60 melt mixed SMA/PMMAe blend.....	135

List of figures (continued)

FIGURE	PAGE
6.14	A scanning electron micrograph picture of a fracture of tensile tested specimen for the 40/60 melt mixed SMA/PMMAe blend, which was phase separated at 220 °C inside the late stage region of spinodal decomposition 135
6.15	The scanning electron micrograph pictures of the fracture from tensile test of the 40/60 melt mixed SMA/PMMAe phase separated at 220 °C at different stages of phase separation: (a) early stage, (b) intermediate stage, (c) late stage..... 136
6.16	The TEM pictures of the 20/80 melt mixed SMA/PMMAe phase separated at 220 °C at different stages of phase separation: (a) early stage, (b) intermediate stage, (c) late stage 138
6.17	The TEM pictures of the 40/60 melt mixed SMA/PMMAe phase separated at 220 °C at different stages of phase separation: (a) early stage, (b) intermediate stage, (c) late stage..... 140
6.18	Illustration of inter-domain distance..... 142
6.19	Comparison of inter-domain distance from light scattering and from TEM for the blends phase separated at 210 °C..... 142
6.20	Comparison of inter-domain distance from light scattering and from TEM for the blends phase separated at 220 °C..... 143
6.21	The inter-domain distance plotted as a function of reduced time for SMA/PMMAe blends. The closed objects represent 20/80 SMA/PMMAe blends while the open objects represent 40/60 SMA/PMMAe..... 144
6.22	Plots of tensile strength at break as a function of inter-domain distance for 20/80 SMA/PMMAe blends..... 145
6.23	Plots of tensile strength at break as a function of inter-domain distance for 40/60 SMA/PMMAe blends..... 146

List of tables

TABLE	PAGE
4.1 Properties of PMMAe and SMA.....	62
4.2 Phase separation times and temperature of the heat treated specimens for tensile tests.....	74



สถาบันวิทยบริการ
จุฬาลงกรณ์มหาวิทยาลัย

Nomenclature

Abbreviation

AFM	Atomic force microscopy
CPE	Chlorinated polyethylene
dPS	Deuterated Polystyrene
DMTA	Dynamic mechanical thermal analyser
DSC	Differential scanning calorimeter
EVA	Copolymer from ethylene and vinyl acetate
FTIR	Fourier transform infrared spectroscopy
GPC	Gel permeation chromatography
IPN	Interpenetrating network
LCST	Lower critical solution temperature
MA	Maleic anhydride
MEK	Methyl ethyl ketone
NG	Nucleation and growth
NMR	Nuclear magnetic resonance spectroscopy
PC	Polycarbonate
PEMA	Poly(ethyl methacrylate)
PMMA	Poly(methyl methacrylate)
PMMAe	Copolymer of poly(methyl methacrylate) and ethyl acrylate
PS	Polystyrene
PVAc	Poly(vinyl acetate)
PVME	Poly(vinyl methyl ether)
SAN	Copolymer from polystyrene and acrylonitrile
SANS	Small angle neutron scattering
SAXS	Small angle X-ray scattering
SD	Spinodal decomposition
SEM	Scanning electron microscope

SMA	poly(styrene-co-maleic anhydride)
TEM	Transmission electron microscopy
THF	Tetrahydrofuran
TMPC	Tetramethyl bisphenol A polycarbonate
UCST	Upper critical solution temperature
WAXS	Wide angle X-ray scattering

Symbols

a	Step length of the primitive chain $\sim N_e^{1/2}b$
a_{i+1}^+	The attachment rate of molecules
a_{i+1}^-	The detachment rate of molecules
b	Kuhn statistical segment length
$c(\mathbf{r},t)$	Concentration at the position of vector \mathbf{r} and time t
$c(\mathbf{q},t)$	Fourier transformation of $c(\mathbf{r},t)$
$C_o(q)$	Parameter related to elastic energy
D	Droplet diameter
D_{app}	Apparent diffusion coefficient
D_i	Adjustment factor
E_i	Intermolecular energy of state i
ΔE^v	Energy of vaporisation
$f(c)$	Volumetric free energy due to concentration fluctuation
F_{FHdG}	Free energy of the Flory-Huggins-de Gennes theory
$F(X)$	Scaling function
g	Empirical term
Δg	Volumetric change in Gibbs free energy between the new and present phase
ΔG_m	Gibbs free energy of mixing
ΔH_m	Enthalpy of mixing
I	Interaction term

$I(q,t)$	Scattered intensity
\bar{I}_m	Reduced scattering intensity
J^*	The nucleation rate in the vicinity of the critical size
$J(\mathbf{r},t)$	Inter-diffusion flux
k	Boltzman constant : 1.38×10^{-23} J/K
L	Length of the tube according to the reptation theory
M	Molecular mobility
\bar{M}_n	Number average molar mass
\bar{M}_w	Weight average molar mass
n	Refractive index of the blend
n_i	number of molecule of component i in the lattice model
n_c	Coarsening exponent
$n_q(t)$	Term analogous to the thermal fluctuation in Cook's theory
N	Total number of molecule in the system
N_A	Degree of polymerisation of polymer A
N_B	Degree of polymerisation of polymer B
N_e	Number of monomer between entanglement parts
N_i	Number of the i -mer in the system following the classical nucleation theory
P	Particular properties such as elastic modulus or thermal conductivity of blend
P_i	Particular properties of component I
P^*	Critical pressure
\tilde{P}	Reduced pressure
q	Scattering wave number
q_c	Critical value of q
q_m	Maximum value of q
\bar{q}_m	Reduced maximum scattering wave number
Q_{12}	non-combinatorial entropic correction

r_d	Radius of cluster
r_i	Number of segment per chain molecule of polymer i
\bar{r}	Average number of segment
R	Gas constant; 8.31432 J/mole-degree
R_g	Radius of gyration
$R(t)$	Radius of droplet
S	Total contact area of the system
$S(q,t)$	Structure function
$\tilde{S}(X)$	Universal scaling function
S_i	Number of intermolecular contact site of composition
$S_x(q)$	Structure function at the equilibrium
ΔS_m	Entropy of mixing
t	time
t_c	Characteristic time
T	temperature
T^*	Critical temperature
\tilde{T}	Reduced temperature
T_g	Glass transition temperature of blend
T_{gi}	Glass transition temperature of component i
T_m	Melting temperature
U	Internal energy
V	Volume of the system
V^*	Critical volume
\tilde{V}	Reduced volume
W	Work of formation of a fluctuation
X	Dimensionless parameter = q/q_m
X_i	Weight fraction of component i

Greek alphabets

α	The exponent of time evolution of the maximum wave vector q_m
α_T	Thermal expansion coefficient
A	Helmoltz free energy
β	The exponent of time evolution of the maximum intensity I_m
γ	Thermal pressure coefficient
γ_s	Surface tension of the system
Γ	Prefactor related to the molecular mobility
δ	Solubility parameter
ε	Strain
E	Young 's modulus
E_i	Intermolecular energy of state
ζ	Friction coefficient of a monomer
Z	Canonical partition function
η_{ij}	Intermolecular energy
$\langle \eta^2 \rangle$	Mean square of refractive index fluctuation
θ	Scattering angle
ϑ	Site fraction of component i
κ	Compressibility
K	Gradient energy
λ	Wavelength of the radiation
Λ	Inter-domain distance of each percolating domain
$\Lambda(q)$	Onsager coefficient
$\Delta\mu$	Chemical potential
ν_p	Poisson 's ratio
σ	Stress
τ	Reduced time
τ_D	Delay time
ϕ_i	Volume fraction of component I

ϕ_0	Average volume fraction of the system
$\chi(q,t)$	Susceptibility of the system
χ_{12}	Flory-Huggins interaction parameter
X_{12}	Exchange energy parameter for unlike concentration
ψ_i	Segment fraction of polymer I
ψ_0	Total number of segment
Ω	Total number of a way of arranging molecule in the lattice site



สถาบันวิทยบริการ
จุฬาลงกรณ์มหาวิทยาลัย

Chapter I

Introduction

The consumption of polymer increased considerably in the past few decades. Various types of polymers apparently have been discovered and commercially produced to serve a variety of usage. However it has been known that to synthesise a truly new and acceptable polymer requires such a high investment cost, this consequently has triggered the ideas of simply mixing two polymers or copolymers. The product is usually called polymer blend or polymer alloy. This sort of technique can offer several economic benefits. For example, it generates the lower production cost with acceptable properties. Moreover, as the growing importance of reactive processing, the blending technology offers new types of materials characterised by controlled chemical constitution and morphology, which can be more precisely tailored the specific requirements. With the synergistic properties, the better properties of products can be obtained. In addition, due to the world waste crisis today, the technique of blending also enables recycling controllable and easier.

Basically polymer blend can be classified into three categories according to micro-phased structure, namely miscible, immiscible and partially miscible blends. Miscible blends always show a stable homogeneous single-phase structure with one glass transition while immiscible blends exhibit 2-phase structure and 2 glass transitions of original components for all conditions. Partially miscible blends, on the other hand, can show either a homogeneous single phase or heterogeneous phase, depending on certain conditions; a large number of commercial alloys and blends usually fall into this category.

A major problem of polymer blend so far is trying to predict its properties. Many features such as composition of the mixture, temperature, pressure, shear rate, etc. can lead to a wide diversity of polymer properties. A very favourable dipole-dipole interaction energy between the polymer components generally results in synergistic, i.e., better properties while the disruption of interaction somehow influences the nonsynergistic, i.e., worst properties, which usually happens in

immiscible blend. The blend, which shares properties of both pure polymer components, is called additive. The general equation to predict properties or processing characteristics is:

$$P = P_1\phi_1 + P_2\phi_2 + I\phi_1\phi_2 \quad (1.1)$$

where P is a particular property, I is interaction term that may be negative (nonsynergistic), zero (additive) or positive (synergistic) and ϕ_i is the volume fraction of component i .

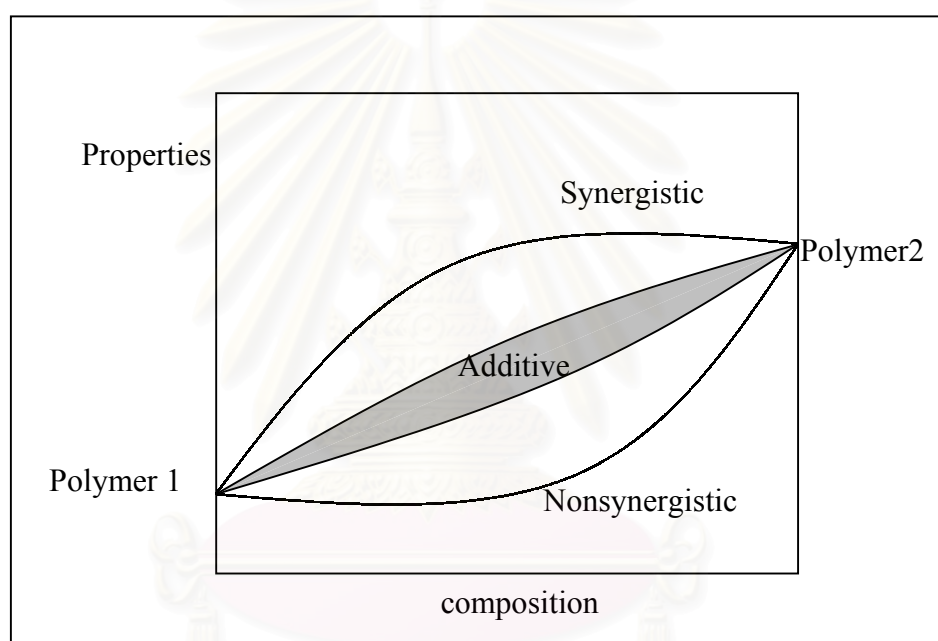


Figure 1.1: Schematic diagram illustrates three types of properties of polymer blend

1.1 Methods of blending

Owing to the substantial use of polymer blends nowadays, numerous preparation techniques have been developed and brought into action. Among those, there are two main techniques, which are worth noting, namely mechanical mixing and solution casting. The mechanical mixing or so-called the melt mixing process has been known to be the most well-known method and dominates the usage of blends due to the economic reason and high scale production. Polymer blends can be obtained by applying heat or force to two pure components however many parameters

are needed to be taken into account such as viscosity, phase separation temperature, T_g , T_m , etc.

The solution casting or sometimes called solvent casting is another main method, in fact it is also popular and maybe not less than the previous one, nonetheless this method can be applied only in small scale especially in laboratory work. Polymer blend can be prepared by dissolving two pure components in a common soluble solvent. The solvent is later eliminated. Generally three methods have been widely utilised to remove solvent. The first one is the common technique and mostly used, starting by allowing solvent to evaporate at room temperature, then putting in a vacuum oven and continually increasing temperature. The heating rate is dependent on polymer system. The second one can result powder by freezing and storing products under vacuum, however the product may be difficult to detect by normal DSC owing to the very tiny size [Paul et al. 1978]. The last method is used for the high boiling point common solvent [Thongyai 1992]. By putting polymer solution in non-solvent can lead to the precipitation and result in powder-formed product.

1.2 Methods of study miscibility and phase separation phenomena

It is clear that polymer blends have different properties from pure components and among those blends, there are still differences between miscible blends and immiscible blends as well. So far a large number of methods have been introduced in order to study polymer blends easier and more accurately. Four main groups with respect to the ways of study are briefly discussed herein; T_g study, scattering study, morphology study, and infrared spectroscopy.

1.2.1 T_g study

It is generally known that miscible blend always exhibits one T_g whereas immiscible blend has 2 T_g 's. In the case of partial miscibility, 2 shifted T_g 's can be obtained. However, it should be borne in mind that a single T_g does not mean complete miscibility. Size of components has strong influence on the capability of equipment. This is clearly demonstrated in the work by Shultz *et al.*[1980], who studies PS/PMMA in naphthalene by using differential scanning calorimeter (DSC).

Nowadays there are several varieties of techniques to determine T_g , among those, the most popular one is the thermal analysis technique using DSC. Details of which are described in Chapters 4 and 5. One other technique, which should be mentioned, is the mechanical technique using dynamic mechanical thermal analyser, DMTA. By subjecting polymers to small amplitude cyclic, deformation can yield important information concerning transitions occurring on the molecular scale. Moreover, not only can 2 aforementioned techniques be used to determine T_g but many others are also used, e.g., dielectric technique, dilatometric technique, radioluminescence spectroscopy, etc.

1.2.2 Scattering study

For normal amorphous systems, homogeneous mixtures are usually transparent whereas heterogeneous mixtures are cloudy unless the components of the mixture have identical refractive indices. By variations of temperature, pressure and compositions of the mixture, it can change the miscible blends from being transparent to cloudy. The first appearing of cloudiness denotes the cloud point. Using light scattering technique, one can investigate phase separation phenomena, namely nucleation & growth and spinodal decomposition. So far it should be noted that to employ scattering technique, not only laser light source can be used, x-ray and neutron is available as well. However, since the operation cost is very high and there are few equipment in the world, it results in those methods being uncommon.

1.2.3 Morphology study

Using highly powerful microscopes, it can reveal the internal structure, e.g., interpenetrating phase, which is impossible to see with bare eyes. The normal technique, which can be used to observe phase boundary under normal light, is optical microscope. However, as some blends have very tiny components, other more powerful techniques are required, i.e., transmission electron microscope TEM, scanning electron microscope SEM, atomic force microscope AFM. It should be noted that in order to see the structure clearly, preliminary treatments are sometimes necessary, for example, etching, or staining.

1.2.4 Infrared spectroscopy

This technique indirectly detects miscibility by investigating some sort of specific interaction in the blend, e.g., hydrogen bond. The knowledge of molecular interaction then can be used to explain the shape of phase diagrams, i.e., UCST or LCST [Saito *et al.* 1987; Cowie 1991].

It is apparent that in reality there is no perfect technique, which can be used to study all systems. The characteristics of system, time, operating cost and the limitations of each equipment are necessary to be taken into consideration. Figure 1.2 shows approximate limit ranges of the above mentioned techniques.

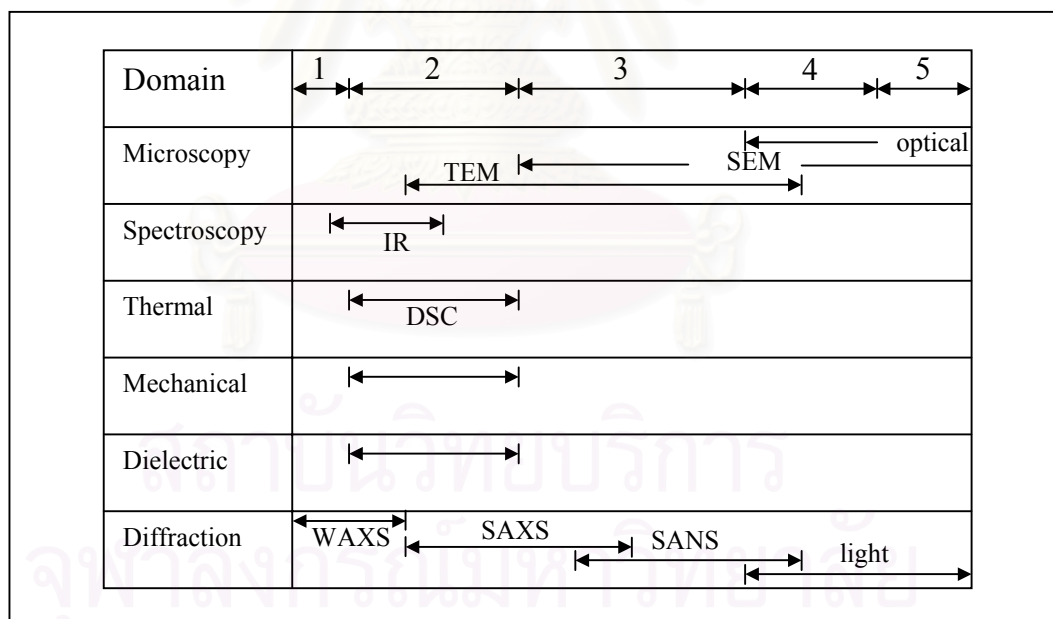


Figure 1.2: Approximate ranges of experimental techniques to study blend morphology of: (1) interatomic; (2) molecular, spherulites; (3) filler aggregates, compatibilised blends; (4) reinforcements, noncompatible blends; (5) voids [Utracki 1989].

1.3 Literature reviews

A number of papers [Robard 1977; Reich 1981; Vernell 1981; Inoue 1985; Saldanha 1987; Neo1992; Nishimoto 1991; Woo 1996; Gaurab 1996] have shown that several parameters are able to affect miscibility and phase boundary conditions of polymer blends, for example, film thickness, substrates, types of solvent, evaporation rate of solvent, etc. Among these, an interesting parameter is the effect of solvent since most experimental works so far usually employed the solution casting method. They are of course vulnerable to the interference of solvent; hence it is very interesting if the thermodynamics and kinetics of phase behaviour in blends are observed in the blends, which do not mingle with all solvent, i.e., melt mixed blends. A previous study by Gaurab *et al.*[1996] using a differential scanning calorimeter (DSC) on blends, which were prepared by 2 different techniques, viz., solution casting and melt mixing from co-precipitated samples, showed that the latter provided the most compatible blends. However, the co-precipitation method cannot in fact be considered to be the melt mixing as pointed out by Gopakumar *et al.* [1998]. The blends of poly(phenylene sulphide) and poly(ethylene terephthalate-co-oxybenzoate) prepared by precipitation and melt mixing show different morphology and the melt transition. The co-precipitated blends exhibit more uniform and continuous morphology compared to the melt mixed blends. Other measurements by Thongyai [1994] on tetra methyl-bis-phenyl-A polycarbonate with polystyrene (TMPC/PS) and Manda [1998] on poly (styrene-co-maleic anhydride) with polymethyl methacrylate (SMA/PMMAe) using solution cast and melt mixing methods show that to employ a direct melt mixing method in the blend can lower the cloud point curve. They suggested that the cloud point curve of the melt mixed samples might coincide with the binodal curve because the large number of heterogeneties in such samples provide multiple nucleating sites for the nucleation and growth mechanism once the sample is inside the metastable region. However to date no spinodal curve of melt mixed samples has been reported.

Although the miscibility and phase separation phenomena have been extensively studied, few works have dealt with the effect of phase separation on mechanical properties. Kim *et al.* [1991] and Abtal *et al.* [1996], who studied

PS/PVME blend by varying annealing time and temperature, followed by mechanical test, e.g., tensile test, concluded that phase separation can cause inferior properties as the result of less connectivity and weak interface, while the appearance of superior properties in some compositions is caused by the shift of T_g . Besides, two works by Kodama, who studied PC/PMMA [Kodama 1993a] and SAN/PMMA [Kodama1993b], show that as temperature is higher and annealing time is longer, diameter of phase separated structure increases resulting in the decrease of specific gravity that means the occurrence of void during phase separation, hence tensile properties deteriorate. On the contrary Kyu *et al.* [1991], who studied PC/PMMA, mentioned that the blends which have the interconnected spinodal structure manifest better toughness in relation to the melts without it. Furthermore a study on CPE/EVA by Xie *et al.* [1993] manifested that the storage and loss modulus of blend increased with time in the early and intermediate stages of spinodal decomposition; they however decreased as phase separation proceeded. In short, it can be seen that there is no mention about network-like structure or spinodal structure in the first four works, while it has been taken into account by just the last two. So far, it is still equivocal about the real effect of spinodal decomposition on mechanical properties.

Interestingly, a recent work by Pavawongsak [1996] has shown that during the isothermal heating of blend inside the spinodal region, there appears one surprising phenomenon called delay time. The phenomenon refers to a time period after a jump to a temperature inside the spinodal, during which no apparent phase separation occurs - at least as observed by light scattering. Relatively few studies so far have mentioned this behaviour, among which we cite [Bank 1972; Binder 1986; Thongyai 1994; Clarke 1997; Manda 1998; Gerard 1999]. Previous work on the polystyrene/poly(vinyl methyl ether) (PS/PVME) blend system from Bank *et al.* [1972] using optical microscopy showed that the delay times decrease as temperature increases. A theoretical approach developed by Binder [1986] was used to describe the interaction between the rheological relaxation mechanisms of the polymers and the concentration fluctuations. However, there was no comparison between the theory and experimental data. The model, which was subsequently elaborated by Clarke *et*

al. [1997], showed that entanglement networks were the key factor causing delay times. This proposition was supported by light scattering experiments on ultra high molecular weight polystyrene-polyvinyl methyl ether (PS/PVME) blends [Pavawongsak 1996]. A study by Thongyai [1994] on TMPC/PS blends using light scattering suggested that the delay time phenomena could be observed in this system only for certain compositions, notably those with a high percentage of TMPC, which is the high T_g component. Experimental work by Manda *et al.* [1998] also showed that delay times can also be detected in the SMA/PMMAe blend system. Shear-induced phase separation in PS/PVME blends studied by Gerard *et al.* [1999] showed that not only can delay times be observed in thermally induced phase separation, but also in shear-induced phase separation.

1.4 Scope of work

This work aims to investigate the effects of sample preparation methods on mixing and the kinetics of phase separation of polymer blends. The blend of poly(methyl methacrylate) (PMMA) and poly(styrene-co-maleic anhydride) (SMA) received attention since it has been known that mixing PMMA and SMA can extend the used temperature of PMMA owing to the high glass transition temperature (T_g) of styrene maleic anhydride copolymer. Furthermore, adding SMA to PMMA also improves the chemical resistance of PMMA. The spinodal curves of melt mixed samples were measured and compared with the solution cast samples. The kinetics of phase separation of both solution cast and melt mixed samples were explored in some detail. In addition, as it is believed that the spinodal structure or the interpenetrating network-like structure might be able to offer synergistic properties, the effect of phase separation on mechanical properties is studied, coupled with the morphological observation. It is rather interesting since so far the morphology of blends, which were phase separated at different periods of time, has been widely investigated only on solution cast blends [Okada *et al.* 1993, 1995; Ribbe *et al.* 1997; Ermi *et al.* 1998], while to date no morphology study in respect of phase separation has been carried out on melt mixed blends. The comparison of morphological development in light scattering experiments and in compression moulding process was carried out. Finally,

the effects of composition, temperature, and sample preparation on delay time behaviour which, is apparently the hot subject nowadays, were also observed. The schematic diagram of this work is shown in Figure 1.3.

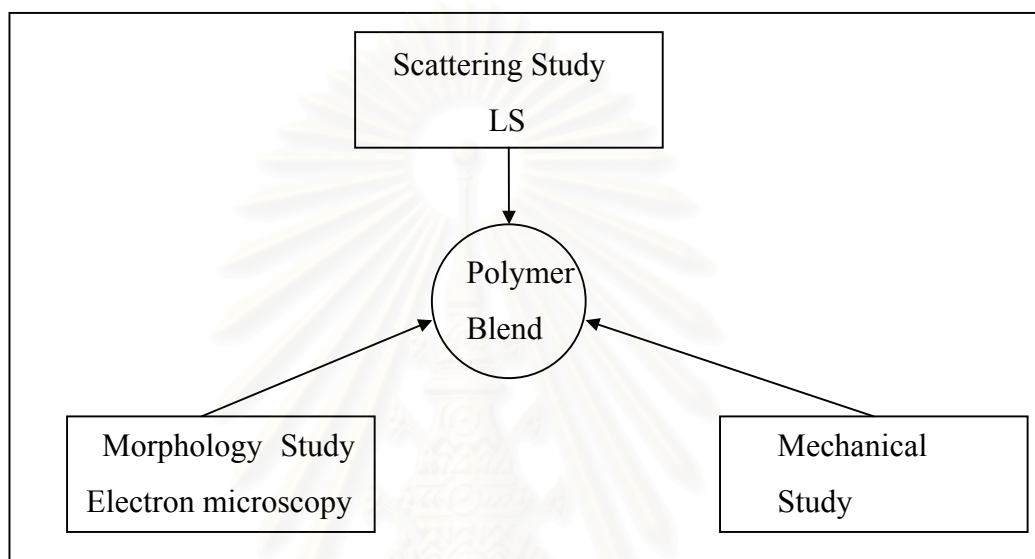


Figure 1.3: The schematic diagram of work

1.5 Organisation of Thesis

This thesis comprises 7 chapters. The first chapter introduces general ideas and scope of this work. The next chapter deals with thermodynamics of polymer blends while the kinetics of phase separation is in Chapter 3, followed by the manifestation of materials and preparation method in Chapter 4. Kinetics of phase separation study as well as mechanical and morphological investigations are covered with in Chapters 5 and 6 respectively. Conclusions and recommendation are reviewed in the last chapter.

Chapter II

Thermodynamics of Polymer Blends

The characteristics of polymer blends are somewhat sophisticated - some miscible blends, which are clear at room temperature, can become turbid after raising or lowering temperature. Hence, to be able to foretell the phase behaviour of mixture is essential. Not only does it enable us to create the specific properties of mixture, but it also minimises the operating cost. So far, a number of scientists have attempted to develop thermodynamic theories to describe phase behaviour. However, since some polymers possess grotesque characteristics, for example the dendrimer, liquid crystal polymer, those theories appear to be valid in some systems and fail in others. Recently, thanks to the development of statistics, physics and fundamental thermodynamics, the knowledge of phase behaviour has been considerably understood. According to the statistical thermodynamic methodology, there are 2 ways to formulate the theory of chain molecular liquids and their mixtures. The first one is dependent on the ideas of predicting the probability of finding polymer segments in particular configurations, for example the Ising model and the mean field model, whereas the second one is attributed to the assumption of regular lattice structure of crystalline solids. Regarding the latter, it results in the so-called lattice model, free volume theory, or the hole theory [Olabisi *et al.* 1979].

This chapter introduces the general models used to describe properties of polymer blend. It starts with classical thermodynamics, followed by other related theories based on the lattice model, e.g., classical Flory-Huggins theory, Flory equation of state, etc. The difference between nucleation-growth and spinodal decomposition in respect of the free energy change during phase separation is manifested, and finally the alternative way of calculating the miscibility and stability of blend based on the solubility parameter is reviewed.

2.1 General Principles for Polymer-Polymer Miscibility

The basic and very useful thermodynamic equation that will be able to describe the miscibility of two polymers is the Gibbs free energy equation:

$$\Delta G_m = \Delta H_m - T\Delta S_m \quad (2.1)$$

where ΔG_m is the Gibbs free energy mixing

ΔH_m is the enthalpy of mixing

ΔS_m is the entropy of mixing

T is the temperature in Kelvin

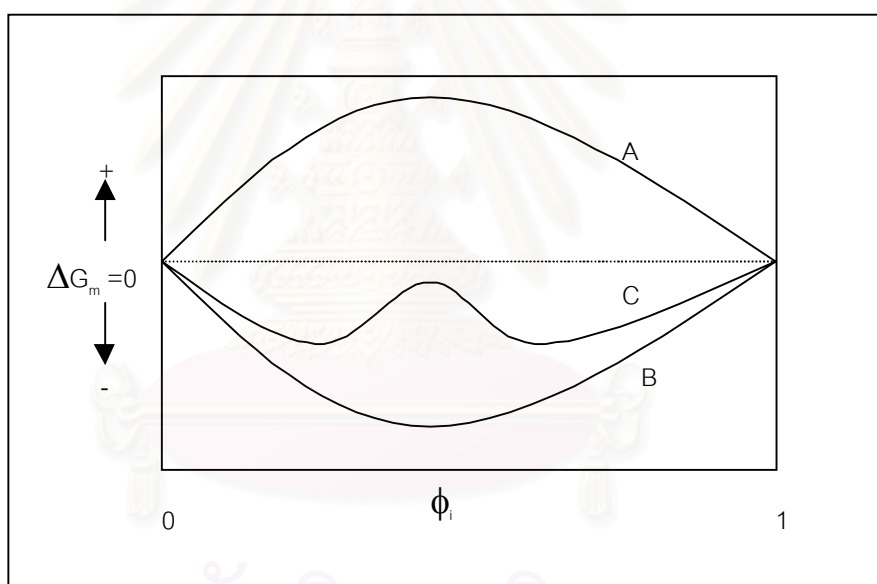


Figure 2.1: Plots of Gibbs free energy of mixing as a function of composition for a binary mixture exhibiting three types of mixing behaviour; immiscibility (A), complete miscibility (B) and partial miscibility (C).

Equation 2.1 apparently can predict whether a blend is miscible, immiscible, or partially miscible by taking into account the sign of ΔG_m as seen in Figure 2.1. With the positive sign of Gibbs free energy, the blend is immiscible, whereas the negative can be seen in a miscible blend. Nevertheless, some can exhibit partially miscible, even with the negative sign of ΔG_m . Thus, the second criteria (the sign of

the second derivative of ΔG_m) is required to specify the difference between partially miscibility and miscibility. Systems always exhibit miscibility if they satisfy this following condition:

$$\frac{\partial^2 \Delta G_m}{\partial \phi_i^2} > 0 \quad (2.2)$$

Concerning the partially miscible blend, it appears that some homogenous systems phase separate if temperature becomes higher demonstrating the LCST behaviour, while some change from being inhomogeneous at room temperature to homogenous at higher temperature called the UCST behaviour. Not only can Equations 2.1 explain the miscibility of mixture, it can also demonstrate what kind of phase diagram the blend should exhibit. Polymer blends generally exhibit the UCST behaviour since, as temperature decreases, $T\Delta S$ term should decrease as well. And as the consequence of which, the free energy term becomes positive and phase separation then takes place indicating the UCST behaviour. On the other hand, some blends appear to show the LCST behaviour, this might be as the result of the enthalpy of mixing increases as temperature increases, leading the free energy to be positive and phase separation occurs. There are two explanations for such behaviour [Strobl 1997, Cowie 1991]. First, once mixing two polymers, there are two types of interaction competing with each other, viz., the repulsive interaction and the attractive force between specific groups incorporated in the two polymers. With increasing temperature the fraction of closed bonds decreases and the repulsive forces eventually dominate. This may induce the enthalpy of mixing to change from being negative at low temperature to being positive at higher one. The second possibility is related to the volume shrinkage. As temperature increases, the free volume for the local motion of monomers decreases. Hence the mobility is reduced, leading to lowering of the entropy.

For polymer blends it appears that not only do the UCST and LCST phase diagrams have been found, other types of phase diagrams can also be observed.

Figure 2.2 presents a schematic representation of various types of phase diagrams for polymer mixture, and for the sake of clarity, the discussion here will be restricted to monodisperse binary mixture. As can be seen from Figure 2.2a, there is no instability regime indicating that the blend appears completely miscible. Figs 2.2 b-c clearly show that the UCST and the LCST exist separately, whereas in Figs 2.2 d-f, the UCST merges with the LCST. This therefore can produce a distinctive hour glass type

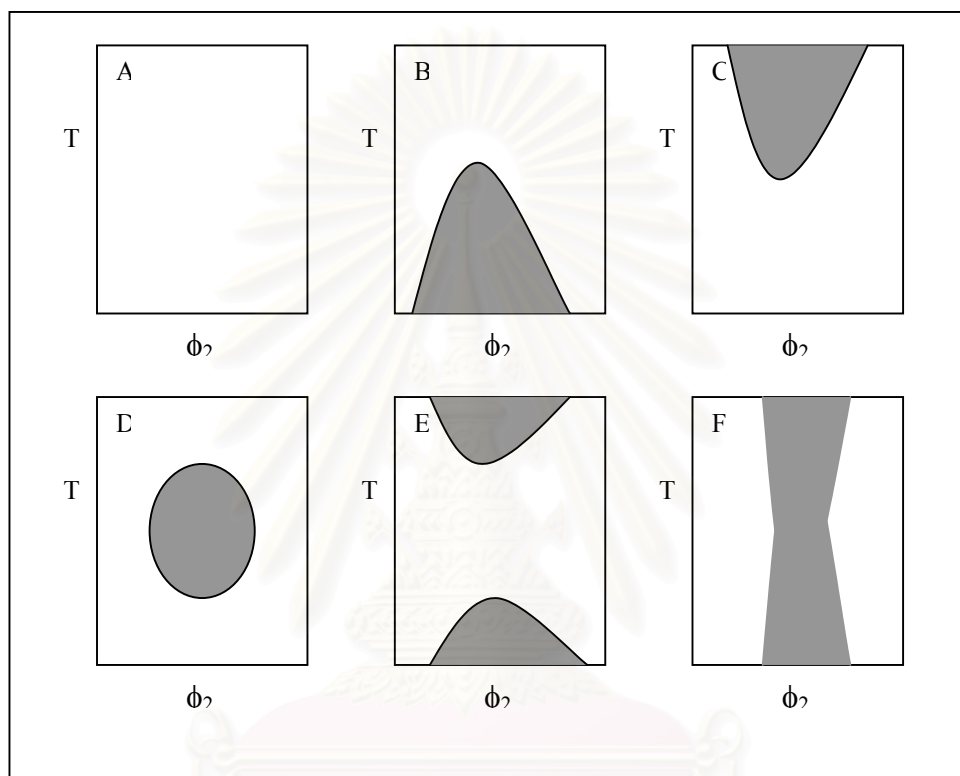


Figure 2.2: Schematic of liquid-liquid temperature-composition phase diagrams. Shade areas represent the temperature-composition regimes of a solution instability where phase separation occurs [Olabisi *et.al.* 1979].

of phase diagram as seen in Fig 2.2 f.

2.2 The Mechanism of Phase Separation

The phase separation phenomena in partially miscible blend at various conditions are dependent on the combined effects of the thermodynamics of the system (i.e. the extension, location and the nature of the miscibility gap in the temperature composition behaviour) and the properties of the different polymers

[Olabisi 1979]. It appears that once the system gets into phase separation regime, it can undergoes 2 different mechanisms: spinodal or nucleation and growth depending on which regime it falls in. One example of the relationship between the Gibbs free energy and phase diagram is shown in Figure 2.3. The line, which separates the unstable and metastable region, is called the spinodal line, whereas the line between the metastable and stable region is the binodal line. Each point in phase diagram comes from the change of Gibbs free energy curve at different temperatures.

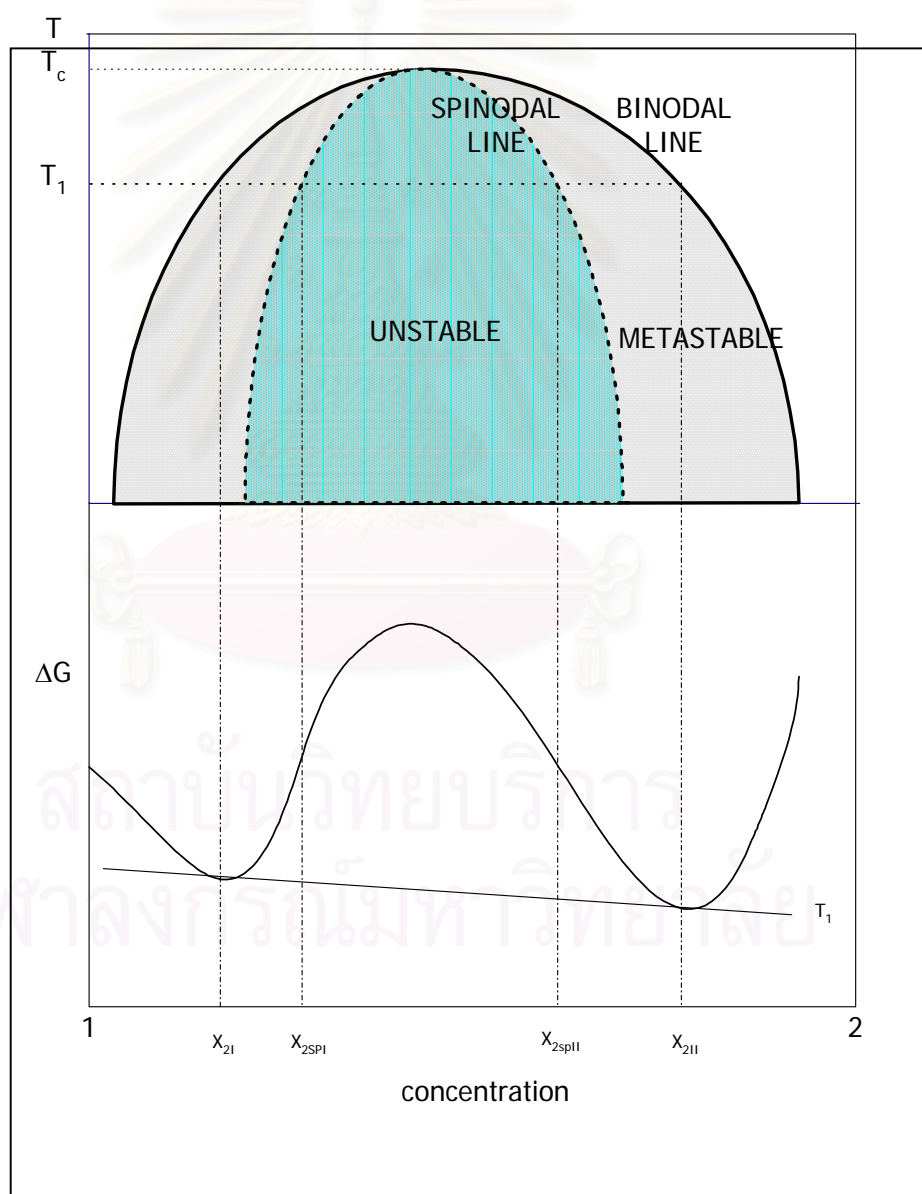
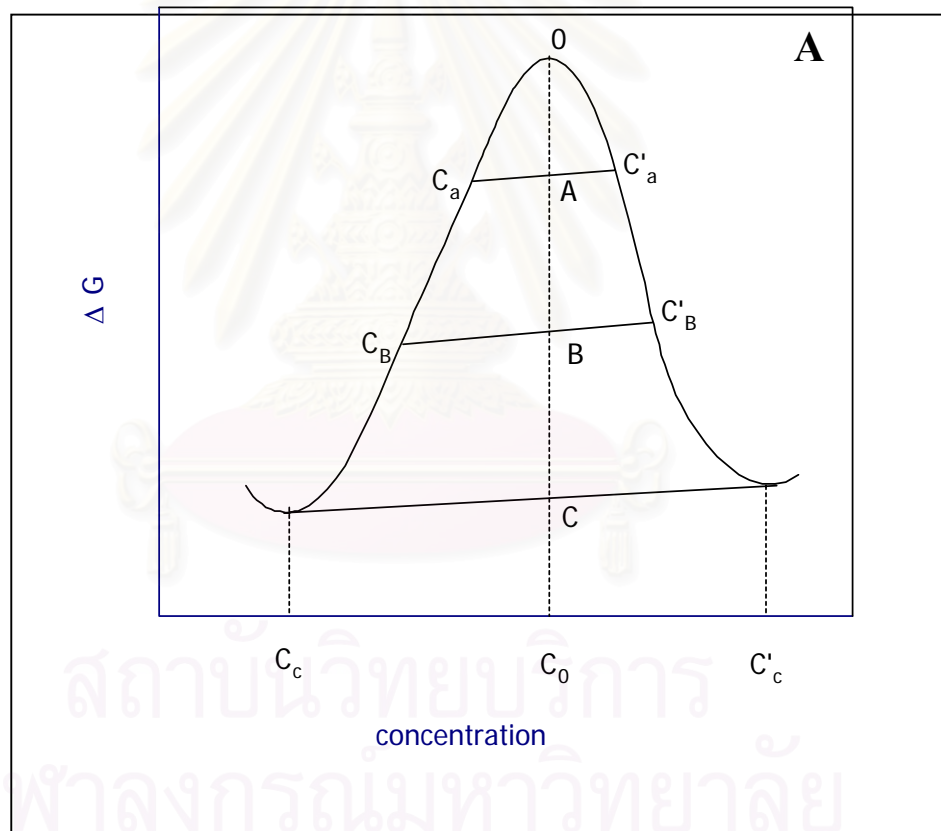


Figure 2.3: Schematic illustration of the relationship between phase diagram and the free energy of mixing

The Free energy-concentration diagram clearly illustrates how the system changes [Cahn 1968]. Considering Figures 2.4 a and b, it can be seen when the original system is in unstable phase as shown with C_0 in Figure 2.4(a) receives such a few perturbation, the free energy of homogeneous phase will move toward the lower free energy, making system more stable, whereas in the case of metastable state as shown in Figure 2.4(b), the homogeneous system needs activation energy to overcome the boundary hill and moves toward the lowest energy state, i.e. point C_a and C_a' in Figure 2.4(b). The limit of metastability is the lowest free energy represented by the tie line C_a-C_a' , and it is defined as the binodal, whereas the unstable change is called spinodal.



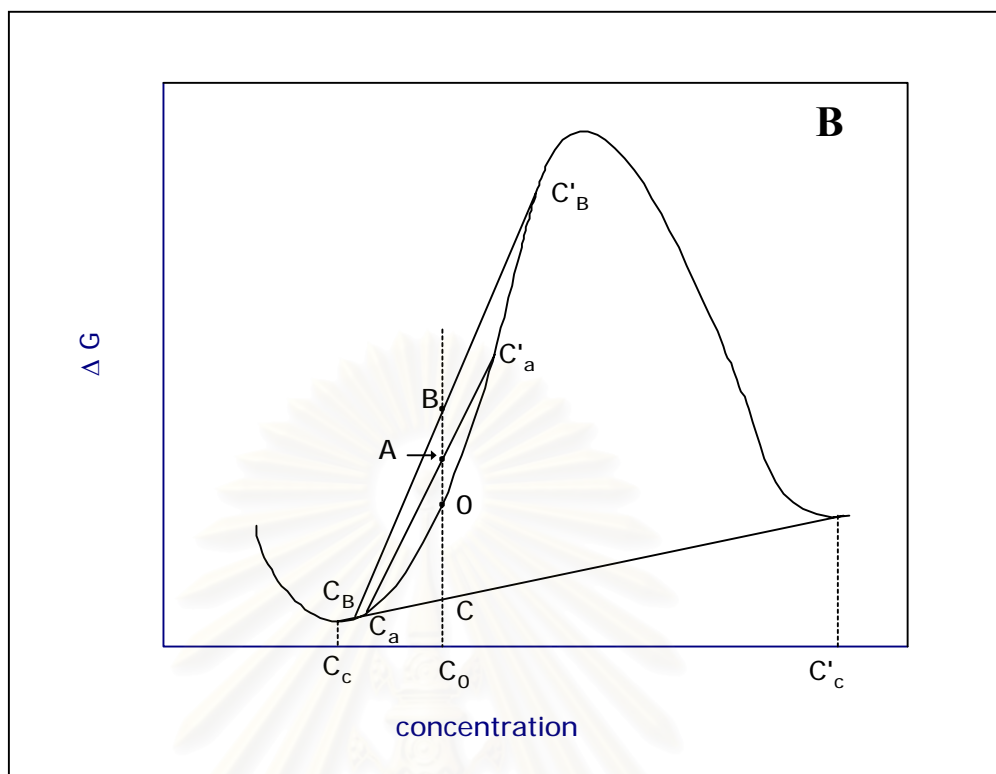


Figure 2.4: Schematic illustration of the free energy –concentration diagrams: (A) unstable region, (B) metastable [Olabisi *et al.* 1979]

2.2.1 Nucleation and Growth

Nucleation and growth is a process, which starts within the metastable state. The system begins with the activated sides called nuclei. The nuclei are different from an equal number of nearest neighbour molecules because they possess an excess of surface energy which produces the aggregate as a new phase [Olabisi *et al.* 1979]. The nuclei grow in their sizes and number with a decrease in free energy; however, their concentration still remains constant. The growth process can be represented by Figure 2.5

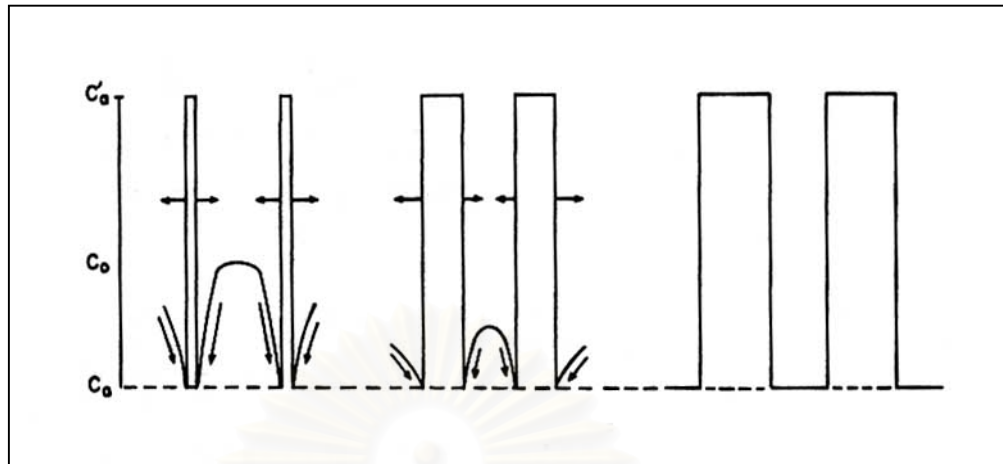


Figure 2.5: Schematic illustration of a phase separation by the nucleation and growth mechanism.

As seen in Figure 2.5, the droplets grow by diffusion of macromolecules into the nucleated domain. The rate of this process has been suggested by different theories, one of which is the Ostwald ripening equation [Ostwald 1900],

$$D \propto t^{1/n_c} \quad (2.3)$$

where D is the droplet diameter

n_c is the coarsening exponent $\cong 3$

Systems, which undergo nucleation and growth mechanism, must have negative second derivative of free energy,

$$\frac{\partial^2 \Delta G_m}{\partial \phi_i^2} < 0 \quad (2.4)$$

Moreover, following the nucleation and growth with respect to the binodal curve, this important condition should be met: the chemical potentials $\Delta\mu$ for the components 1 and 2 are the same in both coexistent phase A and B

$$\Delta(\mu_1)_A = \Delta(\mu_1)_B \quad (2.5)$$

$$\Delta(\mu_2)_A = \Delta(\mu_2)_B$$

2.2.2 Spinodal Decomposition

Spinodal decomposition is a kinetic process, which takes place spontaneously and isothermally once the system falls in the unstable region. No activation energy is required for this process. The growth originates, not from nuclei, but from a small amplitude of concentration fluctuation. The interwoven structures at the beginning become coarser and larger as the spinodal proceeds, and eventually turn into droplet in order to reduce the surface energy. The amplitude and the wavelength of the concentration fluctuation continue growing until reaching the equilibrium. The schematic diagram of spinodal decomposition has been shown in Figure 2.6.

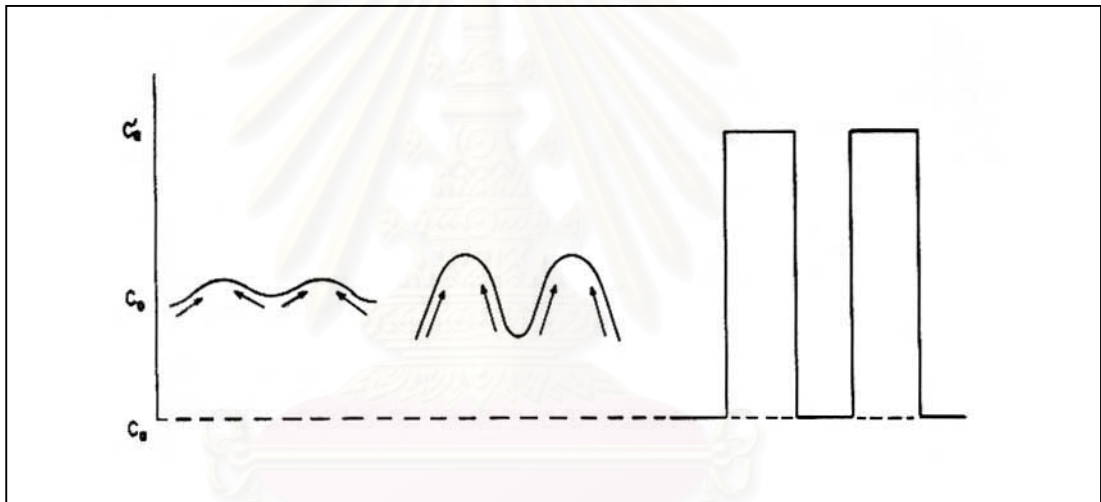


Figure 2.6: Schematic illustration of phase separation by the spinodal mechanism.

Surprisingly, Figure 2.6 shows the diffusion of concentration fluctuation moves uphill, i.e., the diffusion coefficient is negative. This is due to the driving force for the spinodal diffusion is not the concentration difference but the chemical potential difference.

The spinodal line, or the limit between the metastable and unstable regions, can be defined by:

$$\frac{d(\Delta\mu_i)}{d\phi_2} = 0 \quad (2.6)$$

where ϕ_2 is the volume fraction of component 2

In contrast to the nucleation and growth mechanism, systems undergoing spinodal should show positive value of the second derivative of free energy,

$$\frac{\partial^2 \Delta G_m}{\partial \phi_i^2} > 0 \quad (2.7)$$

Several theories have been developed to describe both mechanisms of phase separation. Among these theories, the most important and well-known one is Cahn-Hilliard theory. The kinetics of phase separation via spinodal and nucleation and growth will be discussed in more detail in the following chapter.

2.3 The Statistical Thermodynamics of Polymer Systems

A number of thermodynamic theories for polymer systems have been developed in the past 50 years, for example, the well-known Flory-Huggins theory in 1940s, equation of state by Patterson and Flory in 1960s, and several other polymeric equation of states later on. All of these theories have one thing in common - they are based on the same basic ideas: the lattice model. First assume we have a box, which contains so many small boxes inside, then calculate the probability of putting small balls inside those small boxes, allowing one ball for each small box. By relating that probability to basic thermodynamic values, for example, entropy, this can lead to the Flory-Huggins theory. In the case of each box gaining some sorts of interaction, if the partition function is applied, we then can obtain the equation of state theories.

2.3.1 The General Principle of Statistical Thermodynamics

It will be very helpful for the discussion of following theories, if the concept of statistical thermodynamics is first mentioned. Concerning the ways of each molecule of polymer forming each conformation, e.g., gauche or trans, these ways have the same point of view to the quantum mechanics, which describes how small particles move. Let us first start with the partition function, which can be related to several basic thermodynamic values. Assuming the magnetic field is neglected, the simple canonical partition function, Z , can be defined as:

$$Z = \sum_i e^{\frac{-E_i}{kT}} \quad (2.8)$$

where E_i is an intermolecular energy of state i . Details of this equation can be seen in Mc Clelland [1973], Callen [1985].

By using the statistical thermodynamic approach, all general thermodynamic values such as entropy or internal energy can be obtained via the partition function. First, the Helmholtz free energy, A , is proportional to the logarithm of the partition function:

$$A = -RT \ln Z \quad (2.9)$$

The entropy is given by

$$S = -\left(\frac{\partial A}{\partial T}\right)_V = R \ln Z + RT \left(\frac{\partial Z}{\partial T}\right)_V \quad (2.10)$$

From general law of thermodynamics, the internal energy, U , is the summation of Helmholtz free energy, A , and the entropic energy TS ,

$$U = A + TS = RT^2 \left(\frac{\partial \ln Z}{\partial V} \right)_T \quad (2.11)$$

Pressure, P, is given by

$$P = - \left(\frac{\partial A}{\partial V} \right)_T = RT \left(\frac{\partial \ln Z}{\partial V} \right)_T \quad (2.12)$$

2.3.2 The Flory-Huggins Approach

This theory is based on the idea of arranging chains of small molecules inside the lattice free cell. As shown in figure 2.7, the entropy of mixing based on the Boltzman law is derived as:

$$\Delta S_M = k \ln \Omega \quad (2.13)$$

where Ω is the total number of a way of arranging molecule in the lattice sites, as for example in Figure 2.7 the way to arrange n_1 and n_2 molecules on a regular lattice comprising $N = n_1 + n_2$ cells is

$$\Omega = \frac{N!}{n_1! n_2!} \quad (2.14)$$

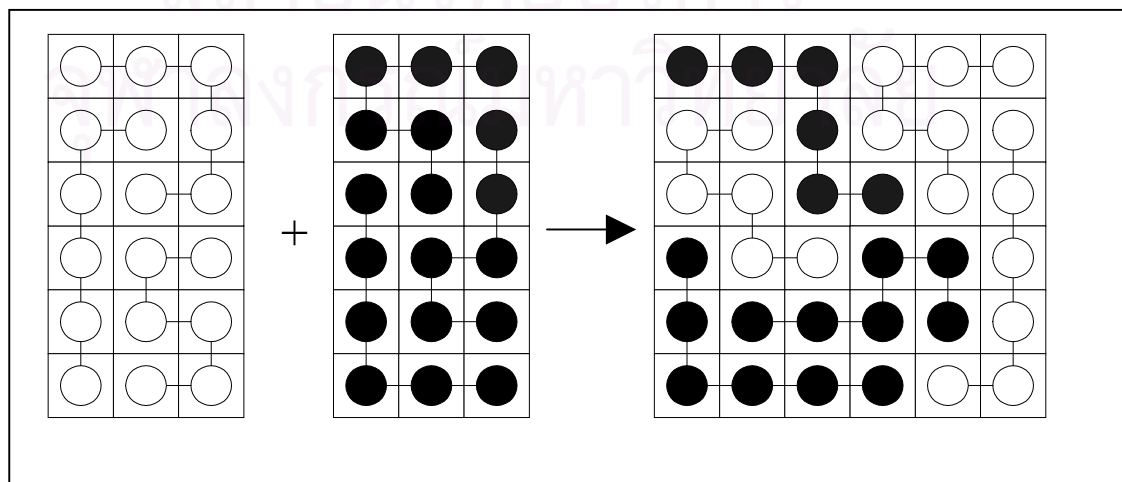


Figure 2.7: A schematic illustration of an example of a possible arrangement in a polymer chain, each contain six segments of molecules.

In 1930s Fowler and Rushbrooke (1937) introduced the concept of a regular arrangement of rigid lattice, whose sites are occupied by a polymer segment and a solvent molecule. This is considered to be a fundamental of following theories. A couple of years later Flory and Huggins [Flory 1941, 1942; Huggins 1941, 1942] suggested the entropy equation for the athermal mixing of monomer and chain molecule liquid. This then has been extended to the polymer-polymer mixture, and experimented. The entropy equation, which was derived is

$$\Delta S_M/k = -[(\psi_1/r_1) \ln \psi_1 + (\psi_2/r_2) \ln \psi_2]\psi_0 \quad (2.15)$$

where ψ_i is the segment fraction polymer i

ψ_0 is total number of segment

r_i is the number of segment per chain molecules of polymer i

k is the boltzman constant (1.38×10^{-23} J/K)

Note that there are several assumptions for this equation, e.g., the molecular weights of polymers are much higher than the solvent, polymer molecules comprise uniform flexible segments, which can be put into the lattice. By substitution ψ_i , r_i in Equation 2.4 with the volume fraction, ϕ_i , the general equation can be obtained.

$$\Delta S_M/k = -(n_1 \ln \phi_1 + n_2 \ln \phi_2) \quad (2.16)$$

where n_i is number of molecules of component i

To calculate the Gibbs free energy for polymer-polymer system, the enthalpy of mixing which shows the interaction between the adjacent molecules should be known. From the Van Laar expression the enthalpy of mixing can be written [Olabisi *et al.* 1979] as:

$$\Delta H_M/kT = \psi_1\psi_2\chi_{12}\psi_0 \quad (2.17)$$

where χ_{12} is Flory-Huggins interaction parameter (dimensionless). The χ_{12} is negative in exothermic mixing, while the χ_{12} is positive in endothermic mixing.

The Gibbs free energy is then written as

$$\Delta G_M = kT[(\psi_1/r_1) \ln \psi_1 + (\psi_2/r_2) \ln \psi_2]\psi_0 + kT\psi_1\psi_2\chi_{12}\psi_0 \quad (2.18)$$

Considering the Flory-Huggins theory above, it still possesses several limitations in describing polymer blends. For example, it neglects to take into account the free volume. As seen in Figure 2.7, all lattice sites are occupied by molecules and that makes it impossible to describe the volume change upon mixing. Furthermore, the F-H theory cannot explain the shape of phase diagram, the temperature and the composition dependence of the interaction parameter. From Equation 2.18, since the entropic contribution to free energy generally is marginal, and if χ_{12} becomes negative or the system is exothermic, the system will be miscible in all temperature range. This clearly shows that the Flory-Huggins theory fails to explain the LCST behaviour. In addition, the original interaction parameter χ_{12} was supposed to be independent of concentration, temperature, and molecular weight. However, many later works have found that the F-H interaction parameter in fact depends on temperature, composition and pressure. Tompa [1956] has taken into account the effect of composition dependence and suggested the extensive expression of F-H interaction parameter as,

$$\chi = \chi_1 + \chi_2\psi + \chi_3\psi^2 + \dots \quad (2.19)$$

Koningsveld [Olabisi *et al.* 1979] furthermore introduced the substitution of an empirical term g for χ . The expression of g relation can be written as,

$$g = \sum_{k=0}^n g_k \psi^k \quad k = 0, 1, 2, 3, \dots, n \quad (2.20)$$

where any coefficient g can be written as a function of temperature:

$$g_k = g_{k,1} + g_{k,2}/T + g_{k,3}T + g_{k,4}\ln T \quad (2.21)$$

Though a lot of modification to the Flory-Huggins theory has been performed, such modified theory still fails to explain the effect of chain flexibility to miscibility, as well as the effect of molecular structure, for example, linear, star, graft or comb polymers.

2.3.3 The Flory Equation of State Approach

From many shortcomings of the well-known Flory-Huggins theory, around 1950s Prigogine *et al.* [1959] applied a configuration partition function based on the Hirsch-felder-Eyring partition function [Eyring *et al.* 1937] to a lattice model theory and then solved the problem of neglecting free volume in the Flory-Huggins theory. Following the formalism of Prigogine, Flory and co-workers [Flory 1965, Eichinger and Flory 1968] replaced the generalised Lennard-Jone potential by a van der Waals type potential in the partition function. They considered the thermodynamic properties of mixture from the interaction between each pure component. The corresponding equation of state can be written as:

$$\frac{\tilde{P}\tilde{V}}{\tilde{T}} = \frac{\tilde{V}^{1/3}}{\tilde{V}^{1/3} - 1} - \frac{1}{\tilde{V}\tilde{T}} \quad (2.22)$$

where \tilde{P} , \tilde{V} , \tilde{T} are the reduced pressure, volume and temperature respectively. These reduced values are defined as:

$$\tilde{P} = \frac{P}{P^*} \quad (2.23)$$

$$\tilde{V} = \frac{V}{V^*}$$

$$\tilde{T} = \frac{T}{T^*}$$

where P^*, V^*, T^* are the characteristic pressure, volume and temperature respectively.

Those three reduced properties apparently are difficult to measure directly. So let us first consider three measurable fundamental coefficients, namely the thermal expansion coefficient α_T , the thermal pressure coefficient γ , and the compressibility κ , which can be written in reduced expressions as:

$$\alpha_T = \frac{1}{V} \left(\frac{\partial V}{\partial T} \right)_P = \left(\frac{\tilde{T}}{T\tilde{V}} \right) \left(\frac{\partial \tilde{V}}{\partial \tilde{T}} \right)_{\tilde{P}} \quad (2.24)$$

$$\gamma = \left(\frac{\partial P}{\partial T} \right)_V = \left(\frac{\tilde{T}P}{T\tilde{P}} \right) \left(\frac{\partial \tilde{P}}{\partial \tilde{T}} \right)_{\tilde{V}} \quad (2.25)$$

$$\kappa = \frac{\alpha_T}{\gamma} = -\frac{1}{V} \left(\frac{\partial V}{\partial P} \right)_T = - \left(\frac{\tilde{P}}{P\tilde{V}} \right) \left(\frac{\partial \tilde{V}}{\partial \tilde{P}} \right)_{\tilde{T}} \quad (2.26)$$

In the limit of pressure going to zero, the equation of state can be reduced to the simplest form

$$\frac{(\tilde{V}^{1/3} - 1)}{\tilde{V}^{4/3}} = \tilde{T} \quad (2.27)$$

The thermal coefficient is therefore can be written via temperature and the reduced volume as:

$$\alpha_T T = \frac{3(\tilde{V}^{1/3} - 1)}{1 - 3(\tilde{V}^{1/3} - 1)} \quad (2.28)$$

The thermal pressure coefficient is similarly obtained as follows,

$$\gamma = \frac{P^*}{T\tilde{V}^2} \quad (2.29)$$

Considering a binary system and by making an assumption that the characteristic volumes of both components are equal, let them be where V^* :

$$V_1^* = V_2^* = V^* \quad (2.30)$$

The enthalpy of mixing and the entropy of mixing can be expressed via the following forms [Flory 1965, Olabisi *et al.* 1979]:

$$\Delta H_M = \bar{r}NV^* \left[\psi_1 P_1^* \left(\frac{1}{\tilde{V}_1} - \frac{1}{\tilde{V}} \right) + \psi_2 P_2^* \left(\frac{1}{\tilde{V}_2} - \frac{1}{\tilde{V}} \right) + \frac{\psi_1 \psi_2 X_{12}}{\tilde{V}} \right] \quad (2.31)$$

$$\begin{aligned} T\Delta S_M = & -RT \left[\frac{\psi_1}{r_1} \ln(\psi_1) + \frac{\psi_2}{r_2} \ln(\psi_2) \right] \\ & - 3\bar{r}NV^* \left[\psi_1 P_1^* \tilde{T}_1 \ln \left(\frac{\tilde{V}_1^{1/3} - 1}{\tilde{V}^{1/3} - 1} \right) - \psi_2 P_2^* \tilde{T}_2 \ln \left(\frac{\tilde{V}_2^{1/3} - 1}{\tilde{V}^{1/3} - 1} \right) \right] \end{aligned} \quad (2.32)$$

where N is the total number of molecules in the system

n_i is the number of molecule of component i in the system

\bar{r} is the average number of segments:

$$\bar{r} = \frac{r_1 n_1 + r_2 n_2}{N} = \frac{1}{\left(\frac{\psi_1}{r_1} + \frac{\psi_2}{r_2} \right)} \quad (2.33)$$

S_i is the number of intermolecular contact site of component i

S is the total contact area of the system

$$S = \psi_1 S_1 + \psi_2 S_2 \quad (2.34)$$

ϑ_i is the site fraction of component i:

$$\vartheta_i = \frac{S_2 r_2 n_2}{(S_1 r_1 n_1 + S_2 r_2 n_2)} = \frac{S_2 r_2 n_2}{S \bar{r} N} = \frac{S_2}{S} \psi_2 \quad (2.35)$$

and X_{12} is the exchange energy parameter for unlike interaction, which can be defined as

$$X_{ij} = S_i \Delta \eta_{ij} / 2(V_i^*)^2 \quad (2.36)$$

where η_{ij} is intermolecular energy. From the Berthelot relationship [Rowlinson 1959]

$$\eta_{ij} = (\eta_{ii} \eta_{jj})^{1/2} \quad (2.37)$$

For the homo-polar components, whose interaction are dominated by the intermolecular dispersion energy, the intermolecular energy can be written as [Flory 1965]:

$$\Delta \eta_{ij} = (\eta_{ii}^{1/2} - \eta_{jj}^{1/2})^2 \quad (2.38)$$

$$= \eta_{ii} + \eta_{jj} - 2\eta_{ij} \quad (2.39)$$

The free energy from this theory, however, always shows the deviation from the experimental data, which is believed to have come from the underestimation of the entropic term. An empirical entropic parameter therefore has been added in order to provide the better fit to experiment. The new entropy of mixing equation can be written as [Olabisi *et al.* 1979]:

$$\begin{aligned}
T\Delta S_M = & -RT \left[\frac{\Psi_1}{r_1} \ln(\psi_1) + \frac{\Psi_2}{r_2} \ln(\psi_2) \right] - \bar{r}NV^* \psi_1 \vartheta_2 TQ_{12} \\
& - 3\bar{r}NV^* \left[\psi_1 P_1^* \tilde{T}_1 \ln \left(\frac{\tilde{V}_1^{1/3} - 1}{\tilde{V}^{1/3} - 1} \right) - \psi_2 P_2^* \tilde{T}_2 \ln \left(\frac{\tilde{V}_2^{1/3} - 1}{\tilde{V}^{1/3} - 1} \right) \right] \quad (2.40)
\end{aligned}$$

where Q_{12} is the non-combinatorial entropic correction

By using the alternative ways of calculating the characteristic properties [Walsh *et al.* 1985], one can obtain the pressure, P^* , and temperature, T^* , from

$$P^* = \phi_1 P_1^* + \phi_2 P_2^* - \phi_1 \vartheta_2 X_{12} \quad (2.41)$$

The chemical potential of component 1 is given by [Chai *et al.* 1983; Rostami *et al.* 1984]

$$\Delta\mu_1 = \left. \frac{\partial \Delta G_M}{\partial \phi_1} \right|_{T, \tilde{V}, \phi_2} \quad (2.42)$$

$$\begin{aligned}
& = RT \left[\ln \phi_1 + \left(\frac{r_2 - r_1}{r_2} \right) \phi_2 \right] \\
& \quad + P_1^* V_1^* \left[3\tilde{T}_1 \ln \left(\frac{\tilde{V}_1^{1/3} - 1}{\tilde{V}^{1/3} - 1} \right) + \tilde{V}_1^{-1} - \tilde{V}^{-1} + \tilde{P}_1 (\tilde{V} - \tilde{V}_1) \right] \\
& \quad + (X_{12} - T Q_{12} \tilde{V}) \left(\frac{V_1^* \vartheta_2^2}{\tilde{V}} \right) \quad (2.43)
\end{aligned}$$

Likewise, the chemical potential of component 2 can be expressed as:

$$\Delta\mu_2 = \left. \frac{\partial \Delta G_M}{\partial \phi_2} \right|_{T, \tilde{V}, \phi_1} \quad (2.44)$$

$$= RT \left[\ln \phi_2 + \left(\frac{r_1 - r_2}{r_1} \right) \phi_1 \right]$$

$$\begin{aligned}
& + P_2^* V_1^* \frac{r_2}{r_1} [3\tilde{T}_2 \ln \left(\frac{\tilde{V}_2^{1/3} - 1}{\tilde{V}^{1/3} - 1} \right) + \tilde{V}_2^{-1} - \tilde{V}^{-1} + \tilde{P}_2 (\tilde{V} - \tilde{V}_2)] \\
& + (X_{12} - T Q_{12} \tilde{V}) \left(\frac{V_1^* \vartheta_2^2 S_2 r_2}{\tilde{V} S_1 r_1} \right) \quad (2.45)
\end{aligned}$$

Using Equations 2.34 and 2.36 and the binodal condition (i.e. Equation 2.4), the binodal curve then can be calculated. Furthermore from the condition of spinodal, Equation 2.5, by differentiating Equation 2.34 with the volume fraction of component 2, the equation for the spinodal curve can be obtained:

$$\begin{aligned}
& \frac{1}{\phi_1} + \left(1 - \frac{T_1}{r_2}\right) - \left(\frac{P_1^* V_1^* D}{RT_1^* (\tilde{V} - \tilde{V}^{2/3})} \right) + \left(\frac{P_1^* V_1^* D}{RT} \right) \left(\frac{1}{\tilde{V}^2} + \tilde{P}_1 \right) \\
& + \left(\frac{V_1^* X_{12}}{RT} \right) \left(\frac{2\vartheta_1 \vartheta_2^2}{\tilde{V} \phi_1 \phi_2} - \frac{\vartheta_2^2 D}{\tilde{V}^2} \right) - \frac{2V_1^* Q_{12} \vartheta_1 \vartheta_2^2}{R \phi_1 \phi_2} = 0 \quad (2.46)
\end{aligned}$$

Mc Master [1973] used the Flory equation of state to calculate the spinodal and binodal curves of hypothetical polymer mixtures. The effect of chain length, thermal expansion coefficient, thermal pressure coefficient, exchange energy parameter and polydispersity were investigated. The result demonstrates that such theory can offer the basic idea of what will happen if those parameters have been changed, i.e., the miscibility regime will decrease if $(\alpha_1 - \alpha_2)$ or $(\gamma_1 - \gamma_2)$ increase. Additionally the theory can be used to predict both the LCST and the UCST behaviours individually or simultaneously. He also suggested that the effect of pressure should be taken into consideration at any nonzero pressure.

The validation of Flory equation of state in real systems has been proved by several scientists, for example, poly(caprolactone) and poly(vinyl chloride) by Olabisi

[1975], poly(methyl methacrylate) with chlorinated polyethylene and poly(butyl acrylate) with chlorinated polyethylene by Chai *et al.*[1983], ethylene-vinyl acetate copolymers with chlorinated polyethylene by Rostami *et al.* [1984]. They demonstrate that the equation of state theory of Flory and co-worker can be used to predict the LCST spinodal and binodal curve of high molecular weight polymer mixtures while in some cases, the adjustments of the non-combinatorial entropic correction (Q_{12}) and the interaction parameter (X_{12}) are required. However, it should be noted that the Flory equation of state still neglects the effect of free volume. This problem later was solved by Simha *et al.* [1969] and was further elaborated by other researchers [Lacombe *et al.* 1976; Sanchez *et al.* 1976; Kleintjens 1983; Lablans-Vinck *et al.* 1985].

2.3.4 Other Thermodynamic Approaches

2.3.4.1 Cell-hole model

It is apparent that one of the major flaws of the Flory equation of state is the neglect of the free volume. In the late 1960 Simha and Somcynsky [1969] introduced a set of couple equations, which provides the relationship between free volume and pressure and temperature. This model however was too sophisticated and sensitive to offer the accuracy of each parameters, especially P^* [Utracki 1989].

2.3.4.2 Sanchez and Lacombe's Equation of State

Sanchez and Lacombe [1976] introduced the vacant lattice sites into the lattice model and obtained the reduced equation of state as:

$$\frac{\tilde{P}\tilde{V}}{\tilde{T}} = \left(\frac{1}{r} - 1\right) + \tilde{V} \ln\left(\frac{\tilde{V}}{1 - \tilde{V}}\right) - \frac{1}{\tilde{V}\tilde{T}} \quad (2.47)$$

All general reduced properties are similar to the Flory equation of state except the reduced volume, which contains the vacant site N_0 .

This model can successfully describe the shape of phase diagram, viz., UCST, LCST [Sanchez *et al.* 1978] and the effect of pressure and shear on cloud point curve [An *et al.* 1998]. Nonetheless, this model is still not able to describe polymer melt at a wide range of pressure [Zoller 1980]. Furthermore, the effect of polymer's structure somehow cannot be explained by this model.

2.3.4.3 Polymer Reference Interaction Site Model

This is the first theory, which is successful in describing the effect of structure of polymer. It suggests that each polymer structure has a unique structure factor that, in principle, can be calculated [Sanchez *et al.* 2000]. The result applied to PVC/PMMA blend shows a good agreement with the experimental data [Honeycutt 1994]. However, it should be noted that using different routes to the equation of state can yield different results, due to the problem of thermodynamic consistency [Sanchez *et al.* 2000].

2.3.4.4 Lattice Cluster Model

Recently Dudowicz and Freed [1998] modified the Flory-Huggins theory by including the effect arising from packing and induced local correlations. They added the entropic contribution to the F-H interaction parameter χ_{ij} as well. This model can be used to investigate the effects of polymer structure on miscibility. The influence of stiffness, monomer molecular structure, and energetic asymmetry on the miscibility recently has been studied on polyolefin blends using this model [Freed *et al.* 1998]. This theory furthermore has been extended to cover the characteristics of copolymer blend [Freed *et al.* 2000].

2.4 The Solubility Parameter Mixing Approach

To be able to predict the miscibility of blend has somehow interested a number of scientists so far. Paul and Barlow [1979], for example, predicted a polymer - polymer miscibility from the heat of mixing obtained from an adiabatic calorimeter. This successful experiment has spurred other researchers later to concentrate on ΔH_M . However such a huge step of the polymer-polymer miscibility study is still an elaborate work since experimental work is necessary [Woo *et al.* 1985; Ellis 1989, Shah *et al.* 1986]. It is therefore rather useful if the enthalpy of mixing can be evaluated without any physical measurement, one way to achieve this is by utilising the solubility parameter.

The solubility parameter was first introduced for the characterisation of strength of interaction in simple liquids by Hildebrand [1964]. It was further developed by Bohn [1973] in order to use with polymer system. The parameter depends on the cohesion of the material or the strength of attraction between the molecules making up the materials and can be defined as [Olabisi 1979]:

$$\delta \equiv \sqrt{\frac{\Delta E^v}{V}} \quad (2.48)$$

where δ is solubility parameter, ΔE^v is energy of vaporisation and V is volume of the systems.

To obtain the solubility parameter from those values is somewhat difficult, hence by utilisation the so-called group contribution method based on the summation of the specific values of each structural group obtained by regression analysis [Olabisi 1979], the solubility parameter is rather easy to be evaluated. The basic thermodynamic values can be written in the simplest form of solubility parameter as [Olabisi 1979]:

$$\frac{\Delta H_M}{V} = (\delta_1 - \delta_2)^2 \phi_1 \phi_2$$

(2.49)

$$-\frac{T\Delta S_M}{V} = kT \left(\frac{n_1}{V} \ln \phi_1 + \frac{n_2}{V} \ln \phi_2 \right)$$

(2.50)

Gibbs free energy of mixing can be obtained via the summation of Equations 2.49 and 2.50. The knowledge of phase behaviour can be received with the help of the spinodal and binodal equations (Eqs. 2.5, 2.6).

2.5 Conclusions

In summary, the principle of thermodynamics has been described in Section 2.1. The general Gibbs free energy of mixing equation is easily capable of being used to estimate the miscibility and phase separation curve with respect to ordinary thermodynamic functions. Details of each function have been dealt with in Section 2.3. In Section 2.2, the mechanism of phase separation has been illustrated. It appears that phase separation in polymer blends can take place via 2 routes, viz., spinodal decomposition and nucleation & growth, depending on the variation of their free energy curve. Spinodal decomposition takes place spontaneously once a blend is quenched into a thermodynamically unstable state, while in the case of nucleation and growth once a blend is quenched into metastable state, it requires some sort of perturbation such as impurity. The line that separates the metastable state and stable state is called the binodal line, while the spinodal line divides the metastable state and unstable state. In Section 2.3, applications of statistical thermodynamics on polymer system have been presented. The basic partition function was introduced. Two main theories namely Flory-Huggins theory and the Flory equation of state as well as other recent developed theories have been shown. The Flory-Huggins theory is very general and can be extended to several other theories. It appears that this theory is still used nowadays, albeit a number of flaws. One of the most successful theories, which takes

into account the interaction of each pure component, is the Flory equation of state. Other thermodynamic theories have been developed from those two theories based on different corrections leading to the ability to better predict miscibility. All possible effects on miscibility, for instance, pressure, shear, composition, stiffness, stereoregularity, etc. have been taken into consideration. Recent developed theories are not only able to predict just homopolymer system, yet they can be used for copolymer blend as well.



สถาบันวิทยบริการ
จุฬาลงกรณ์มหาวิทยาลัย

Chapter III

Kinetics of Phase Separation in Polymer Blends

Kinetics of phase separation has attracted great interest recently, especially for anyone who desires to control the morphology by playing with temperature or pressure variation. As shown in the previous chapter, a miscible polymer blend can undergo nucleation and growth or spinodal decomposition depending on whether it is brought into metastable state [Elicabe *et al.* 1997, 1998; Muller *et al.* 1997; Mazumder *et al.* 1999] or into unstable state [Chen *et al.* 1997; Ribbe *et al.* 1997; Mecke *et al.* 1997; Takeno *et al.* 1998]. Each mechanism has a unique concentration and morphology evolution. The rate of phase separation and the resulting morphology depend on many parameters such as annealing time and temperature, concentration, physical properties of the blend constituents. Regarding the spinodal decomposition mechanism, many works so far [Hashimoto *et al.* 1991; Takenaka *et al.* 1992; Cummings *et al.* 1992; Hashimoto 1993; Edel 1995] reported that the growth of concentration fluctuation and the structure formation can be classified into at least 3 stages: early stage, intermediate stage and late stage.

As shown in Figure 3.1a, only the amplitude of the concentration fluctuation grows with time in the early stage of spinodal decomposition, while the wavelength remains constant. The concentration distribution is described well by the linearised theory [de Gennes 1980; Binder 1983]. During the intermediate stage both the wavelength and amplitude of concentration fluctuation grow with time while the nonlinear effect becomes more essential. In the late stage, the local concentration reaches equilibrium, only the wavelength change then can be observed. The scaling analysis has been recently developed for this stage.

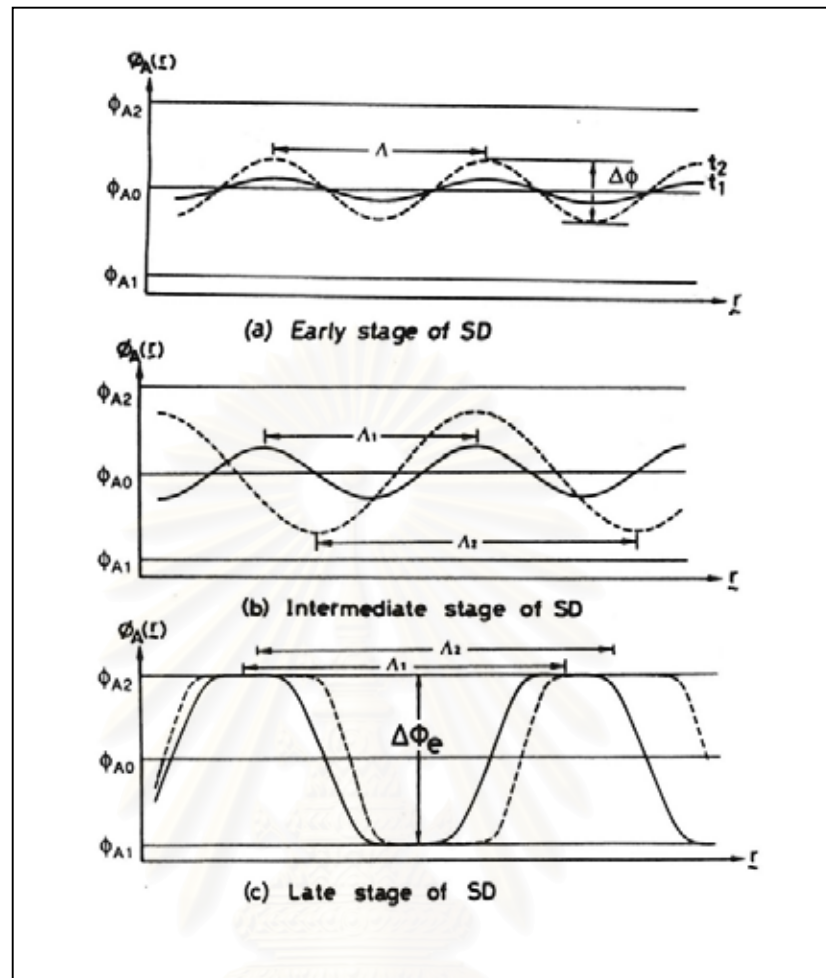


Figure 3.1: Schematic diagrams show the concentration fluctuation in the early (a), intermediate (b) and late stage of spinodal decomposition(c) [Hashimoto 1993]. $\Delta\phi = \phi_{A1} - \phi_{A0}$ is the amplitude of fluctuation, Λ is the wavelength of concentration fluctuation.

In this chapter the fundamental theories of phase separation via both nucleation and growth, and spinodal decomposition are discussed. The basic concept of nucleation and growth theory is first reviewed, starting from the classical nucleation theory, followed by the density function theory and the diffuse interface theory. Spinodal decomposition is discussed next: it begins with the Cahn-Hilliard linearised theory, followed by its limitation and related theories such as Cahn-Hilliard-Cook theory, Langer-Barlon-Miller's equation, Cahn-Hilliard-deGennes theory, etc. In the final part of this section the scaling analysis regarding the late stage of spinodal decomposition is reviewed.

3.1 Nucleation & Growth

As mentioned in the previous chapter, nucleation and growth (N&G) phenomenon always takes place in the metastable region by having some sort of perturbation such as an impurity as a driving force. The process begins with the formation of heterogeneous fluctuations which for the sake of simplicity such fluctuations are considered as spherical particles. This thesis reviews three well-known theories, which deal with the kinetics of formation of those particles. The derivation of the classical nucleation theory is shown first, followed by other modified theories based on it.

3.1.1 Classical Nucleation Theory

This theory is based on the droplet approximation introduced by Gibbs [1932] in order to study the stability of phases. It is assumed that the spherical particles display bulk properties right up to the dividing surface. As a consequence of which, the work of formation of a fluctuation can be written as:

$$W = -\frac{4\pi r_d^3}{3} \cdot \Delta g + 4\pi r_d^2 \gamma_s \quad (3.1)$$

where r_d is the radius of the cluster, Δg is the volumetric Gibbs free energy difference between the new and parent phases, and γ_s is the surface tension. The work of formation shows a maximum at the respective critical size

$$r_d^* = 2\gamma_s / \Delta g \quad (3.2)$$

while the maximum work is

$$W^* = \frac{16\pi}{3} \cdot \frac{\gamma_s^3}{\Delta g^2} \quad (3.3)$$

Concerning the master equation for describing particle distribution and regarding only single molecule attachment and detachment, that equation can be expressed as [Granasy 1997]:

$$dN_1/dt = a_2^+ N_2 - a_1^- N_1 \quad (3.4)$$

$$\text{and } dN_i/dt = a_{i+1}^+ N_{i+1} - a_{i-1}^- N_{i-1} - (a_{i+1}^+ - a_{i-1}^-) N_i, \text{ for } 1 < i < \infty, \quad (3.5)$$

where the coefficients $a_{i+1}^+ = O_{i+1} \Gamma \exp[-(W_{i+1}-W_i)/2kT]$ and $a_{i-1}^- = O_{i-1} \Gamma \exp[-(W_{i-1}-W_i)/2kT]$ are the attachment and detachment rates of molecules, N_i is the number of the i -mers in the system, O_{i+1} is an adjustable parameter, and the prefactor Γ is related to the molecular mobility.

The initial condition can be obtained from the fact that the distribution shows a sharp maximum at the monomer or the beginning,

$$N_i(0) = N \exp[-W_i(T_0)/kT_0] \quad (3.6)$$

where N is the total number of molecules and $T_0 > T_{eq}$, T_{eq} is the equilibrium temperature.

The number of large cluster is continuously increasing as the nucleation and growth phenomenon is proceeding until it reaches the steady state condition in the vicinity of the critical size (i^*). The nucleation rate J^* thus tends to be constant and can be expressed as:

$$J^* = a_i^+ N_i^* - a_{i+1}^- N_{i+1}^* \quad (3.7)$$

Equation 3.7 was then simplified and simulated by Kelton *et al.* [1983]. The simple form of the steady state nucleation rate equation is:

$$J^* = J_0 \exp(-W^*/kT) \quad (3.8)$$

where $J_0 \propto \Gamma$.

This theory apparently provides a qualitative picture of nucleation processes [Elicabe *et al.* 1997, 1998]; however, it frequently fails in reproducing the correct magnitudes. A number of works have shown that this theory always underestimates the drop count [Strey *et al.* 1986; Hung *et al.* 1989, 1990]. This is related to several severe assumptions being made during the derivation of the nucleation rate equation; for example, they took bulk physical properties as the representatives of properties of few molecules in nuclei, the real interface is not as sharp as they assumed, etc.

3.1.2 Density Function Theories

Numerous following theories attempt to tackle those mistakes in the classical nucleation theory. All approaches in this group begin by concentrating on the correction of work of formation (W). They consider that work as a function of order parameter instead of the bulk difference. The first important approach is the van der Waals/Cahn-Hilliard theory. They estimated the work of formation using Taylor expansion approximation and the Helmholtz free energy. It seems that this theory provides a better result. Nevertheless they still neglect molecular interactions [Adams *et al.* 1984].

Oxtoby and co workers [Oxtoby *et al.* 1988; Nyquist *et al.* 1995; Talanquer *et al.* 1995] also consider free energy as a function of order parameter, but recently they included the effect of molecular interactions in the work of formation as well. The

consequent result shows much more improvement [Adams *et al.* 1984]. Nonetheless, this theory still neglects the fluctuation such as the capillary waves on the surface of droplets. Furthermore it cannot describe the system which has complex structure.

3.1.3 Diffuse Interface Theory

This is the simplest form of the classical nucleation theory. Instead of including several predicted parameters, it just replaces approximate parameters with as many measurable values as possible. Several experimental data are employed such as an interfacial free energy (surface tension), the characteristic length, etc. This theory apparently shows an excellent agreement with experiments [Granasy 1996].

3.2 Spinodal Decomposition

Several theories have been developed in order to explain spinodal decomposition correctly. The first well-known theory is the Cahn-Hilliard linearised theory. This is rather general and considered to be a fundamental theory of later developed theories like the role that the Flory-Huggins theory does to the thermodynamic polymer field. Other important theories are Cahn-Hilliard-Cook theory, Flory-Huggins-de Gennes's theory, the scaling analysis, etc.

3.2.1 The Cahn-Hilliard Linearised Theory

Basically the linearised theory of Cahn and Hilliard is based on deriving and solving a general diffusion equation. They firstly neglected the effect of material flow and estimated the total free energy of an incompressible and isotropic binary system as a function of order parameter, which herein refers to the composition using Taylor's expansion and neglecting the third and higher-order terms. The generalised

free energy equation over the total volume V of the system can be written [Cahn *et al.* 1959; Hilliard 1970] as:

$$F = \int_V [f(c) + K(\nabla c)^2] dV \quad (3.9)$$

where $f(c)$ is the free energy per unit volume of a homogeneous system of a concentration c and K is a gradient energy which is defined as:

$$K = -\frac{\partial^2 f}{\partial c \partial (\nabla^2 c)} + \left(\frac{1}{2}\right) \frac{\partial^2 f}{(\partial |\nabla c|)^2} \quad (3.10)$$

They related thermodynamics to the diffusion equation by introducing the chemical potential $\mu(\mathbf{r},t)$ as a driving force for diffusion of the system once developing spinodal decomposition into the general diffusion equation. It is assumed that there is no reaction and free movement, the inter-diffusion flux $J(\mathbf{r},t)$ can be expressed as:

$$J(\mathbf{r},t) = -M \nabla \mu(\mathbf{r},t) \quad (3.11)$$

where M is the diffusion mobility and for the sake of simplicity, it was assumed constant.

The chemical potential $\mu(\mathbf{r},t)$ is defined as

$$\mu(\mathbf{r},t) = \frac{\partial F}{\partial c} \quad (3.12)$$

Note that the bold letter in each equation is related to vector form. Inserting the inter-diffusion flux from Equation 3.4 into an equation of motion, it finally yields

$$\frac{\partial c}{\partial t} = -\nabla J(\mathbf{r},t)$$

$$= M\nabla^2\mu(\mathbf{r},t) \quad (3.13)$$

This equation can be solved if the chemical potential $\mu(\mathbf{r},t)$ is known, they again estimated it using Taylor expansion, and neglected the third and higher-order term [Cahn *et al.* 1958]. The Fourier transform was applied to Equation 3.6 in order to make it easier to solve. However, unfortunately, the Fourier amplitudes cannot be measured. Rindman and Hilliard [1967] then showed that X-ray intensity measurements are sufficient for testing the theory. The structure function $S(\mathbf{q},t)$, which can be related to scattering experiments is defined as:

$$S(\mathbf{q},t) = \langle |c(\mathbf{q},t)|^2 \rangle \quad (3.14)$$

where $c(\mathbf{q},t)$ is the Fourier transform of $c(\mathbf{r},t)$ which is defined as:

$$c(\mathbf{q},t) = \frac{1}{(2\pi)^{3/2}} \int c(\mathbf{r},t) e^{-i\mathbf{q}\cdot\mathbf{r}} d\mathbf{r} \quad (3.15)$$

where $\mathbf{q} = \mathbf{q}_f - \mathbf{q}_0$, \mathbf{q}_f being a vector of magnitude $(2n\pi)/\lambda$ that points from the center of each particle to the point where scattered light is detected and \mathbf{q}_0 a vector of magnitude $(2n\pi)/\lambda$ that points in the direction of the incident light. The scattering wave vector q is the magnitude of \mathbf{q} :

$$q = \frac{4n\pi}{\lambda} \sin\left(\frac{\theta}{2}\right) \quad (3.16)$$

where λ is the wavelength of the radiation which is used to study the concentration fluctuation, θ is the scattering angle and n is the refractive index of the blend.

With those assumptions, eventually the modified equation of motion for the structure function can be written as:

$$\frac{\partial S(\mathbf{q},t)}{\partial t} = -2Mq^2 \left[\left(\frac{\partial^2 f}{\partial c^2} \right)_{c_0} + 2Kq^2 \right] S(\mathbf{q},t) \quad (3.17)$$

where $\left(\frac{\partial^2 f}{\partial c^2}\right)_{c_0}$ is the second derivative of free energy at the average concentration c_0 .

The solution of Equation 3.17 is a generalised Cahn-Hilliard linearised equation, which can be written in an exponential function,

$$S(q, t) = S(q, 0) e^{2R(q)t} \quad (3.18)$$

where $R(q)$ is the q dependent growth rate of concentration fluctuations, given by,

$$R(q) = -q^2 M \left[\left(\frac{\partial^2 f}{\partial c^2}\right)_{c_0} + 2K q^2 \right] \quad (3.19)$$

Generally, the growth or decay with time depends on whether $R(q)$ is positive or negative. In metastable region, $R(q)$ is always negative; consequently concentration fluctuation always decays. On the other hand, in the unstable region where the blend undergoes spinodal decomposition, $R(q)$ is positive for q less than the critical value (q_c), indicating that the fluctuation grows with time. The critical value q_c can be expressed as,

$$q_c = \sqrt{-\frac{(\partial^2 f / \partial c^2)_{c_0}}{2K}} \quad (3.20)$$

Equation 3.19 has a maximum at

$$q_m = \frac{1}{2} \sqrt{-\frac{(\partial^2 f / \partial c^2)_{c_0}}{K}} \text{ or } \frac{q_c}{\sqrt{2}} \quad (3.21)$$

Inserting the maximum wave vector q_m into Equation 3.19, the highest relative growth rate $R(q_m)$ is:

$$R(q_m) = \frac{M}{8K} \left(\frac{\partial^2 f}{\partial c^2} \right)_{c_0}^2 \quad (3.22)$$

Apparent diffusion coefficient, D_{app} are defined as,

$$D_{app} = -M \left(\frac{\partial^2 f}{\partial c^2} \right)_{c_0} \quad (3.23)$$

or

$$D_{app} = \frac{2R(q_m)}{q_m^2} \quad (3.24)$$

Note that since M , $(\partial^2 f / \partial c^2)_{c_0}$ and K are assumed to be constant in the derivation of Eq 3.18, then q_c (Eq.3.20), q_m (Eq. 3.21), $R(q_m)$ (Eq. 3.22) and D_{app} (Eq. 3.23) will become constant as well. Concerning Eq. 3.19, a plot of $R(q)/q^2$ vs q^2 yields a straight line with a slope of $2MK$ and an intercept of D_{app} . Furthermore q_m and $R(q_m)$ also can be obtained by those slopes and intercepts as follows,

$$q_m = \sqrt{\frac{\text{intercept}}{-2\text{slope}}} \quad (3.25)$$

$$R(q_m) = \frac{(\text{intercept})^2}{-4\text{slope}} \quad (3.26)$$

3.2.2 Shortcomings of the Cahn-Hilliard Linearised Theory

The linearised theory has been accepted and utilised to describe a number of experiments so far [Snyder *et al.* 1983; Guo *et al.* 1990]; nonetheless, several recent experiments showed some discrepancies from the simple Cahn-Hilliard theory. For example, $R(q)/q^2$ does not decrease linearly with q^2 [Nojima *et al.* 1982; Sasaki *et al.* 1984; Perreault *et al.* 1995], q_m shift toward low q after spinodal decomposition has

taken place for a long time [Hashimoto *et al.* 1986; Tomlins *et al.* 1989; Izumitani *et al.* 1990], the calculated q_m and $R(q_m)$ deviate from the observed values [Hill *et al.* 1985; Sato *et al.* 1988; Onuki *et al.* 1989], etc. All these discrepancies have built up the clear picture that there are a number of severe assumptions during the derivation of the linearised theory.

i. Neglecting the effect of the lattice anisotropy of the solid

For a crystalline solid the interfacial free energy becomes isotropic at the critical point while generally the interfacial free energy between co-existing A-rich and B-rich phases depends on the orientation of the interface [Binder 1991].

ii. The composition independence of M , K and the second derivative of free energy

This assumption is again only valid near the critical point whereas in general it may be incorrect [Binder 1991].

iii. Neglecting the q -dependence of mobility M

de Gennes and co-workers [de Gennes 1980; Pincus 1981; Binder 1983] showed that the mobility term should be replaced by the wave vector dependent Onsager coefficient $\Lambda(q)$. This modification receives a support from some experiments [Fruitwala 1988; Higgins 1989a].

iv. Neglecting thermal fluctuation

Cook [1970] suggested that there always appears some small fluctuation even when the spinodal decomposition reaches equilibrium.

v. Neglecting all nonlinear terms

Langer [1973] pointed out that the way that Cahn and Hilliard neglected all nonlinear terms is acceptable at the beginning of fluctuation; however, as soon as the concentration fluctuation proceeds toward the equilibrium that assumption becomes invalid. This suggestion gained some supports from Binder [1983] and Snyder *et al.* [1985] who indicated that the nonlinear terms should be included.

v. Neglecting some slowly relaxation variables

Binder [1986] demonstrated that the linearised theory failed to describe phase separation near glass transition. Moreover some entanglements, which can cause relaxation during the beginning of phase separation, should be taken into account as well.

3.2.3 The Cahn-Hilliard-Cook Theory

In order to overcome the problem of thermal fluctuation, Cook [1970] introduced a term analogous to the well-known fluctuation force in the theory of Brownian motion to the diffusion equation. The modified equation of structure function then can be written as:

$$\frac{\partial S(q, t)}{\partial t} = -2Mq^2kT S_x^{-1}(q) [S(q, t) - S_x(q)] \quad (3.27)$$

where $S_x(q)$ is the structure function at the equilibrium representing the effect of thermal fluctuation which can be defined as:

$$S_x(q) = kT / \left[\left(\frac{\partial^2 f}{\partial c^2} \right)_{c_0} + 2Kq^2 \right] \quad (3.28)$$

The solution of Eq. 3.27 can be expressed as:

$$S(q,t) = S_x(q) + [S(q,0) - S_x(q)]e^{(2R(q)t)} \quad (3.29)$$

The relaxation growth rate $R(q)$ here is equivalent to the one from the linearised theory. This theory therefore still relies on the linear approximation of chemical potential. Consequently it is applicable at the very stage of phase separation only whereas at the later stage it still fails to explain phase separation behaviour. This theory was further probed by a number of scientists. Okada and Han (1986) showed that if the system is quenched very deep inside the spinodal regime, the effect of thermal fluctuation can become insignificant. Higgins *et al.* [1989b] later suggested that such an effect might be a system dependent criterion. Recently Jinnai *et al.* [1993], who explored the memory effect in a polymer blend, reported that this theory describes satisfactorily the early stage SD.

3.2.4 The Nonlinear Theory

After Cook [1970] introduced the theory taking into account the effect of thermal fluctuation, Langer and co-workers [1973, 1975] then presented another successful theory which includes all higher terms in the approximation of $\partial f / \partial c$. The modified equation of structure function can be written as:

$$\frac{\partial S(q,t)}{\partial t} = -2Mq^2 [A(t) + 2Kq^2] S(q,t) + 2Mq^2 kT \quad (3.30)$$

where $A(t)S(q,t)$ can be defined as

$$A(t)S(q,t) = \sum_2^{\infty} \frac{1}{(n-1)!} \left(\frac{\partial^n f}{\partial c^n} \right)_{c_0} S_n(q,t) \quad (3.31)$$

Unfortunately, this equation cannot be simply solved. As a consequence of this, it requires a transformation to a single point distribution function, which can be replaced by a sum of two Gaussian functions and eventually approximated by numerical calculation. In spite of the requirement of the elaborate solving, this theory is successful in describing the shift of q_m to smaller q as time goes on. Moreover, to date several works have shown that the higher order terms of composition fluctuations play a crucial role in the deviation from the linearised theory especially the curvature of $R(q)/q^2$ vs q^2 curve.

3.2.5 The Flory-Huggins-deGennes Theory

It is apparent that all aforementioned theories have one thing in common, i.e., they used Taylor's expansion to approximate free energy and df/dc . De Gennes and co-workers [de Gennes 1979, 1980; Pincus 1981; Binder 1983] later suggested that instead of using such an approximation they borrowed the concept of lattice model from Flory-Huggins theory to approximate free energy. An additional term arising from the effect of concentration gradient was inserted into the classical Flory-Huggins equation, the new free energy equation for a binary system therefore can be expressed as [de Gennes 1980]:

$$F_{\text{FHdG}}/kT = \frac{\phi}{N_A} \ln \phi + \frac{(1-\phi)}{N_B} \ln(1-\phi) + \chi \phi(1-\phi) + \kappa (\nabla \phi)^2 \quad (3.32)$$

where ϕ is the volume fraction of polymer A, N_A , N_B are the degree of polymerisation of A and B which are assumed to be equal, and κ is a measure of the interfacial energy, determined from the random phase approximation as,

$$\kappa = \frac{b^2}{36\phi(1-\phi)} \quad (3.33)$$

where b is the Kuhn statistical segment length and for simplicity, the average value is assumed for the two polymers.

In the case of both polymers having equivalent degree of polymerisation defined as N , the modified structure equation based on the C-H-C theory is then [Binder 1983],

$$\frac{\partial S(q, t)}{\partial t} = -2\Lambda(q)q^2 \left\{ \frac{1}{N\phi_0(1-\phi_0)} - 2\chi + 2\kappa q^2 \right\} S(q, t) + n_q(q, t) \quad (3.34)$$

where ϕ_0 is the average volume fraction of the system, $n_q(t)$ is the term analogous to the thermal fluctuation in Cook's theory, and $\Lambda(q)$ is an Onsager coefficient representing the capability of polymer chains to move. It should be noted that Equation 3.34 follows the linearised theory if the mobility parameter is constant and the thermal fluctuation is neglected.

De Gennes [1980] approximated $\Lambda(q)$ by using the reptation model and found that for the concentration fluctuation of the short wavelength ($qR_0 \gg 1$, R_0 is an end to end distance), such coefficient is approximated as:

$$\Lambda(q) \cong \phi_0(1-\phi_0)N_e D_1 (qb)^2 \quad (3.35)$$

where N_e is the number of monomers between entanglement points and D_1 is an adjustment factor. Equation 3.35 eventually yields $\Lambda(q) \propto q^2$. It should be noted that this is based on the assumption of a single relaxation time for a non-interacting chain in a melt, which is incorrect in reality. In contrast to de Gennes, Pincus [1981] suggested that $\Lambda(q) \propto q^{-2}$ instead of q^2 . Despite he still used the reptation model, he incorporated the influence of an external longitudinal force field. Consequently he obtained,

$$\Lambda(q) \cong \phi_0(1-\phi_0) \frac{2k_B T}{\zeta} \frac{1}{q^2 L^2} [1 - \exp(-q^2 R_g^2)] \quad (3.36)$$

where ζ is the friction coefficient of a monomer, L is the length of the tube which is defined as,

$$L \cong NN_e^{-1/2}b \quad (3.37)$$

and R_g is the radius of gyration, which is defined as

$$R_g^2 = \frac{R_0^2}{6} \quad (3.38)$$

Binder [1983] however derived a different kind of equation,

$$\Lambda(q) \cong \phi_0(1-\phi_0) \frac{4k_B T}{\zeta} \frac{1}{q^2 L^2} \left\{ 1 - \frac{1}{q^2 R_g^2} [1 - \exp(-q^2 R_g^2)] \right\} \quad (3.39)$$

Equation 3.39 is, however, less famous. It was pointed out later by Semenov that Binder used the wrong expression for the dynamic structure factor of a reptating polymer [Clarke 1994]. Experimental works by Schwahn *et al.* [1992,1995] reported that $\Lambda(q) \propto q^{-n}$ where n equals 2 for large q and decreases as q decreases.

The concern recently is not only the wavevector dependence of mobility, since in reality polymers possess different length and dynamic properties resulting in the difference of rate of inter-diffusion and the relaxation and growth. Therefore it is of interest whether the fast or the slow components of a binary blend control the rate. A theoretical approach by Brochard *et al.* [1983] and Binder [1983] suggested that the slower component would control the dynamics, and the general equation derived by Binder is:

$$\frac{1}{\Lambda(q)} = \frac{1}{\phi M_A(q)} + \frac{1}{(1-\phi) M_B(q)} \quad (3.40)$$

It should be noted that this equation is based on the assumption that the fluxes of two different polymers are equal and opposite across the rather sharp interface, and the motion is purely diffusive.

On the contrary, the other approach pointed out that the interface should not be absolutely sharp since a bulk can always flow across the interface. Kramer *et al.* [1984] and Sillescu [1984] concluded that the fast component is the one that controls the mutual diffusion.

$$\Lambda(q) = \phi(1-\phi)[\phi M_A(q) + (1-\phi)M_B(q)] \quad (3.41)$$

It appears that to date the final conclusion is still equivocal since there have been a number of works supporting either of them [Composto *et al.* 1988; Akcasu *et al.* 1995, 1997].

สถาบันวิทยบริการ
จุฬาลงกรณ์มหาวิทยาลัย

3.2.6 Viscoelastic Effects and Kinetics of Phase Separation

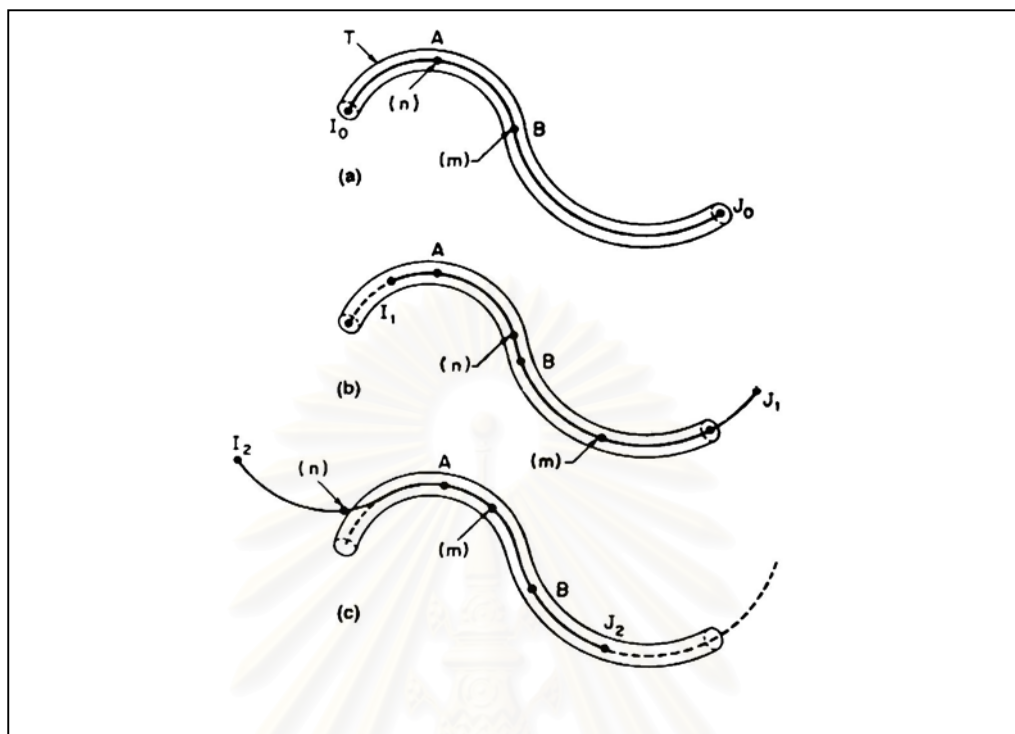


Figure 3.2: Free successive situations for a reptation chain: (a) the chain is trapped in its original tube; (b) the chain moves to the right and a certain portion ($I_0 I_1$) of the original tube disappears; (c) the chain moves to the left and a portion ($J_0 J_2$) of the original tube disappears [de Gennes 1979].

Considering the motion of long linear polymer chains, it is usually different from the short ones. This has been suggested that when the concentration and molecular weight are high enough, the effect of entanglement in polymer will play an important role [Doi 1996]. The theory, which successfully describes this phenomenon, was first introduced by de Gennes [1971] called the reptation or tube model. A polymer chain is assumed to be trapped and only move in a hypothetical tube while the tube itself can change with time. Once the concentration is high enough it seems that the neighbour chains turn to be obstacles and confine the chain movement. The chain is not allowed to cross over other chains but it is able to wriggle along between them. The chain will leave some part of the tube and create some new

parts as shown in Figure 3.2. The relaxation time τ for the chain to complete its motion through the original tube is written as [Doi *et al.* 1986]:

$$\tau = \frac{\zeta}{\pi^2 k_B T} \frac{b^4}{a^2} N^3 \quad (3.42)$$

where ζ is the friction coefficient of a monomer and a is the step length of the primitive chain which is of the order of $N_e^{1/2}b$.

A recent work by Clarke *et al.* [1997] showed that the effect of entanglement on phase separation for high molecular weight polymer systems could be described by introducing a transient elastic energy term into the Cahn-Hilliard equation. Two cases were considered: A-B entanglements, in which both components are mutually entangled, and A-A entanglements which are dominated by one component. By taking an assumption that mobility constant is independent of q and the rates associated with concentration fluctuation dynamics are much slower than the rheological rates, i.e., $R_T \ll R_{CO}, R_V$, the resultant scattering function may be written as,

$$\frac{S(q, t)}{S(q, 0)} \approx A_1 \exp\{-(R_V + R_{CO})t\} + (1 - A_1) \exp\left\{-\left(\frac{R_T R_V}{R_V + R_{CO}}\right)t\right\} \quad (3.43)$$

where $R_T = 2q^2 M \left[\frac{1}{N\phi_0(1-\phi_0)} - \chi + 2\kappa q^2 \right]$, $R_{CO} = 2C_0(q)Mq^2$, $R_V = 1/\tau$, and $A_1 = R_{CO}/(R_V + R_T)$. The magnitude of the effect of the elastic energy is determined by the form of the parameter $C_0(q)$, which for A-B entanglements is written in the form}

$$C_0(q) = \frac{36}{N_e^2 b^2 q^2} \quad (3.44)$$

where N_e is the number of monomers between entanglement points. For A-A type entanglements, the elastic energy arises due to swelling of the entanglement network, and

$$C_0(q) = \frac{3\phi_A}{N_e} \quad (3.45)$$

The magnitude of rate R_T is identical to the relaxation growth rate, $R(q)$ of the Cahn-Hilliard equation. It represents the thermodynamic mode, whereas the other two rates, namely R_{CO} and R_V give rise to additional viscoelastic modes. The summation of R_V and R_{CO} in the first term of Equation 3.41 is always positive whereas the product of R_T and R_V in the second term on the right hand side can be either positive or negative depending on R_T . Hence the first term represents a decaying mode, while the second one represents a growing mode. It should be noted that the aforementioned assumptions are valid for very highly entangled chains, whose length scale is greater than the distance between entanglements, i.e., $1/q > N_e b^2$.

3.2.7 The Scaling Theories

All aforementioned theories apparently have one thing in common: they neglect the nonlocality arising from the formation of the droplet, leading all of them fail to describe in the late stage of phase separation. Two main mechanisms so far have been suggested to describe the droplet growth namely the evaporation-condensation process, the diffusion-reaction process. Furukawa [1978] then followed the ideas of the diffusion-reaction process and introduced another form of structure function, details of which is reviewed later.

3.2.7.1 The Evaporation-Condensation Process

Lifshitz and Slyozov [1961] suggested that droplets cannot move but can grow by the diffusion of numerous tiny atoms from smaller droplets, just like tiny atoms evaporate from small droplets and condense into larger droplets. This is as the result of smaller droplets having a larger chemical potential due to the surface tension. They found that droplets grow according to the power law behaviour:

$$R(t) \sim q_m(t)^{-1} \propto t^{1/3} \quad (3.46)$$

where $R(t)$ is the radius of droplet.

3.2.7.2 The Diffusion-Reaction Process

Binder and Stauffer [1974] later suggested the other aspect of process, instead of considering the stagnant droplet they regarded droplets as free Brownian particles. Each droplet can travel freely until it meets another and once two droplets meet, they coalesce into one larger droplet. Likewise the evaporation-condensation process, the droplet growth rate follows the power law behaviour,

$$R(t) \propto t^{1/n} \quad (3.47)$$

Two regimes were distinguished and the factor n depends on which regime it belongs. First, at low temperature $T < T^*$, $n = d + 3$ where d is the spatial dimensionality. The second regime occurs for T near T^* and above, where the concentration difference between a typical fluctuation and its environment is rather small, and hence the factor n is approximately 2.

3.2.7.3 Furukawa's approach

The most striking theory in the past two decades for analysing the late stage of spinodal decomposition was proposed by Furukawa. He substituted the free energy equation previously obtained by Taylor's expansion method with the modified Landau-Ginzburg free energy incorporating with the ideas of the diffusion-reaction process. The free energy function can be written as [Furukawa 1978],

$$F(c(q,t)) = \frac{1}{2} \chi(q,t)^{-1} |c(q,t)|^2 \quad (3.48)$$

where $\chi(q,t)$ is the susceptibility of the system and can be written as [Furukawa 1985],

$$\chi(q,t)^{-1} = q_m(t)^d [\alpha' + \beta' (q/q_m(t))^{d+1}] \quad (3.49)$$

where d is dimension of the system

α' and β' are constants of the order unity.

As the result of this revision, the equation of motion for the structure function can be expressed as [Furukawa 1978]:

$$\frac{dS(q, t)}{dt} = 2Mq^2 [k_B T - \chi(q, t)^{-1} S(q, t)] \quad (3.50)$$

Furukawa [1985] proposed that the scaling solution of Equation 3.50 can be represented by the dimensionless scaling function $\tilde{S}(q/q_m(t))$ such that

$$S(q, t) = q_m(t)^{-d} \tilde{S}(X) \quad (3.51)$$

where $X = q/q_m(t)$, $\tilde{S}(X)$ is a universal scaling function which is independent of time and varies from zero to unity.

Several tests of the scaling structure function were carried out by both numerical simulations and experimental studies [Furusaka *et al.* 1985; Katano *et al.* 1984; Porod 1982]. It was observed that the scaling function is proportional to X^2 for wave vector less than $q_m(t)$, i.e., $X < 1$. While for $X > 1$, i.e., wave vectors greater than q_m , the scaling function was found to be proportional to whether X^{-4} or X^{-6} depending on the morphology of the mixture. If the phase separated clusters are isolated then X^{-4} dominates; however, if the clusters are not isolated but percolate through the structure then, X^{-6} dominates. In order to express this in general form both criteria were combined to a simple power $X^{-\gamma'}$ where in 3-dimension system γ' is equal to $d + 1$ for cluster regime and is equal to $2d$ for percolation regime. Combining all criteria for the whole X , a universal scaling function $\tilde{S}(X)$ is obtained:

$$\tilde{S}(X) = \frac{(1 + \gamma'/2)X^2}{\gamma'/2 + X^{2+\gamma'}} \quad (3.52)$$

3.3 Conclusions

So far, various theoretical approaches regarding the kinetics of phase separation via both spinodal decomposition and nucleation and growth phenomena of a binary system have been reviewed. It is clear that the diffuse interface theory, which appears to utilise more measurement values, exhibits an excellent agreement with the experimental investigation. However, the classical nucleation theory should not be taken for granted since this is the fundamental of all following theories with respect to nucleation and growth phenomenon. On the other hand, due to the fascinating evolution of spinodal morphology several current attempts have been devoted to studying the process of spinodal decomposition. The first and most well-known theory so far is the Cahn-Hilliard linearised theory. It shows that the scattering intensity keeps growing while the maximum wave vector is constant as time proceeds. This fits quite well with a number of experiments especially at the certain range of time in the early stage of phase separation. Consequently, it has been suggested that the linearised theory might be used to approximately indicate the early stage of phase separation while beyond that the effect of thermal fluctuation, nonlinearity of the approximate chemical potential and the droplet growth should be taken into consideration. These are presented in Cahn-Hilliard-Cook and Langer-Baron-Miller theories.

The gargantuan change in the evolution of polymer field was conducted by De Gennes nearly two decades ago. The clear picture of the effect of viscoelasticity on polymer and the other way of considering free energy were introduced. Additionally, owing to viscoelasticity of polymer, entanglement sometimes plays an important role during phase separation causing a relaxation or here so-called delay time. The modified linearised model by Clarke, who introduced a term defined as the elastic energy to the classical free energy equation, is presented. It appears that this model comprises two main modes in the structure function equation: the normal decaying mode and the impeding decaying mode. Previous simulation on high molecular weight polymers using this model showed a satisfactory result.

In the last section the processes of droplet formation are explained. The scaling analysis, which includes the effect of droplet formation, is presented. The universal scaling function proposed by Furukawa is described. A number of experimental studies by neutron, light and x-ray scattering have shown that this approach is applicable for the whole range of spinodal decomposition and the most important thing is the fact that this theory can distinguish the beginning of the late stage of spinodal decomposition.

Since the development of phase separation theories has progressed dramatically, it seems that recent interests have been laid on not only the static phase separation but also on the moving fluid such as in the presence of shear. Due to the presence of pressure loss and shear loss, Navier-Stoke equation has been introduced, coupled with the continuity equation in some recent studies [van Noije *et al.* 2000; Nestler *et al.* 2000]. Furthermore, concerning the realistic phase separation a new kind of equation has been suggested in order to cope with the problems of the confined area or the presence of some particles [Binder 1998].

สถาบันวิทยบริการ
จุฬาลงกรณ์มหาวิทยาลัย

Chapter IV

Materials and Experimental Techniques

This chapter explains the characteristics of materials used in this work as well as all experimental techniques. Two materials namely the commercial poly(methyl methacrylate) (PMMA) and poly(styrene-co-maleic anhydride) (SMA) are of interest. The chemical structure and the physical behaviour of those materials are first discussed. Sample preparations consisting of solution casting, and melt mixing are next considered. Lastly, several important techniques, which were employed, are manifested, viz., differential scanning calorimeter, Fourier transform infrared spectrometer, gas permeation chromatography, light scattering and scanning electron microscope.

4.1 Material Characteristics

Poly(methyl methacrylate) is best known as the polymer, which shows excellent transparency. In addition, it also exhibits good rigidity, abrasion resistance, outstanding weather ability, and good general chemical resistance except for some organic solvents. Owing to its prominent optic properties, the main products of poly(methyl methacrylate) are automotive tail-light lenses, safety and security glazing, sky lights, illuminated signs, and optical fibers. It is sometimes used for coating, such as floor waxes, and in emulsion (latex) paints. The chemical structure of this polymer is shown in Figure 4.1.

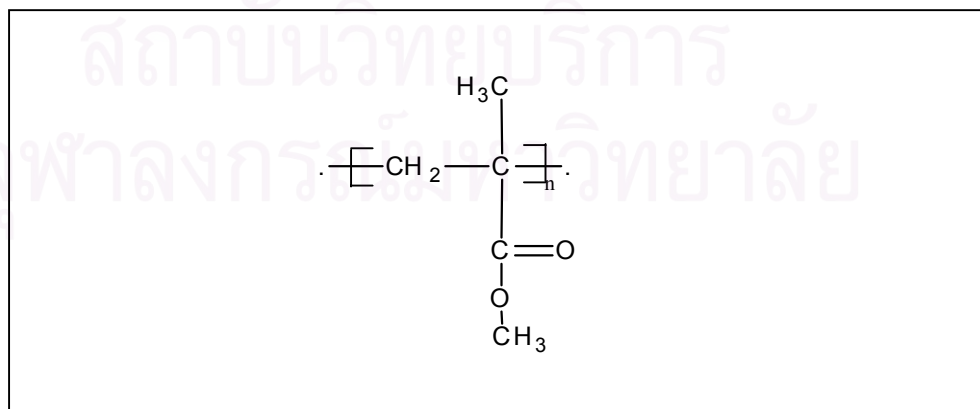


Figure 4.1: The chemical structure of poly(methyl methacrylate) (PMMA)

Poly(styrene-co-maleic anhydride) (SMA) was commercially introduced in the early 1930s [Wang 1997]. It has several excellent properties such as low melt flow-rate, ease of colouring, high thermal resistance and improved chemical resistance as compared to other engineering thermoplastics such as carbonate and modified polyphenylene oxide. Owing to the functionality of the anhydride ring and the high glass transition temperature (T_g), it offers a wide variety of applications [Tacx *et al.* 1996]. The low-molecular-mass SMA copolymer can be found as a levelling agent in floor polishes, embattling/anti-resoil agents in rug shampoos, and pigment dispersant in paints [Brydson 1979]. Since SMA copolymer can provide the combined rigidity and thermal properties necessary in roof and floor consoles, it has been widely used in automotive interiors. The major area of application is instrument panel support components. The glass-reinforced SMA polymers are used extensively in supporting padded instruments panels, while un-reinforced products are used in a variety of interior trim parts and exterior mirror housings. SMA with flame-retardant materials is used in switch covers, modems and a number of business- machine applications. SMA resins have also been approved for packaging materials that come in contact with food.

SMA copolymers are usually made by mass copolymerisation using a free-radical initiator. There is a strong tendency to form 1:1 equimolar copolymer unless the maleic anhydride (MA) concentration is held at an extremely low level during the entire polymerisation sequence [Brydson 1979]. If the number of styrene monomer units is larger than that of maleic monomer units, excess styrene units will combine with each other to form blocks of styrene units in the polymer chain [Buchak *et al.* 1976].

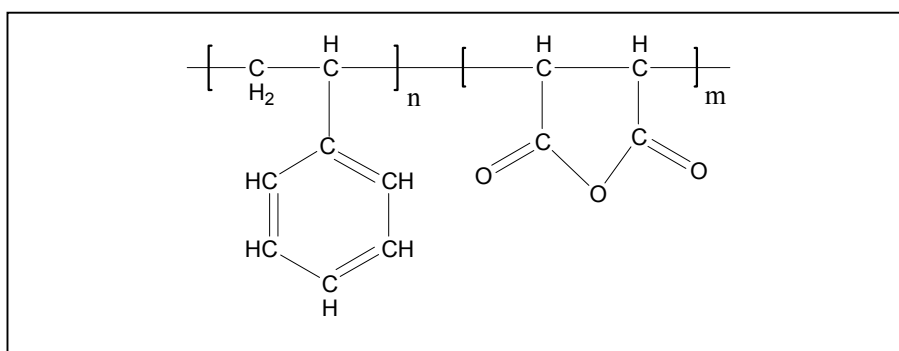


Figure 4.2: The chemical structure of poly(styrene-co-maleic anhydride) (SMA)

Blends of PMMA and SMA are becoming of interest nowadays owing to the high T_g of styrene maleic anhydride copolymer which can elevate the processing temperature in blends. The miscibility of this blend has been previously investigated by several groups. For example, the previous work by Brannock *et al.* [1991] using differential scanning calorimetry measurements (DSC) showed that the miscibility of the blend was dependent on maleic anhydride content. Using pure polyethyl methacrylate (PEMA) instead of pure PMMA lowered the cloud point curve. Light scattering experiments carried out on a similar blend but with a commercial PMMAe sample (with ethyl acrylate co-monomer) by Manda *et al.* [1998] showed similar results to the PMMA system but with a slightly lower cloud point due to the co-monomer. Feng *et al.* [1995] investigated the mechanism for miscibility of SMA/PMMA blends using NMR, FTIR and DSC. It was suggested that a strong intermolecular interaction between the phenyl groups in SMA and the carbonyl groups in PMMA resulted in the miscibility at a molecular level. The strength of the interaction depends on the compositions of the blends. The effect of shear mixing and de-mixing on blends using the commercial PMMAe have been reported by Aelmans *et al.* [1999, 2000] and Chopra *et al.* [1998].

The random copolymer of styrene maleic anhydride (SMA) used in this work, containing 32% by weight of maleic anhydride (MA), was kindly provided by DSM (The Netherlands). Owing to its hygroscopic nature, it was stored in a dry atmosphere (dessicator) and heated prior to use. The commercial grade of poly(methyl methacrylate) (PMMAe), containing 10 wt% copolymerised ethyl acrylate comonomer was supplied by ICI (UK). It comprises ca. 0.75 wt% of lubricating agent, 0.02% UV stabiliser, and 0.1 wt% heat stabiliser. The commercial PMMAe polymer was chosen for these studies because the cloud point of general SMA/PMMA blends usually exists at high temperature [Brannock *et al.* 1992] leading samples being very vulnerable to thermal degradation during phase separation investigations. Furthermore a preliminary work on the pure PMMA material showed that it is difficult to detect phase boundaries at slow heating rates because of degradation. At the high temperatures used to follow spinodal decomposition inside

the phase boundary, degradation became prohibitive. Using the commercial PMMAe grade both lowers the phase boundary and greatly increases thermal stability. Characteristics of both polymers are shown in table 4.1.

Material	\bar{M}_w	\bar{M}_w / \bar{M}_n	T_g^c	Density (g/cm ³) ^d	Refractive index ^e
PMMAe	120,000 ^a	2.2	100.4	1.185	1.489
SMA	80,000 ^b	2.3	175.7	1.182	1.564

Table 4.1: Properties of PMMAe and SMA

4.2 Sample Preparations

Both polymers were heated at 120 °C in a vacuum oven for 4 hours prior to use to remove absorbed water. Two main preparation techniques were employed in this study.

4.2.1 Solution casting

Blends of different weight compositions were dissolved in a homogeneous solution of methyl ethyl ketone. The total amount of polymer in solution is 10% (w/v). The solution was coated onto the top of 16 mm diameter glass cover slips. To minimise the effects of film thickness in diminishing the scattered intensity because of reduced transmission as phase separation develops, thin film samples (0.1-0.2 mm.) were used in this work. In order to obtain the same thickness, the same concentration and number of drops were applied each time. Samples were placed inside petri dishes to avoid dust and to allow the solvent to evaporate slowly. They were kept at room temperature for 1 day and further dried in a vacuum oven starting at 60 °C. The temperature was raised gradually until at least 20 °C above the glass transition

^a Determined by gel permeation chromatography analysis using PS standards (GPC)

^b Provided by the supplier: DSM (The Netherlands)

^c Determined by differential scanning calorimeter (DSC)

^d Determined by pycnometer micromeritics accupyc 1330

^e Determined at 21°C for SMA and 23°C for PMMA [Brandrup *et al.* 1992]

temperatures of the blend (approximately 2 weeks) and constant weight was reached. The prepared samples were kept in a dessicator to avoid moisture absorption.

Solution cast specimens were prepared by mixing 10 %(w/v) different weight compositions of blends in methyl ethyl ketone. The solution was coated onto the top of 16 mm diameter glass cover slips and kept at room temperature for 1 day. It was further dried in a vacuum oven in which the temperature was raised gradually until at least 20 °C above the glass transition temperatures of the blend (approximately 2 weeks) and constant weight was reached.

4.2.2 Melt mixing

A PRISM twin screw extruder at the polymer group, Department of Chemical Engineering and Chemical Technology, Imperial College was used to mix the samples. The schematic diagram of this machine is shown in Figure 4.1, details of which will be described later on. Both polymers were first mixed as pellets and stirred outside the extruder. They were then put into the extruder, which was operated at torque 60%, screw speed at 20 rpm and temperature between 200-210 °C. This is the lowest temperature that can be used to mix completely since experience showed that at temperatures lower than this inhomogeneity was found in the samples [Manda 1998]. Moreover, at low temperatures, the viscosity appears to be rather high, which can result in high torque and could lead to damage of the extruder. Samples from the extruder were cut into small beads using a PRISM pelletiser. The size of bead can be controlled by the speeds of the pelletiser and the twin screws. The beads were passed through the extruder a second time in order to improve mixing. It was clear that this did not cause degradation to the blends since GPC traces showed no significant difference in the molar weight distributions of single passed and twin passed blends. Moreover, as reported by Chrysostomou *et al.* [1998], it appeared that the mechanical properties such as strength and modulus in both extension and flexures tests were apparently independent of the number of reprocessing cycles. The temperatures used in the extruder here fell inside the phase separation regime hence producing two-phase samples consisting of two mixed phases with different compositions. These

samples were as a consequence somewhat cloudy, and it was therefore necessary to anneal inside the miscible regime prior to use. The beads were heated overnight at a temperature 20 degrees above their glass transition temperatures after which they became perfectly transparent. Thin film samples (approximately 0.1-0.15 mm.) for light scattering experiment were obtained using a hydraulic hot press machine.

4.2.2.1 Twin screw extruder

The machine consists of a twin screw extruder which is fed by a controllable feeder. The barrel contains the two intermeshing screws, which operate in a co-rotating mode to provide a uniform and controllable stress field suitable for mixing polymers, with a regular composition distribution in the product [Utracki 1991]. There are some kneading paddles in the middles of the screws, which are effective in both the melting and the dispersion of the polymer; they provide a more well-mixed flow. The extruder is heated along its length to variable set point temperatures by electrical heaters. Temperature is controlled by three temperature sensors. At the end, the slit die viscometer is connected and also electrically heated along its length to a given set point temperature. Along the midpoint of the vertical wall are two horizontally aligned pressure transducers, at distance L apart. There are also two corresponding temperature sensors in the die.

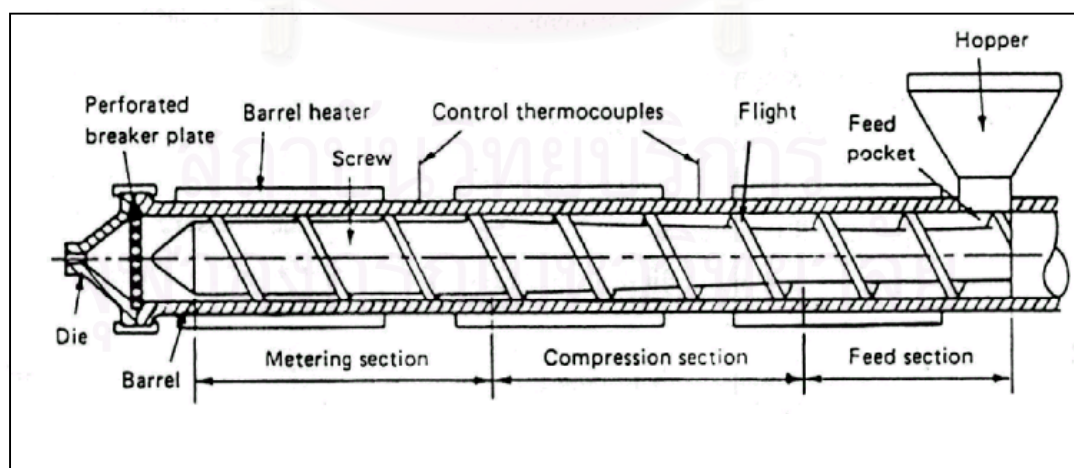


Figure 4.3: Illustration of a plasticating extruder [McCrum *et al.* 1997].

4.3 Experimental Techniques

4.3.1 Differential scanning calorimeter (DSC)

This machine was used to detect T_g of the blends and of the pure polymers. It has been known that a miscible binary blend generally exhibits one T_g which lies between the T_g 's of two components while an immiscible blend exhibits 2 T_g 's at exactly the same position as the individual ones. A partially miscible blend exhibits 2 T_g 's which shift to lie between the T_g 's of two constituents.

As shown in Figure 4.4, the sample and reference are simultaneously heated at a fixed rate until they reach the set point. In the case of ideal thermal symmetry the temperature of both cells is similar. When a transformation occurs, the temperature between two cells is different. The controller thus tries to compensate the heat difference by increasing or decreasing an addition heating power. Details of which can be found elsewhere [Wendlandt 1986]

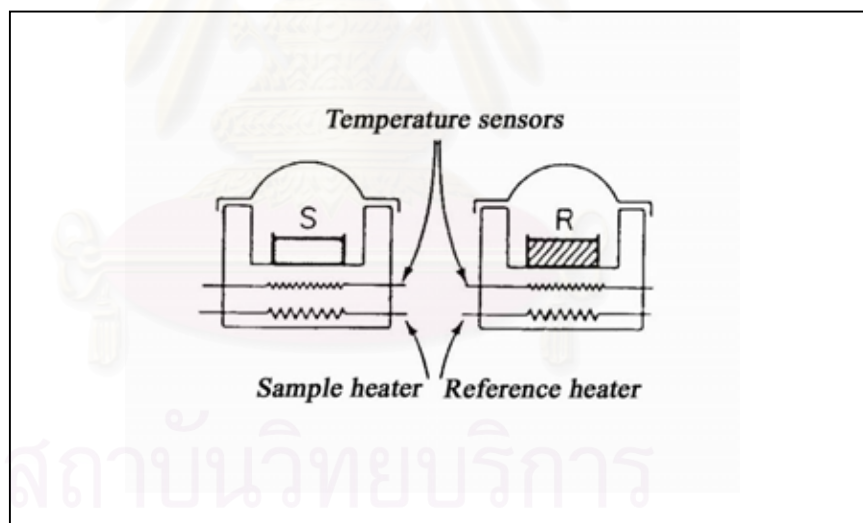


Figure 4.4: A schematic diagram of differential scanning calorimeter [Wendlandt 1986].

A Perkin Elmer (DSC 7) was used to detect T_g in this work. The weight of each sample was 10-15 mg. Samples were placed on the aluminium pan and heated at the rate of 20 °C/min from room temperature to approximately 20 degrees beyond the end of the T_g transition, then quenched to room temperature, held for 5 minutes and heated again at the same rate. The T_g value is the mid point of the specific heat change. The second run T_g was used in order to avoid the effect of thermal history.

4.3.2 Fourier transform infrared spectrometer (FTIR)

A Fourier transform infrared spectrometer is apparently used as a tool to observe functional groups. Infrared radiation is generated by electrically heating a source, which is usually fabricated from a binder and oxides of zirconium, thorium, and cerium. The radiation splits into two beams, one beam is of fixed length, the other of variable length (movable mirror), as shown in Figure 4.5. The combined beam then passes through a sample cell and once molecules absorb infrared radiation, each molecule can emit different kinds of molecular rotation and vibration reflecting its functional groups. An analog signal is detected and transformed into a digital signal, which is then analysed by a computer. Details of this machine can be found elsewhere [Silverstein *et al.* 1991].

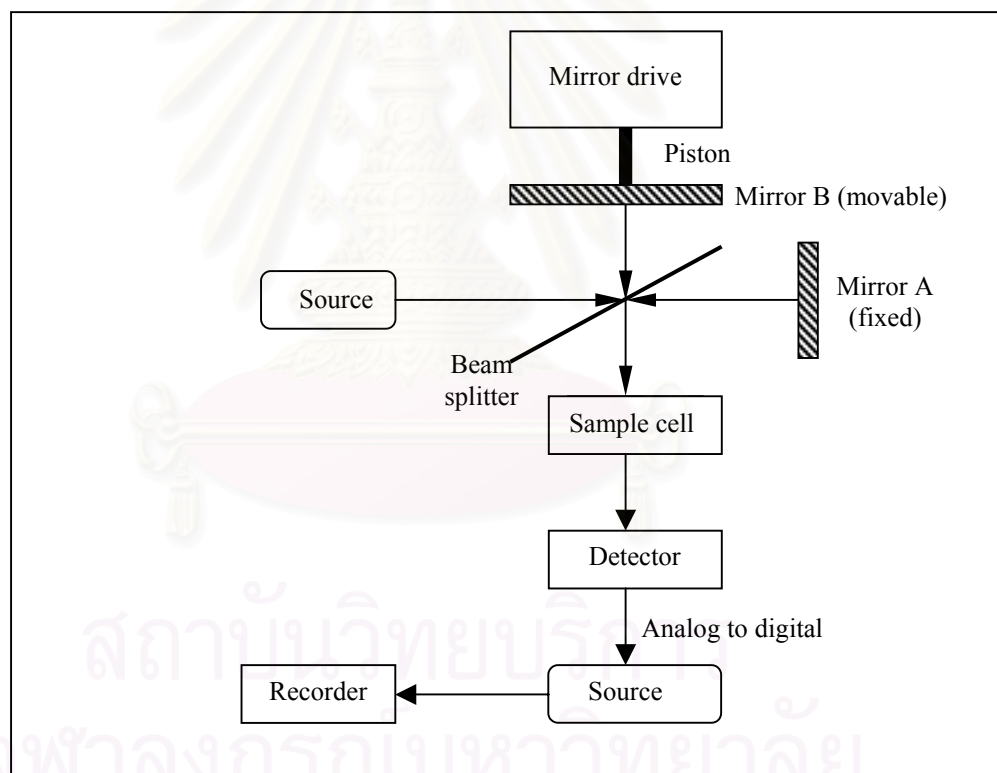


Figure 4.5: A schematic diagram of an FTIR spectrometer [Silverstein *et al.* 1991].

A FTIR-1760 Perkin Elmer spectrometer at the Scientific and Technological Research Equipment Centre, Chulalongkorn university was employed in this study. Measurements were taken at 0.5 cm^{-1} resolution. Samples were first ground and mixed with potassium bromide using a small vibration ball mill. They were then

pressed into cylindrical plates and mounted on a holder for subsequent measurement of the spectra. The shift of some important bands in the blend such as phenyl or carbonyl peaks can be used as a tool to indicate some sort of interaction occurring. Furthermore, comparing the absorbance peak of blends with that of pure SMA allows approximate concentrations of the blends to be obtained.

4.3.3 Gel permeation chromatography (GPC)

Gel permeation chromatography, one of size exclusion chromatography techniques, was first introduced by Moore in 1964 [Moore 1964]. It is usually used to separate high polymer systems. In principle, the polymer of interest is first dissolved in a solvent and then passed through a long tube packed with beads of rigid porous glass or porous highly cross-linked polystyrene. As the dissolved polymer molecules flow past the porous beads, they can diffuse in or out of the holes in the beads depending on their size. The large molecules can enter only a small fraction of holes, or are completely excluded, therefore they pass through the column rapidly. The smaller molecules can penetrate a larger fraction of holes, so they show the larger retention time or volume. The amount of polymer at the end of the column is detected by spectrophotometric method, i.e., refractive index measurement. The molecular size distribution can be obtained by comparing the retention time or volume with the calibration curve generally from polystyrene. Details of which can be found elsewhere [Billmeyer 1984].

Gel permeation chromatography experiments in this thesis can be divided into two sections, in which different apparatuses and methods were employed depending on experimental places. The first part was carried out in the United Kingdom at the Department of Chemistry, Imperial College, in order to investigate the effect of number of processing cycles on the fraction of molar weight, in other words degradation. A polymer solution for gel permeation chromatography was obtained by dissolving 10 mg of sample in 5 ml of chloroform. The complete mixed solution then was injected into a series of packing columns containing porous gel with the rate of 1 cm³/min at ambient temperature. An external differential refractometer (DRI) was

used to measure the difference in the refractive index between the solvent and the eluent. The initial result was obtained as a chromatogram, i.e., a plot of concentration versus retention volume. Conversion of the chromatogram to a molar weight distribution curve was performed on the basis of the molar weight calibration of polystyrene standards. Figure 4.6 shows the comparison of plots of concentration against retention time of the sample obtained from different number of run in the extruder. It was found that those two curves are quite similar, manifesting two peaks corresponding to PMMA peak (first appearing) and SMA peak (second appearing). It might indicate that there is no sign of degradation by the second passing sample through the extruder.

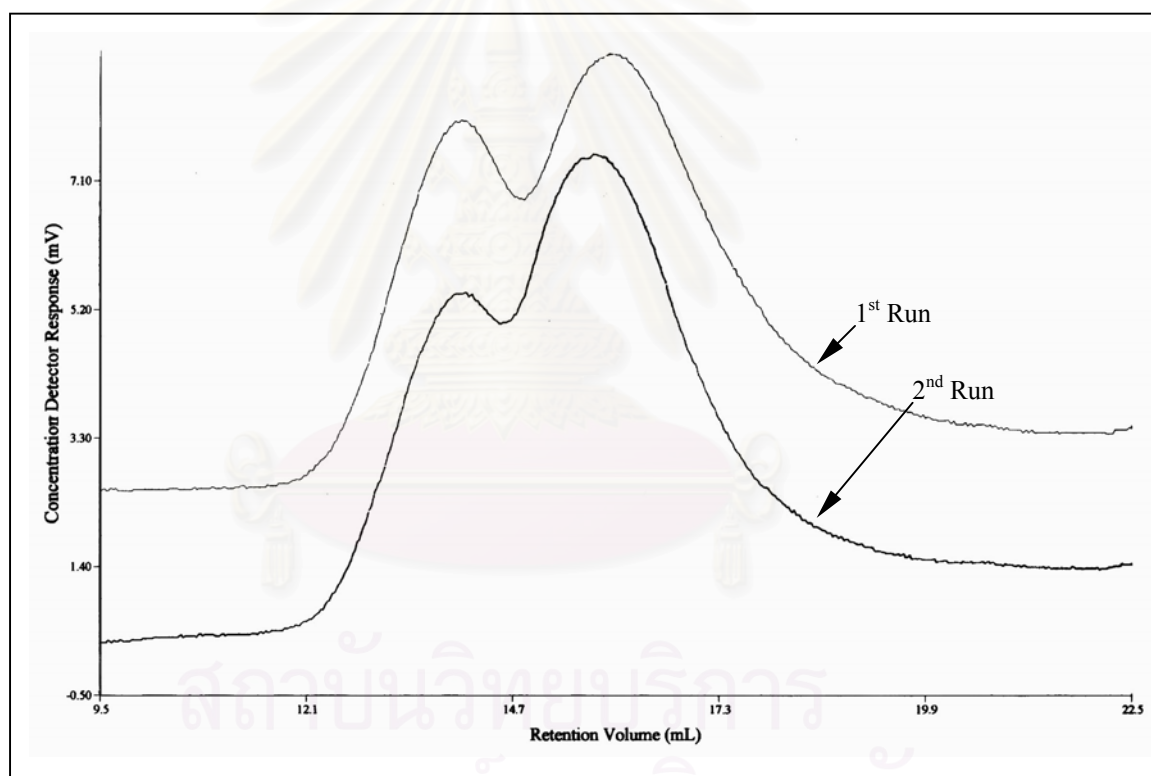


Figure 4.6: A schematic illustration shows that numbers of processing cycles do not cause molar weight fraction in melt mixed polymer blends.

The second part of the GPC experiments was carried out in Thailand at the National Metal and Materials Technology Centre in order to trace the sign of degradation due to molecular fraction in finished phase separated specimens. The Waters Chromatography 150-CV was employed here; however, unfortunately this is not the same GPC column used in the United Kingdom. Owing to its wide range of

molar weight observation ($500\text{-}10 \times 10^6$ dalton) leading low resolution, some working conditions therefore were required to be revised here in order to obtain unequivocal results, i.e., the concentration of polymer solution was increased to raise the output signal, the flowing rate in the column is decreased in order to observe minor difference of molar weight. Firstly, 15 mg of specimens for tensile testing prepared from different conditions was dissolved in 5 ml of tetrahydrofuran (THF), and after being left overnight to completely dissolve, the solution was filtered through a 0.45-micron paper. The complete solution was then injected into a series of packing columns with the rate of $0.273 \text{ cm}^3/\text{min}$ at ambient temperature. The output concentration and retention volume was later detected by the differential refractometer and converted to molar weight distribution by comparing with the calibration curve using polystyrene.

4.3.4 Light Scattering (LS)

Kinetic experiments were performed using a light scattering apparatus at the polymer laboratory, the Department of Chemical Engineering (Imperial College, UK). The equipment is schematically shown in Figure 4.7.

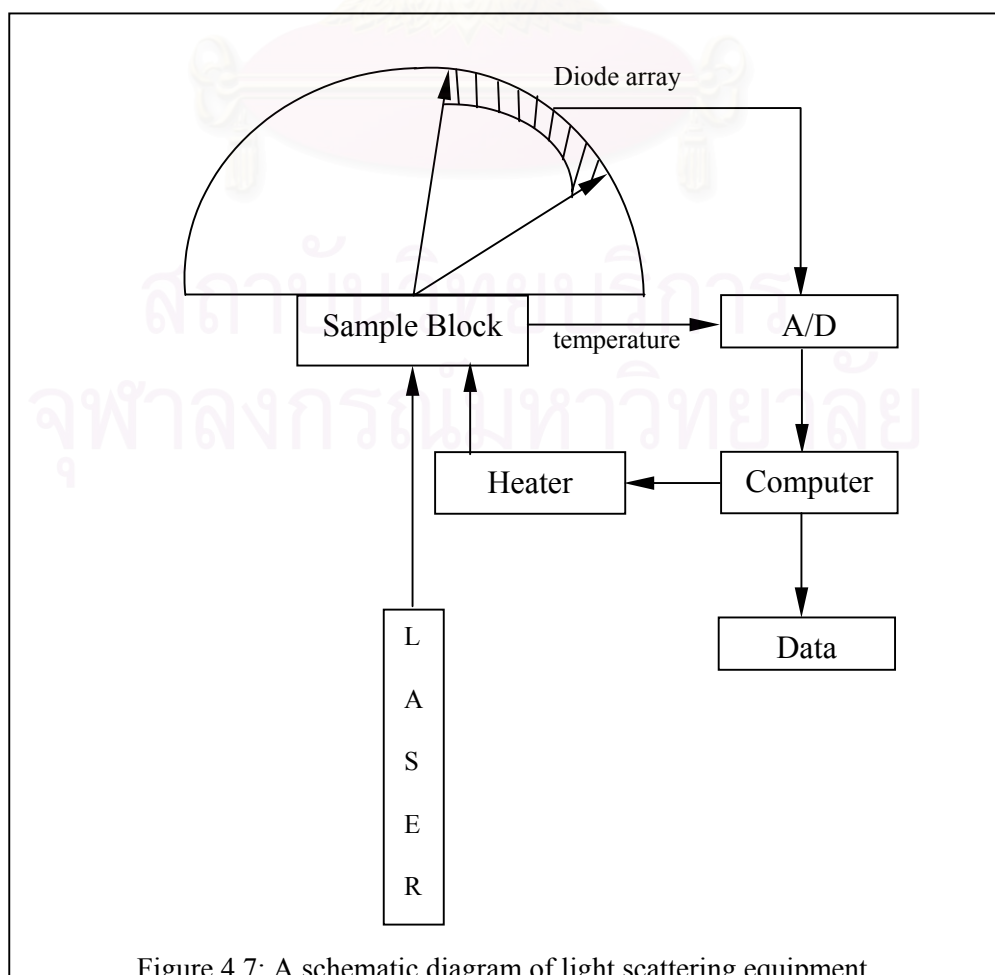
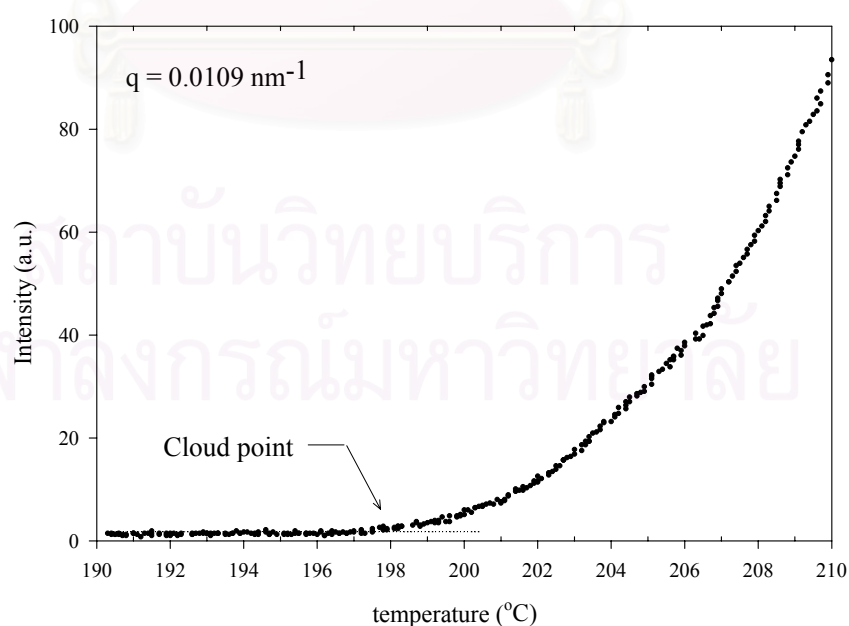


Figure 4.7: A schematic diagram of light scattering equipment

An Aerotech model 1105P He/Ne laser of 5 mW ($\lambda = 632.8$ nm) is used as an incident light source. Samples were placed inside a sample holder, which was mounted between laser and a series of photo diodes. The temperature inside the sample holder was controlled by a computer. The scattering light is detected by a photo diode array, mounted on an arc between 5 - 67 degrees at 2-degree intervals. The signal from diodes is converted in a multi-channel analogue/digital converter, and transfer to analyse using the computer.

Two different experimental techniques were employed using the light scattering apparatus, viz., a cloud point experiment, and a temperature jump experiment. In the former case, a number of dry films of each composition were heated at different heating rates. The point at which the scattered intensities start to increase is defined as the cloud point. As shown in Figure 4.8, the cloud point temperature is approximately 198 °C. Since cloud point values depend on the rate at which phase separation in the sample responds to the temperature changes, as a rule, the lower the heating rate the lower the cloud point value. Extrapolating heating rate to zero is then used to obtain a value close to the true cloud point. Several heating rates, viz., 0.1 °C/min, 0.2 °C/min, 0.3 °C/min, 0.5 °C/min and 1 °C/min were chosen



for the cloud point measurement.

The second set of experiments was designed to determine the spinodal temperatures, by following the spinodal decomposition process after a temperature jump inside the phase boundary. Homogeneous blends were annealed first at approximately 160 °C (i.e. above the T_g and below the cloud point temperature) for 10 minutes and then transferred quickly into the sample holder, which was pre-heated to the desired temperature inside the phase boundary.

4.3.5 Scanning Electron Microscopy.

The SEM was originally devised in Germany in the 1930s by Knoll & von Ardenne, and has been considered as an original of the early electrical facsimile machine [Joy 1993]. In scanning electron microscope, a fine beam of electron is first scanned across the surface of an opaque specimen. Once such an electron beam touches the surface, a difference of electron density in the specimen results a variety of scattering electron and photon emission. Those electrons are detected, modified and used to modulate the brightness of the second beam scanned synchronously in cathode ray tube (CRT). A big collected signal produces a bright spot on the CRT while a small signal produces a dimmer spot. Details of this technique can be found elsewhere [Bozzola 1992].

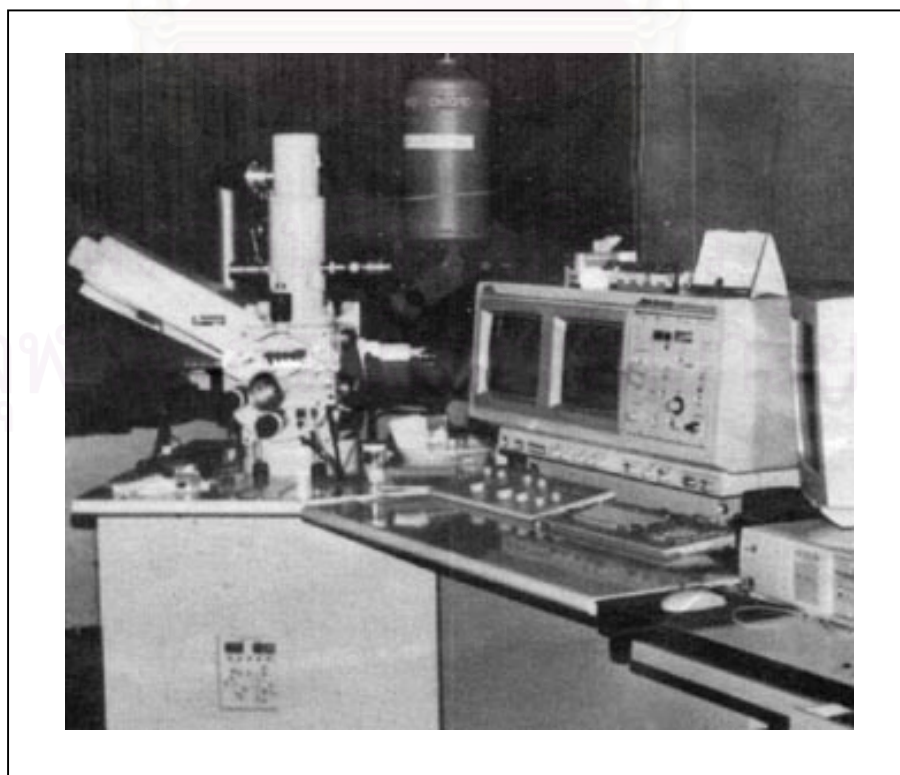


Figure 4.9: A photographic illustration of SEM model JSM-6400.

Phase separation morphologies of the fractured surface in this thesis was observed by using a scanning electron microscope JEOL JSM-6400 at the Scientific and Technological Research Equipment Centre, Chulalongkorn university as shown in Figure 4.9. Since this technique requires the sample to be good at electron conducting, it is necessary to provide conduction to specimens by evaporating a thin metal layer (i.e. gold was used in this work). The coated specimens were kept in dry place before experiment. It was operated at 15 kV. This is considered to be a suitable condition since too high energy can cause burning to samples.

4.3.6 Transmission Electron Microscopy

Transmission Electron microscopy (TEM) measurements were carried out at the Scientific and Technological Research Equipment Centre, Chulalongkorn university. Following the standard procedure of this centre [Nopanitaya 1985], the samples were firstly cut into tiny pieces and embedded in epoxy resin prior to slicing into thin film in order to avoid curling. The samples and epoxy resin in capsules were annealed at 70 °C for 8 hours, after which they completely polymerise, becoming hard and ready to cut into thin film. The obtained samples were sectioned into thin film (≈ 90 nm thick) using a low-temperature ultramicrotome (LKB- ultratome V) with a diamond knife. The ultrathin film was attached on a copper grid and stained in 2% aqueous OsO_4 for 2 hours prior to monitoring in order to increase the contrast between two phases. Attachment of osmium atoms to unsaturated hydrocarbon repeating units results in a darker image for those portions. The samples were viewed with a TEM (JEOL - JEM 200CX) at 100 kV. The light area in the resulting micrographs corresponds to the PMMAe-rich phase while the dark area is related to the SMA-rich phase.

4.3.7 Tensile Measurement

Tensile properties in this thesis were measured by using a LLOYD model 2000 as shown in Figure 4.10.



Figure 4.10: A photographic illustration of LLOYD model 2000.

Thin sheet samples of the melt mixed 20/80 and 40/60 SMA/PMMAe blends for tensile tests were obtained by the compression moulding method using a hydraulic hot press machine. Two compositions were chosen for the tensile test as these have rather low spinodal temperatures compared to other compositions leading the phase separation temperatures being not so high, thus the problem of thermal degradation can be avoided. Furthermore since both compositions lie two sides of the critical composition (30/70) and show nearly the same spinodal temperatures, this is very interesting to compare the difference caused by phase separation. All samples were heat treated at different phase separation temperatures and times inside the hydraulic hot press machine depending on the stage of phase separation as shown in Table 4.2. The method of identification of each stage of spinodal decomposition is briefly described in Appendix C. The blends, which firstly were transparent, became whitened after phase separation. Strips of uniform width and thickness of rectangular specimens of 100 mm x 10 mm were carefully cut from the thin sheeting (≈ 0.07 mm) using a razor blade. The cutting edge of each sample was polished in order to get rid of imperfections. All specimens were kept in a dessicator prior to test in order to

avoid moisture absorption. The test specimens were held at the ends by the grips lined with rubber sheet in order to avoid slippage. They were pulled at a constant crosshead speed of 5 mm/min with the operated at temperature between 23 and 25 °C. The initial gage length of 50 mm was employed. Since this blend is considered to be an isotropic material even though it is phase separated as shown by Matsuoka *et al.* [1998], at least five specimens were used for each sample, any specimens showed failure at the grips were discarded. Since all samples usually show a toe region in a stress-strain curve, which in fact does not represent a property of the material. It may be an artifact caused by a takeup of slack and alignment or seating of the specimens. In order to remove such an artifact, the specimen was subjected to a marginal force first, followed by capturing data of the actual experiment.

Phase Separation Temperature (°C)	Phase separation time (sec)		
	Early stage SD	Intermediate stage SD	Late stage SD
210	1800	3600	6000
220	600	1200	2400

Table 4.2: Phase separation times and temperatures of the heat treated specimens for tensile tests

Chapter V

Miscibility and Kinetics of Phase Separation of SMA/PMMAe Blends

Theoretical discussions on thermodynamic and kinetic points of view in Chapters 2 and 3 have rigorously shown that several parameters have already been taken into account, for example, pressure, molecular weight, shear, stereoregularity, stiffness, etc. However, besides those effects, experimental studies via a variety of techniques such as thermal analysis, scattering techniques and microscopic observation recently manifested that both miscibility and kinetics of phase separation can also be affected by other parameters, such as thickness, substrate, sample preparation, etc., which to date cannot be clearly explained by any equations.

Guo *et al.* [1990], who studied TMPC/PS blend using light scattering technique, found that cloud point depends on the film thickness: as film thickness increases, the cloud point decreases dramatically at first and then levels off. It was suggested that owing to the closeness of the refractive indexes of PS and TMPC, a significant signal can only be achieved with the thicker film. Another work by Woo *et al.* [1996] on PC/PMMA blend supports that result. They used SEM to observe morphology of the blend and suggested that the effect of film thickness might be in fact related to the kinetic rate of solvent evaporation, i.e. the faster rate of evaporation in the thin film results in a greater extent of chain entanglements and thus lower extent of heterogeneity compared to the thicker ones. On the other hand Reich *et al.* [1981] and Geoghegan *et al.* [1995] found that besides the thickness, the effect of substrate is essential as well. A study on PS/PVME blend showed that film on gold substrate exhibits increased miscibility as the film thickness decreases, while film on glass substrate exhibits the opposite way. They suggested that this might be the result of the substrate-polymer interaction, electrostatic interaction or selective adsorption of polystyrene on the substrate. However, it should be noted that these studies were conducted only on the very thin film (thickness is smaller than 1 μm). Another work, which shows the effect of solvent on miscibility, was carried out by Neo *et al.* [1992]. They used DSC to investigate PVAc/PBEMA blends and found that the blends cast

from THF are completely immiscible while those cast from MEK are miscible at low temperature and show the LCST behaviour upon heating. This is in agreement with the recent experiment by Serrano *et al.* [2000], who used the latest technique namely the epifluorescence microscopy. It was found that the variation of concentration in the film depends on composition and type of solvents. So far since it has been illustrated that a solvent can play an important role on miscibility, it is therefore interesting to compare phase behaviour of the blends, which are free of solvent during processing with the blends which pass the way of dissolving in some kind of solvent.

The first part of this chapter illustrates the studies of miscibility and kinetics of phase separation of SMA/PMMAe blends from early to late stage of spinodal decomposition with respect to the effect of sample preparation. It starts with phase boundary investigations, followed by miscibility and kinetic discussion. Then the test of Cahn-Hilliard theory for phase separation in the early stage is dealt with, followed by the scaling analysis for phase separation in the intermediate and the late stages. Finally, the delay time behaviour, which to date is still equivocal, is clearly discussed.

5.1 Phase Boundary Investigations

5.1.1 Cloud point Determination

As the temperature was continuously elevated, the blends, which at first were clear, became cloudy after the temperature reached the cloud point temperature as observed by the rise of scattered intensity. It has been found that the observed cloud point temperatures are dependent on the heating rate as shown in Figure 5.1. This is in agreement with other works, which suggested that it might be the result of the viscous and highly entangled nature of polymers [Guo 1990; Thongyai 1994; Pavawongsak 1996; Soontaranun 1997; Manda 1998]. In order to diminish the effect of relaxation and heating rate dependence, the method of extrapolation to zero heating rate was used to obtain the real cloud point temperature. Furthermore since this blend can show the delay as observed by temperature jump experiments. It raises the concerns of the observed cloud point temperature overshooting the real cloud point temperature. As a

consequence of this, using the heating rate as low as possible supports the idea of receiving data close to the real cloud point temperature.

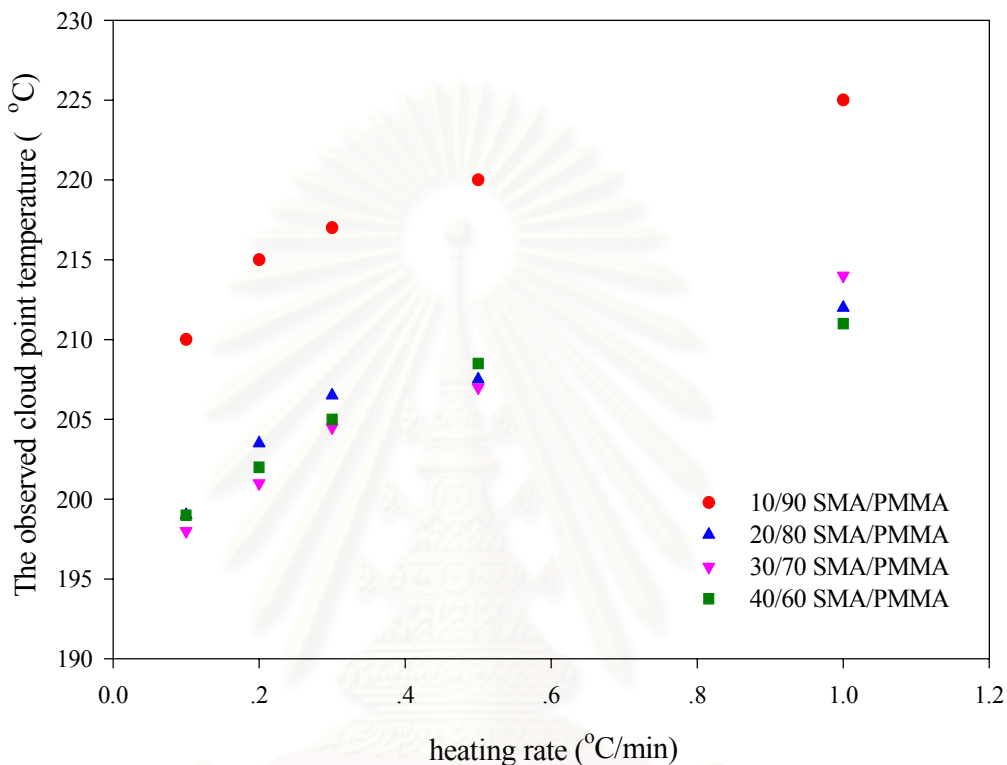


Figure 5.1: Dependence of heating rate on the observed cloud point temperature of solution cast SMA/PMMAe blends at various compositions. Note that error bars have been omitted herein for the sake of clarity.

As shown in Figure 5.1, the observed cloud point temperatures do not change linearly over the whole ranges of heating rate. This has been recently reported by Pavawongsak [1996] and Manda [1998] that for some systems there is a distinct change in the slope of the curve of cloud point with heating rate, and it has been suggested that two mechanisms may be detected. The faster process, which shows up at the higher heating rate could then be spinodal decomposition, while the slow response could be nucleation and growth. If this is the case, then extrapolation of the two lines to zero heating rate will give an indication of both the spinodal and binodal temperatures of the blend.

Several techniques have been suggested to indicate whether a blend undergoes SD or NG mechanism. One easy way among those techniques can be performed by using light scattering. Sasaki *et al.* [1984] suggested that for the blend phase separating via NG, the scattered intensity does not increase exponentially with time, whereas the blend undergoing spinodal exhibits a contrary result. Mazumder *et al.* [1999] and Lefebvre *et al.* [1999], on the other hand, suggested inspecting the way the scattered intensity changes as a function of scattering wave number: for NG mechanism, since the phase separation process is relatively slow, there might appear a fluctuation relaxation at the very beginning of phase separation, and especially at a low scattering wave number. No maximum peak can be observed for NG mechanism. On the contrary, for SD mechanism, one usually observes a maximum peak of scattered intensity showing up at a particular angle and then moving toward lower angles as phase separation proceeds.

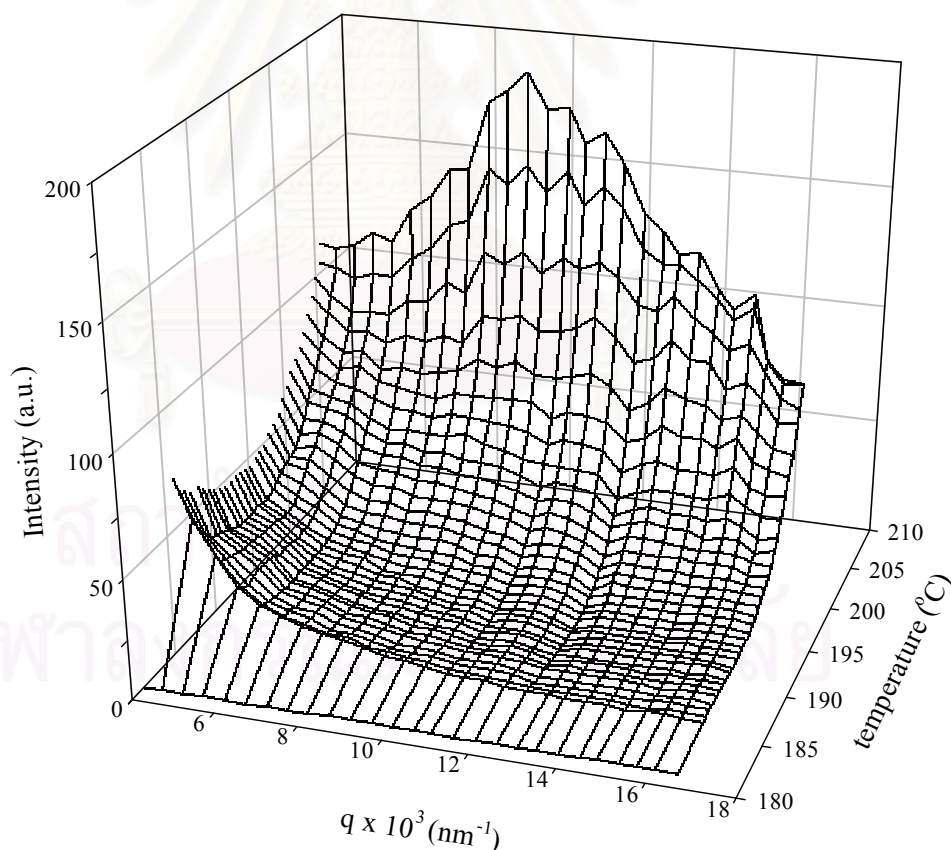


Figure 5.2: The plot of angular dependence 20/80 melt mixed SMA/PMMAe blends at the heating rate of 0.1 °C/min.

3-dimensioned curves of scattering wave number, intensity and temperature were plotted herein to examine those mechanisms. One example of the plot of angular dependence of scattered intensity in Figure 5.2 shows that phase separation proceeded via spinodal decomposition. Since spinodal peaks like this were observed for all experiments, it seems that the used heating rates are rather high, leading the occurrence of spinodal decomposition during the cloud point temperature observation of this system. It has been suggested by Pavawongsak [1996] and Soontaranun [1997] that by employing an infinitely slow heating rate, i.e., extrapolation to zero heating rate, this results in the blends having more time to relax and developing slowly through metastable regime, providing the binodal curve.

5.1.2 Spinodal Determination

According to temperature jump experiments, the blends were heated inside the spinodal region. Surprisingly, the intensity does not change at the beginning of phase separation as called in this work a delay time, indicating a deviation from the Cahn-Hilliard-Cook theory. However, after that distinctive period, the scattered intensity increases exponentially following the linearised theory as shown in Figure 5.3.

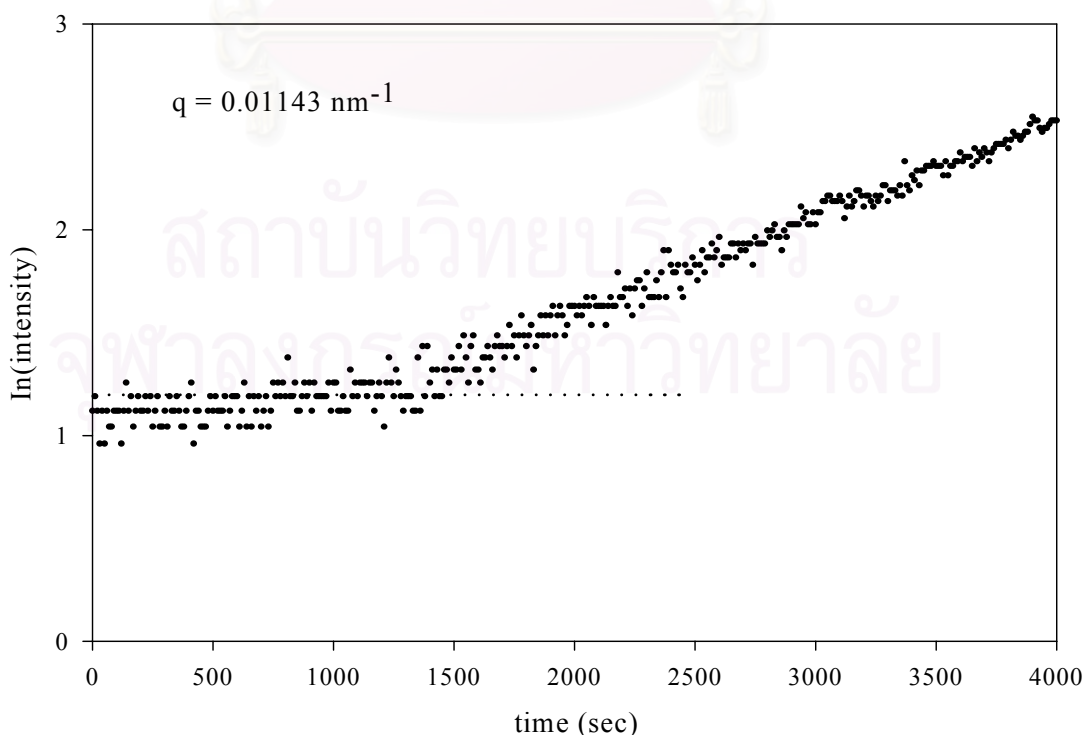


Figure 5.3: A plot of $\ln(\text{intensity})$ against time for melt mixed SMA/PMMAe (20/80) blends, obtained from a temperature jump experiment at 205 °C.

Considering the period, which the experimental data obey the Cahn-Hilliard theory, the change of natural logarithm of intensity with time (after any delay time) provides the double value of Cahn-Hilliard growth rate $R(q)$ as shown in Equation 3.18. From Equation 3.19 and the definition of the apparent diffusion coefficient D_{app} , it can be seen that $D_{app} = [R(q)/q^2]_{q \rightarrow 0}$, i.e., the intercept of a plot of $R(q)/q^2$ versus q^2 . As depicted in Figure 5.4, it appears that $R(q)/q^2$ versus q^2 curve becomes nonlinear as temperature is higher; this is in agreement with what have been found in other systems [Cook 1970; Pincus 1981; Binder 1983; Manda 1998; Binder *et al.* 1986; Clarke *et al.* 1997; Pavawongsak 1996]. Several reasons have been suggested, for example, thermal fluctuations, polymer relaxation, wave vector dependent mobility, etc. Owing to the aforementioned nonlinear dependence, it raises the problem of how to get the real D_{app} . However, since it has been recently demonstrated by Pavawongsak [1996] that despite different ranges of q are selected, the received spinodal temperatures are still close to each other. Consequently, the high q -data range was chosen in this work, as this is less likely to be contaminated by any initial inhomogeneities in the sample such as dust or unmixed polymers. Spinodal points can be obtained by extrapolating the apparent diffusion coefficient to zero since thermodynamic force decreases as getting close to the spinodal point.

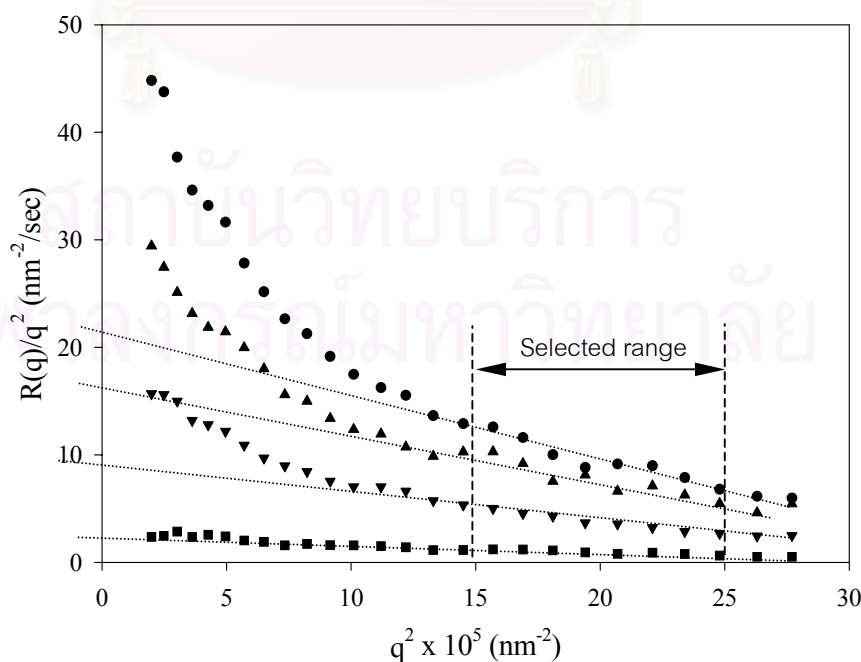


Figure 5.4: Plots of $R(q)/q^2$ against q^2 for melt mixed (40/60) SMA/PMMAe blends obtained from different jump temperatures. ●: 210 °C; ▲: 208.5 °C; ▼: 205 °C; ■: 200 °C.

5.2 Effect of Sample Preparation on Miscibility

Cloud point and spinodal curves of melt mixed and solution cast blends are shown in Figure 5.5.

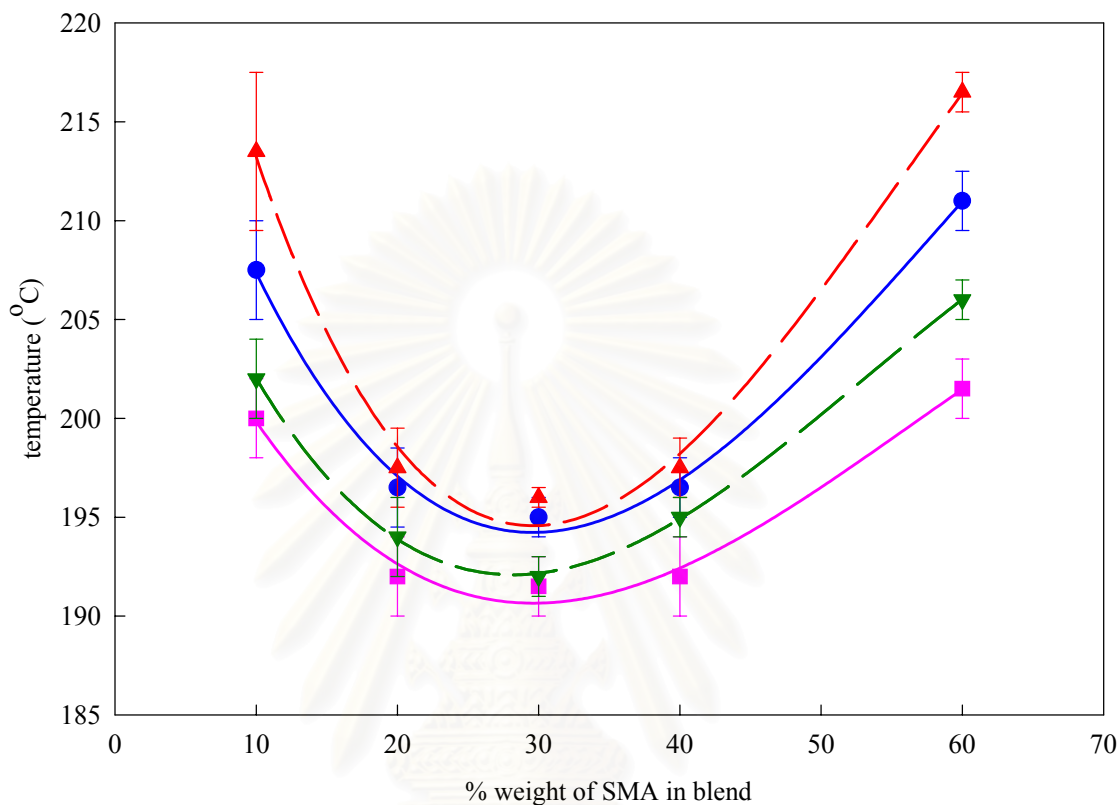


Figure 5.5: Phase diagrams of SMA/PMMAe blends prepared by solution cast and melt mixed methods. ●: cloud point (solution cast); ■: cloud point (melt mix); ▲: spinodal (solution cast); ▼: spinodal (melt mix).

As seen in Figure 5.5, cloud point curves, which may represent the binodal lines are slightly lower than spinodal curves in the vicinity of critical composition (approximately 30 weight % of SMA in blends). The gap between those curves becomes larger as compositions are further from the critical composition. Comparing between two different preparation methods, although there is a considerable scatter in the data, there does appear to be a real shift of about 5°C between the values for the melt mixed and solution cast samples. The melt mixed samples appear to exhibit systematically lower spinodal and cloud point curves than solution cast samples. This indicates that at the same composition if both samples are heated simultaneously, the melt mixed samples will become cloudy signalling demixing first. This may be the result of the solution cast method allowing polymers to mix completely at a molecular

level and facilitating specific interactions between them. The solution cast blends subsequently require much more energy than the melt mixed blends do in order to break the molecular interactions before phase separation proceeds.

It has been pointed out in the previous work by Feng *et al.* [1995] that there exist strong intermolecular interactions between phenyl groups in SMA and carbonyl groups in PMMA as the result of electron transfer interactions, proved by solid state NMR and FTIR experiments. FTIR results in that work furthermore showed that the phenyl bands of SMA shift up to higher frequencies as the SMA content increases, indicating the stronger interaction. Since some kinds of shift in IR experiments might be able to illustrate the change of interaction, the FTIR experiments then have been carried out in this work in order to monitor some sort of shift in phenyl band due to sample preparation methods, using very fine resolution (i.e. 0.5 cm^{-1}). Figure 5.6 illustrates the spectra of the blends prepared by different methods in the region of the phenyl group vibration in the styrene unit of SMA (702 cm^{-1}). It was found that there is no distinctive difference between two methods. This might be as the result of the difference of interaction between two preparation methods being marginal, leading the observation with FTIR spectroscopy being impossible. It is therefore required more powerful technique such as solid state NMR or another way to observe the change in interaction such as the interaction parameter, χ_{ij} , using SANS.

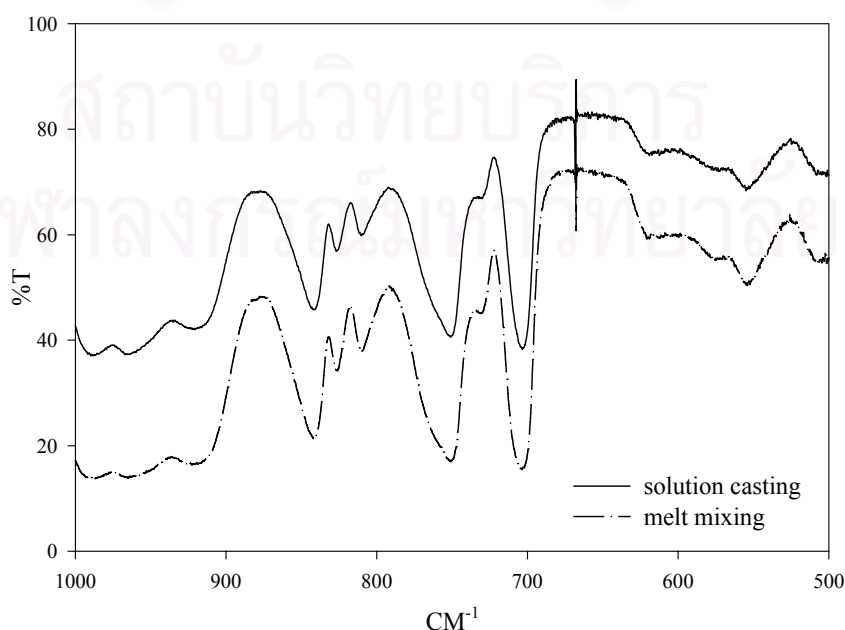


Figure 5.6: The comparison of phenyl bands of 20/80 SMA/PMMAe blends prepared by two sample preparation methods.

A thermal analysis has been conducted to trace any solvents that might cause the higher of glass transition temperature for solution cast blends as suggested by Porter *et al.* [2000]. It was found that a single T_g , intermediate between those of the two components, was observed for all compositions of the as-prepared samples demonstrating the miscibility of these two polymers. The thermograms of these experiments are shown in Appendix D. Experimental results obtained from DSC show only very minor differences between T_g of solution cast and melt mixed samples as seen in Figure 5.7. These fall within the experimental errors, and confirm that all solvent in the solution cast blends has been removed. The Fox equation [1956] was used to predict T_g of the blend,

$$\frac{1}{T_g} = \frac{X_1}{T_{g1}} + \frac{X_2}{T_{g2}} \quad (5.1)$$

where T_{gi} is glass transition temperature of i component

X_i is the weight fraction of i component

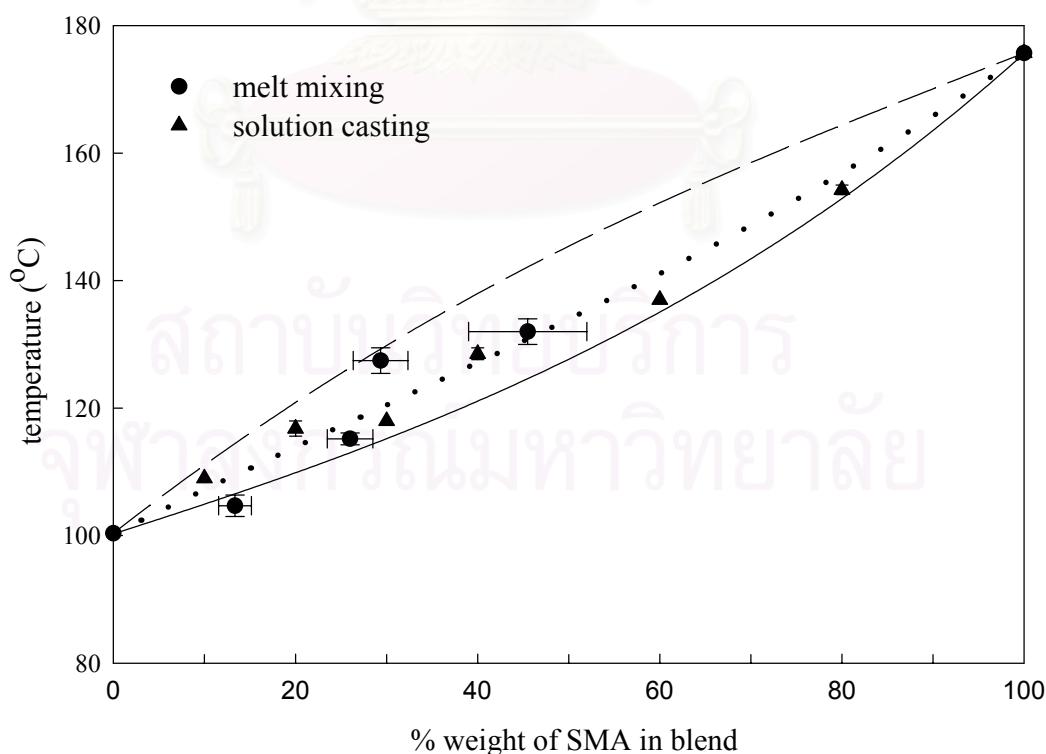


Figure 5.7: Plots of glass transition of SMA/PMMAe blends. The solid line presents the Fox equation. The broken and dotted lines illustrate the Gordon-Taylor Kwei equation using $k = 1.62$, $\alpha = 65K$, and $k = 1.75$, $\alpha = 25K$ respectively.

Figure 5.7 manifests that all compositions show a positive deviation from the Fox equation. The Gordon-Taylor-Kwei empirical equation [Chopra *et al.* 1998], which takes into account the influence of interactions, was then employed in this work.

$$T_g = \frac{X_1 T_{g1} + kX_2 T_{g2}}{X_1 + kX_2} + \alpha X_1 X_2 \quad (5.2)$$

The first term on the right hand side of Equation 5.2 is identical with the widely used Gordon-Taylor expression [Gordon *et al.* 1952], while the second term represents the effect of polymer-polymer interaction, e.g., hydrogen bonding. Chopra *et al.* [1998] exploited this equation by using $k \approx T_{g1} / T_{g2} = 1.62$, $\alpha = 65$ K and found that the calculated values fit very well with experimental data. This work however obtains slightly overestimated values using the same parameters, this might be the result of the used materials. Therefore values of $k = 1.75$ and $\alpha = 25$ were used; consequently, it provides a reasonable fit to the data as seen in Figure 5.7. Such a fit is typical evidence, which shows some specific interactions between the component polymers.

5.3 Sample Preparation Dependence on Kinetics of Phase Separation

The growth rates of phase separation are discussed in two specific ways with respect to the change in scattered intensity. It is clear that the scattered intensity increases exponentially with time in the early stage of spinodal decomposition and the growth rate of spinodal decomposition during this time can be represented by the Cahn-Hilliard growth rate $R(q)$. However, the scattered intensity changes differently as soon as spinodal decomposition approaches the intermediate stage and the maximum scattering wave number q_m moves toward the lower q . The rate of phase separation now is described by the change of q_m with time.

5.3.1 The Cahn-Hilliard Growth Rate ($R(q)$)

The Cahn-Hilliard growth rate ($R(q)$) from the half slope of $\ln(\text{intensity})$ and time for four compositions of blends, which were separated at nearly the same quench

depth, are shown in Figures 5.8 - 5.11. Comparing melt mixed and solution cast blends at the same temperature, since the former is deeper inside the spinodal regime than the latter (see Figure 5.5), it might be expected that the melt mix blend should phase separate faster than the solution cast blend due to the larger quench depth. However, a much more complicated effect was observed in practice. It was found that $R(q)$ obtained from the melt mix method for SMA/PMMAe (10/90) is higher than from the solution cast method, while for other compositions the opposite effect was observed. For the SMA/PMMAe (30/70) blend, which is believed to be at the critical composition (as seen in Figure 5.5), the solution cast blend phase separates much faster than the melt mix blend does, whereas for 20/80 and 40/60 compositions the solution cast blends phase separate slightly faster than the melt mixed blends. The gap becomes bigger as quench depth is larger as shown in Figure 5.12. This may imply complex differences in the thermodynamic behaviour of the blends. A variation with both temperature and composition of the Gibbs free energy derivative, $\partial^2 G/\partial\phi^2$, which provides the thermodynamic driving force for phase separation if dependent on preparation technique would lead to the preparation-dependent relative growth rates.

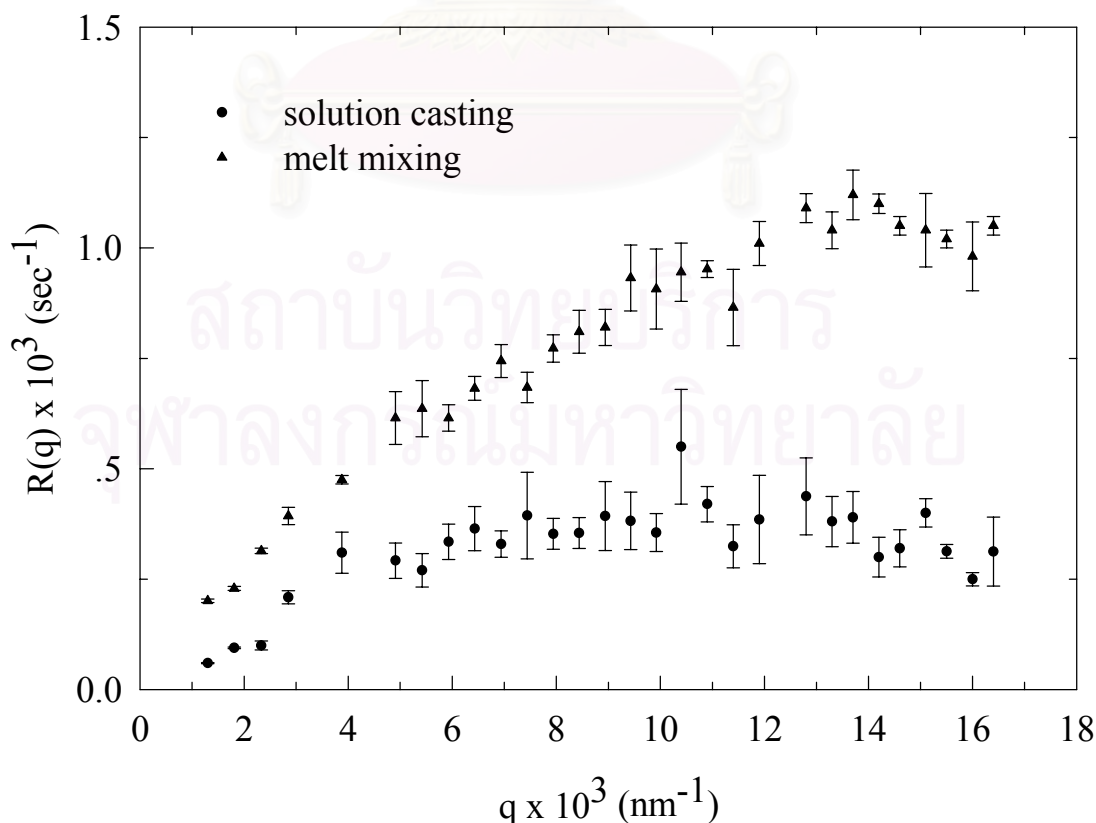


Figure 5.8: Effects of preparation method on $R(q)$ for SMA/PMMAe (10/90) blends, obtained from temperature jump experiments at 220 °C.

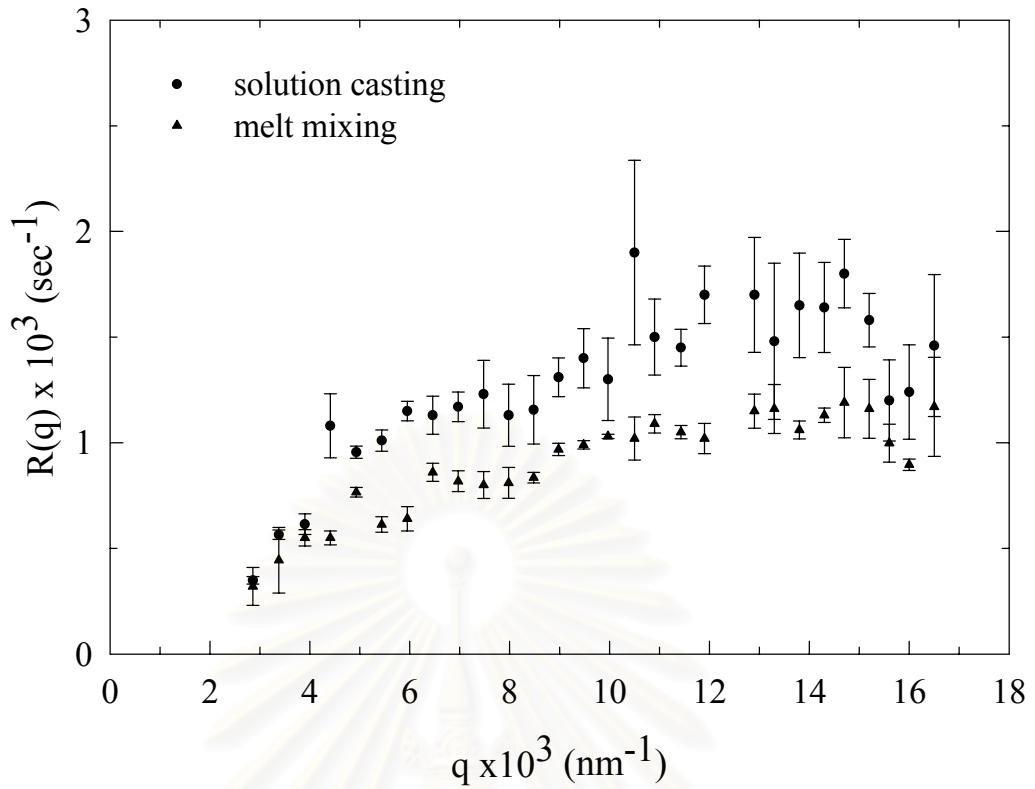


Figure 5.9: Effects of preparation method on $R(q)$ for SMA/PMMAe (20/80) blends, obtained from temperature jump experiments at 210 °C.

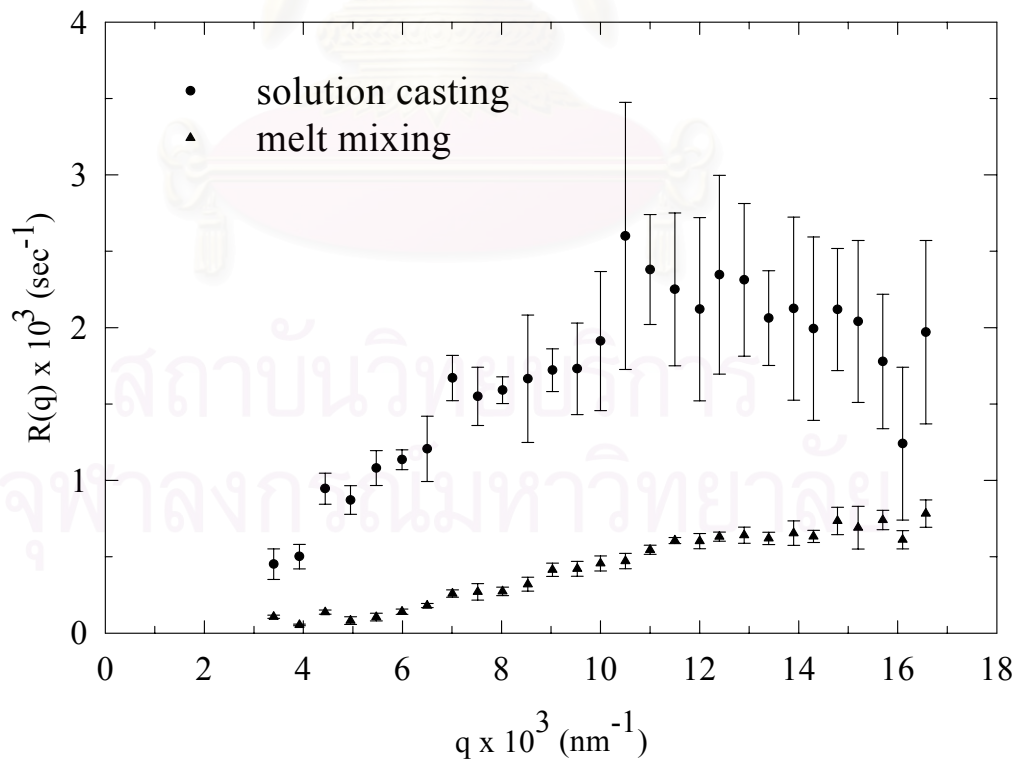


Figure 5.10: Effects of preparation method on $R(q)$ for SMA/PMMAe (30/70) blends, obtained from temperature jump experiments at 210 °C.

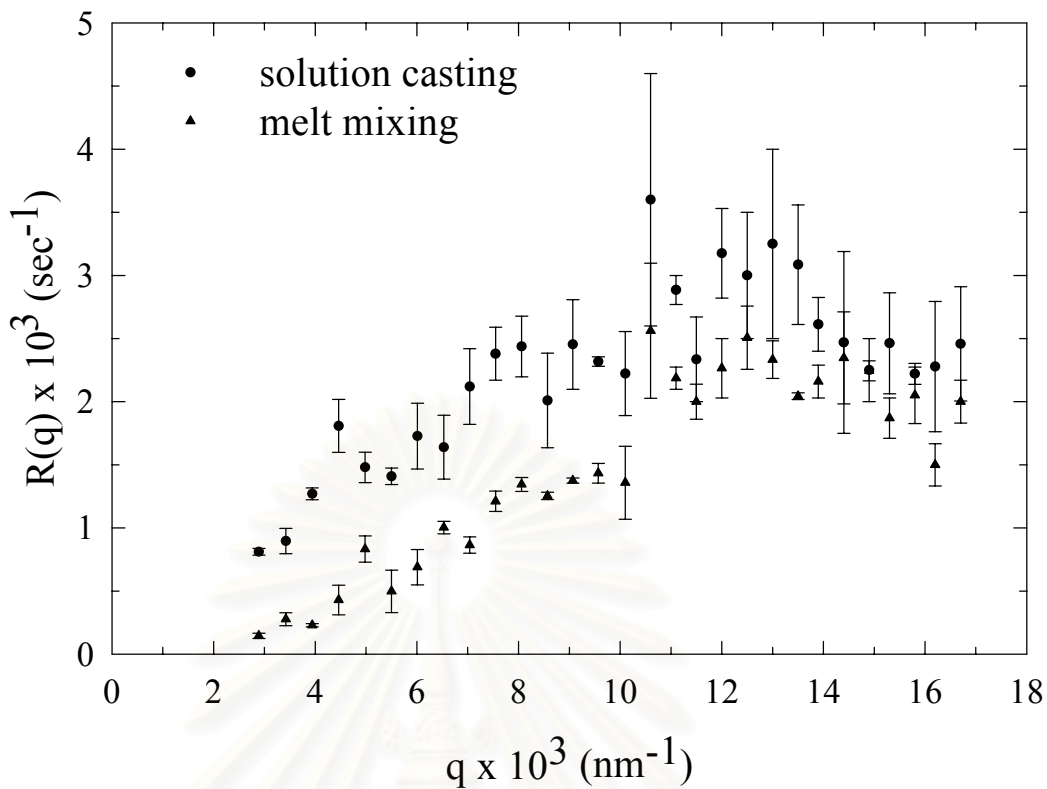


Figure 5.11: Effects of preparation method on $R(q)$ for SMA/PMMAe (40/60) blends, obtained from temperature jump experiments at 210 °C.

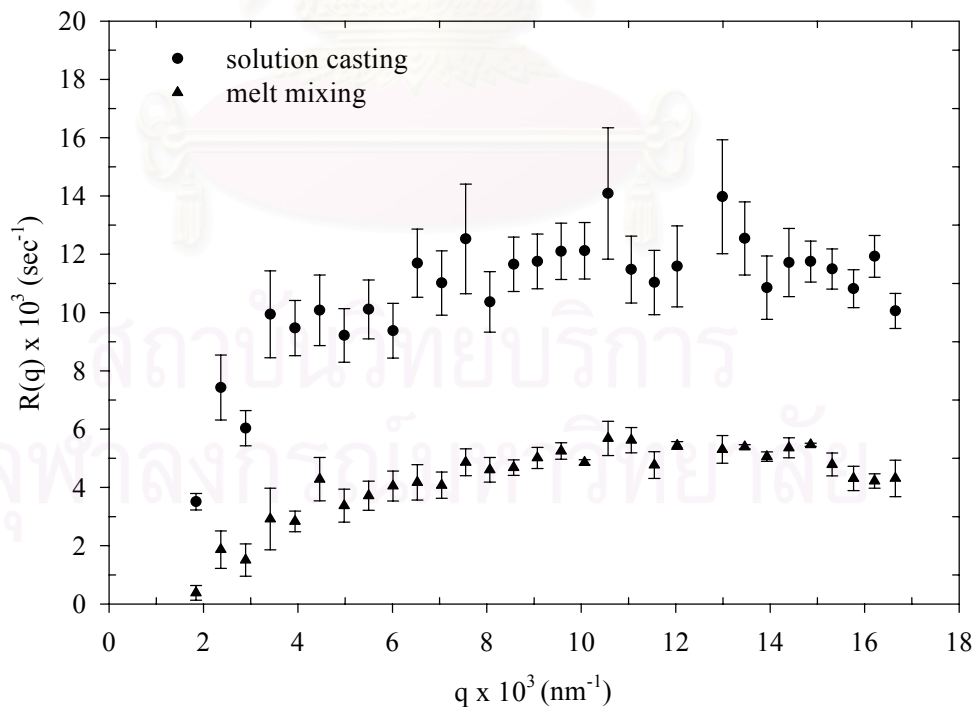


Figure 5.12: Effects of preparation method on $R(q)$ for SMA/PMMAe (40/60) blends, obtained from temperature jump experiments at 220 °C.

According to the linearised theory, the growth rates $R(q)$ should have a quadratic dependence on q^2 as shown in Equation 3.19 but in practice the curvature is much flatter than that as has been frequently reported in other literatures [Pavawongsak 1996; Manda 1998]. Non instantaneous temperature jumps have been suggested as a possible cause of such flat $R(q)$ curves [Carmesin *et al.* 1986]. Fernandez *et al.* [1989], who studied the blend of EVA and SCPE, attributed this to the result of off-scaled q_m .

5.3.2 The Growth Rate of Spinodal Decomposition between Intermediate and Late Stages

Comparisons of time changes in the maximum scattered intensity I_m and wave number q_m between solution cast and melt mixed blends at different compositions are shown in Figures 5.13 and 5.14 respectively. As seen in these figures, the maximum intensity and wave number follow the simple power law,

$$q_m \propto t^\alpha \quad (5.3)$$

and
$$I_m \propto t^\beta \quad (5.4)$$

where different values of exponents α and β have been suggested so far, for example, $\alpha = 1/3$ by Lifshitz and Slyozov [1961], $\alpha = 0.212$ and $\beta = 0.81$ by Langer *et al.* [1975], $\alpha \approx 1/3 - 1$ by Siggia [1979], $\alpha = 1/4$ by Siegert *et al.* [1993], or $\alpha = 0.9$ by Takeno *et al.* [1999]. This work, on the other hand, found that exponential values depend not only on sample preparation but also on phase separation time, temperature and composition. As seen in Figures 5.13 and 5.14, the exponent α of both compositions changes from zero in the early stage to about 0.6 in the intermediate SD and finally to 1.2 in the late stage of spinodal decomposition. However, the exponent β depends on composition, i.e., it changes from 2.7 in the intermediate stage SD to about 1.7 in the late stage SD for 20/80 SMA/PMMAe blends while for 40/60 SMA/PMMAe blends the exponent β decreases from about 2.2 to 2 in the case of solution casting and to 1.6 in the case of melt mixing. The

high value of exponent α as observed in this work might be due to the strong hydrodynamic contribution after each chain is released from the interconnecting lock as shown via the delay in the beginning of phase separation. However, the exponents β decreases at the longer time limit, thus the relationship between α and β deviates from the previous suggestion [Hashimoto et al. 1986a, 1986b, Tomlins et al. 1989, Lauger et al. 1995] where $3\alpha < \beta$ in the intermediate stage of spinodal decomposition, and $3\alpha = \beta$ in the late stage. This might be the result of multiple scattering since each specimen is too thick.

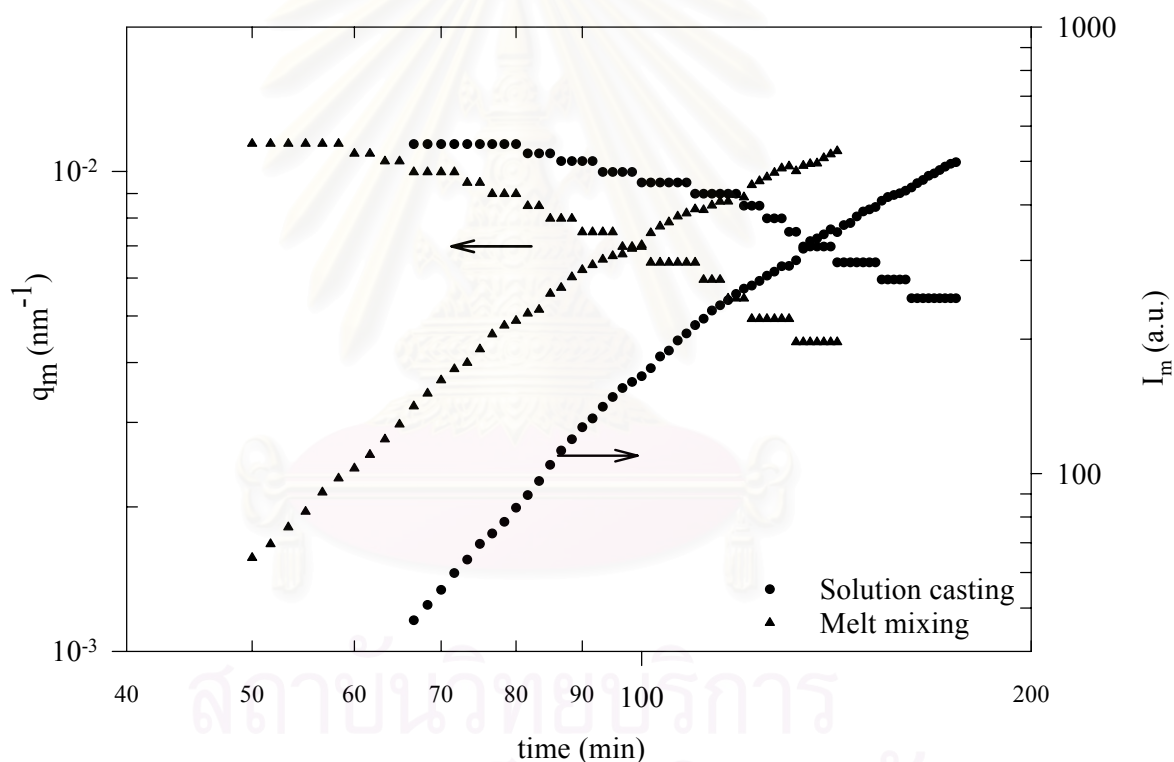
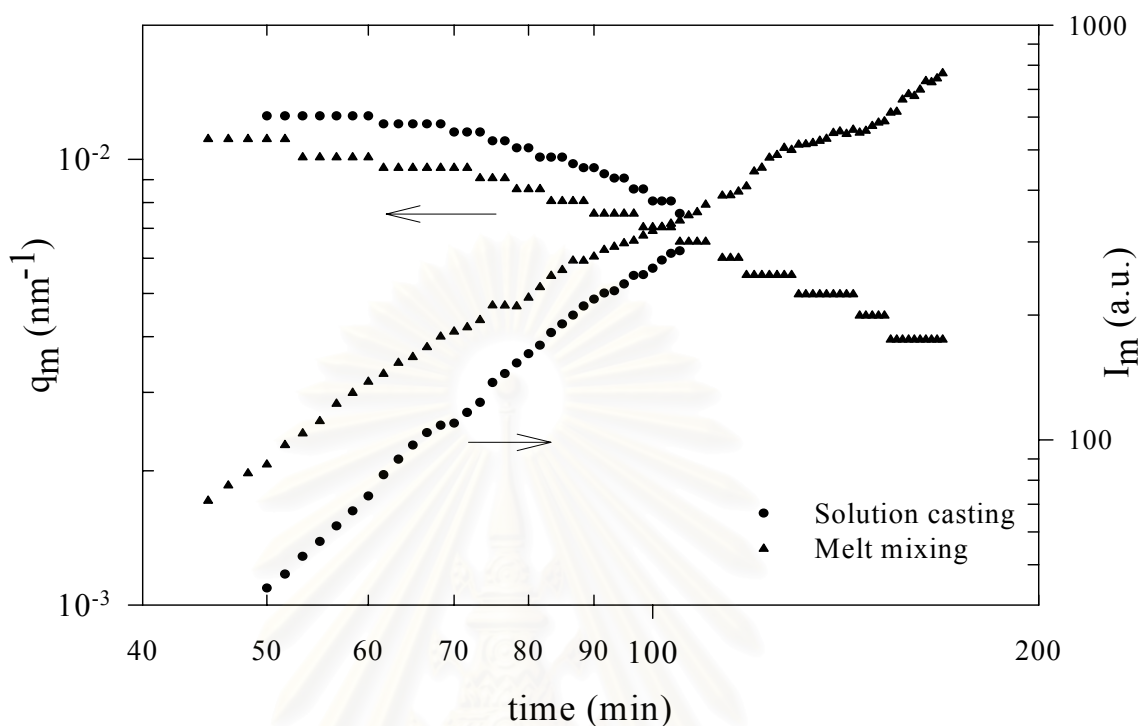


Figure 5.13: Time-change of q_m and I_m as observed by light scattering for solution cast and melt mixed 20/80 SMA/PMMAe blends at the temperature jump of 210 °C.



As seen in Figures 5.13 and 5.14, interestingly although both blends were phase separated at the same temperature, the melt mixed blends appear to advance to the late stage of spinodal decomposition faster than the solution cast ones. This is surprisingly inconsistent with other work by Cabral et al. [2000], who studied TMPC/dPS blends using neutron scattering technique. This is due to the fact that the spinodal boundary of that system occurs at higher temperature for melt mixed blends than for solution cast ones. It has been suggested that the fast phase separation for melt mixed blend of this system might be the result of the difference of the spinodal boundary: the spinodal boundary of melt mixed blends is lower than the solution cast blends. Furthermore, due to the effect of polymer relaxation, the melt mixed blends, which are extruded and suddenly quenched in the glassy state, seem to be away from equilibrium than solution cast blends, which slowly change during preparation. Comparing Figure 5.13 and Figure 5.14, it can be seen that the

Figure 5.14: Time change of q_m and I_m as observed by light scattering for solution cast and melt mixed 40/60 SMA/PMMAe blends at the temperature jump of 210 °C.

melt mixed 20/80 SMA/PMMAe blends phase separate much faster than the solution cast ones compared to the composition of 40/60 SMA/PMMAe. This might be attributed to the fact that the gap between spinodal curve of solution cast and melt mixed blends is closer at the composition of 40/60 SMA/PMMAe than at the composition of 20/80 SMA/PMMAe.

The dimensionless or reduced parameters of time, scattering wave number and intensity have been introduced in order to create a single master curve of each blends, which phase separated at different temperature jumps: the reduced time τ suggested by Chou and Goldberg [1979] is defined as,

$$\tau \equiv t/t_c \quad (5.5)$$

where t_c is the characteristic time of the system,

$$t_c = \frac{1}{q_m^2 D_{app}} \quad (5.6)$$

and the reduced wave number \bar{q}_m and intensity \bar{I}_m suggested by Hashimoto et al. [1986] are defined as,

$$\bar{q}_m = q_m(t) / q_m(t=0) \quad (5.7)$$

$$\bar{I}_m = I_m(t) q_m^3(t=0) / \int_{q_{min}}^{q_{max}} q^2 I(q, t) dq \quad (5.8)$$

As the consequence of these, the time changes in q_m and I_m from Figures 5.13 and 5.14 are replotted in Figures 5.15 and 5.16 using reduced variables: τ , \bar{q}_m , \bar{I}_m . Interestingly, the reduced wave vectors \bar{q}_m and the reduced maximum intensity \bar{I}_m from different compositions and preparation methods follow the same trend with nearly the same exponents. Imaginary lines have been drawn to illustrate the relationships between \bar{q}_m and τ , \bar{I}_m and τ . However, they fail to fall onto a single master curve as predicted by other literatures [Hashimoto et al. 1986b] especially the reduced intensity of each curve, which shows a noticed deviation from the single master curve indicating an invalidity of Equations 5.7 and 5.8. This could be due to the effect of preparation methods leading to different temperature dependence of

concentration fluctuation, which again might result from the difference of thermodynamic behaviour. In addition, an irregularity of the structure due to impurities, which might be trapped in the melt mixed samples, can result in different phase separation growth rates. Concerning the relationship between the exponents α and β , similar to the previous discuss, it still deviates from general suggestions.

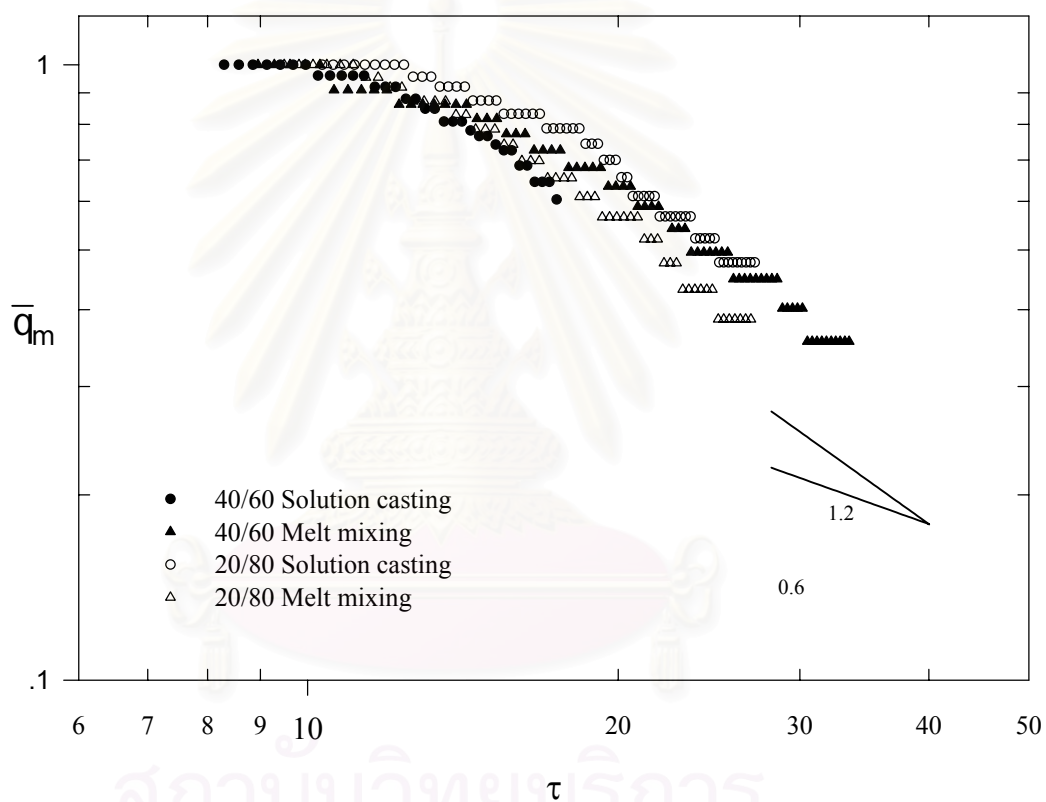


Figure 5.15: Plots of reduced time and the reduced maximum scattering wave number for SMA/PMMAe blends at different compositions and preparation methods obtained from a temperature jump experiment of 210 °C.

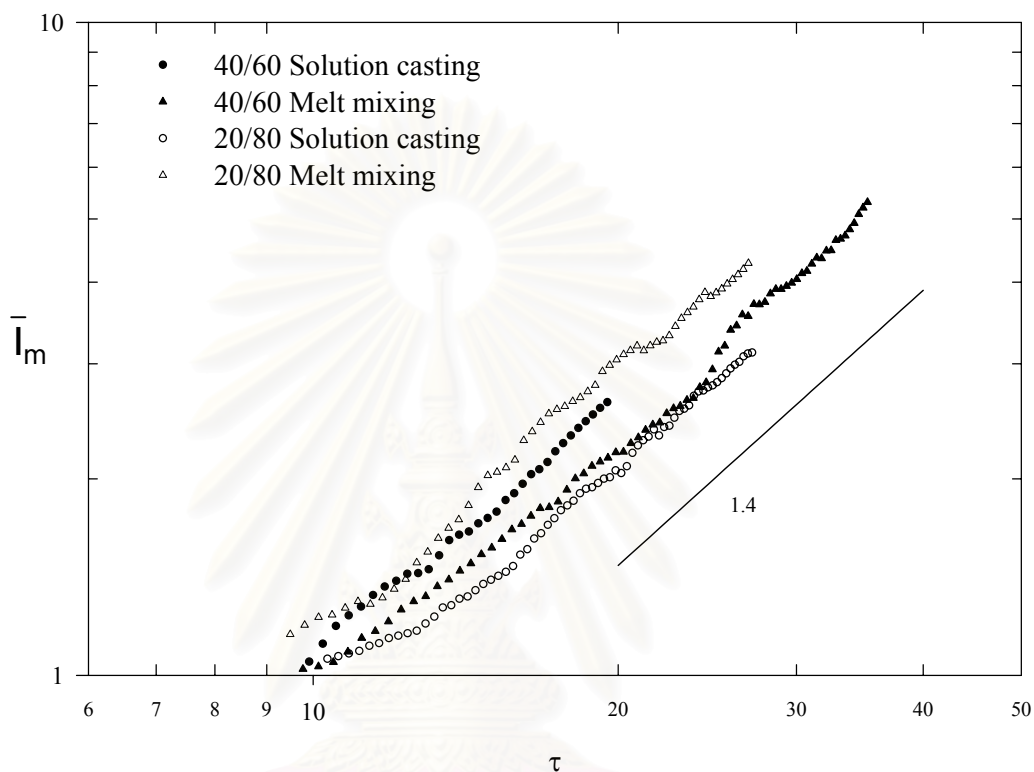


Figure 5.20 Plots of reduced time and the reduce maximum intensity \bar{I}_m for SMA/PMMAe blends at different compositions and preparation methods obtained from a temperature jump experiment of 210 °C.

5.4 The validity of Cahn-Hilliard Theory

The validity of Cahn-Hilliard theory was monitored via several criteria. According to such theory, the scattered intensity should increase exponentially with time providing the double $R(q)$ from the slope of the $\ln(I)$ versus time plot. Furthermore, from Equation 3.19 it is clear that the value of $R(q)q^2$ varies linearly with q^2 while the maximum scattering wave number q_m and growth rate $R(q_m)$ can be obtained from the intercept and slope of such plot as shown in Equations 3.25 and 3.26 respectively. Apparently, at the certain period our scattered intensity does follow

the exponential move as expected yet it fails to show the linear plot of $R(q)/q^2$ versus q^2 with several reason as already mentioned. Nonetheless, so far it is quite interesting to compare q_m and $R(q_m)$ from the Cahn-Hilliard theory with the directly observed data from light scattering experiment.

5.4.1 The maximum scattering wave number (q_m)

The maximum wave numbers q_m obtained from direct observation and calculation from the Cahn-Hilliard theory are shown in Figure 5.17. It can be clearly seen that the calculated data are in good agreement with the observed ones within the experimental error indicating the positive validity. On the other hand, interestingly as seen in Figure 5.17, both data appear to be virtually independent of temperature (i.e. of quench depth). The apparent non-dependence of q_m on quench depth has been reported for other systems [Higgins *et al.* 1989b]. It may result from the fact that to reach the deeper quenches, the sample passes through a long region of instability, and that the initial phase separation domain size simply reflects an early stage in this passage. Furthermore, it has been suggested that as the temperature is increased, the dissimilarity then increases and in order to deal with this the polymers will adjust their conformation resulting the increase of radius of gyration [Bates *et al.* 1994].

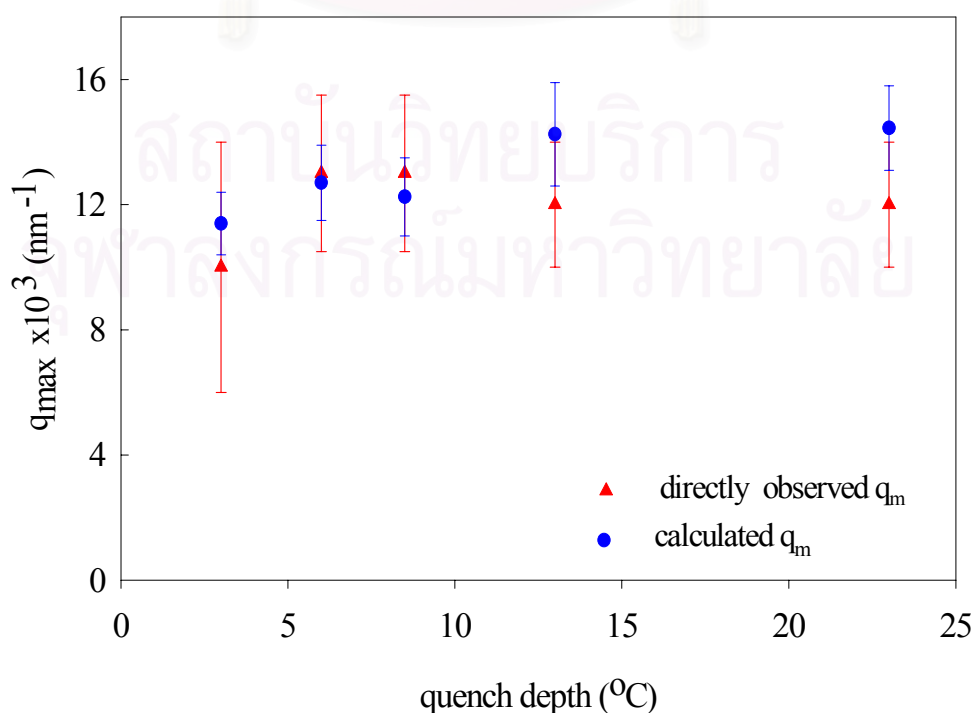


Figure 5.17: Comparison of q_m from direct observation and calculating from Cahn-Hilliard theory for solution cast SMA/PMMAe (30/70) blends

5.4.2. The maximum growth rate ($R(q_m)$)

Likewise the maximum wave number, the comparison of maximum growth rate $R(q_m)$ from direct observation and calculation are illustrated as the plot of $\sqrt{R(q_m)}$ with temperature. As can be seen from Figure 5.18, $\sqrt{R(q_m)}$ increases linearly with quench depth and follows the prediction from Cahn-Hilliard theory. However, since it changes with temperature, this is in contrast to the behaviour of q_m described in the previous section, and implies that, if q_m may reflect what happens at the instant of passing through the spinodal (or at least very soon afterwards), $R(q)$ is determined much more closely by the final temperature at which the phase separation develops. From Equation 3.34 if the thermal fluctuation term is neglected as well as the Onsager coefficient is assumed to be constant, the resulting equation will follow the classical Cahn-Hilliard linearised theory, where the alternative form of growth rate $R(q)$ can be written as,

$$R(q) = -q^2 M [\chi_s - \chi + \kappa q^2] \quad (5.9)$$

where M is mobility constant and χ_s is the interaction parameter at the spinodal temperature (T_s), which for a binary system can be given by the function,

$$2\chi_s = \frac{1}{N\phi_0(1-\phi_0)} \quad (5.10)$$

where ϕ_0 is the volume fraction of component A at equilibrium and degree of polymerisation of both polymers are assumed to be equivalent (approximately N).

From Equation 5.9, the maximum relative growth rate ($R(q_m)$) can be expressed as,

$$R(q_m) = \frac{M[\chi - \chi_s]^2}{2K} \quad (5.11)$$

Inserting the usual $\chi \propto 1/T$ variation into Equation 5.11, we then obtain

$$R(q_m)^{1/2} \propto (T - T_s) \quad (5.12)$$

which clearly manifests how $R(q_m)$ relates to square of the quench depth.

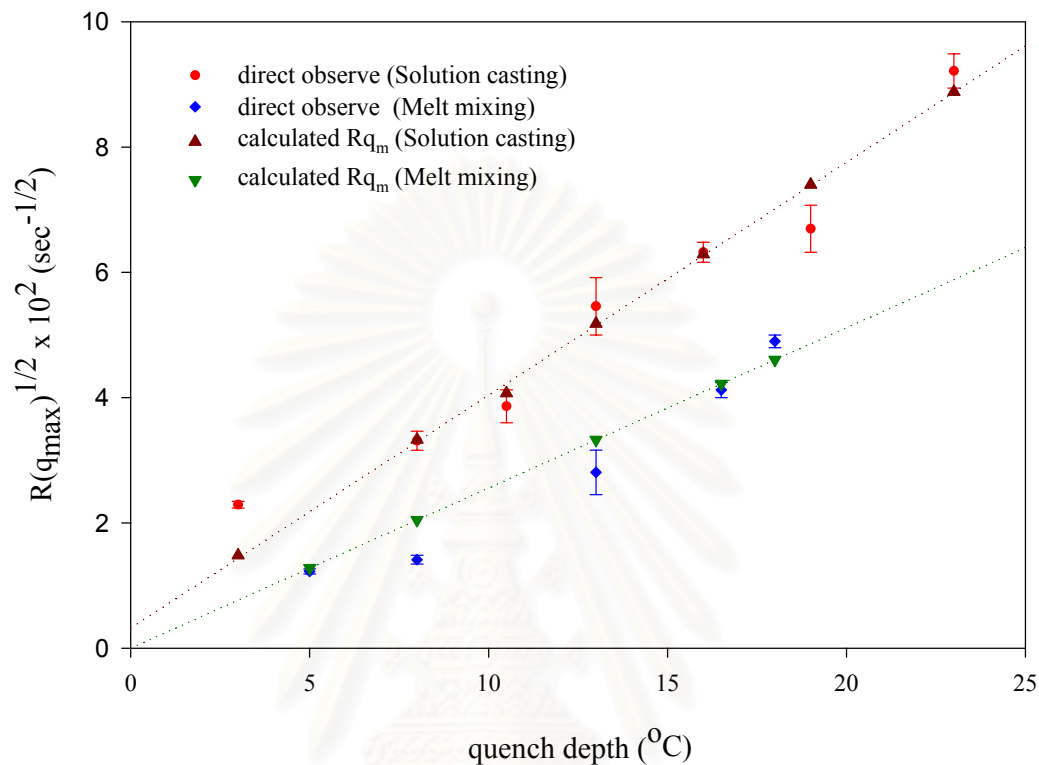


Figure 5.18: Comparisons of the maximum growth rate $R(q_m)$ from direct observation and calculation from the Cahn-Hilliard theory for SMA/PMMAe (40/60) blends. The imaginary lines indicate the trend of $R(q_m)$.

Considering the same quench depth, the solution cast blends appear to show higher maximum growth rates than the melt mixed ones which is not as would be expected from the relative positions of the phase boundaries, and would again imply differences in the thermodynamic behaviour.

5.5 The Scaling Analysis for the Intermediate and Late Stage of Spinodal Decomposition

5.5.1 The analysis of scaling function $F(X)$

Following the scaling analysis as reviewed in Chapter 3, Furukawa [1985] has introduced the well-known scaled solution of an equation of motion for a d -dimensional isotropic system (Eq. 3.51), which is apparently very useful since it can describe the kinetics of phase separation in the late stage very well even after the formation of droplets. Hashimoto et al. [1986a, 1991], on the other hand, suggested that the scattered intensity $I(q,t)$ can be generally related to the universal scaling function, $\tilde{S}(X)$, as

$$I(q,t) \sim \langle \eta^2 \rangle q_m(t)^{-3} \tilde{S}(X) \quad (5.13)$$

where $\langle \eta^2 \rangle$ is the mean square of refractive-index fluctuations, which apparently depends on the concentration fluctuation $\delta c(t)^2$.

The scaling function $F(X)$, which is defined as

$$F(X) \equiv I(q,t) q_m(t)^3 \quad (5.14)$$

therefore can be related to the universal scaling function by

$$F(X) = \langle \eta^2 \rangle \tilde{S}(X) \quad (5.15)$$

Figure 5.19 Plots of reduced time and reduce scattering wave vector \bar{q}_m for SMA/PMMAe blends at different compositions and preparation methods obtained from a temperature jump experiment of 210 °C. According to Equation 5.15, it is clearly seen that in the intermediate stage

SD, where the amplitude of concentration still increases with time resulting in an increase in $\langle \eta^2 \rangle$, consequently the scaling function $F(X)$ increases with time. However this breaks down as soon as the $\langle \eta^2 \rangle$ reaches equilibrium in the late stage, leading the universality of the scaling function.

Figures 5.19-5.22 manifest time evolution of the scaling function $F(X)$ constructed on the basis of Equation 5.14. In part (a) of each figure, $F(X)$ is apparently time dependent; this range is consequently defined as the intermediate stage of phase separation. However, after that period, $F(X)$ is apparently independent of time, the master curve then can be obtained. This has been known as the late stage of spinodal decomposition. Comparing Figures 5.19 and 5.20, it appears that the slopes of scaling function become steeper with increasing the

temperature jump. In addition, the blend, which was phase separated at shallow quench depth, also exhibited the single master curve slower than the one which was annealed at deeper quench depth. No clear evidence of any difference of the slopes between the solution cast and melt mixed blends was observed as shown in Figures 5.20 and 5.21; nonetheless, the melt mixed blend appears to get into the late stage of phase separation slightly faster than the solution cast blends. It should be noted that these two figures are examples to show the difference between solution cast and melt mixed blends. The blends from other compositions and phase separation temperatures may actually show some minor differences, yet they follow the same trend as previously mentioned. Surprisingly, the slopes of 40/60 SMA/PMMAe blends are much steeper than the 20/80 SMA/PMMAe blends and this might be the result of the fact that 40/60 SMA/PMMAe blends undergo phase separation faster than 20/80 as they contain less PMMA, which has an unusually high monomeric friction coefficient. This result is consistent with the previous discussion about the Cahn-Hilliard relative growth rate, $R(q)$, (Section 5.3.1), i.e., comparing at the same phase separation temperatures, $R(q)$ of 40/60 SMA/PMMAe blends is always higher than that of 20/80 SMA/PMMAe blends, indicating faster phase separation.

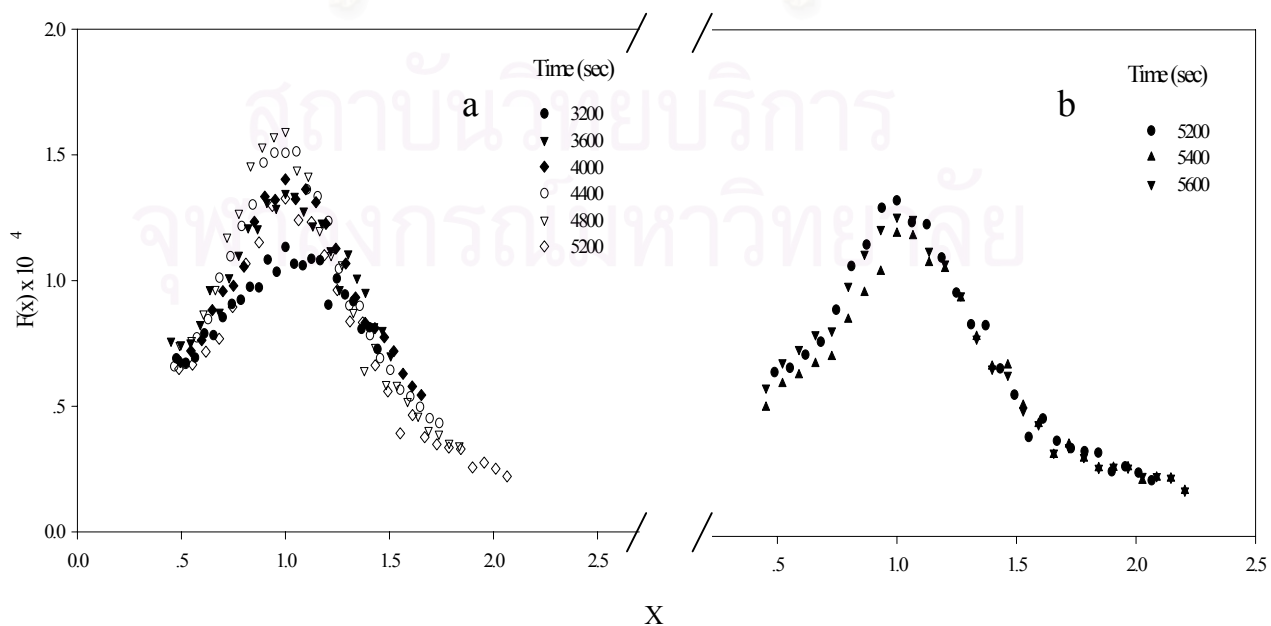
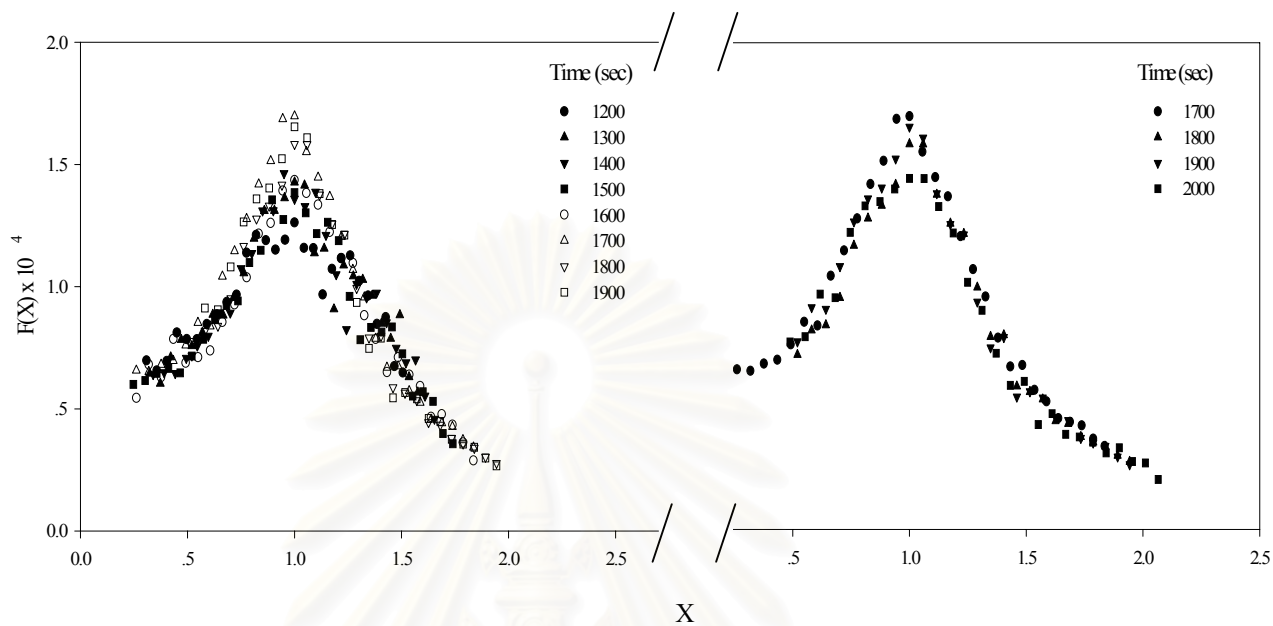


Figure 5.19: Time evolution of the scaling function $F(X)$ for a melt mixed 20/80 SMA/PMMAe, quench to 210 °C. Figure 5.19 (a) illustrates region where $F(X)$ depends



SMA/PMMAe, quench to 220 °C. Figure 5.20 (a) illustrates region where $F(X)$ depends on time, while Figure 5.20 (b) shows $F(X)$ being independent of time, indicating the late stage of spinodal decomposition.

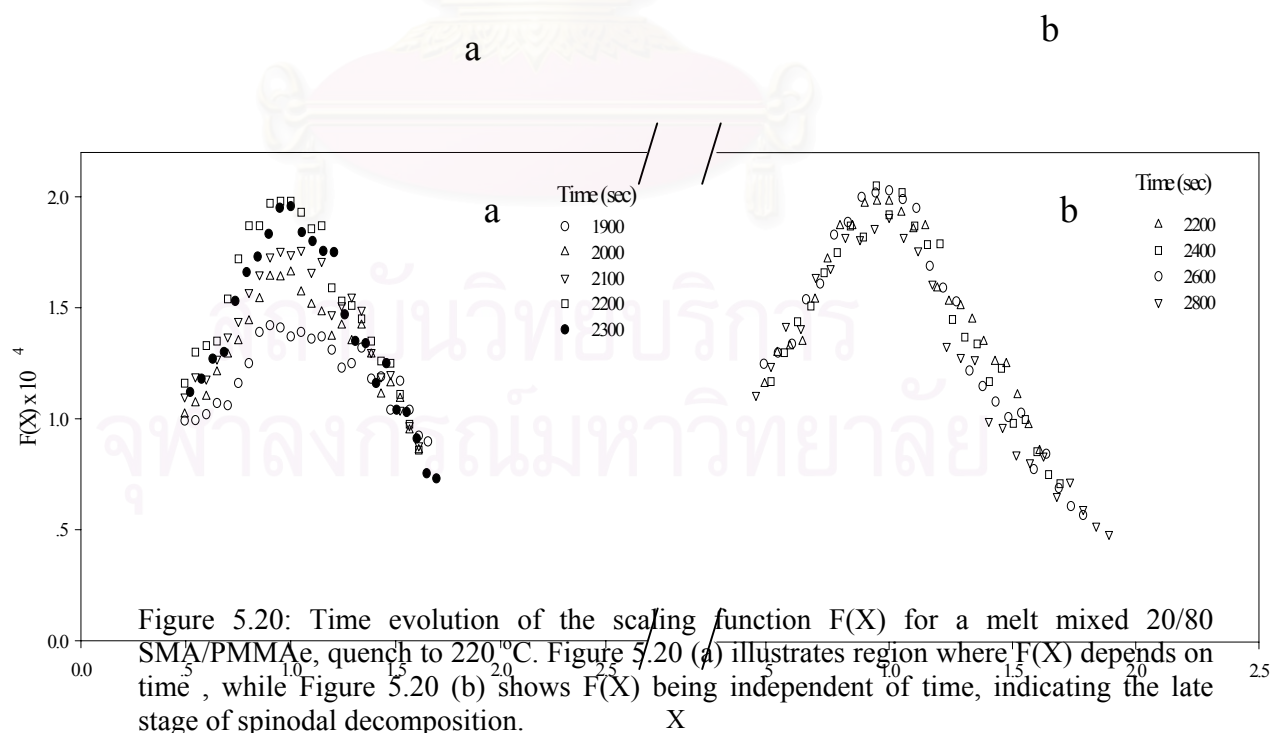
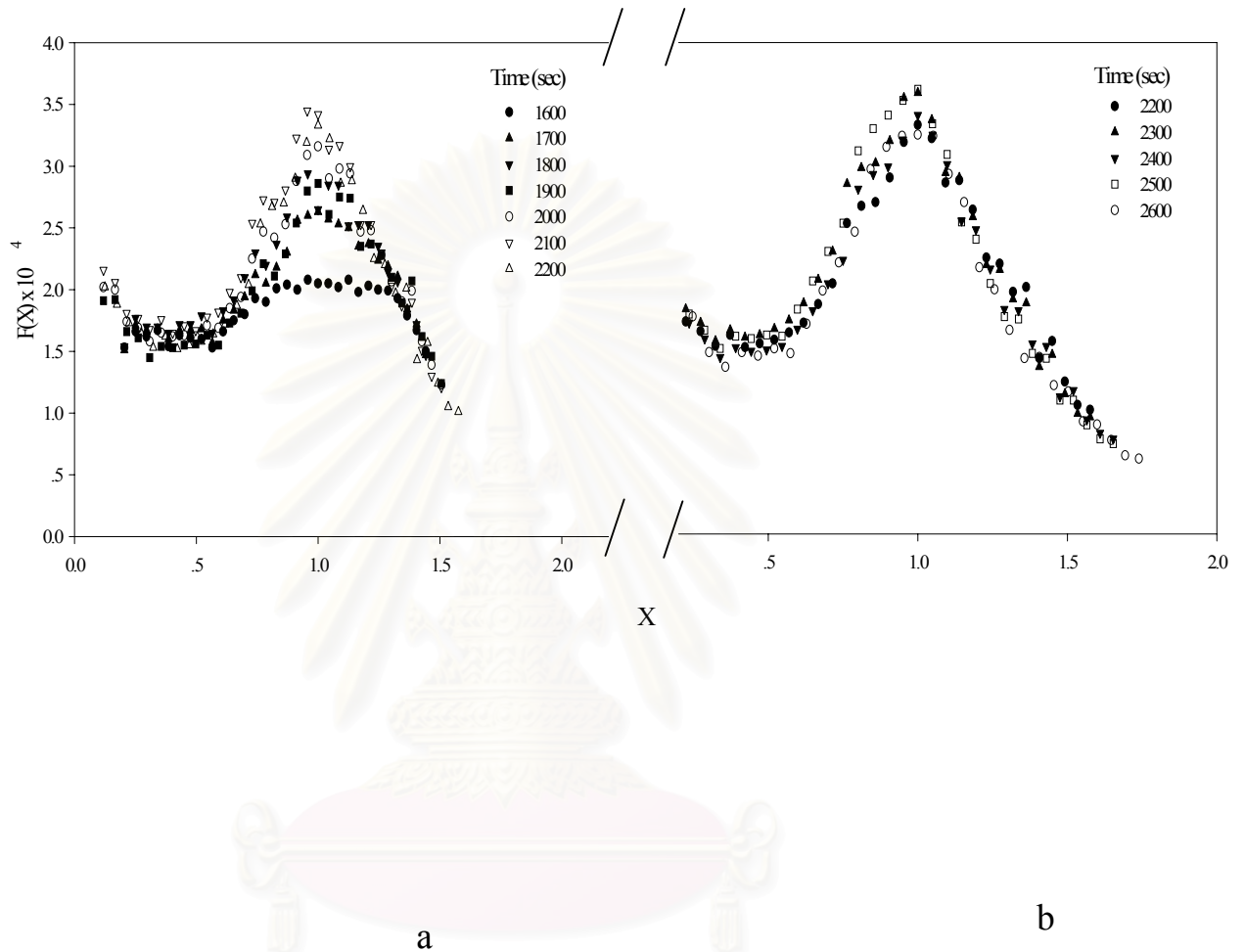


Figure 5.20: Time evolution of the scaling function $F(X)$ for a melt mixed 20/80 SMA/PMMAe, quench to 220 °C. Figure 5.20 (a) illustrates region where $F(X)$ depends on time, while Figure 5.20 (b) shows $F(X)$ being independent of time, indicating the late stage of spinodal decomposition.

Figure 5.21: Time evolution of the scaling function $F(X)$ for a solution cast 20/80 SMA/PMMAe, quench to 220 °C. Figure 5.21 (a) illustrates region where $F(X)$ depends on time, while Figure 5.21 (b) shows $F(X)$ being independent of time, indicating the late stage of spinodal decomposition.



5.5.2 Comparison with Theoretical Scaling Structure Function

In order to facilitate the comparison of the experimental result with an estimated equation, the scaling function can be normalised [Marro *et al.* 1979; Komura *et al.* 1985] as,

$$\tilde{F}(X) = \frac{F(X)}{\int_{q_{\min}}^{q_{\max}} q^2 I(q, t) dq} \int_{X_{\min}}^{X_{\max}} X^2 \tilde{S}(X) dX \quad (5.16)$$

where $\tilde{S}(X)$ is the universal scaling function as defined in Chapter 3, X_{\min} and

Figure 5.22: Time evolution of the scaling function $F(X)$ for a solution cast 40/60 SMA/PMMAc, quenched to 220 °C. Figure 5.22 (a) illustrates region where $F(X)$ depends on time, while Figure 5.22 (b) shows $F(X)$ being independent of time, indicating the late stage of spinodal decomposition.

$$\int q^2 I(q, t) dq = \int X^2 F(X) dX \quad (5.17)$$

Following a number of numerical simulations and fittings with experimental results as pointed out in Chapter 3.2.7.3, Furukawa elegantly introduced two types of the universal scaling function profile $\tilde{S}(X)$ depending on the surface transitions:

$$\tilde{S}(X) = \frac{4X^2}{3 + X^8} \text{ for the change in percolating regime} \quad (5.18)$$

$$\tilde{S}(X) = \frac{3X^2}{2 + X^6} \text{ for the change in cluster regime} \quad (5.19)$$

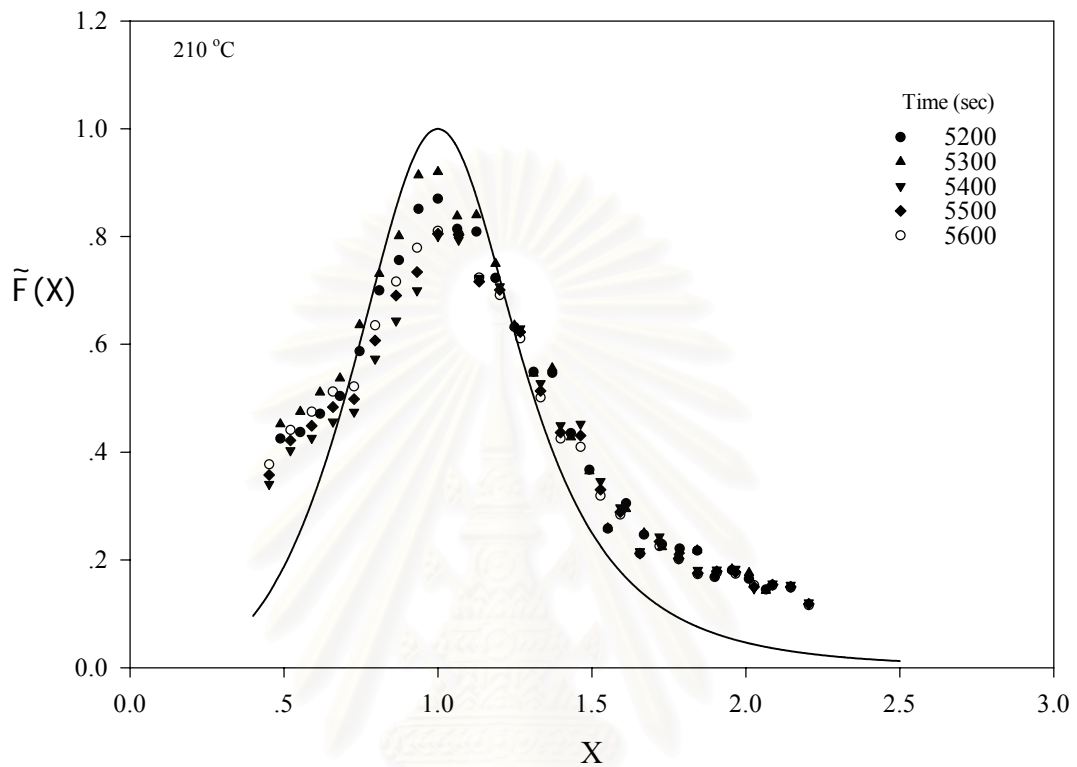
Hashimoto *et al.* [1986a] and Takeno *et al.* [1999] suggested that Equation 5.18 is suitable for critical mixture since each phase always keeps percolation even in the late stage of phase separation, while for off-critical mixture the minority phase cannot keep percolation even longer; the system subsequently undergoes percolation to cluster transition. Thus Equation 5.19 is preferable.

Recently, Furukawa [1986] proposed that for a deep quench, $\tilde{S}(X)$ should be proportional to X^3 rather than X^2 [Furukawa 1986], as a consequence of which the scaling function is given as,

$$\tilde{S}(X) = \frac{3X^3}{2 + X^9} \quad (5.20)$$

Figures 5.23 – 5.25 show different plots of the normalised scaling function based on Equation 5.16 using different kinds of universal scaling function. It appears that the normalised curve based on the cluster regime profile (Eq 5.19) fits with the theoretical profile better than the theoretical profile for percolation regime especially at high X . This is in agreement with the previous literatures by Hashimoto *et al.* [1986a] and Takeno *et al.* [1999] since both compositions used in this work are off-critical as depicted in Figure 5.5. Although the quench depth in this present work is

quite deep (approximately 17 °C for the temperature jump of 210 °C and 27 °C for the temperature jump of 220 °C), the fit with the theoretical scaling function for a deep



quench shows less agreement than such the simple function for cluster regime especially at high X values. This might be as the result of system dependence since Equation 5.20 actually was obtained from fitting with other experimental data and due to the extraordinary slow phase separation of our system this might lead to a deviation of the plot.

สถาบันวิทยบริการ
จุฬาลงกรณ์มหาวิทยาลัย

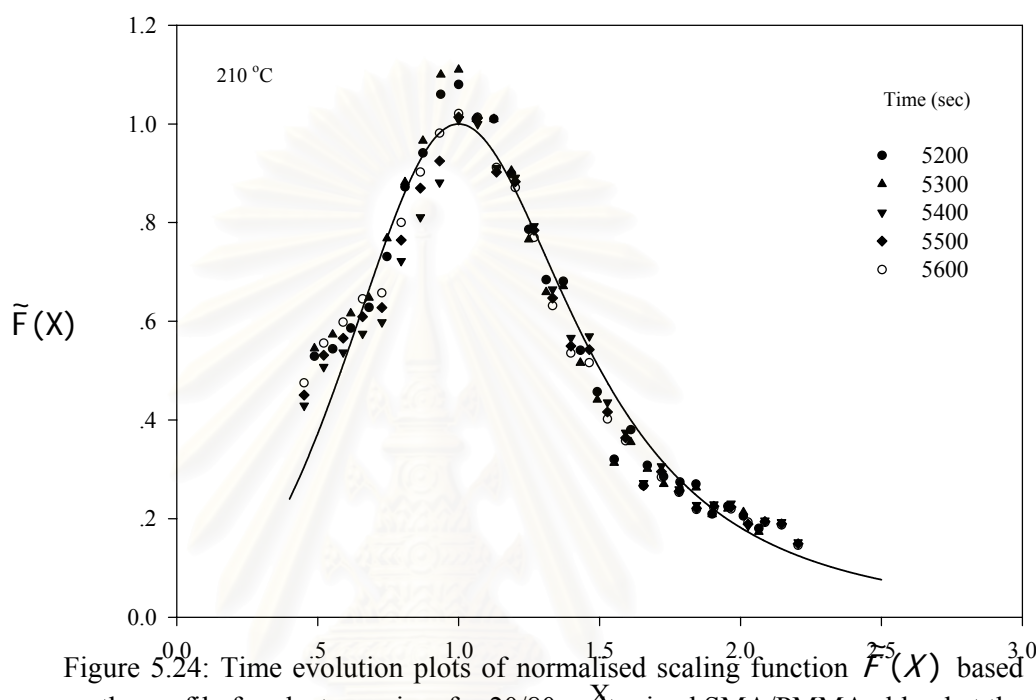


Figure 5.24: Time evolution plots of normalised scaling function $\tilde{F}(X)$ based on the profile for cluster regime for 20/80 melt mixed SMA/PMMAe blend at the jump temperature of 210 °C. The solid line corresponds to the theoretical scaling function for cluster regime (eq. 5.19).

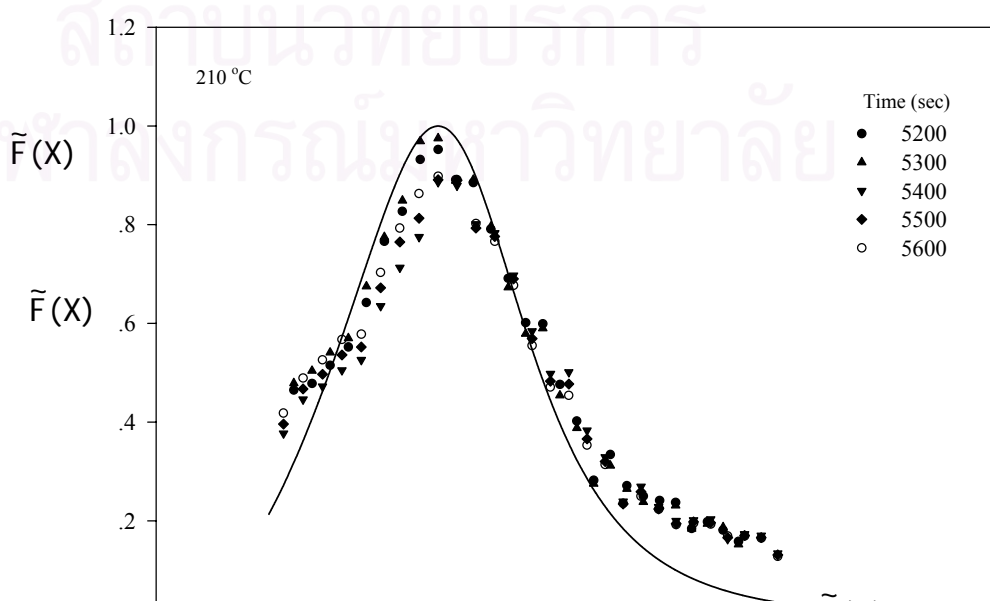


Figure 6.24: Time evolution plots of normalised scaling function $\tilde{F}(X)$ based on the profile for cluster regime for 20/80 melt mixed SMA/PMMAe blend at the jump temperature of 210 °C. The solid line corresponds to the theoretical scaling function for cluster regime (Eq. 5.19).

Figures 5.26-5.28 show normalised scaling function $\tilde{F}(X)$ at different jump temperatures and different compositions. The profile for cluster regime can still describe the phase separation behaviour at the late stage very well even at deeper quench depth (220 °C) and other compositions.

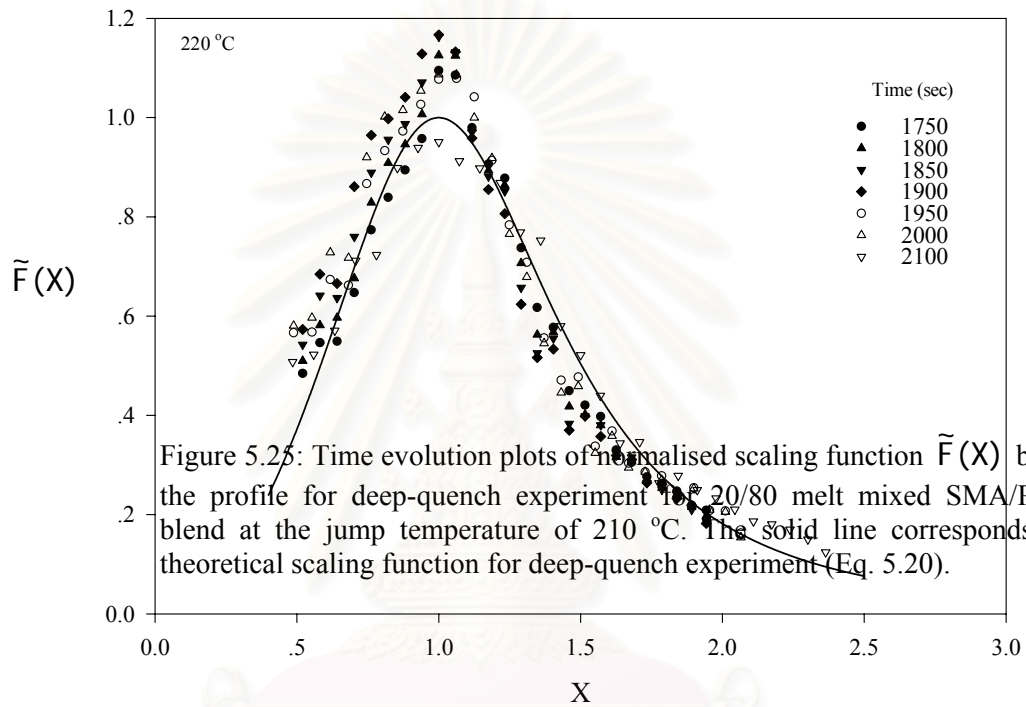


Figure 5.26: Time evolution plots of normalised scaling function $\tilde{F}(X)$ based on the profile for cluster regime for 20/80 melt mixed SMA/PMMAe blend at the jump temperature of 220 °C. The solid line corresponds to the theoretical scaling function for cluster regime (Eq. 5.19).

จุฬาลงกรณ์มหาวิทยาลัย

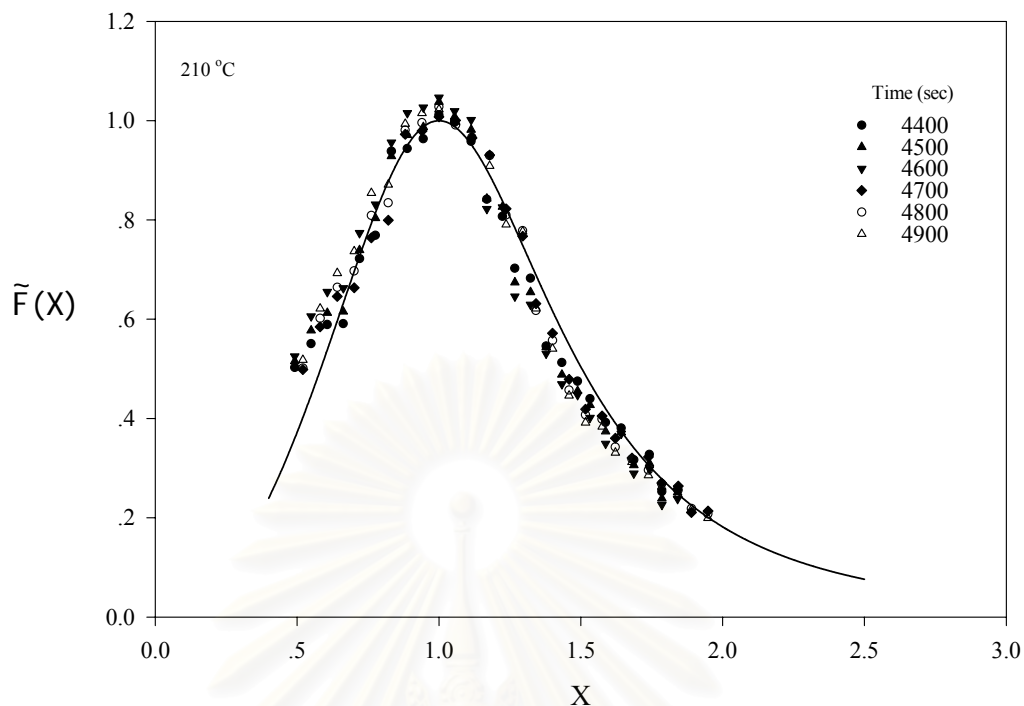


Figure 5.27: Time evolution plots of normalised scaling function $\tilde{F}(X)$ based on the profile for cluster regime for 40/60 melt mixed SMA/PMMAe blend at the jump temperature of 210 °C. The solid line corresponds to the theoretical scaling function for cluster regime (Eq. 5.19).

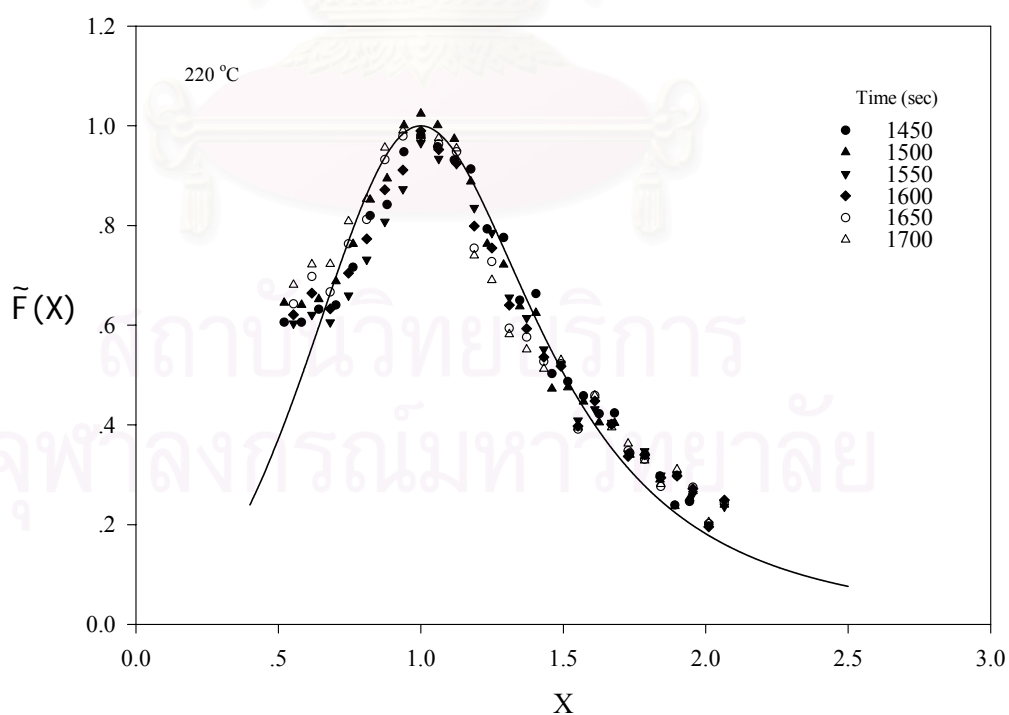


Figure 5.28: Time evolution plots of normalised scaling function $\tilde{F}(X)$ based on the profile for cluster regime for 40/60 melt mixed SMA/PMMAe blend at the jump temperature of 220 °C. The solid line corresponds to the theoretical scaling function for cluster regime (Eq. 5.19).

5.6 Delay Time Discussion

According to the Cahn - Hilliard theory, the phase separation via spinodal decomposition should occur spontaneously after heating into the phase separation regime. Surprisingly, it was however found that a delay time frequently appears at the beginning of phase separation (shown in Figure 5.3). Caution should be shown in interpreting these delays in terms of physical behaviour because there are a number of potential limitations in the technique which may show up as artefacts such as the delay time. The response time of the light scattering used in this work is believed not to be a problem since from Figure 5.3 intensities increase exponentially after such a delay time conforming the linearised theory, indicating that the intensities do still fall in the early stage. The peak first grows at a particular angle and then shifts toward the low wave vector as would be expected for spinodal decomposition (shown in Figure 5.29).

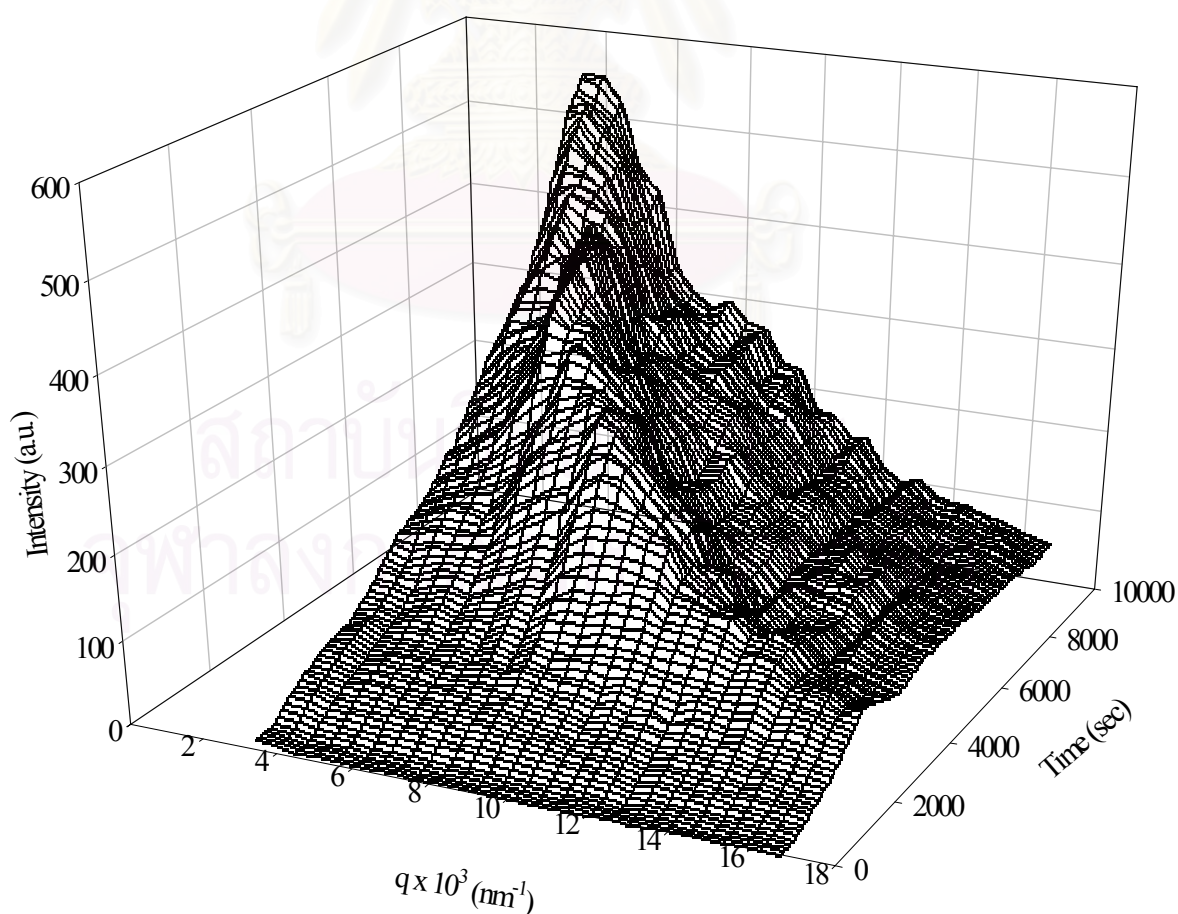


Figure 5.29: A typical plot of intensity against time and q for melt mixed (40/60) SMA/PMMAe blends, obtained from a temperature jump experiment at 210 °C.

5.6.1 Effect of Scattering Wave Number

Figure 5.30 reveals one important behaviour: the delay time at high q is less than at low q . In other words, the scattered intensity with shorter characteristic length r or higher wave vector q proceeds toward spinodal faster than that having a long r or lower q . This is expected for early and intermediate stage as small fluctuations grow in amplitude earlier than the long wavelength ones.

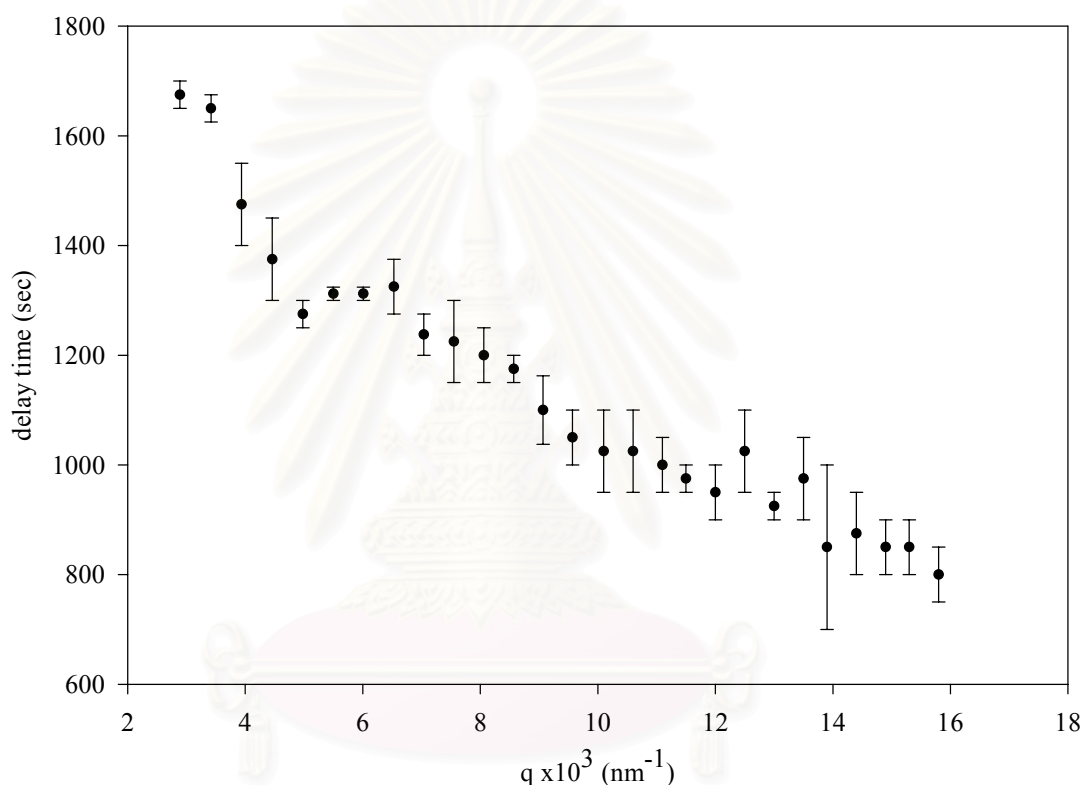


Figure 5.30: A plot of delay time against q for melt mixed SMA/PMMAe (40/60) blend, from a temperature jump experiment at 205 °C.

5.6.2 Effect of Composition

Figures 5.31-5.32 display the variation of the delay times with the quench depth for several compositions. Dotted lines show the trend of variation for each composition. It should be noticed that the error bar of quench depth was omitted herein for the sake of clarity. As quench depth decreases, the delay time increases substantially. This is due to the reduction in phase separation driving force as quench

depth decreases. There is no clear difference among composition within experimental error since if the error from estimation spinodal point is included, this can shift each curve almost 2 °C to either left or right. Considering all composition, it appears that delay time is inversely related to $R(q)$, i.e., those which have high $R(q)$, have low delay time.

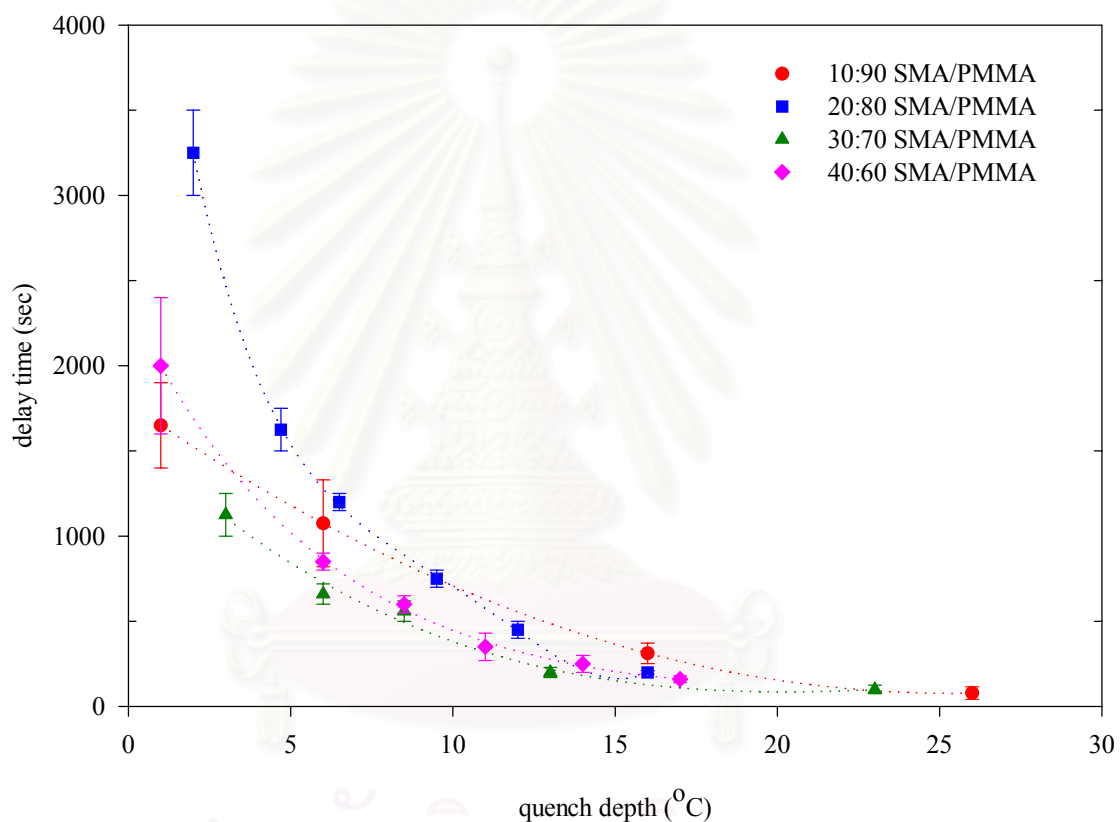


Figure 5.31: Plots of delay time against quench depth for solution cast SMA/PMMAe blends at different compositions.

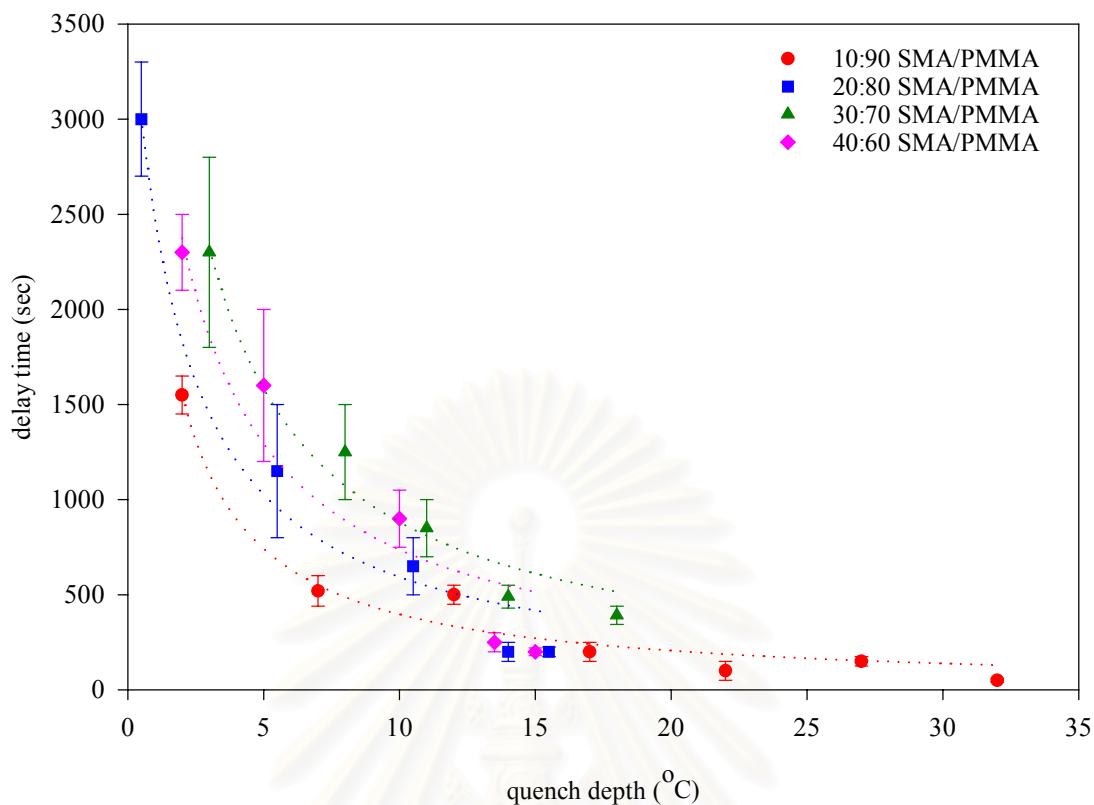
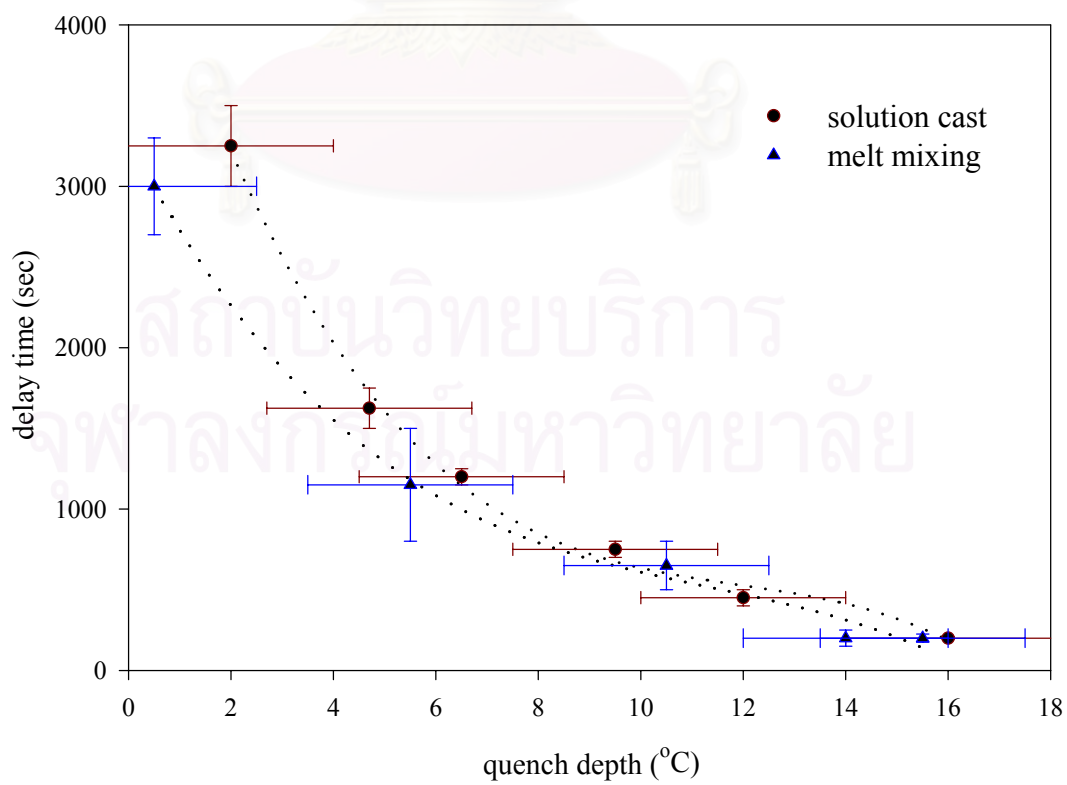
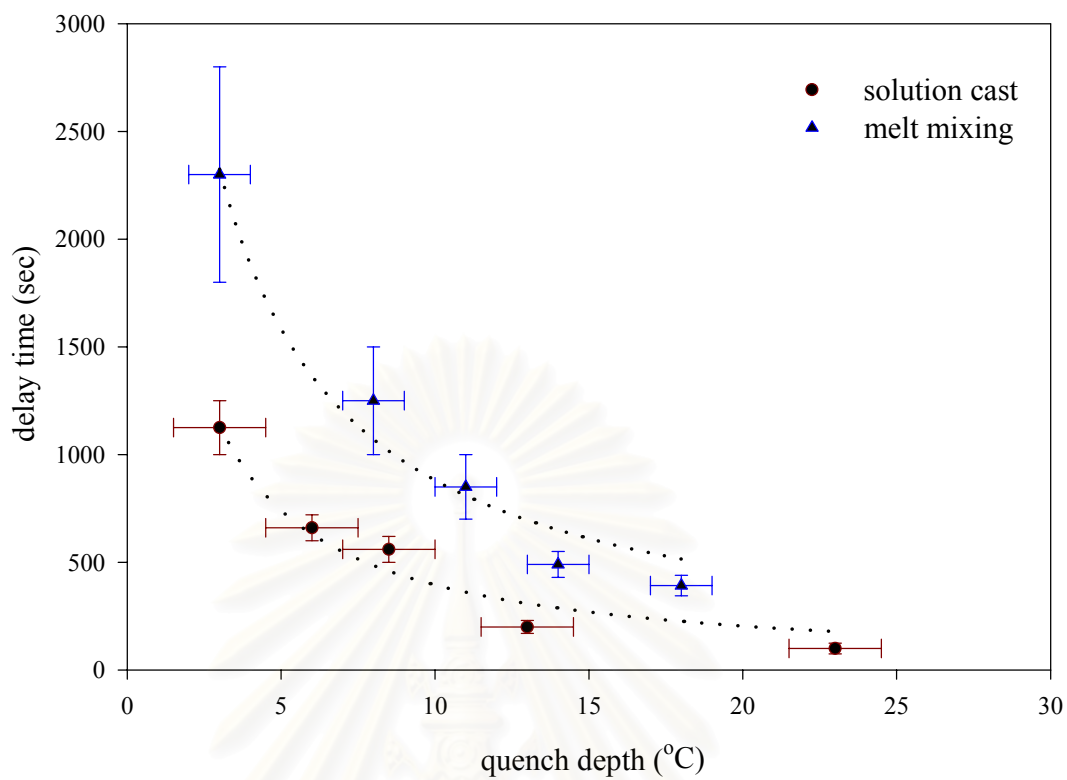


Figure 5.32: Plots of delay time against quench depth for melt mixed SMA/PMMA blends at different compositions.

5.6.3 Effect of sample preparation

It was found the pronounced difference between two preparation methods in 30/70 SMA/PMMA blends, which is believed to be the critical composition - the melt mixed blends show much higher delay time than the solution cast one as seen in Figure 5.33. Nevertheless, there appear only small differences within experimental errors between both methods for other compositions as shown in Figure 5.34.



5.6.4 Theoretical approach

Clarke *et al.* [1997] recently demonstrated that the effect of viscoelasticity due to entanglements can delay the onset of phase separation. According to the modified Cahn-Hilliard model by Clarke, starting from Equation 3.43 in Chapter 3, if we first assume that the delay time τ_d is given by the relation, $S(q, \tau_d) \approx S(q, 0)$, and after that time the decaying term is negligible, then we have

$$1 \approx (1-A_1) \exp\{-R_2\tau_d\} \quad (5.21)$$

where R_2 is related to the observed modified growth rate, which includes the slowing down due to viscoelasticity. For the sake of simplicity, R_2 thereafter is replaced by $R(q)$. From Clarke's paper [Clarke *et al.* 1997], if we assume that the rates associated with concentration fluctuation dynamics are much slower than the rheological rates, Equation 5.21 then can be written as,

$$|R(q)\tau_d| \approx \ln(1+2C_0(q)M\tau q^2) \quad (5.22)$$

The mobility of concentration fluctuations M may be written as,

$$M = \frac{kTNe}{3\zeta N} \quad (5.23)$$

so that,

$$M\tau \approx \frac{N^2 b^2}{3\pi^2} \quad (5.24)$$

which is independent of the monomeric friction coefficient.

As C_0 relies on types of entanglement dominating the system, it can be seen that Equation 5.22 depends on the model chosen. If the A-B entanglement model is chosen, it results in the product of delay time and the relative growth rate being independent of q ,

$$|R(q)\tau_d| \approx \ln\left(1 + \frac{24N^2}{\pi^2 Ne^2}\right) \quad (5.25)$$

On the other hand, if we assume that PMMA dominates the rheological properties of the system, i.e., the system behaves as an A-A entanglement network, Equation 5.22 can be written as:

$$|\mathbf{R}(q)\tau_d| \approx \ln \left(1 + \frac{2\phi_{\text{PMMMA}}N^2b^2}{\pi^2N_e}q^2 \right) \quad (5.26)$$

Equations 5.25 and 5.26 can be used to test whether observed delay times and growth rates are consistent with known rheological data. The principal advantage of Equations 5.25 and 5.26 is that the effect of the quench depth have been factored out. As shown in Equations 5.25 and 5.26, it can be seen that the values of $\tau_d\mathbf{R}(q)$ can be used to distinguish whether A-B or A-A entanglement networks are appropriate for this system. For A-B entanglements, the product of delay time and growth rate should be independent of q , whereas in the case of A-A entanglements $\tau_d\mathbf{R}(q)$ depends on q . $\tau_d\mathbf{R}(q)$ was plotted against q for both solution cast and melt mixing methods as shown in Figure 5.35. It was found that $\tau_d\mathbf{R}(q)$ apparently depends on sample preparation method; solution cast blends show higher $\tau_d\mathbf{R}(q)$ values than those of melt mixed one.

In Figure 5.35 we plotted the variation with q of Eq 5.26 using upper and lower limits of N_e , coupled with the use of $b = 0.22$ nm.[Brandrup *et al.* 1992] and $N = 1200$. Not only is it clear that the experimental q -variation is very much less than predicted, but the values of N_e required to fit the data are nonsense, being of order unity or less! On the other hand, if we assume there is effectively no q -variation and use Eq 5.25 to obtain values of N_e from the average values of $\tau_d\mathbf{R}(q)$ in Fig 5.35 we also obtain nonsensical values of order N ! There is clearly a serious problem here which may be due to experimental limitations or to approximations in the theory. In particular if for some reasons the rheological relaxation time is very long due to some long lived specific interactions, the assumptions which lead to Equation 3.43, which is an approximation to Equation 13 of Clarke's paper [Clarke *et al.* 1997] may become invalid, and the subsequent development breaks down. In order to utilise the exact expression, detailed knowledge of the rheological response of the blend is further required.

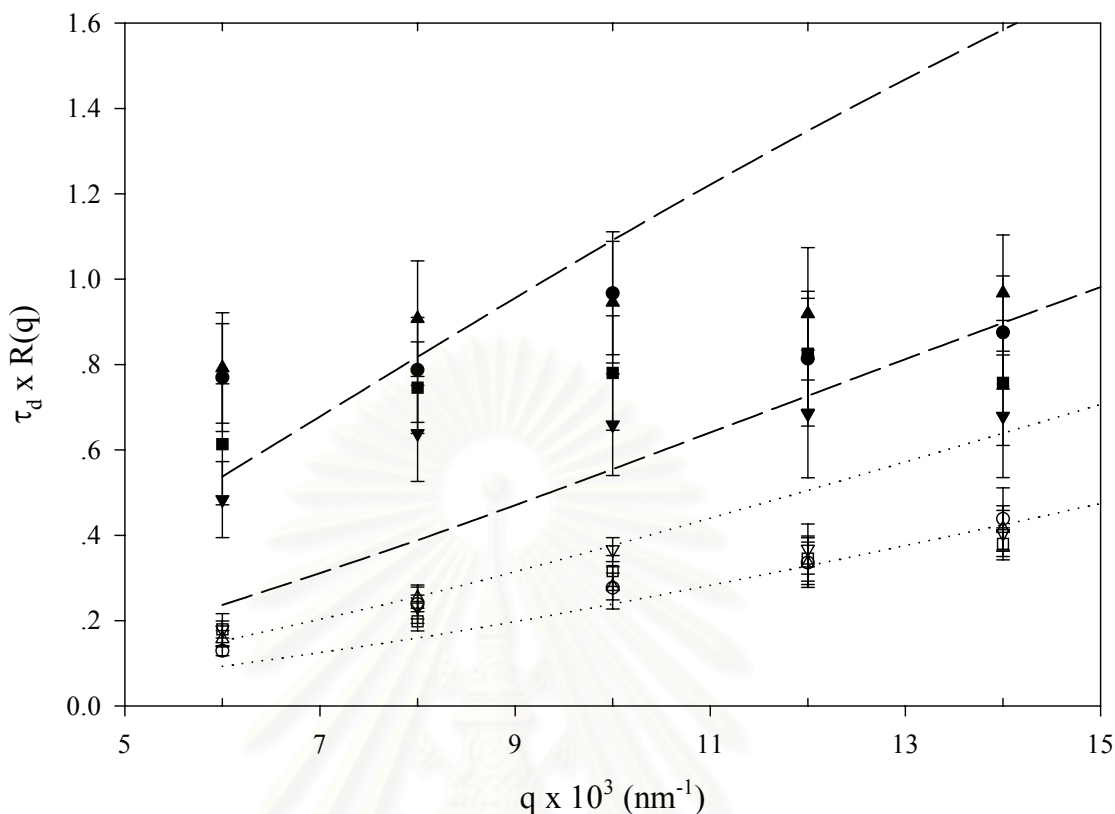


Figure 5.35: Plots of $\tau_d \times R(q)$ against q for 30/70 SMA/PMMAe blends. (● : $T_{\text{jump}} = 200$ °C, solution cast blend; ▲ : $T_{\text{jump}} = 205.5$ °C, solution cast blend; ▼ : $T_{\text{jump}} = 210.5$ °C, solution cast blend; ■ : $T_{\text{jump}} = 220$ °C, solution cast blend; ○ : $T_{\text{jump}} = 195$ °C, melt mixed blend; △ : $T_{\text{jump}} = 200$ °C, melt mixed blend; ▽ : $T_{\text{jump}} = 206$ °C, melt mixed blend; □ : $T_{\text{jump}} = 210$ °C, melt mixed blend).

5.6 Conclusions

Cloud point and spinodal determinations have been clearly demonstrated. The results reported here show clear influences of sample preparation methods on phase behaviour, i.e., spinodal and cloud point curves of melt mixed samples are lower than those of solution cast blends. It is suggested that the stronger intermolecular interactions facilitated in solution cast blends by the more intimate mixing might play a crucial role in producing the differences arising from sample preparation method. The DSC experiments do not find any evidences of solvent, which may be trapped inside the solution cast blends. The Gordon-Taylor-Kwei equation, which take into account the effect of interactions between polymers, shows good agreement with the glass transition temperature data confirming the existence of specific interactions in

this blend. Since no shift of the phenyl band has been clearly observed using FTIR experiments, this may raise the question of how much the difference of interaction arising from sample preparation. It is therefore interesting to investigate more closely by using other powerful techniques such as solid state NMR or SANS.

The Cahn-Hilliard growth rates $R(q)$ vary in a complex way depending on concentration and sample preparation. Delay time behaviour was investigated closely. It was found that sample preparation, composition, temperature, and q affect the delay time. The values of $\tau_d R(q)$ appear to depend on preparation methods. Comparison of the observed delay times with the predictions of viscoelastic theory shows serious contradictions, which may indicate the origin of the apparent delays lies elsewhere, i.e., the detected data may have already passed the early stage SD in this case. However, some evidences in the data indicate that phase separation still proceeded through the early stages of spinodal decomposition after the delay. For example, intensities increase exponentially after the delay time as expected from the linearised theory, and this suggests that the intensities do still fall in the early stages. Since it is more difficult to rule out a lack of sensitivity to the refractive index difference in the very early stages or a phase separation outside the q -range accessible by light scattering, X-ray or neutron scattering experiments might be able to answer this question. However, both techniques have serious experimental difficulties for this blend, for instance, the problem of deuterating and how to receive the clear contrast from this blend using X-ray scattering. On the other hand, since some rheological terms were omitted after a lapse of delay, this may be able to cause a serious deviation in fitting as well.

The characteristics of time evolution of scaling function depending on phase separation temperature, preparation methods and compositions have been demonstrated. The time dependent scaling function is clearly observed during the intermediate stage of phase separation. As soon as it reaches the late stage of phase separation, the scaling function profile then becomes a single master curve. The simple normalised scaling function profile for cluster region proposed by Furukawa

can describe experimental data very well, while the profile for deep quench, which was recently suggested, showed more discrepancies; this might be the effect of system dependence.

The tests of the Cahn-Hilliard theory showed that such theory is still valid at the certain range of time, providing the satisfying prediction of q_m and $R(q_m)$. From the Cahn-Hilliard theory, light scattering experiments can be used to classify each stage of phase separation. Two criteria are used to illustrate the early stage SD, namely the time independence of q_m and the consistence with the linearised theory, i.e., scattering intensities increase exponentially with time. The period, in which phase behaviour obeys the linearised theory, is considered to be the early stage of spinodal decomposition. As soon as q_m starts moving or the scattered intensity deviates from the early slope of $\ln(I)$ versus time plot, this is considered to be the beginning of the intermediate stage of spinodal decomposition. It enters the late stage of spinodal decomposition as soon as the time-independence of $F(X)$ occurs.

Chapter VI

Mechanical Properties and Morphologies of SMA/PMMAe Blends

The relationship between morphology and properties of polymer blend has received much attention recently. It has been known that many properties of polymer blends strongly depend on their structure; thus one of the crucial keys to utilise polymer blend effectively is controlling their structure. Phase separation kinetic is considered to be an excellent way to generate irregular spatial patterns from the homogeneous systems. A miscible polymer blend generally undergoes spinodal decomposition after exposure to temperatures in the unstable two-phase regime. The rates of phase separation and the resulting morphology depend on many parameters, e.g., time of heat treatment, temperature, concentration, and physical properties of the blend constituents.

The effects of phase separation on mechanical properties and morphologies of SMA/PMMAe blends are dealt with in this chapter. It starts with a discussion on mechanical properties of polymer blends consisting of general principle, the characteristic of breaking phenomena, and the result of tensile test. The morphology observation is demonstrated thereafter. The characteristic of microstructure at various phase separation times and temperatures are reviewed through scanning electron microscopic pictures. The comparison between the characteristic length scale during phase separation obtained from the direct measurement using the scanning electron micrograph pictures and calculation from the temperature jump experiment using light scattering are illustrated in order to confirm each stage of spinodal decomposition.

6.1 Mechanical Properties

6.1.1 A Principle of Linear Viscoelastic Behaviour of Amorphous Polymers

Basically the mechanical properties of elastic solid can be described by Hooke's law, which states that an applied stress is proportional to the resultant strain but is independent of the rate of strain. However, for liquid system the stress is usually independent of the strain but proportional to the rate of strain, which is described by the well-known Newton's law. In many cases, a material may exhibit the characters of both a liquid and a solid and neither of the limiting laws will adequately describe its behaviour. The system is then said to be in a viscoelastic state. Among several systems, plastic such as silicone is a good example to exhibit viscoelastic behaviour.

Homogeneous isotropic elastic materials possess the simplest mechanical properties. Under a simple tension such as shown in Figure 6.1

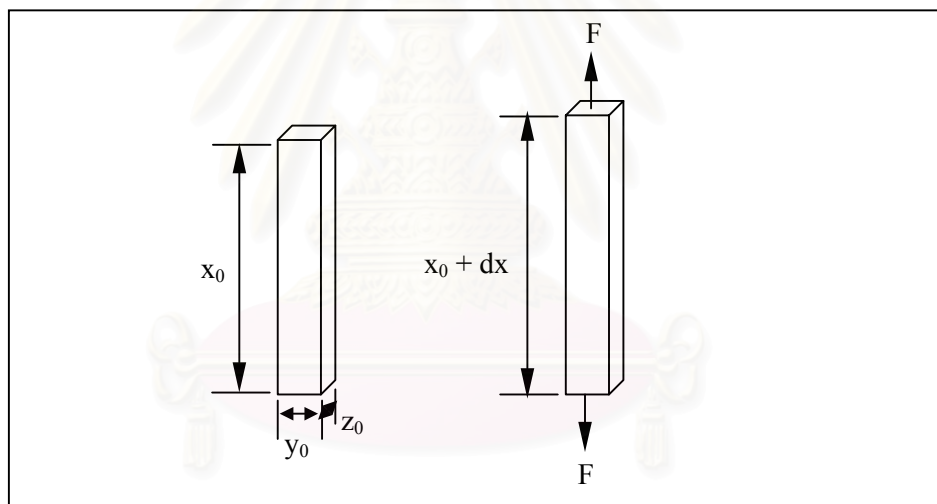


Figure 6.1: Tensile stressing of a bar.

This object of cross-sectional area $A_0 = y_0 z_0$ is subjected to a balance of pairs of tensile force F . If its length changes by an increment dx so that $x_0 + dx = x$, Hooke's law is obeyed and the tensile stress σ is proportional to the tensile strain ϵ . The constant of proportionality known as the Young's modulus can be expressed as:

$$\sigma = E\epsilon \quad (6.1)$$

where E is Young's modulus

The stress σ is a measure of the force per unit area (F/A), and the strain or elongation is defined as the extension per unit length, i.e. $\epsilon = (dx/x_0)$. For an isotropic material, it should be noticed that the change in length per unit length is related to the change in width per unit of length as,

$$\nu_p = (dy/y_0)/(dx/x_0) \quad (6.2)$$

where ν_p is known as Poisson's ratio and varies from 0.5, when no volume change occurs, to about 0.2 [Cowie 1991].

6.1.2 Stress-Strain Measurements

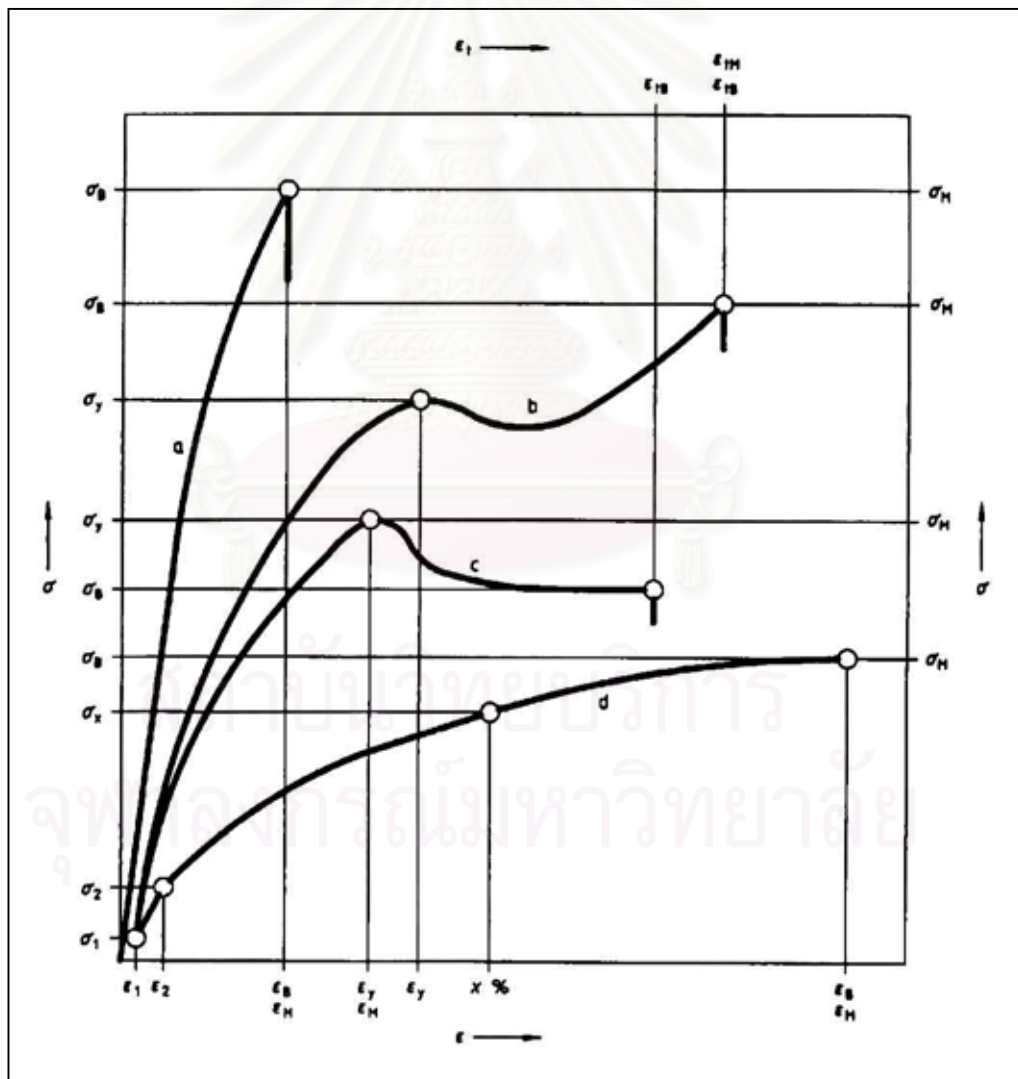


Figure 6.2: Typical stress-strain curves [BSI 1996]

The data obtained from stress-strain measurements on thermoplastics are quite important from a practical point of view, since they can provide information on the modulus, the brittleness, the ultimate and yield strength of the polymers. By subjecting the specimens to a tensile force applied at a uniform rate and measuring the resulting deformation, typical stress-strain curves as shown in Figure 6.2 can be constructed.

As shown in Figure 6.2, curve A represents brittle materials and the stress initially rises in an approximately linear manner as the applied strain increases and once it reaches yield point (ϵ_y, σ_y), which is defined as a point at which an increase in strain occurs without an increase in stress, the materials suddenly fracture indicating by a plunge of stress. Curves B and C represent tough materials, once the stress passes their yield point the materials entirely deform or stretch until they finally break at (ϵ_b, σ_b). The stress may increase as curve B due to the strain hardening which can increase the effective stiffness of the materials. Curve C represents tough material without yield point, in this case the tensile stress at x % strain can be used for the yield stress. The maximum stress sustained by the test specimen during a tensile test (σ_M) is named as the tensile strength. The whole area under the stress-strain curve is proportional to the energy required for the fracture of material.

6.1.3 Breaking Phenomena

Concerning the rupture of a typical glassy polymer such as poly(methyl methacrylate) or poly(styrene), Berry [1959] suggested that as crack propagates, work is expended in the alignment of polymer chains ahead of the crack, consequently leaving an oriented layer on the fracture surface, forming a so-called craze at the crack tip of the fracture surface. Dugdale [1960] proposed that the craze profile was very similar to the plastic zone model for metal. In contrast to the idea of the presence of an infinite stress at the crack tip, it was suggested that the stress concentration at the crack tip can be released by the formation of a craze. The stress singularity at the crack tip is cancelled by the superposition of a second stress field in which the

stresses are compressive along the length of the crack as shown in Figure 6.3. A constant compressive stress is assumed, and is identified with the craze stress.

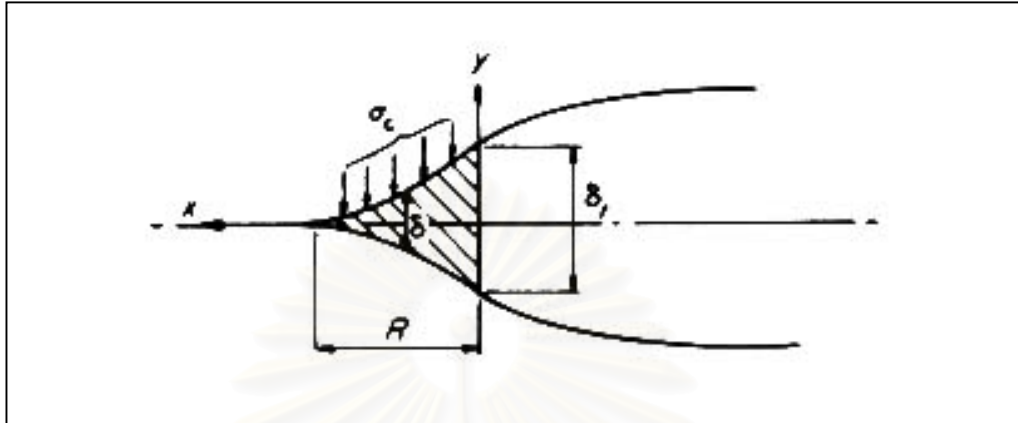


Figure 6.3: The Dugdale plastic zone model for a craze [Ward *et al.* 1993]

Understanding the craze development is quite important since the craze at the crack tip plays such a crucial role in determining the fracture toughness of materials. The studies of the craze structure by Kramer and his co-workers [Donald *et al.* 1982] demonstrate that the craze structure is not uniform along its length. Argon and his colleagues [1977] proposed that the craze front advances by a meniscus instability mechanism in which craze tufts are produced by the repeated break-up of the concave air/polymer interface at the crack tip, as illustrated in Figure 6.4.

สถาบันวิทยบริการ
จุฬาลงกรณ์มหาวิทยาลัย

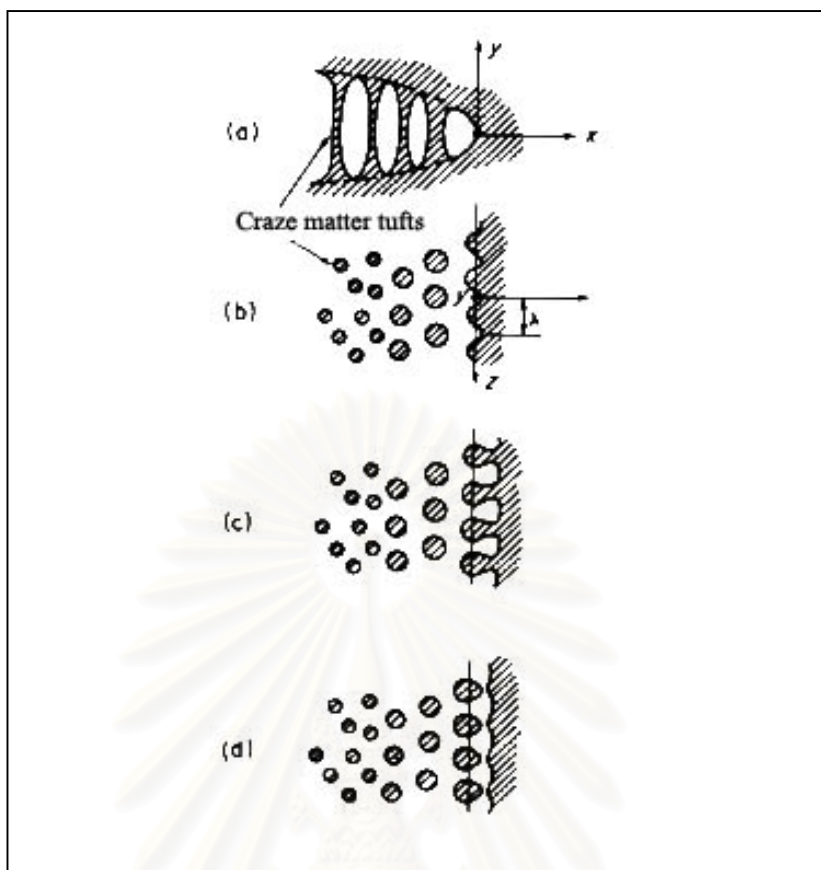


Figure 6.4: A Schematic diagram shows craze formation by the mechanism of meniscus instability; (a) outline of a craze tip; (b) cross-section in the craze plane across craze matter tufts; (c), (d) advance of the craze front by a completed period of interface convolution [Argon *et al.* 1977].

6.1.4 Results and Discussion

6.1.4.1 Tensile Test

Figure 6.5 shows an example of the stress-strain curves for PMMAe and 20/80 SMA/PMMAe blends, which were phase separated at 210 °C at different stages of phase separation. It can be clearly seen that the tensile stresses of all samples increase rapidly at the beginning and once they reach the yield point, the samples suddenly break, demonstrating a characteristic of brittle materials. Young's moduli and tensile stress at break of the miscible blends are higher than those of PMMAe. It has been suggested that an exothermic heat of mixing or a negative volume change on mixing, which exists for some miscible blends, might result in a synergistic increase in modulus of the blends [Nishi *et al.* 1975; Kleiner *et al.* 1979; Kim *et al.* 1991]. However, the elongation at break of the miscible blend becomes much lower implying

that the toughness property of the blend appears to be inferior compared to PMMAe. After phase separation, Young's modulus of the blends increases slightly, while the elongation at break decreases.

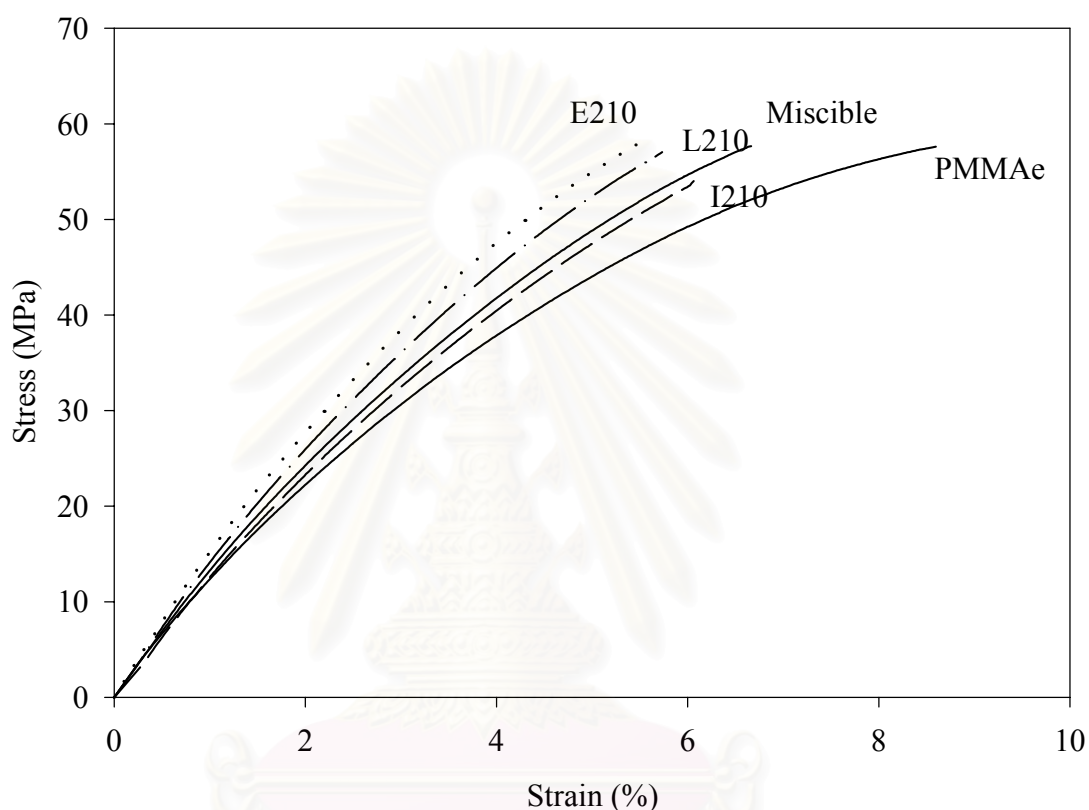
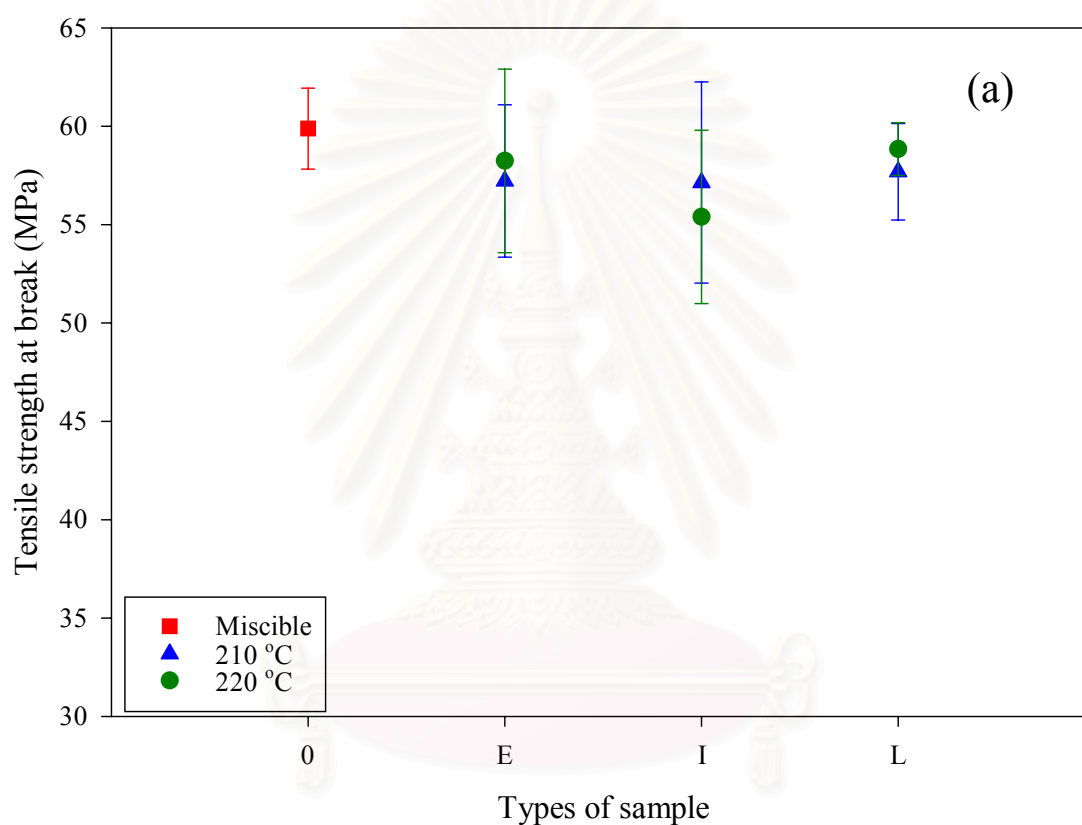


Figure 6.5: Stress-strain curves of PMMAe and 20/80 SMA/PMMAe blends, which are miscible and phase separated at 210 °C at different stages of SD. Note that E 210 represents the early stage of phase separation (15 min.), I 210 represents the intermediate of phase separation (60 min.) and L 210 represents the late stage of phase separation (100 min.).

Young's modulus, tensile strength at break and elongation at break of 20/80 SMA/PMMAe blends are clearly shown as a function of phase separation temperature and each stage of spinodal decomposition in Figures 6.6a - c. As seen in Fig 6.6a, there is a minor decrease of tensile stress at break for phase separated blends compared to the miscible blend; however, regarding the effect of phase separation time and temperature, no clear difference of tensile stress at break within

experimental errors was found. From Figure 6.6b, the tensile modulus of the blends, which were phase separated at 210 °C, increases slightly in the early stage of SD, then decreases in the intermediate stage of SD and surprisingly increases again in the late stage of SD. The first increase in modulus might be the result of the change in composition due to phase separation, i.e., the PMMAe-rich phase, which is close to the pure PMMAe, exists. Since it appears that the higher concentration of SMA, the poorer tensile properties, then making the low concentration of SMA might result in the excellent mechanical properties. As phase separation proceeds, the co-continuous structures increase in their size (as will be discussed thoroughly in Section 6.2.3.2) and this was suggested by Kim *et al.* [1991] that it may result in less connectivity and weaker interface between phases leading lower modulus and strength. This was supported by the prediction by Lipatov *et al.* [1985], who suggested that the series model which represents the miscible blend shows higher modulus than the combination of series and parallel elements, which on the contrary represents the phase separated blend. Furthermore, considering the fracture surface of broken specimens, the group of craze fibrils at only the PMMAe-rich phase for phase separated blends especially in the late stage of SD rather than well distributed craze fibrils for miscible blends might result in the weakness for some areas of specimens (this will be mentioned again in Section 6.2.3.1). The latest increase of tensile modulus for blends phase separated within the late stage of SD might be attributed to the structural recovery. It was suggested by Scheirs [2000] that once polymers are annealed long enough, this might allow them to have sufficient time to relax, each polymer chain can slowly re-organise and pack more closely, turning them from unstable and non-equilibrium toward equilibrium, eventually. As a consequence of this, an increase in yield stress and modulus is expected, however, the fracture energy, impact strength and ultimate elongation might decrease. It can be seen in Figure 6.6c that the elongation at break decreases for the blends phase separated in the late stage of SD. The tensile modulus of blends, which were phase separated at 220 °C, increase slightly first after phase separation inside the early stage of SD, then decrease marginally as phase separation continues. The minor decrease of tensile modulus here in the late stage of SD raises the question that whether it is possible for the tensile

modulus to increase if the samples are annealed long enough. However, owing to heating polymers at high temperature for a long time, this might cause a problem of thermal degradation, resulting in the lower mechanical properties.



สถาบันวิทยบริการ
จุฬาลงกรณ์มหาวิทยาลัย

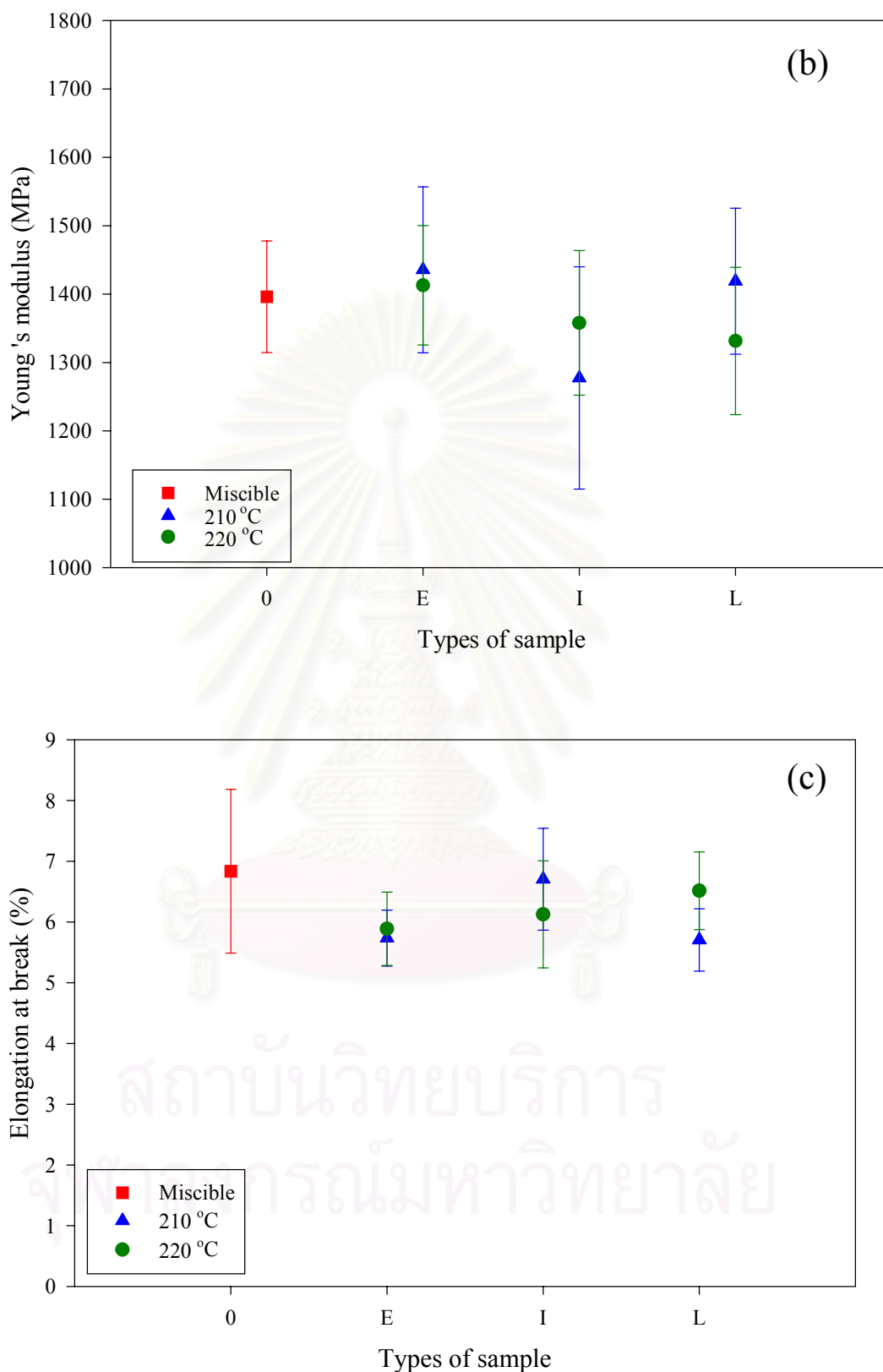


Figure 6.6: Comparisons of (a) tensile strength at break, (b) Young's modulus and (c) elongation at break for 20/80 SMA/PMMAe blends, which are either miscible or phase separated at different times and temperatures. Note that 0 = no phase separation (miscible); E = early stage of phase separation; I = intermediate stage of phase separation; L = late stage of phase separation.

Figure 6.7 illustrates the stress-strain curves of PMMAe and 40/60 SMA/PMMAe blends, which were phase separated at 210 °C at different stages of phase separation. Concerning the miscible blend, it appears that mechanical properties become deteriorate as the content of SMA is increased, i.e., Young's modulus, tensile stress at break and elongation at break of the miscible 40/60 SMA/PMMAe blends are quite low relative to those of the miscible 20/80 SMA/PMMAe blends. The effect of phase separation time on the change of stress-strain curves is somewhat similar to the 20/80 SMA/PMMAe blends, i.e., the blend, which was phase separated in the early stage of SD, shows the highest tensile stress at break as well as the modulus, while tensile stress at break and modulus decreases for the blends phase separated inside the intermediate of SD. Either the tensile stress at break or modulus increases again in the late stage of SD.

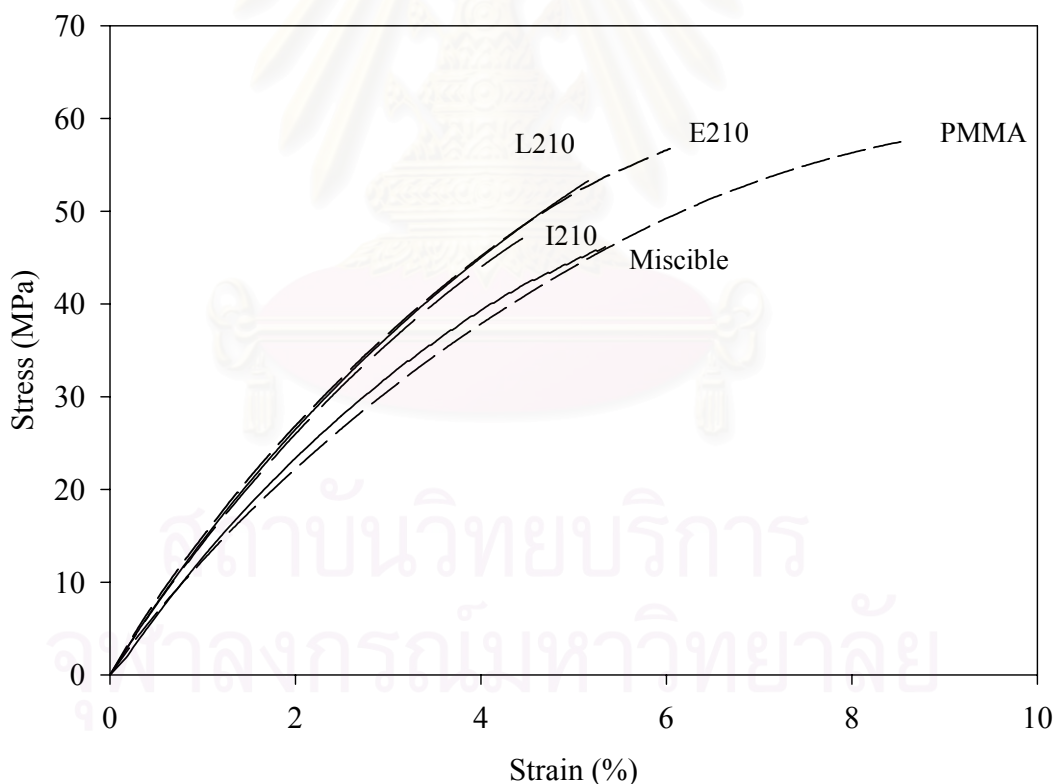
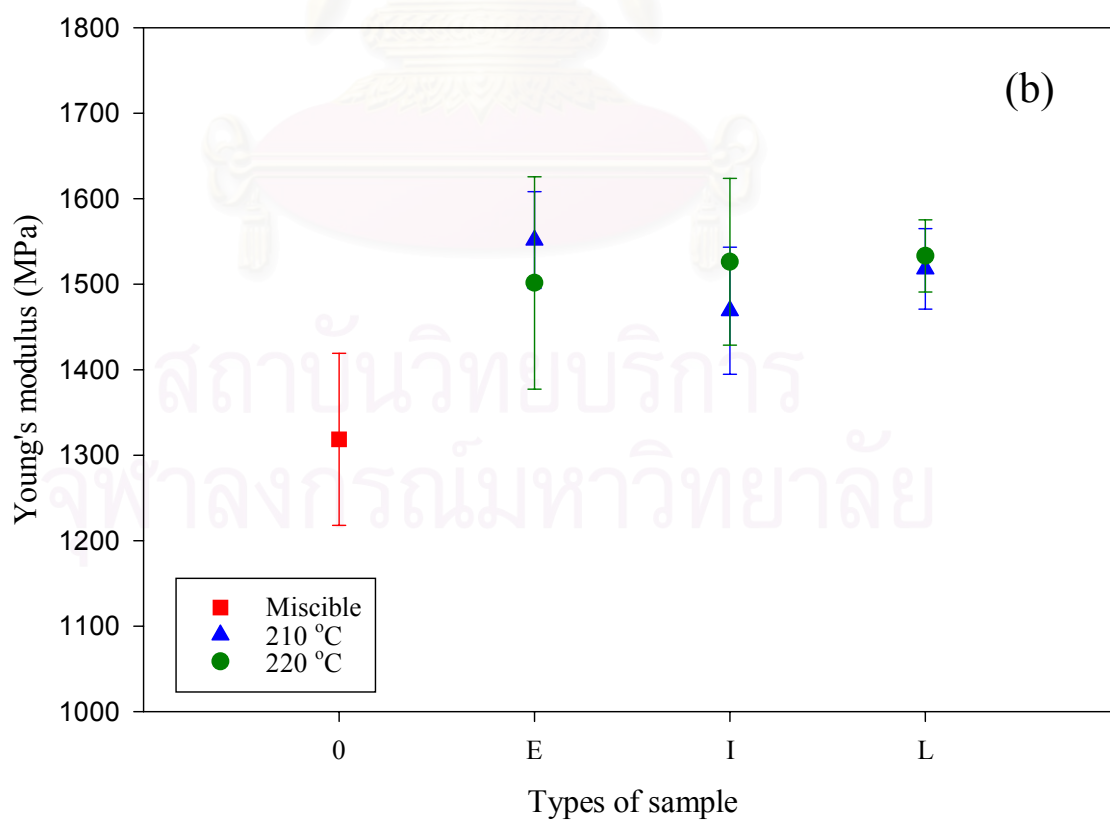
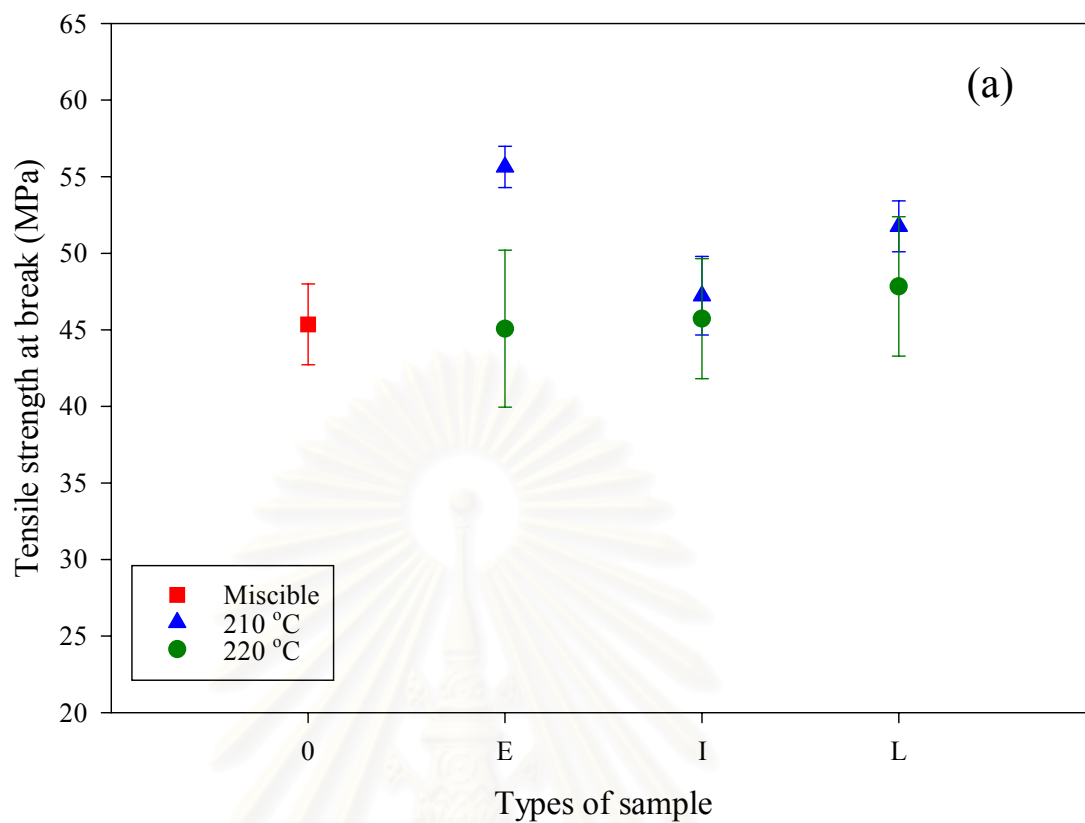


Figure 6.7: Stress-strain curves of PMMAe and 40/60 SMA/PMMAe blends, which are miscible and phase separated at 210 °C at different stages of SD. Note that E 210 represents the early stage of phase separation (15 min.), I 210 represents the intermediate of phase separation (60 min.) and L 210 represents the late stage of phase separation (100 min.).

Figures 6.8a - c show the tensile strength at break, Young's modulus and elongation at break for 40/60 SMA/PMMAe blends, which were phase separated at various temperatures and times. As seen in Figs 6.8a-b, interestingly at the phase separation temperature of 210 °C, there appears a sharp rise of tensile stress at break and modulus for the blend phase separated inside the early stage of SD. The tensile stress at break and modulus drop slightly after the early stage of phase separation but they increase slightly thereafter (i.e. in the late stage of SD). This is rather similar to what we found in the case of 20/80 SMA/PMMAe blends and consequently confirms that such an interesting behaviour can be found not only for 20/80 but also for 40/60. On the other hand, at the phase separation temperature of 220 °C, the tensile stresses at break at various stages of SD are close to each other within experimental errors. The modulus apparently does increase after phase separation but no variation of modulus as the result of the change in stage of SD was found. The elongation at break of all phase separated blends drops compared to the miscible blends as shown in Fig 6.8c - this might be due to the weak interface as the blends phase separate. The tensile stress and elongation at break decrease as increasing phase separation temperature - this might be a significant evidence to illustrate that samples become more brittle after being heated at high temperature.



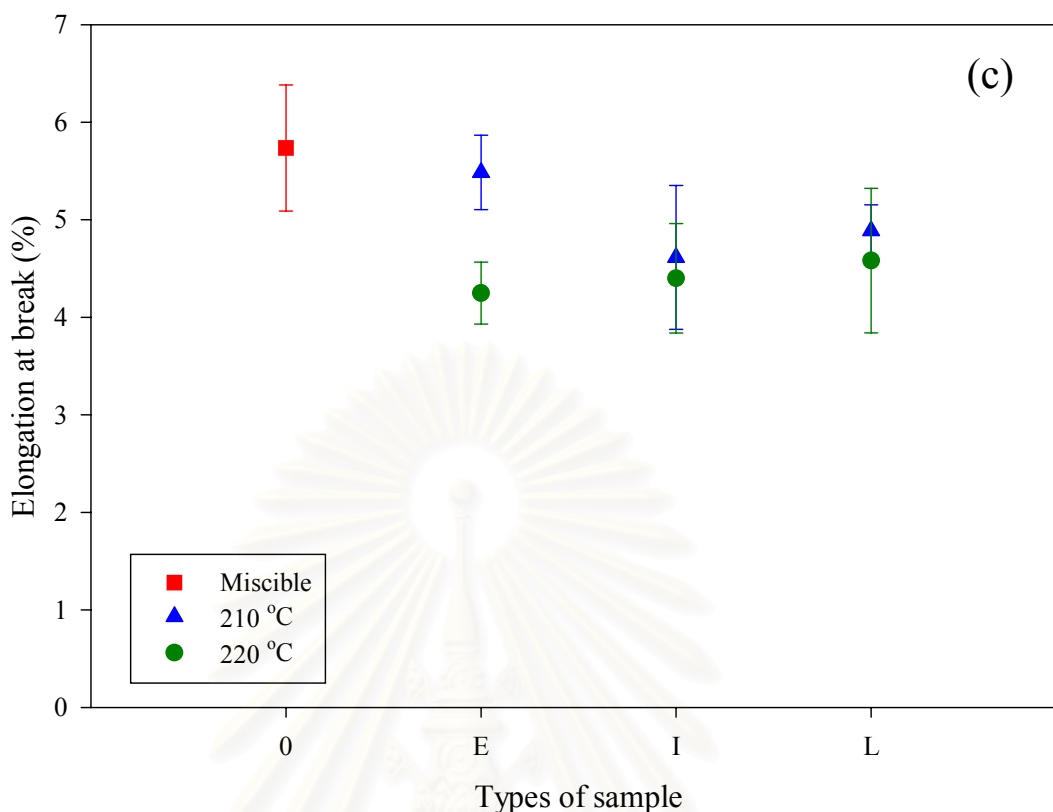


Figure 6.8: Comparisons of (a) tensile strength at break, (b) Young's modulus and (c) elongation at break for 40/60 SMA/PMMAe blends, which are either miscible or phase separated at different times and temperatures. Note that 0 = no phase separation (miscible); E = early stage of phase separation; I = intermediate stage of phase separation; L = late stage of phase separation

Owing to the concern of thermal degradation leading to chain fragmentation, all samples were investigated by using a gel permeation chromatography. As shown in Figure 6.9, it was found that all curves are nearly similar especially blends phase separated in the late stage at 210 °C and in the late stage at 220 °C. these curves are overlapping and similar to the curve of miscible blends, indicating that phase separation time and temperature used in this work do not cause molecular fragmentation at least within the limitation of GPC. It should be noted that the chromatograph curves here are different from curves in Figure 4.6, which exhibits a small hump of SMA separately from PMMA. Comparing to the previous experiments, this might be due to differences of equipment as well as the mobile solvent and flow rate.

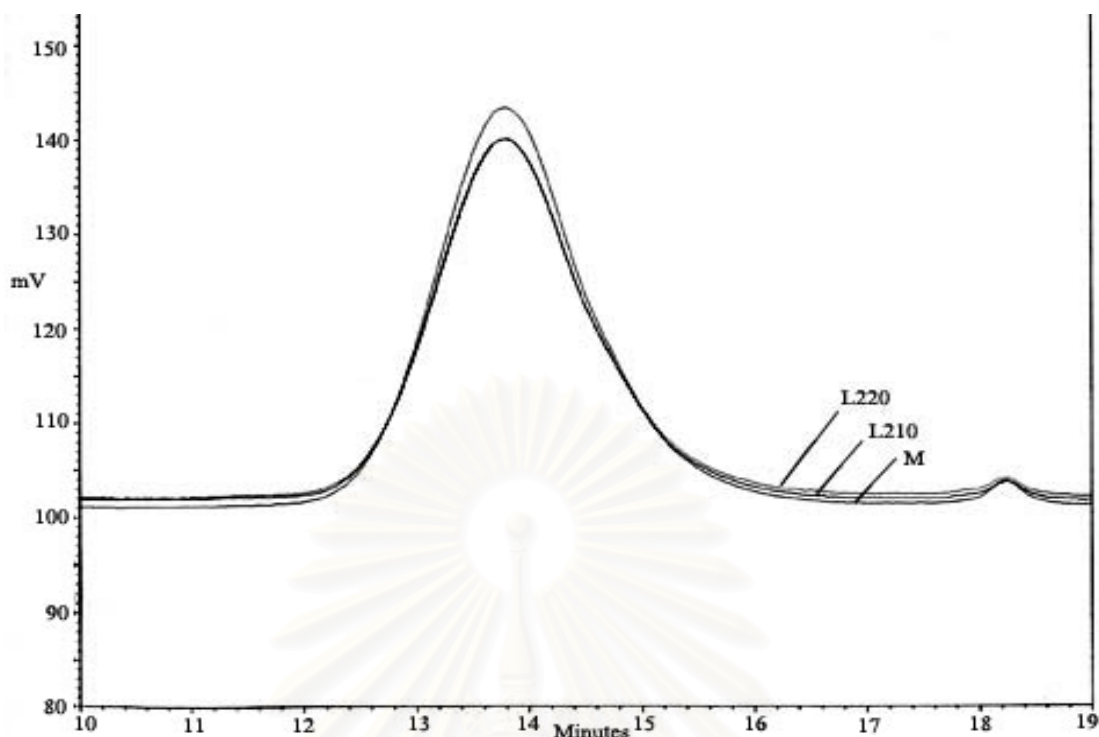


Figure 6.9: GPC results of melt mixed 40/60 SMA/PMMAe blends prepared at different phase separation times and temperatures (L220: phase separation at 220°C in the late stage region, L210: phase separation at 210°C in the late stage region, M: no phase separation).

6.2 Morphology

The morphology of polymer blends results from the spatial arrangement on a supramolecular scale of assemblies of macromolecules. The complexities of these arrangements increase rapidly in going from amorphous homogeneous polymers to the various types of heterogeneous polymers. So far several methods of morphological investigation have been developed in order to deal with those complexities, among those are electron microscopy, small angle x-ray scattering, etc.

6.2.1 Morphology of Homogeneous Polymer Blends

Several morphological features can occur in homogeneous blends depending on their structural arrangement, i.e. crystalline or amorphous. It has been believed for many years that amorphous homogeneous polymers do not have morphological features. However, thanks to the advance technology nowadays, it is clear that even amorphous homogeneous polymers still have unique structure - some studies recently

have reported the evidence of the existence of supramolecular structures in such systems. For example, Yeh [1972] reported the evidence of density variations in atactic polystyrene using TEM.

6.2.2 Morphology of Heterogeneous Polymer Blends

The morphology of heterogeneous systems depends on the arrangement of the constituent phase. For a binary system, three possible cases have been suggested so far – (i) two discontinuous phases, (ii) one discontinuous and one continuous phase and (iii) two continuous phases. The case of two discontinuous phases is usually represented by a random aggregate of two kinds of structural units; for example, the spherulites of crystalline phase A and the spherulites of crystalline phase B coexist in an aggregate without clustering of either type [Bever *et al.* 1974]. The structure consisting of one continuous and one discontinuous phase is generally observed for heterogeneous systems, i.e., the continuous phase usually serves as matrix while the other phase is present as dispersed particles which can be sphere or rods. The two continuous-phase structure is frequently found to form lath-like interpenetrating networks.

6.2.3 Electron Microscopy Results

In this chapter, the supramolecular structure of polymer blends were explored in two aspects, viz., the characteristics of fracture surface and the development of phase separation morphologies, using scanning and transmission electron microscopies.

6.2.3.1 The Fracture of Polymers

Figures 6.10, 6.11 demonstrate morphologies at low magnification (x 2000) of pure SMA and PMMAe respectively. It should be noted that the PMMAe sample for SEM observation was obtained from the fracture of tensile test specimens, while the SMA sample comes from compression moulded bars, which was manual pulled. It can be seen that both polymers show very smooth surface with numerous fracture layers as expected for general brittle materials. Those layers might come from propagation of stress on more than one plane [Saucer *et al.* 1976]. The surface of

SMA is apparently smoother than PMMAe, indicating that SMA can break easier than PMMAe. It is consistent with the result from tensile test, i.e., the energy to break decreases as the content of SMA increases. A number of fracture nuclei were found for the pure PMMAe whereas none was found for SMA. It has been pointed out by Narisawa *et al.* [1993] that such nuclei can be the beginning of craze.

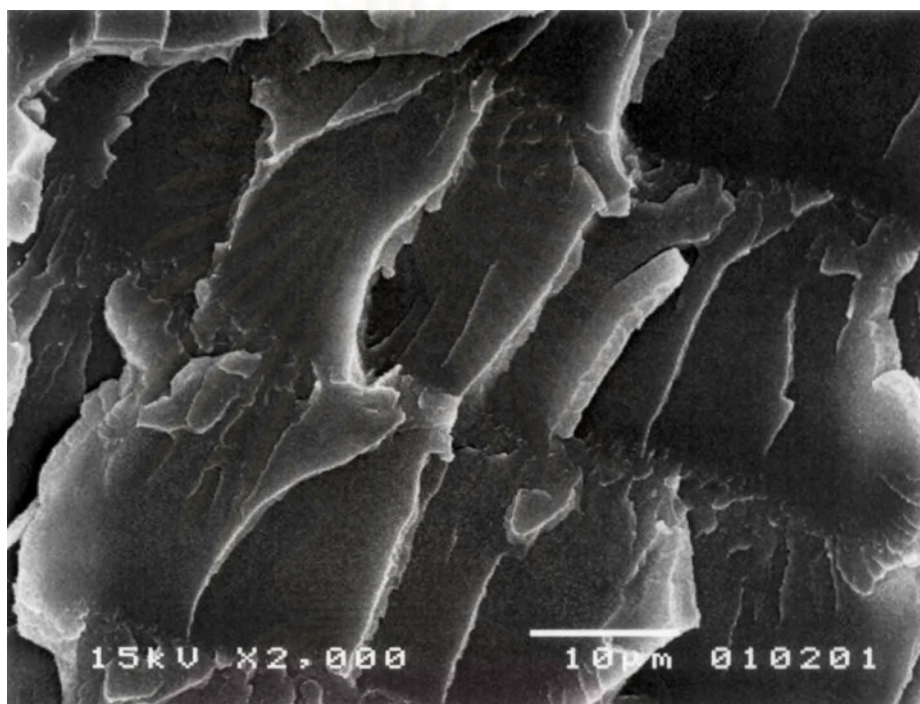


Figure 6.10: A scanning electron micrograph picture of SMA.

สถาบันวิทยบริการ
จุฬาลงกรณ์มหาวิทยาลัย

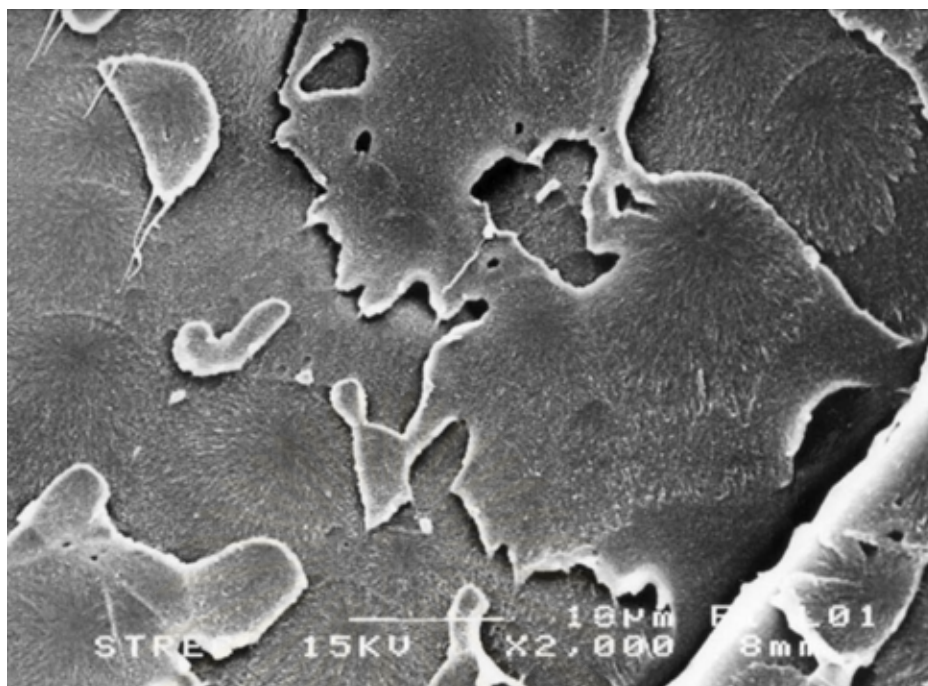


Figure 6.11: A scanning electron micrograph picture of PMMAe.

The high magnification (x10,000) picture of SMA illustrates the weakness interaction between layers and confirms the previous conclusion about the brittleness of SMA. As shown in Figure 6.12, it is clear that the interface is very sharp and smooth with no evidence of craze. Unfortunately, PMMAe cannot be observed at the high magnification since it is very sensitive to electron beam leading to rapid burning and cracking of specimens during observation.

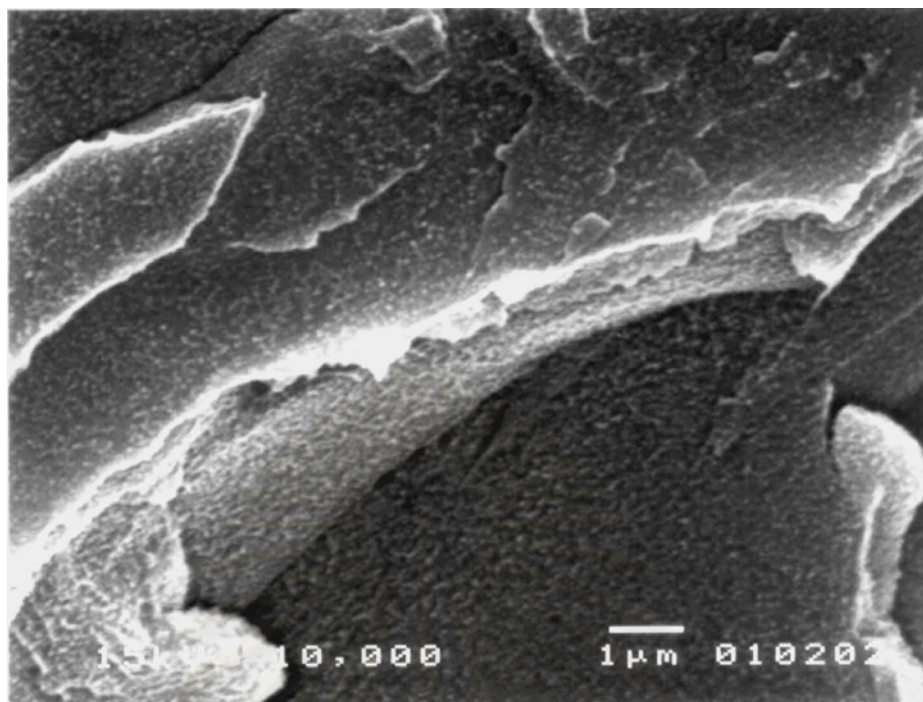


Figure 6.12: A scanning electron micrograph picture of SMA.

The interface between layers of the fracture at high magnification ($\times 10,000$) of miscible blends and phase separated blends are shown in Figures 6.13 and 6.14. Interestingly, there exist fiber-like structures between each layers, which might be considered as groups of large craze forming ahead of the crack. These fibrils appear continuously along the interface for miscible blends whereas in the case of phase separated blends, the fibrils show up only at PMMAe-rich phase. This might indicate that the interaction over a flake-like surface of phase separated blends seem to be strong at some certain portions leading to the reduction of ductility. Furthermore, as shown in Figure 6.14, it is clear that the IPN-like structure was noticed for phase separated blends. This has been reported by other literatures [Okada *et al.* 1993, 1995; Lauger *et al.* 1995; Wagner *et al.* 1998; Dorgan *et al.* 1998] as a distinctive structure due to polymer blends phase separating via spinodal decomposition. Details of which will be discussed later on.

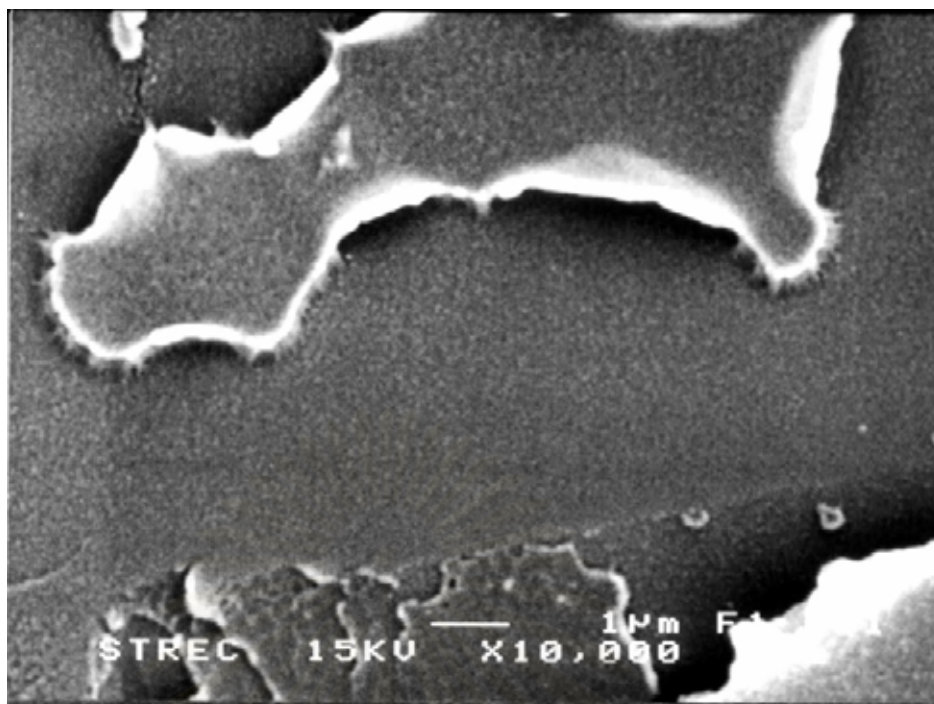


Figure 6.13: A scanning electron micrograph picture of a fracture of tensile tested specimen for a miscible 40/60 melt mixed SMA/PMMAe blend.

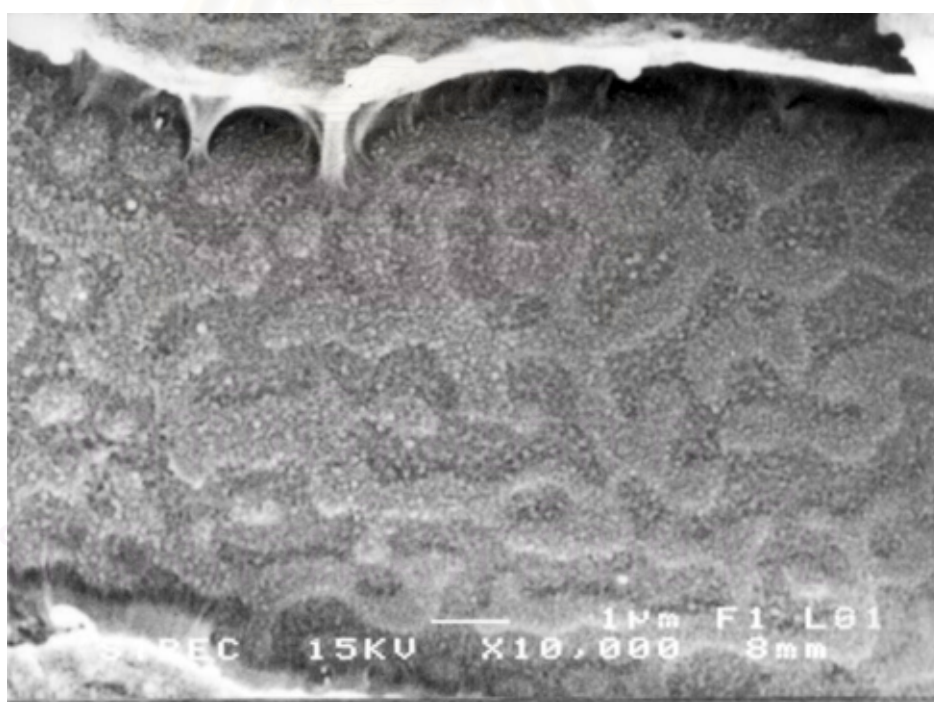
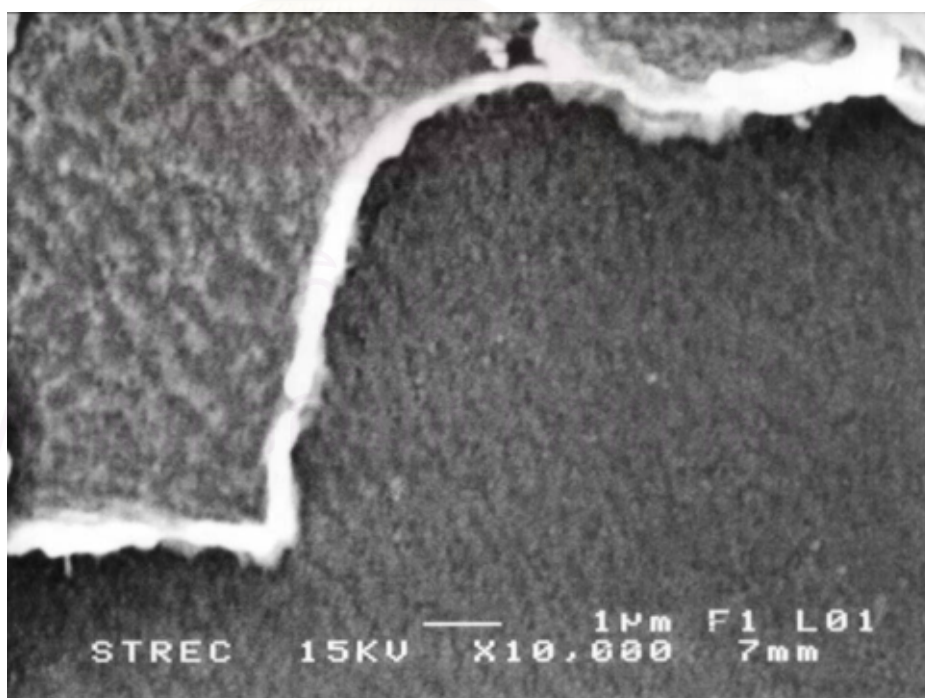


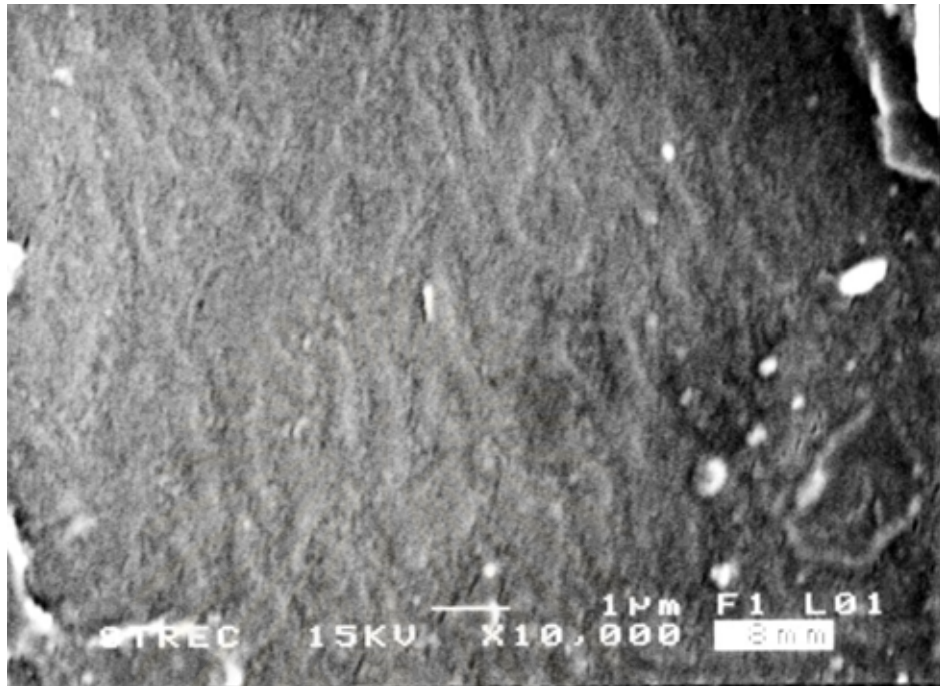
Figure 6.14: A scanning electron micrograph picture of a fracture of tensile tested specimen for the 40/60 melt mixed SMA/PMMAe blend, which was phase separated at 220 °C inside the late stage region of spinodal decomposition.

6.2.3.2 Morphological Development via Spinodal Decomposition of Polymer Blends

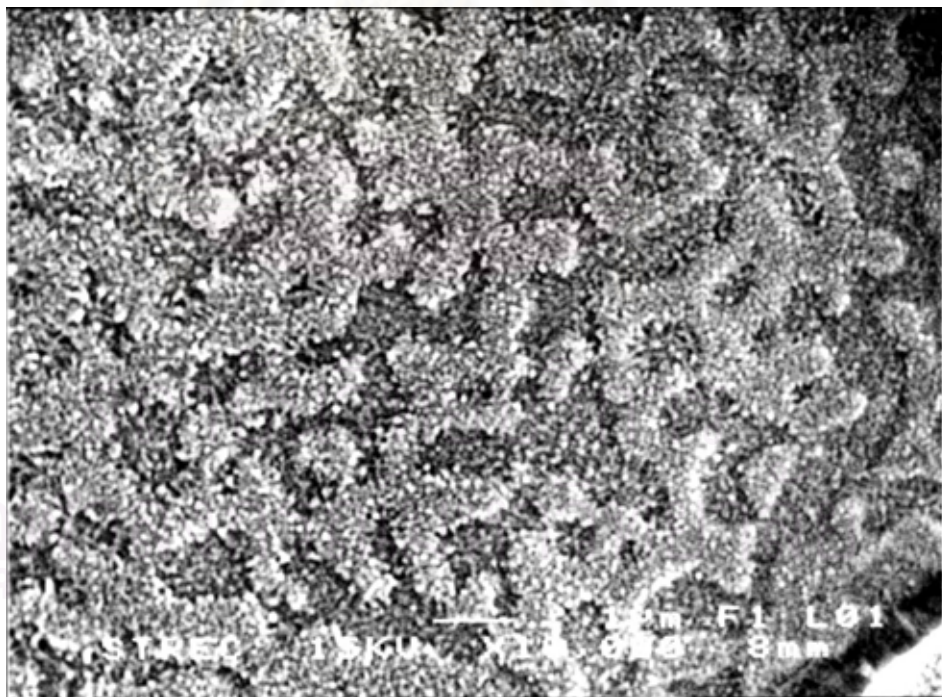
The variation of phase separation morphology (spinodal structure) is clearly discussed in this section. To our knowledge, this is apparently the first work that demonstrates the spinodal structure inside the fracture surface of the melt mixed blends. As shown previously in Fig 6.13, the surface of miscible blends is clearly smooth, indicating no sign of phase separated domain. However, after phase separation, the co-continuous structures develop as depicted in Figures 6.15 a-c. The co-continuous domains formed in the early stage as shown in Figure 6.15a and then develop to larger size as phase separation time increases, demonstrated through Figures 6.15b-c. It should be noted that since PMMA is really sensitive to electron beam the samples are required to be exposed to electron beam for a certain of time in order to obtain the clear contrast between two phases. Nevertheless, this can cause burning to sample surface and damage to the SEM equipment. Another technique, namely TEM is therefore required to observe the morphological development. By staining with OsO_4 , the clear contrast between two phases can be obtained.



a



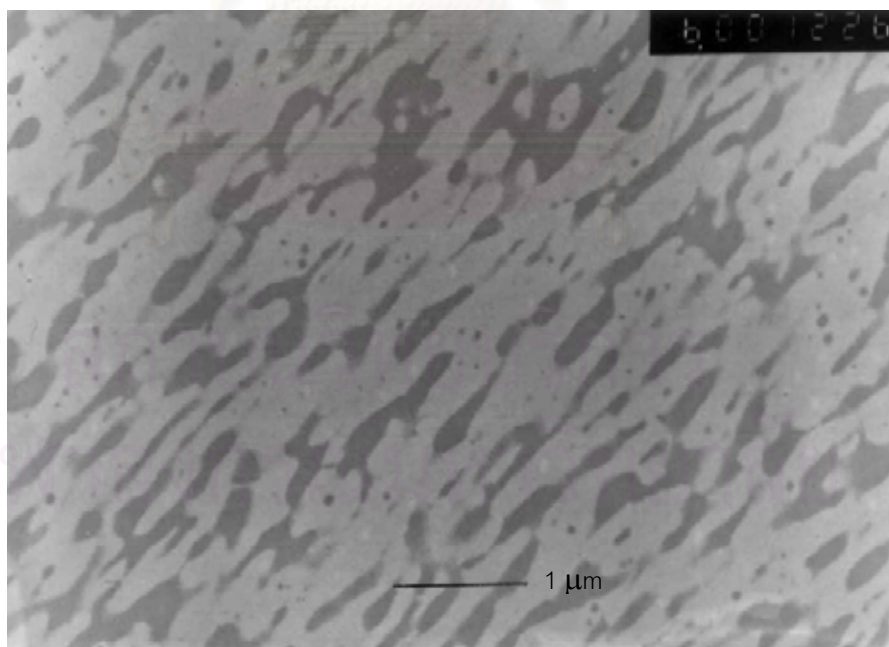
b



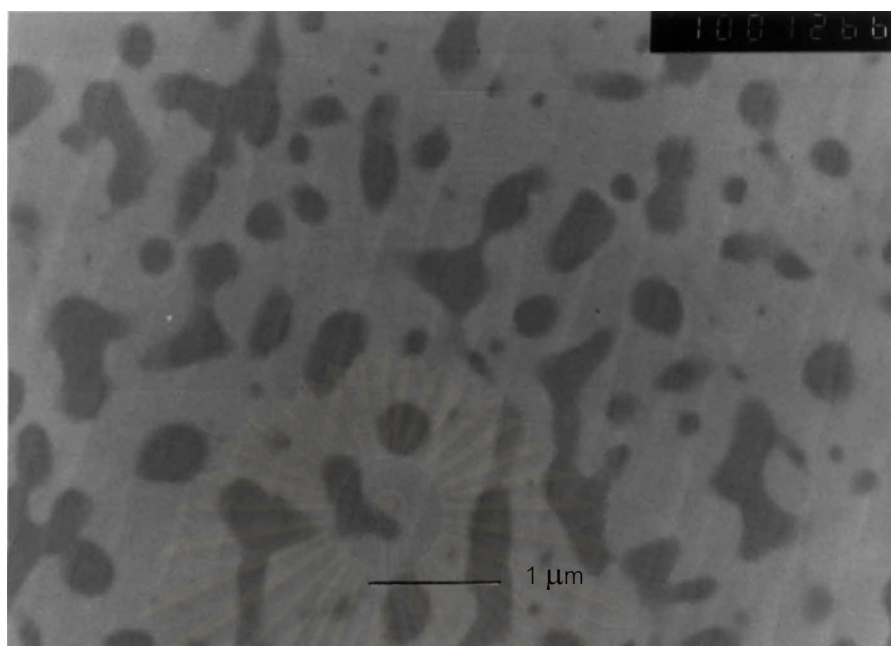
c

Figure 6.15: The scanning electron micrograph pictures of the fracture from tensile test of the 40/60 melt mixed SMA/PMMA phase separated at 220 °C at different stages of phase separation: (a) early stage, (b) intermediate stage, (c) late stage.

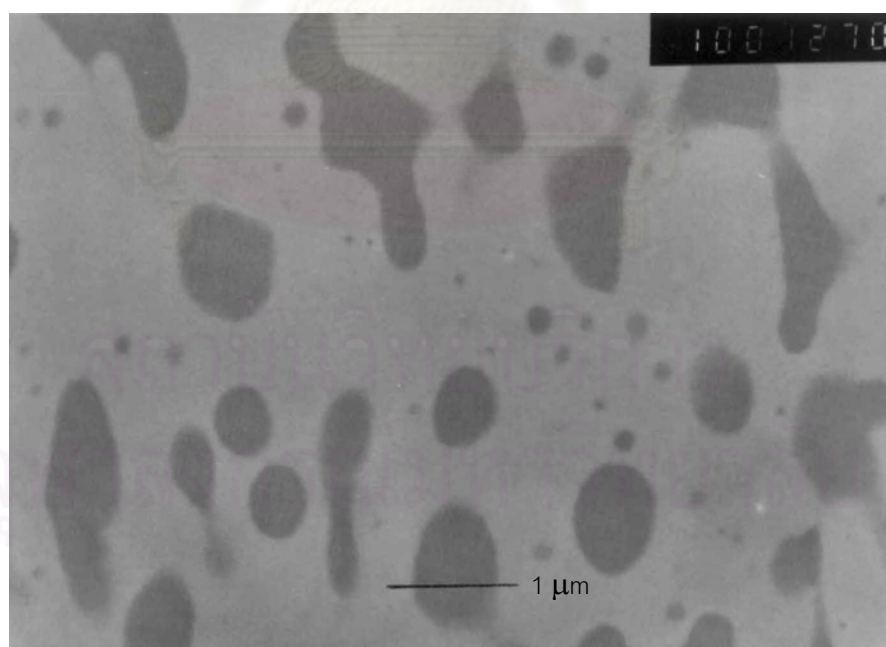
Likewise the SEM technique, the TEM pictures show a co-continuous structure, which is a unique characteristic of spinodal structure. Figures 6.16 a-c and 6.17 a-c illustrate the morphologies at different stage of spinodal decomposition of 20/80 and 40/60 SMA/PMMAe respectively. At 20 wt% of SMA, the domain size of SMA (black region), which herein is a minor phase, appears to grow with phase separation time. Conversely, the domain size of PMMAe (white region) was increased as increasing phase separation time for 40/60 SMA/PMMAe. This is quite interesting since the minor phase is still SMA for this blend. This phenomenon can be simply described by using the lever rule. From the phase diagram in Chapter 5, it should be noted that at a certain phase separation temperature, both compositions of interest nearly lie on the same tie line but on different sides of critical point, which is 30/70 SMA/PMMAe. After 40/60 SMA/PMMAe was phase separated, it is clear that the distance from the original composition to the SMA-rich phase is shorter than to the PMMAe-rich phase. Following the lever rule, this results that the amount of SMA-rich phase is higher than that of PMMAe-rich phase.



a

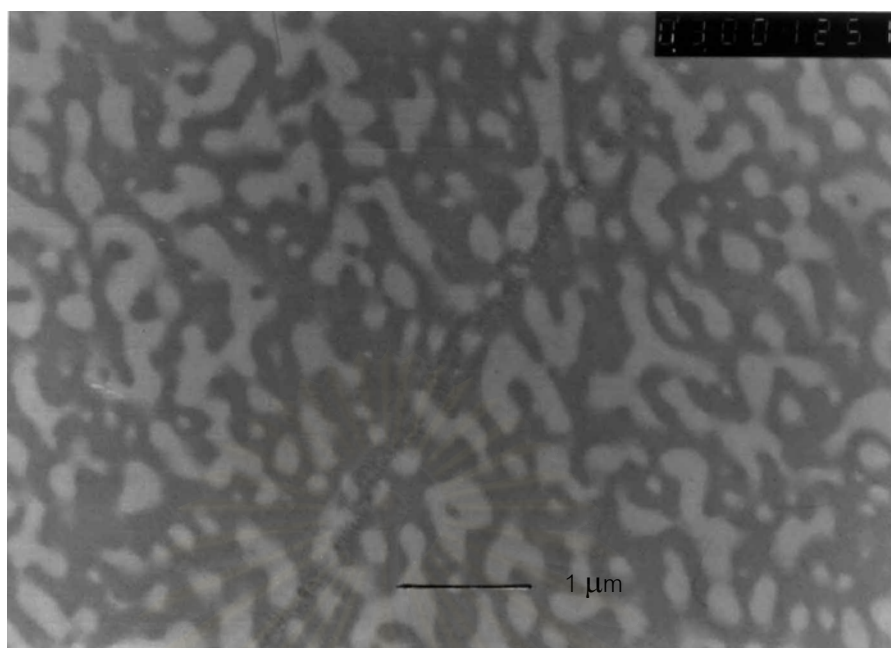


b

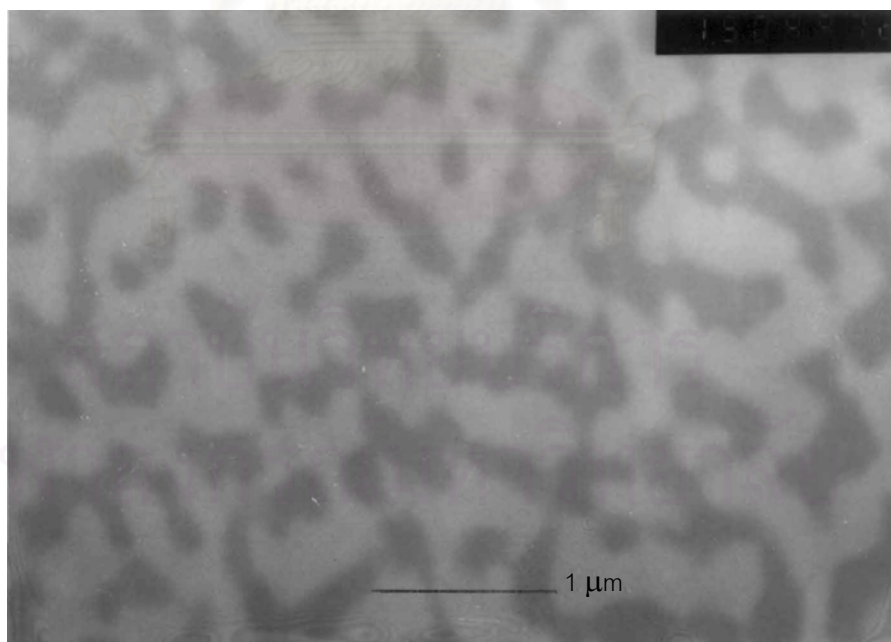


c

Figure 6.16: The TEM pictures of the 20/80 melt mixed SMA/PMMA phase separated at 220 °C at different stages of phase separation: (a) early stage, (b) intermediate stage, (c) late stage.

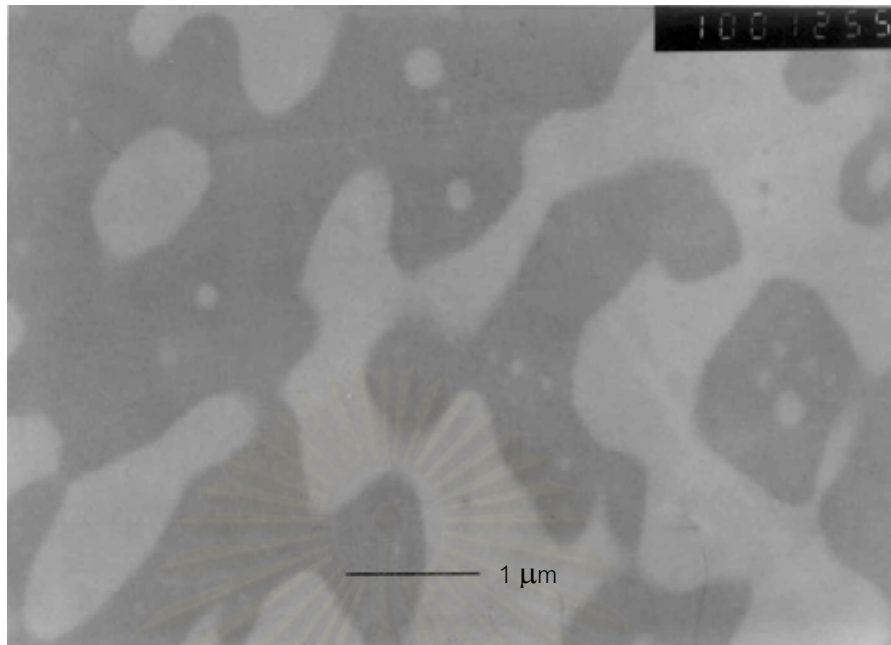


a



b

۰۰۲)



c

Figure 6.17: The TEM pictures of the 40/60 melt mixed SMA/PMMA phase separated at 220 °C at different stages of phase separation: (a) early stage, (b) intermediate stage, (c) late stage.

Interestingly, the kinetic experimental data can be related to morphology through the specific inter-domain distance $\Lambda(t)$, i.e, the wavelength of the dominant mode of the fluctuations. It is related to the scattering wave vector q , which is previously defined $(4n\pi/\lambda)\sin(\theta/2)$ in Chapter 3 as:

$$\Lambda(t) = \frac{2\pi}{q_m(t)} \quad (6.3)$$

The illustration of inter-domain distance of the spinodal structure and the concentration fluctuation are shown in Figure 6.22. Details of which can be seen elsewhere [Hashimoto 1991]

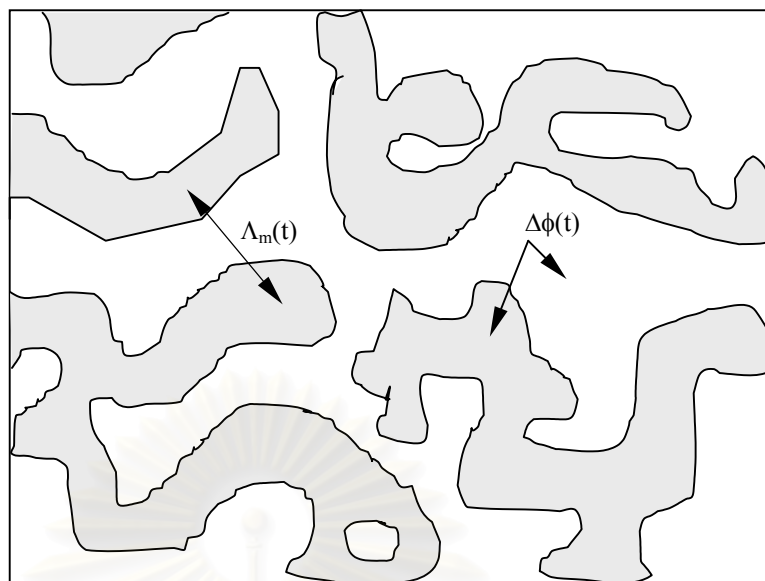


Figure 6.18: Illustration of inter-domain distance [Hashimoto 1991]

The comparisons of the inter-domain at different phase separation times obtained from Equation 6.3 using q_m from light scattering and from direct measurement using TEM are shown in Figures 6.19 and 6.20. The procedure of determining the inter-domain distance is reviewed in Appendix E.

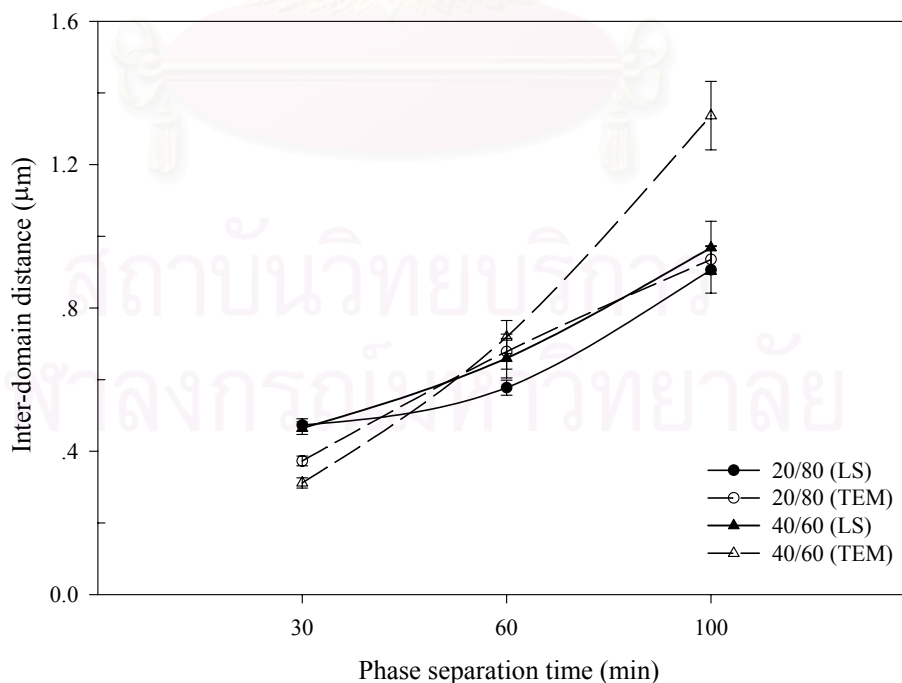


Figure 6.19: Comparison of inter-domain distance from light scattering and from TEM for the blends phase separated at 210 °C. The solid line represents the calculated data from light scattering while the broken line shows the trend of measured data from TEM.

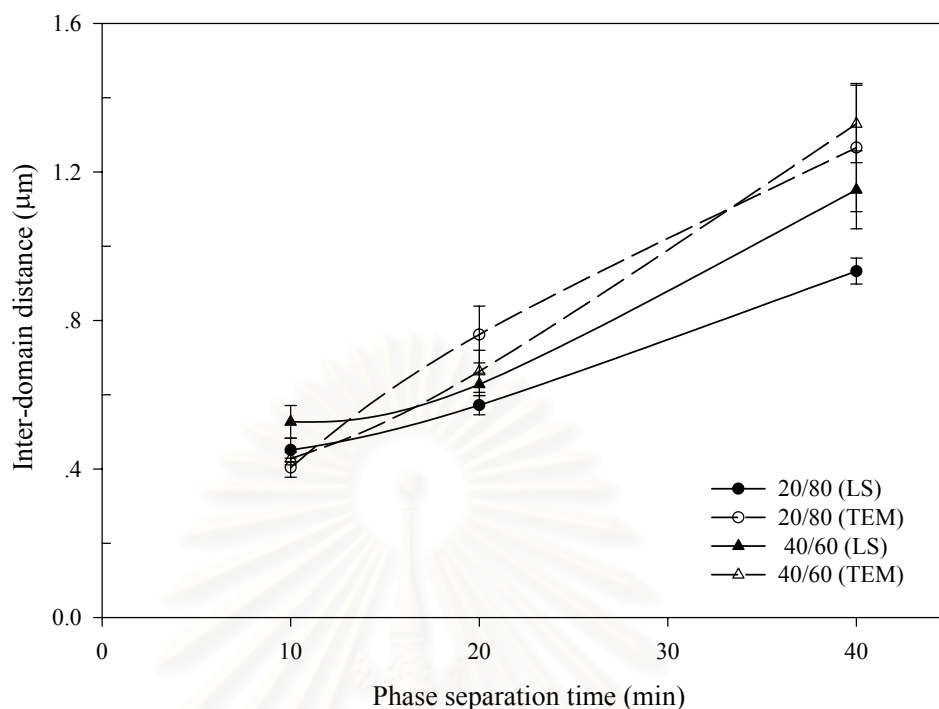


Figure 6.20: Comparison of inter-domain distance from light scattering and from TEM for the blends phase separated at 220 °C. The solid line represents the calculated data from light scattering while the broken line shows the trend of measured data from TEM

As seen in Figures 6.19, 6.20, the discrepancy between two techniques was found – the calculated data from light scattering experiment are higher than the measured data at low phase separation time but become lower at longer phase separation time. This might be attributed to the effect of heat distribution, thickness of the sample and method of heating. It should be noted that the samples for TEM observation were obtained from the fracture of thick sheet while the samples for light scattering experiment were just thin film on glass cover slips. Furthermore, the thick sheet for tensile test was directly heated all over the surface area inside the hydraulic hot press whereas the thin film was heated at only the rim, since inside the heating box, there is a hole at the centre to let the laser beam pass through. At the beginning of phase separation, since the blends for light scattering measurement is thinner than the thick sheet, heat can be transferred to the former easier and faster than to the latter. Consequently, phase separation in thin film is faster than in thick sheet. At longer

phase separation time, since the thick sheet was in complete contact with the heater while the thin film was just contacted at only the rim, this might result in the complete heating in the thick sheet, leading to perfect and faster phase separation. The difference of the inter-domain distance between two techniques becomes significant as the concentration of SMA is higher. This could be the result of the decrease in PMMAe, which exhibits slow dynamics, as described earlier in Chapter 5.

Figures 6.19, 6.20 were combined and replotted as a function of the reduced time τ (as defined in Eq 5.6). It is apparent that the data almost fall onto a master curve, i.e., the inter-domain distances of all blends are quite close to each other at the certain reduced time. This is in agreement with the result of the reduced time evolutions of q_m and I_m in Chapter 5, that also show a master curve as well, indicating that the relationship between q_m and Λ can be well described by Eq 6.3.

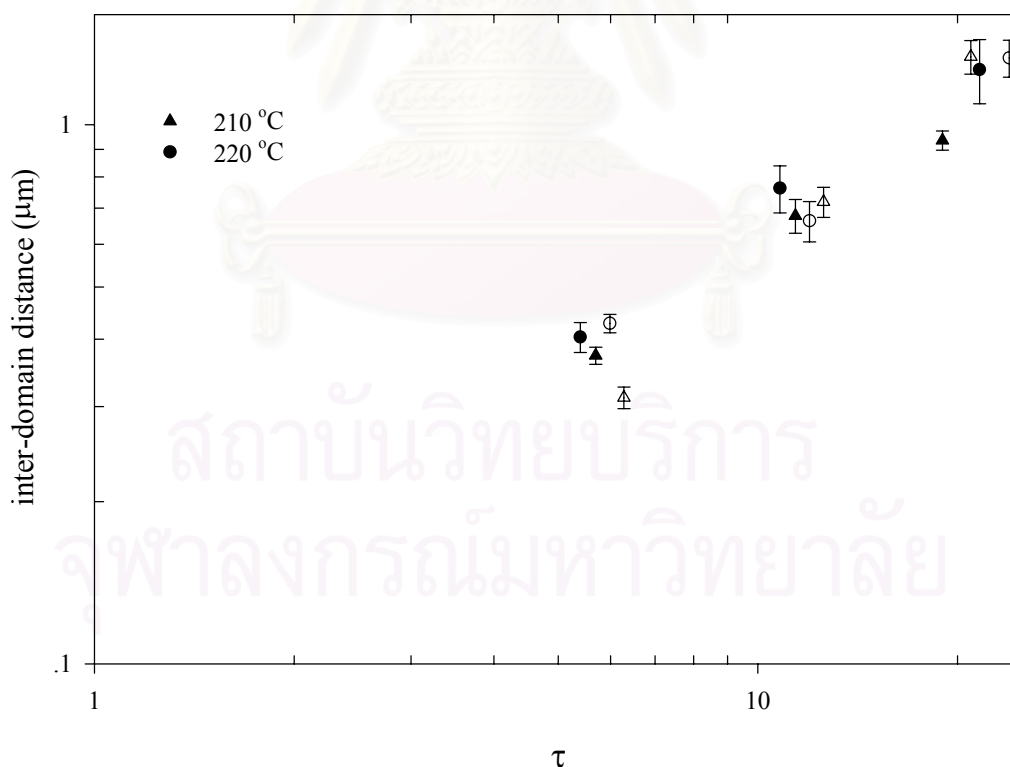


Figure 6.21: The inter-domain distance plotted as a function of reduced time for SMA/PMMAe blends. The closed objects represent 20/80 SMA/PMMAe blends while the open objects represent 40/60 SMA/PMMAe.

The relationship between tensile properties and the inter-domain size is definitely fascinating. Figures 6.6a and 6.8a were therefore replotted as a function of inter-domain distance. As seen in Figure 6.22, despite the same inter-domain distance, the tensile stress at break is still unequal. In addition, for the blends phase separated at 210 °C, the tensile stress at break remains constant as the inter-domain is increased. This is in agreement with what was found in 40/60 SMA/PMMAe. Comparing Figures 6.22 and 6.23, although the inter-domain is the same, the phase separated 20/80 SMA/PMMAe blends always have higher tensile stress at break. Hence, it is clear that the change of phase separating domain via spinodal decomposition has no influence on tensile properties. The change in composition during phase separation and the re-organising of the chain is believed to play a significant role on mechanical properties as the blend is phase separated.

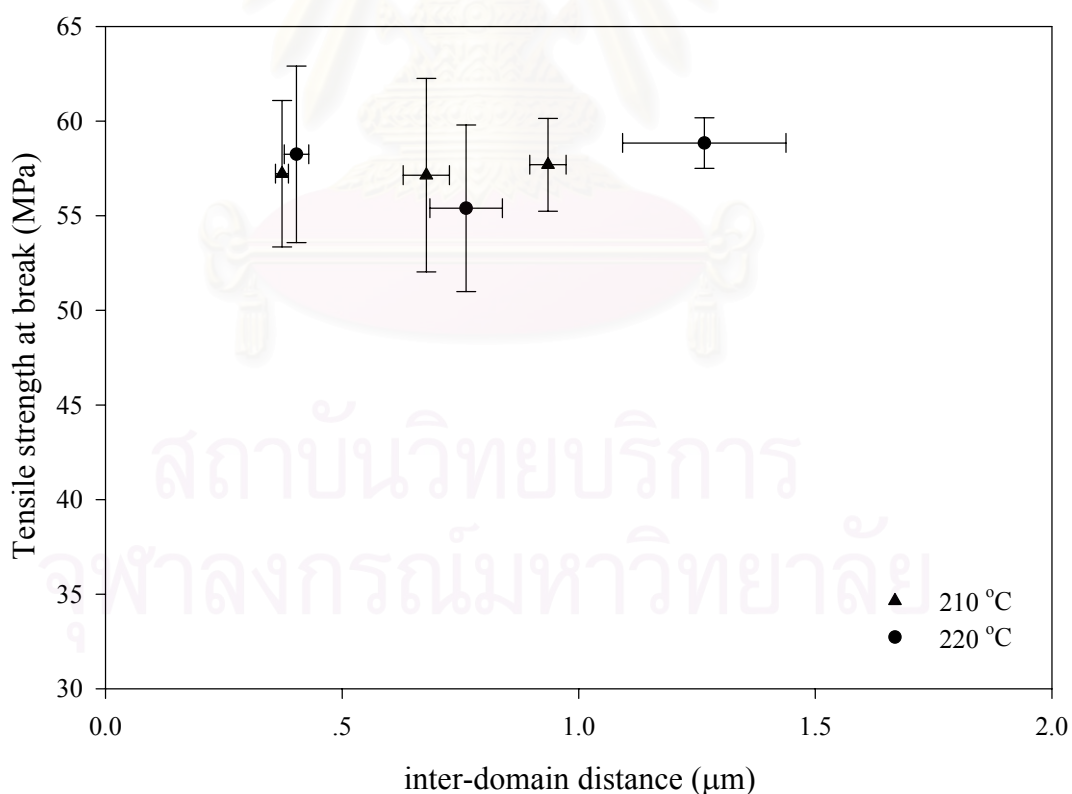


Figure 6.22: Plots of tensile stress at break as a function of inter-domain distance for 20/80 SMA/PMMAe blends.

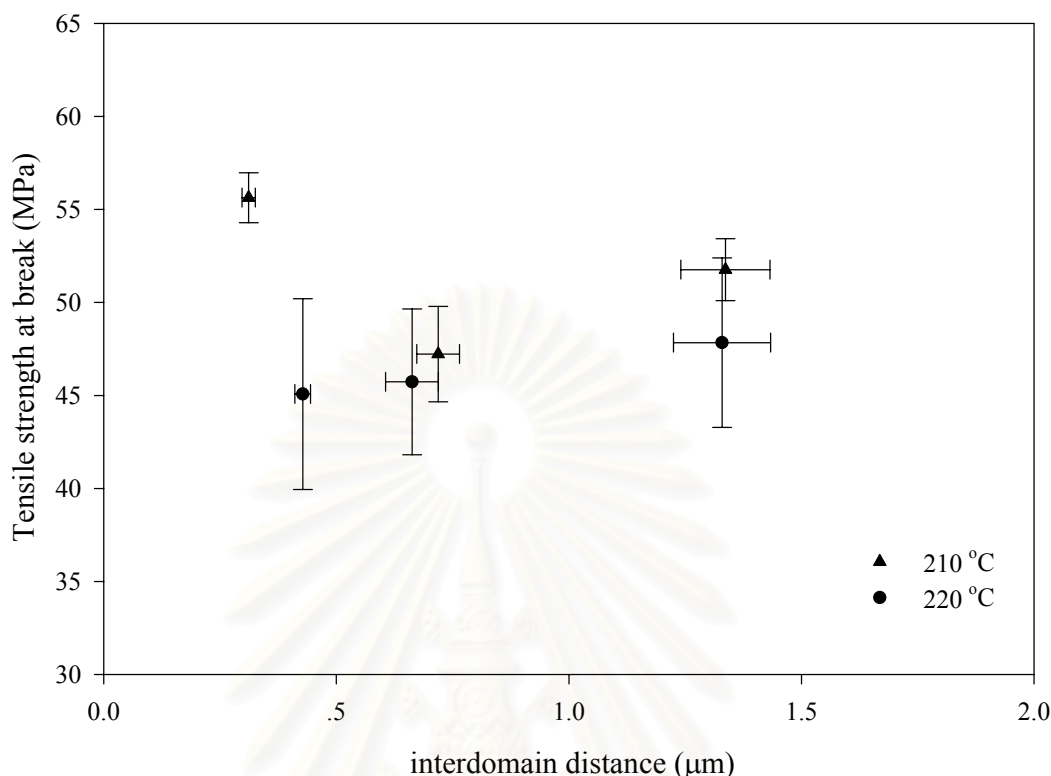


Figure 6.23: Plots of tensile stress at break as a function of inter-domain distance for 40/60 SMA/PMMAe blends.

6.3 Conclusions

It has been shown that electron microscopy can be an alternative way to monitor the development of spinodal decomposition. The co-continuous structure, which is rather unique and considered to be spinodal structure, was found for both compositions. The observed spinodal structure is consistent with what was found by Okada *et al.* [1993, 1995], who suggested that the co-continuous domain structures are produced at compositions close to the critical point, while at a composition far off the critical point, the isolated spherical domain structures are produced. The comparison between inter-domain from light scattering and TEM was carried out. Some discrepancies have been observed. This might be attributed to the effect of heat transfer, thickness and the method of heating.

The change of tensile properties is suggested to be the effect of the change of composition to stronger or weaker compositions. It could furthermore be the result of the change in connectivity between phase separating domain and two components rearranging themselves after heat treatment. It was found that the change in spinodal structure could not affect the tensile properties since the change of inter-domain distance from TEM pictures gives no evidence of size dependence. The change in composition after phase separation is supposed to play an important role in the first increase, while the weaker interface or less connectivity among phase separating domains, which plays a crucial role thereafter, may lead to the decrease in mechanical properties then. The final increase in tensile modulus might be the result of the structure recovery.

It should be noted that since both polymers are glassy and highly brittle materials. The mechanical properties are fairly close to each other. It is then very difficult to make a strong conclusion from mechanical result. It should be easier to investigate the mechanical properties of the blends of ductile and brittle materials.

สถาบันวิทยบริการ
จุฬาลงกรณ์มหาวิทยาลัย

Chapter VII

Conclusions and Recommendations

This work employed three different techniques, viz., light scattering, electron microscopy and tensile test to monitor a binary polymer blend – poly(methyl methacrylate) and poly(styrene-co-maleic anhydride). The miscibility and kinetics of phase separation of SMA/PMMAe blends was investigated using the light scattering technique. The effects of sample preparation methods on mixing and the kinetics phase separation of polymer blends were clearly explored. Furthermore, due to the recent interesting behaviour at the very beginning of phase separation, i.e. delay time, this phenomenon has been studied as well, covering the effect of composition, temperature, and sample preparation on delay time behaviour. From the kinetic data, two compositions, namely 20/80 SMA/PMMAe and 40/60 SMA/PMMAe, which stay on the same tie line but on the different sides of the critical point, were phase separated at different temperatures and stages of SD for tensile test. The effects of phase separation on mechanical properties and morphologies of SMA/PMMAe blends thus have been thoroughly studied.

7.1 Conclusions

Two main curves, which build up phase diagram in this work, consist of cloud point curve and spinodal curve. The cloud point, which is defined as the first rise of scattering intensity during heating samples can be obtained by performing light scattering experiments. It appears that this value depends on heating rate, the real cloud point can then be obtained from extrapolation to zero heating rate. The spinodal point on the other hand can be obtained by the projection to zero D_{app} , which is obtained from the y-axis intercept of $R(q)/q^2$ vs q^2 curve. It is clear that sample preparation do affect miscibility by lowering cloud point and spinodal curves, this might be due to solution cast method allowing enough time for both samples to mix completely. The rate of phase separation depends not only on sample preparation but also on composition of the blends. Comparing to the well-known Cahn-Hilliard linearised theory, the validity was found for a certain period. Delay time decreases

with increasing quench depth, it depends on either composition or sample preparation methods. Surprisingly, it was found that the theoretical approach by Nigal, which takes into account the effect of entanglement, showed a discrepancy with experimental results. This might be due to the effect of severe assumptions since some terms in the equation were omitted.

The scaling analysis was carried out to explore the later stage of phase separation. It appears that the relationship between the exponents α and β in the late stage SD fails to fit this system - this might be the effect of system dependence. The scaling function was found to be in agreement with the cluster model for off-critical composition. In conclusion, the light scattering technique can be used to classify each stage of spinodal decomposition. Furthermore, it should be borne in mind when mixing two polymers since the effect of sample preparation plays an important role.

The development of spinodal structure and tensile properties of phase separated samples were observed using electron microscopy and tensile testing machine. It appears that tensile properties were changed after phase separation. Nevertheless, it is suggested that this may not be the result of the change in spinodal size as observed through TEM. The change of composition, connectivity between phase separating domains and structure recovery could be other possibilities on the change of those properties. Furthermore, since not only do the tensile properties of the blends phase separated inside the early stage of SD decrease, but they also increase, this might be a positive result for processing these blends using an extruder since further anneal to one phase-region is not necessary any more.

The relationship between light scattering technique and electron microscopy technique was performed through the inter-domain distance; however, owing to the difference of thickness and method of heating, these result in the variation of heat transfer and lead to the discrepancy.

7.2 Recommendations

Although several points concerning this blend have been dealt with in this thesis, there still be some interesting points, which should be borne in mind and can be further researched in the future. These are some recommendations.

7.2.1 Effect of Sample Preparation on Kinetics of Phase Separation

It is accepted that sample preparations really have influence on miscibility and kinetics of phase separation. Measurements using FTIR and DSC indicate the stronger interaction in solution cast blend, nonetheless it should be noted that the residual solvent, which might be left in the solution cast blends, can play a significant role on phase separation as well. The powerful techniques such as solid state NMR might be able to trace a tiny amount of solvent as well as monitor the change of interaction between both polymers. The change in the composition of the new phase after phase separation also can be observed using this technique. The other interaction term due to the effect of sample preparation might be discovered and added to the Flory-Huggins classical equation, using SANS experiments.

7.2.2 Effects of Delay Time

Light scattering technique nowadays has utilised widely; nonetheless, it should be borne in mind that such a technique can monitor the change of a system within the limitation of micro-scale. Therefore, it would be interesting to study the change of polymer blend at the low scale limit using powerful techniques such as SANS, SAXS or WAXS. The study of phase separation a high q -scale might be able to explain the mystery of delay time.

As Clarke's model cannot be able to fit the experimental data in this work, it raises the question of how serious all assumptions in that model were made. This can be simply listed, for example, the q -independent mobility, the equal degree of polymerisation, the omission of viscoelastic term, etc. It might be worth considering

the full equation closely. However, in order to fit the full equation, several physical parameters are required such as degree of polymerisation, entanglement molar mass, relaxation time according to the reptation model, the Flory-Huggins interaction parameters, etc.

7.2.3 Mechanical Properties

It is clear that the mechanical properties of each sample from three stages of phase separation are very close to each other. The result, therefore, might become clearer if more samples are added to each stage of phase separation. Furthermore, since SMA used in this work is really a lab-grade material, it thus contains very few solvents or additive and this might be the reason why the blends show inferior properties due to adding SMA.

As suggested by Kyu *et al.* [1991], the toughness of polymer blends can be increased due to phase separation; this might be difficult to accomplish in this work since both materials are glassy and highly brittle polymers. Nevertheless, as this blend is very brittle it should be worth studying the fracture behaviour by preparing a notch sample. A standard test method for plane-strain fracture toughness and strain energy release rate of plastic materials (ASTM D 5045-95) is recommended. Furthermore, to change samples to the blends between ductile and brittle materials can be an alternative way to study the effect of spinodal structure on mechanical properties. Ductile particles can act not only as stress concentrators, initiating crazes in the surrounding matrix but also as craze terminators, preventing uninhibited growth of the cracks, which would result in premature failure. Nonetheless, to choose a particular blend, it should be borne in mind that each component should have a significant difference in T_g since this can facilitate the way to detect phase separation. Furthermore, as the processing temperature inside the extruder is usually high and sometimes is higher than phase separation temperature, the blends are thus required to be annealed for a certain time before making thin sheeting. Consequently, other blends having processing temperature lower than phase separation temperature are

recommended. The miscibility of SMA/PC blend was recently published [Merfeld *et al.* 1998].

7.2.4 Morphology

As shown in the electron micrographs, the variation of co-continuous domain with phase separation time can be clearly seen. The inverse of type of minor phase was found for both compositions, and was discussed earlier based on the lever rule. It is thus worth investigating closely the amount of each phase. A measurement of each area can be further studied. Moreover, it would be interesting to investigate the variation in the size of structural unit of phase separated blends prepared by different methods and at a variety of phase separation times using electron microscopy technique such as TEM since it has been suggested that the preparation methods affect the way each molecule packs inside the blends [Mansour *et al.* 1997].

Alternatively, spinodal structure can be investigated in three dimensions using other techniques such as AFM. The depth and size of each phase can be measured and used to construct a 3-D model. This can be further compared with previous theories such as a linearised theory, de Gennes theory, etc.

References

- Abtal, E ; Prud'homme, R. E. Polymer. 37 (1996) : 3805.
- Adams, G. W.; Schmitt, J. L.; Zalabsky, R. A., J. Chem. Phys. 81 (1984) : 5074.
- Aelmans, N. J. J.; Reid, V. M. C.; Higgins, J. S. Polymer. 40 (1999) : 5051.
- Aelmans, N. J. J.; Reid, V. M. C.; Higgins, J. S. Macromol. Sympo. 149 (2000) : 53.
- Akcasu, A. Z.; Nagele, G.; Klein, R. Macromolecules. 28 (1995) : 6680.
- Akcasu, A. Z. Macromol. Theo. Simu. 6 (1997) : 679.
- Allen, S.G. Comprehensive Polymer Science. London : Pergamon press, 1989.
- An, L.; Wolf, B. A. Macromolecules. 31 (1998) : 4621.
- Argon, A. S.; Hannoosh, J. C.; Salama, M. M. Fracture 1977. Vol. 1, Waterloo, Canada, 1977.
- Bank, M.; Leffingwell, J.; Thies, C. J. Polym. Sci., Part A-2. 10 (1972) : 1097.
- Bates, F. S.; Fredrickson, G. H. Macromolecules. 27 (1994) : 165.
- Berry, J.P. Fracture. Auerbach B.L., *et al.* (eds), New York : John Wiley & Sons, Inc., 1959.
- Bever, M. B.; Shen, M. Mats. Sci. Eng. 15 (1974) : 145.
- Billmeyer, F. W. Textbook of Polymer Science. New York : John Wiley & Sons, Inc., 1984.
- Binder, K.; Stauffer, D. Phys. Rev. Letts. 33, (1974) : 1006.
- Binder, K. J. Chem. Phys. 79 (1983) : 6387.
- Binder, K.; Frisch, H. L.; Jackle, J. J. Chem. Phys. 85 (1986) : 1505.
- Binder, K. Spinodal Decomposition. Cahn, R. W.; Haasen, P.; Kramer, E. J. (eds.), in Materials Science and Technology, Vol. 5, Weinheim : VCH, 1991.
- Binder, K. J. Non-Equilib. Thermodyn. 23 (1998) : 1.
- Bohn, L. Rubber Chem. Technol. 41 (1973) : 37.
- Brandrup, J; Immergut, E. H. Polymer Handbook. vol.1., New York : John-Wiley & Sons, 1992.
- Brannock, G. R.; Barlow, J. W.; Paul, D. R. J. Polym. Sci., Part B: Polym. Phys. 29 (1991) : 413.
- British Standard Institution (BSI) Plastics-Determination of tensile properties: Part 1 General principles. BS EN ISO 527-1, 1996.

- Brochard, F.; Joultrouy, J.; Levinson, P. Macromolecules. 16 (1983) : 1638.
- Brydson, J. A. Plastic Materials. 6th edition, Oxford : Butterworth Heinenmann, 1979.
- Buchak, B. E.; Ramey, K. C. Polym. Lett. Ed. 14 (1976) : 401.
- Cabral, J. T.; Gerard, H.; Clarke, N.; Higgins, J. S. Physica B. 276 (2000) : 408.
- Callen, H. B. Thermodynamics and an introduction to thermostatistics. New York: John Wiley & Sons, Inc., 1985.
- Cahn, J. W. Trans. Metall. Soc. AIME. 242 (1968) : 166.
- Cahn, J. W.; Hilliard, J. E. J. Chem. Phys. 28 (1958) : 258.
- Cahn, J. W.; Hilliard, J. E. J. Chem. Phys. 31 (1959) : 688
- Carmesin, H. O.; Heermann, D. W.; Binder, K. Phys B: Condensed Matter. 65 (1986): 89.
- Chai, Z., Ruona, S., Walsh, D. J., Higgins, J. S. Polymer. 24 (1983) : 263.
- Chai, Z., Walsh, D. J. Makromol. Chem. 184 (1983) : 1549.
- Charrier, J. M. Polymeric Materials and Processing. New York : Hanser Publishers, 1990.
- Chen, C. Y.; Yunus, W. Md. Z. W.; Chiu, H.W.; Kyu, T. Polymer. 38 (1997) : 4433.
- Chopra, D.; Vlassopoulos, D.; Hatzikiriakos, S. G. J Rheology. 42 (1998) : 1227.
- Chou, Y. C.; Goldburg, W.I. Phys. Rev. A. 20 (1979) : 2105.
- Chrystomou, A.; Hashemi, S. J. Mat. Sci. 33 (1998) : 1165.
- Clarke, N. Theoretical Aspects of Linear/Branched Polymer Blends, Ph.D. Thesis, UK: University of Sheffield, 1994.
- Clarke, N.; Mcleish, T. C. B.; Pavawongsak, S.; Higgins, J. S. Macromolecules. 30 (1997) : 4459.
- Coleman, M. E.; Graf, J. F.; Painter, P. C. Specific Interactions and the Miscibility of Polymer Blends. Pennsylvania : Technomic Publishing Company, Inc., 1991.
- Composto, R. J.; Kramer, E. J.; White, D. M. Macromolecules. 21 (1988) : 2580.
- Cook, H. E. Acta Met. 18 (1970) : 297.
- Cowie, J. M.G. Polymers: Chemistry & Physics of Modern Materials. London : Blackie and Son Limited, 1991.
- Cruz, C. A.; Barlow, J. W.; Paul, D.R. Macromolecules. 12 (1979) : 726.

- Cummings, A.; Wilzius, P.; Bates, F. S.; Rosendale, J. H. Phys. Rev. A. 45 (1992) : 885.
- de Gennes, P. G. J. Chem. Phys. 55 (1972) : 572.
- de Gennes, P. G. Scaling Concept in Polymer Physics. New York : Cornell Univ. Press, 1979.
- de Gennes, P. G. J. Chem. Phys. 72 (1980) : 4756.
- Doi, M.; Edwards, S. F. The Theory of Polymer Dynamics. New York : Oxford University Press, 1986.
- Doi, M. Introduction to Polymer Physics. Oxford : Oxford University Press, 1996.
- Donald, A. M.; Kramer, D. J. Polymer. 23 (1982) : 457.
- Dorgan, J. R.; Yan, D. Macromolecules. 31 (1998) : 193.
- Dugdale, D. S. J. Mech. Phys. Solids. 8 (1960) : 100.
- Edel, V. Macromolecules. 28 (1995) : 6219.
- Eichinger, B. E.; Flory P. J. Trans. Faraday Soc. 64 (1968) : 2035.
- Elicabe, G. E.; Larrondo, H. A.; Williams, R. J. J. Macromolecules. 30 (1997) : 6550.
- Elicabe, G. E.; Larrondo, H. A.; Williams, R. J. J. Macromolecules. 31 (1998) : 8173.
- Ellis, T. S. Macromolecules. 22 (1989) : 742.
- Ermi, B. D.; Nisato, G.; Douglas, J. F.; Rogers J. A.; Karim A. Phys. Rev. Lett. 81 (1998) : 3900.
- Eyring, H.; Hirschfelder, J. O. J. Phys. Chem. 41 (1937) : 249.
- Feng, H.; Shen, L.; Feng, Z. Eur Polym J. 31 (1995) : 243.
- Fernandez, M. L.; Higgins, J. S.; Tomlins, P. E. Polymer. 30 (1989) : 3.
- Flory, P. J. J. Chem. Phys. 9 (1941) : 660.
- Flory, P. J. J. Chem. Phys. 10 (1942) : 51
- Flory, P. J. J. Am. Chem. Soc. 87 (1965) : 9.
- Fowler, R. H.; Rushbrooke, G. S. Trans. Faraday Soc. 33 (1937) : 1272.
- Fox, T. G. Bull. Am. Phys. Soc. 2 (1956) : 123.
- Freed, K. F.; Dudowicz, J. Macromolecules. 31 (1998) : 6681.
- Freed, K. F.; Dudowicz, J.; Forman, K. W. J. Chem. Phys. 108 (1998) : 7881.
- Freed, K. F.; Dudowicz, J. Macromolecular Symposia 149 (2000) : 11.

- Fruitwala, H. Phase Separation in Polymer Blends and Its Effects on Mechanical Properties, Ph.D. Thesis, London: Imperial College, 1988.
- Furukawa, H. Prog. Theor. Phys. 59 (1978) : 1072.
- Furukawa, H. Adv. Phys. 34 (1985) : 703.
- Furukawa, H. Phys. Rev. B. 33 (1986) : 638.
- Furusaka, M.; Ishikura, Y.; Mera, M. Phys. Rev. Lett. 54 (1985) : 2611.
- Gaurab, D.; Banerjee, A. N. J. Appli. Polym. Sci. 61 (1996): 1473.
- Geoghegan, M.; Jones, R. A. L.; Clough, A. S., J. Chem. Phys. 103 (1995) : 2719.
- Gerard, H.; Higgins, J. S.; Clarke, N. Macromolecules 32 (1999) : 5411.
- Gibbs, J. W. The Collected Works of J. Willard Gibbs. vol. I, London : Longmans and Green, 1932.
- Gopakumar, T. G.; Ponrathnam, S.; Rajan, C. R.; Fradet, A. Polymer. 39 (1998) : 2221.
- Gordon, M.; Taylor, J. S. J. Appl. Chem. 2 (1952) : 495.
- Granasy, L. J. Chem. Phys. 104 (1996) : 5188.
- Granasy, L. Solid state Phenomena. 56 (1997) : 67.
- Guo, W.; Higgins, J. S. Polymer. 31 (1990) : 699.
- Hashimoto, T.; Itakura, M.; Hasegawa, H. J. Chem. Phys. 85 (1986a) : 6118.
- Hashimoto, T.; Itakura, M.; Shimidzu, N. J. Chem. Phys., 85 (1986b) : 6773.
- Hashimoto, T.; Takenaka, M.; Jinnai, H. J. Appl. Cryst., 24 (1991) : 457.
- Hashimoto, T. Structure and Properties of Polymer. Thomas, E. L. (ed.), in Materials Science and Technology, Vol. 12, Weinheim : VCH, 1993.
- Higgins, J. S.; Fruitwala, H.; Tomlins, P. E. Br. Polym. J. 21 (1989a) : 247.
- Higgins, J. S.; Fruitwala, H.; Tomlins, P. E. Macromolecules. 22 (1989b) : 3674.
- Hildebrand, J. H.; Scott, R. L. The Solubility of Non-Electrolytes. New York, 1964.
- Hill, R. G.; Tomlins, P. E.; Higgins, J. S. Macromolecules. 18 (1985): 2555.
- Hilliard, J. E. Phase Transformations American Society for Metal. New York : Chapman & Hall co., Ltd., 1970.
- Honeycutt, J. D. Macromolecules. 27 (1994) : 5377.
- Huggins, M. L. J. Chem. Phys. 9 (1941) : 440.
- Huggins, M.L. J. Phys. Chem. 46 (1942) : 151.

- Hung, C. H.; Krasnopoler, M. J.; Katz, J. L. J. Chem. Phys. 90 (1989) : 1856.
- Hung, C. H.; Krasnopoler, M. J.; Katz, J. L. J. Chem. Phys. 92 (1990) : 7722.
- Inoue, T.; Ougizawa, T.; Yasuda, O.; Miyasaka, K. Macromolecules. 18 (1985) : 57.
- Izumitani, T.; Takenake, M.; Hashimoto, T. J. Chem. Phys. 92 (1990) : 276
- Jinnai, H.; Hasegawa, H.; Hashimoto, T.; Han, C. C. J. Chem. Phys. 99 (1993) : 4845.
- Katano, S.; Iizumi, M. Phys. Rev. Lett. 52 (1984) : 835.
- Kelton, K. F.; Greer, A. L.; Thompson, C. V. J. Chem. Phys. 79 (1983) : 6261.
- Kim, J. H.; Karasz, F. E.; Malone, M. F. Polym. Eng. Sci. 31 (1991) : 13.
- Kleiner, L. W.; Karasz, F. E.; Macknight, W. J. Polym. Eng. Sci. 19 (1979) : 519.
- Kleintjens, L. A. Fluid Phase Equilib. 10 (1983) : 183.
- Kodama, M. Polym. Eng. Sci. 33 (1993a) : 10.
- Kodama, M. Polym. Eng. Sci. 33 (1993b) : 17.
- Komura, S.; Osamura, K.; Fujii, H.; Takeda, T. Phys. Rev. B. 31 (1985) : 1278.
- Kramer, E. J.; Green, P.; Polmstrona, C. J. Polymer. 25 (1984) : 473.
- Kyu, T.; Saldanha, J. M.; Kiesel, M. J. Two-phase polymer systems progress in polymer processing. Utracki, L.A. (ed.), Carl Hanser Verlag, 1991.
- Lablans-Vinck, A. M.; Koningsveld, R.; Kleintjens, L. A.; Diepen, G. A. M. Fluid Phase Equilib. 20 (1985) : 347.
- Lacombe, R. H.; Sanchez, I. C. J. Phys. Chem. 80 (1976) : 2568.
- Langer, J. S. Acta Met. 21 (1973) : 1649.
- Lange, J. S.; Bar-on, M.; Miller, H.D. Phys. Rev. A. 11 (1975) : 1417.
- Lauger, J.; Lay, R.; Maas, S.; Gronski, W. Macromolecules. 28 (1995) : 7010.
- Lefebvre, A. A.; Lee, J. H.; Jeon, H. S.; Balsara, N. P.; Hammouda, B. J. Chem. Phys. 111 (1999) : 6082.
- Lifshitz, I. M.; Slyozov, V. V. J. Phys. Chem. Solids. 19 (1961) : 35.
- Lipatov, Y. S.; Rosovitskii, V. F.; Maslak, Y. V.; Zakharendo, S. A. Mech. Compo. Mater. 21 (1985) : 484.
- Manda, D., PhD Thesis, London: Imperial College, 1998.
- Manda D.; Higgins J. S.; Aelmans N. J; Reid V. M. C. To be submitted to Polymer.
- Mansour, A. A.; Madbouly, S. A.; Hohne, G.; Dollhopf, W. Polym. Int. 42 (1997) : 143.

- Marro, J.; Lebowtiz, J.L.; Kalos, M. H. Phys. Rev. Lett. 43 (1979) : 282.
- Mazumder, S.; Sen, D.; Batra, I. S.; Tewari, R.; Dey, G. K.; Banerjee, S.; Sequeira, A.; Amenitsch, H.; Bernstorff, S. Phys. Rev. B. 60 (1999) : 822.
- Mc Clelland, B. J. Statistical thermodynamic. London : Chapman & Hall & Science, 1973.
- Mc Crum, N.G.; Buckley, C.P.; Bucknall, C.B. Principles of Polymer Engineering. 2nd edition, Oxford: Oxford University Press, 1997.
- Mc Master, L.P. Macromolecules. 6 (1973) : 760.
- Mecke, K. R.; Sofonea, V. Phys. Rev. E. 56 (1997) : R3761.
- Mendenhall, W.; Sincich, T. A Second Course in Statistics: Regression Analysis. 5th edition, New Jersey : Prentice-Hall International, 1996.
- Merfeld, G. D.; Paul, D. R. Polymer. 39 (1998) : 1999.
- Moore, J. C. J. Polym. Sci. A2 (1964) : 835.
- Muller, G.; Schwahn, D.; Springer, T. Phys. Rev. E. 55 (1997) : 7267.
- Narisawa, I.; Yee, A. F. Crazing and Fracture of Polymers. Thomas, E. L. (ed.), in Materials Science and Technology, Vol. 12, Weinheim : VCH, 1993.
- Neo, M. K.; Gho, S. H. Polymer. 33 (1992) : 2012.
- Nestler, B.; Wheeler, A. A; Ratke, L.; Stocker, C. Physica D. 141 (2000) : 133.
- Nishi, T.; Wang, T.T.; Kwei, T. K. Macromolecules. 8 (1975) : 222.
- Nishimoto, M.; Keskkula, H.; Paul, D. R. Polymer. 32 (1991) : 272.
- Nojima, S.; Tsusumi, K.; Nose, T. Polymer. 14 (1982) : 225.
- Nyquist, R. M.; Talanquer, V.; Oxtoby, D. W. J. Chem. Phys. 103 (1995) : 1175.
- Okada, M.; Kwak K. D.; Chiba, T.; Nose, T. Macromolecules. 26 (1993) : 6681.
- Okada, M.; Sun, J.; Tao, J.; Chiba, T.; Nose, T. Macromolecules. 28 (1995) : 7514.
- Olabisi, O. Macromolecules. 9 (1975) : 316.
- Olabisi, O; Robeson, L. M.; Shaw, M. T. Polymer- Polymer Miscibility. London : Academic Press, Inc. (London) Ltd., 1979.
- Onuki, A.; Hashimoto, T. Macromolecules. 22 (1989) : 879.
- Ostwald, W. Z. Phys Chem. 34 (1900) : 495.
- Oxtoby, D. W.; Evans, R. J. Chem. Phys. 89 (1988) : 7521.

- Paul, D. R.; Newman, S. Polymer blend. Vol. 1&2, London : Academic Press, Inc. (London) Ltd., 1978.
- Pavawongsak, S. PhD Thesis London : Imperial College, 1996.
- Perreault, F.; Prudhomme, R. E. Polym. Eng. Sci. 35 (1995) : 34.
- Pincus, P. J. Chem. Phys. 75 (1981) :1996.
- Porod, G. Small Angle X-ray Scattering. Glatter, O.; Kratky, O. (eds.), London: Academic Press, 1982.
- Porter, C. E.; Plum, F. D. Macromolecules. 33 (2000) : 7016.
- Prigogine, I. The Molecular Theory of Solutions. Amsterdam: North-Holland Publishing Co., 1959.
- Reich, S.; Cohen, Y. J. Polym. Sci., Part B: Polym. Phys. 19 (1981) : 1255.
- Ribbe, A.E.; Hashimoto, T. Macromolecules. 30 (1997) : 3999.
- Robard, A.; Patterson, D. Macromolecules. 10 (1977) : 706.
- Rosato, D. V.; Dimattia, D. P.; Rosato, D. V. Designing with Plastics and Composites a Handbook. New York : Van Nostrands-Reinhold, 1991.
- Rostami, S.; Wash, D.J. Macromolecules 17 (1984) : 315.
- Rowlinson, J. S. Liquid and Liquid Mixtures. London : Butterworth and Co., Ltd., 1959.
- Rundman, K.B.; Hilliard, J. E. Acta Met. 15 (1967) : 1025.
- Saito, H.; Fujita, Y.; Inoue, T. Polymer. 19 (1987) : 405.
- Saldanha, J. M.; Kyu, T. Macromolecules. 20 (1987) : 2840.
- Sanchez, I. C.; Lacombe, R. H. J. Phys. Chem. 80 (1976) : 2352.
- Sanchez, I. C.; Lacombe, R. H. Macromolecules. 11 (1978) : 1145.
- Sanchez, I. C; Stone, M. T. Statistical Thermodynamics of Polymer Solutions and Blends. Paul, D. R.; Bucknall, C. B. (eds.), in Polymer Blends Vol. I: Formulation. New York : John Wiley & Sons, Inc., 2000.
- Sasaki, K.; Hashimoto, T. Macromolecules. 17 (1984) : 2818.
- Sato, T.; Han, C. C. J. Chem. Phys. 88 (1988) : 2057.
- Saucer, J. A.; McMaster, A. D.; Morrow, D. R. J. Macromol. Sci., Phys. B12 (1976) : 535.

- Scheirs, J. Compositional and Failure Analysis of Polymers- A Practical Approach.
Chichester : John Wiley & Sons, Ltd, 2000.
- Schwahn, D.; Janssen, S.; Springer, T. J. Chem. Phys. 97 (1992) : 8775.
- Schwahn, D.; Janssen, S.; Muller G.; Springer, T.; Eckerlebe, H.; Rieger, J. Phys. B
213 (1995) : 688.
- Serrano, B.; Baselga, J.; Bravo, J.; Mikes, F.; Sese, L.; Estaban, I.; Pierola, I. F. J. Fluorescence 10 (2000) : 135.
- Shah, V. S.; Keitz, J. D.; Paul, D. R.; Barlow, J. W. J. Appl. Polym. Sci. 32 (1986) :
3863.
- Shaw, M. T. Polym. Eng. Sci. 25 (1984) : 373.
- Shultz, A. R.; Young, A. L. Macromolecules. 13 (1980) : 663.
- Siegert, M.; Rao, M., Phys. Rev. Letts. 70 (1993) : 1956.
- Siggia, E. D. Phys. Rev. A. 20 (1979) : 595.
- Sillescu, H. Makromol. Chem., Rapid Comm. 5 (1984) : 519.
- Simha, R.; Somcynsky, T. Macromolecules. 2 (1969) : 342.
- Silverstein, R. M.; Bassler, G. C.; Morrill, T. C. Spectrometric Identification of Organic Compounds. New York : John Wiley & Sons, Inc., 1991.
- Snyder, H. L.; Meakin, P.; Reich, S. Macromolecules. 16 (1983) : 757.
- Snyder, H. L.; Meakin, P. J. Polym. Sci.: Polym. Symp. 73 (1985) : 217.
- Soontaranun, W. Effect of Flow on the Miscibility of Partially Miscible Polymer Blends, PhD. Thesis, Londond : Imperial College, 1997.
- Stevens, M. P. Polymer Chemistry, An Introduction. New York : Oxford University Press, 1990.
- Strey, R.; Wagner, P. E.; Schmeling, T. J. Phys. Chem. 84 (1986) : 2325.
- Strobl, G. R. Macromolecules. 18 (1985) : 558.
- Strobl, G. R. The Physics of Polymers: concepts for understanding their structures and behaviour. Berlin : Springer Verlag, 1997.
- Tacx, J. C. J. F.; Meijerink, N. L. J.; Suen, K. Polymer. 37 (1996) : 4307.
- Takenaka, M.; Hashimoto, T. J. Chem. Phys. 96 (1992) : 6177.
- Takeno, H.; Nakamura, E.; Hashimoto, T. J. Chem. Phys. 110 (1999) : 3612.
- Talanquer, V.; Oxtoby, D. W. J. Chem. Phys. 103 (1995) : 3686.

- Thongyai S. PhD Thesis London : Imperial College, 1994.
- Tomlins, P. E.; Higgins, J. S. J. Chem. Phys. 90 (1989) : 6691.
- Tompa, H. Polymer Solutions. London : Butterworth, 1956.
- Utracki, L. A. Polymer Alloys and Blends: Thermodynamics and Rheology. New York : Hanser Publishers, 1989.
- Utracki, L. A. Two-Phase Polymer Systems. New York : Hanser Publishers, 1991.
- Utracki, L. A. Polym. Eng. Sci. 35 (1995) : 2.
- Van Noije, T. P. C.; Ernst, M. H. Phys. Rev. E. 61 (2000) : 1765.
- Varnell, D. F.; Runt, J. P.; Coleman, M. M. Macromolecules. 14 (1981) : 1350.
- Wagner, A. J.; Yeomans, J. M. Phys. Rev. Letts. 80 (1998) : 1429.
- Wang, F. C. J. Chromatography A. 756 (1997) : 279.
- Ward, I. M.; Hadley, D. W. An Introduction to the Mechanical Properties of Solid Polymers. West Sussex : John Wiley & Sons Ltd., 1993.
- Wendlandt, W. W. Thermal Analysis. New York : John Wiley & Sons, Inc., 1986.
- Wiltzius, P.; Bates, F. S.; Heffner, W. R. Phys. Rev. Letts. 60 (1988) : 1538.
- Woo, E. M., Barlow, J.W., Paul, D.R. Polymer. 26 (1985) : 763.
- Woo, E. M.; Su, C. C. Polymer. 37 (1996) : 4111.
- Xie, R.; Liang, H.; Yang, B.; Jiang B.; Zhang, Q.; Xu, Y. J. Appli. Polym. Sci. 50 (1993) : 1397.
- Yeh, G. S. Y. J. Macromol. Sci. Phys. B6 (1972) : 451.
- Zoller, P. J. Polym. Sci.: Polym. Phys. Ed. 18 (1980) : 897.



Appendices

สถาบันวิทยบริการ
จุฬาลงกรณ์มหาวิทยาลัย

Appendix A

Error analyses

Most experimental data in this thesis are reported with the error bar of 95 % confidence. It should be noted that the 95% confidence interval or 0.95 confidence coefficient in fact means if it is assumed that the distribution is the normal probability distribution, 95% of data fall within this region. The value can be defined as;

$$t_{.025}\left(\frac{\sigma}{\sqrt{n}}\right) \quad (\text{A-1})$$

where $t_{.025}$ is the standard normal value of $t_{.025}$ at the degree of freedom of $(n-1)$, as can be seen in figure A-1.

σ is standard deviation

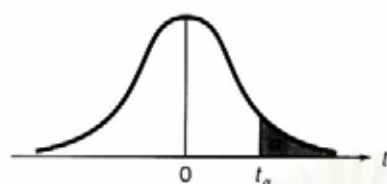
n is number of data

For example

From tensile test, it appears that the standard deviation of tensile modulus of PMMAe is 1.3035 and the number of specimen is five. At the column of $t_{.025}$ and the degree of freedom of 4 in figure A-1, it gives 2.776. The value of 95% confidence therefore is 1.6182.

สถาบันวิทยบริการ
จุฬาลงกรณ์มหาวิทยาลัย

Figure A-1: Critical value for student's t



ν	$t_{.100}$	$t_{.050}$	$t_{.025}$	$t_{.010}$	$t_{.005}$	$t_{.001}$	$t_{.0005}$
1	3.078	6.314	12.706	31.821	63.657	318.31	636.62
2	1.886	2.920	4.303	6.965	9.925	22.326	31.598
3	1.638	2.353	3.182	4.541	5.841	10.213	12.924
4	1.533	2.132	2.776	3.747	4.604	7.173	8.610
5	1.476	2.015	2.571	3.365	4.032	5.893	6.869
6	1.440	1.943	2.447	3.143	3.707	5.208	5.959
7	1.415	1.895	2.365	2.998	3.499	4.785	5.408
8	1.397	1.860	2.306	2.896	3.355	4.501	5.041
9	1.383	1.833	2.262	2.821	3.250	4.297	4.781
10	1.372	1.812	2.228	2.764	3.169	4.144	4.587
11	1.363	1.796	2.201	2.718	3.106	4.025	4.437
12	1.356	1.782	2.179	2.681	3.055	3.930	4.318
13	1.350	1.771	2.160	2.650	3.012	3.852	4.221
14	1.345	1.761	2.145	2.624	2.977	3.787	4.140
15	1.341	1.753	2.131	2.602	2.947	3.733	4.073
16	1.337	1.746	2.120	2.583	2.921	3.686	4.015
17	1.333	1.740	2.110	2.567	2.898	3.646	3.965
18	1.330	1.734	2.101	2.552	2.878	3.610	3.922
19	1.328	1.729	2.093	2.539	2.861	3.579	3.883
20	1.325	1.725	2.086	2.528	2.845	3.552	3.850
21	1.323	1.721	2.080	2.518	2.831	3.527	3.819
22	1.321	1.717	2.074	2.508	2.819	3.505	3.792
23	1.319	1.714	2.069	2.500	2.807	3.485	3.767
24	1.318	1.711	2.064	2.492	2.797	3.467	3.745
25	1.316	1.708	2.060	2.485	2.787	3.450	3.725
26	1.315	1.706	2.056	2.479	2.779	3.435	3.707
27	1.314	1.703	2.052	2.473	2.771	3.421	3.690
28	1.313	1.701	2.048	2.467	2.763	3.408	3.674
29	1.311	1.699	2.045	2.462	2.756	3.396	3.659
30	1.310	1.697	2.042	2.457	2.750	3.385	3.646
40	1.303	1.684	2.021	2.423	2.704	3.307	3.551
60	1.296	1.671	2.000	2.390	2.660	3.232	3.460
120	1.289	1.658	1.980	2.358	2.617	3.160	3.373
∞	1.282	1.645	1.960	2.326	2.576	3.090	3.291

From Mendenhall, W. and Sincich, T., "A Second Course in Statistics: Regression Analysis", 5th edition, Prentice-Hall International, New Jersey, 1996.

Appendix B

The growth rate (A_1) approximation of Clarke's model

From equation 13 in Clarke *et al.* [1997], the definition of A_1 can be defined as;

$$A_1 = \frac{1}{2} \left[1 - \frac{R_v - R_{c0} - R_T}{\sqrt{(R_T + R_v + R_{c0})^2 - 4R_T R_v}} \right] \quad (\text{B-1})$$

and $1 - A_1$ is then

$$1 - A_1 = \frac{1}{2} \left[1 + \frac{R_v - R_{c0} - R_T}{\sqrt{(R_T + R_v + R_{c0})^2 - 4R_T R_v}} \right] \quad (\text{B-2})$$

It is assumed that $R_T \ll R_v, R_{c0}$. This indicates that modes arising from the viscoelastic nature of entangle polymers are much faster than the thermodynamic mode. Equation B-2 can be approximated as

$$1 - A_1 \approx \frac{1}{2} \left[1 + \frac{R_v - R_{c0}}{\sqrt{(R_v + R_{c0})^2}} \right] = \frac{1}{2} \left[1 + \frac{R_v - R_{c0}}{R_v + R_{c0}} \right] \quad (\text{B-3})$$

$$1 - A_1 \approx \frac{1}{2} \left[\frac{2R_v}{R_v + R_{c0}} \right] \quad (\text{B-4})$$

$$\frac{1}{1 - A_1} \approx \frac{R_v + R_{c0}}{R_v} = 1 + \frac{R_{c0}}{R_v} \quad (\text{B-5})$$

Inserting equation B-5 into equation 5.21, equation 5.22 then can be obtained.

Appendix C

The method of identification each stage of phase separation

It has been clearly shown in other literatures [Hashimoto *et al.* 1991, 1993; Tanaka *et al.* 1992; Cummings *et al.* 1992] that spinodal decomposition can be separated into 3 stages, namely, early stage, intermediate stage and late stage. According to those works, the linearised Cahn-Hilliard theory can fit the experimental data in the early stage of SD, whereas the hydrodynamic effect, which plays a significant role later on, causes the linearised theory to fail in the intermediate and late stages respectively. The scaling function $F(X)$ from Furukawa have been introduced to described the later stage which herein refers to the intermediate and late stages SD. The universality of $F(X)$ can be used to indicate the beginning of the late stage SD [Hashimoto *et al.* 1986a].

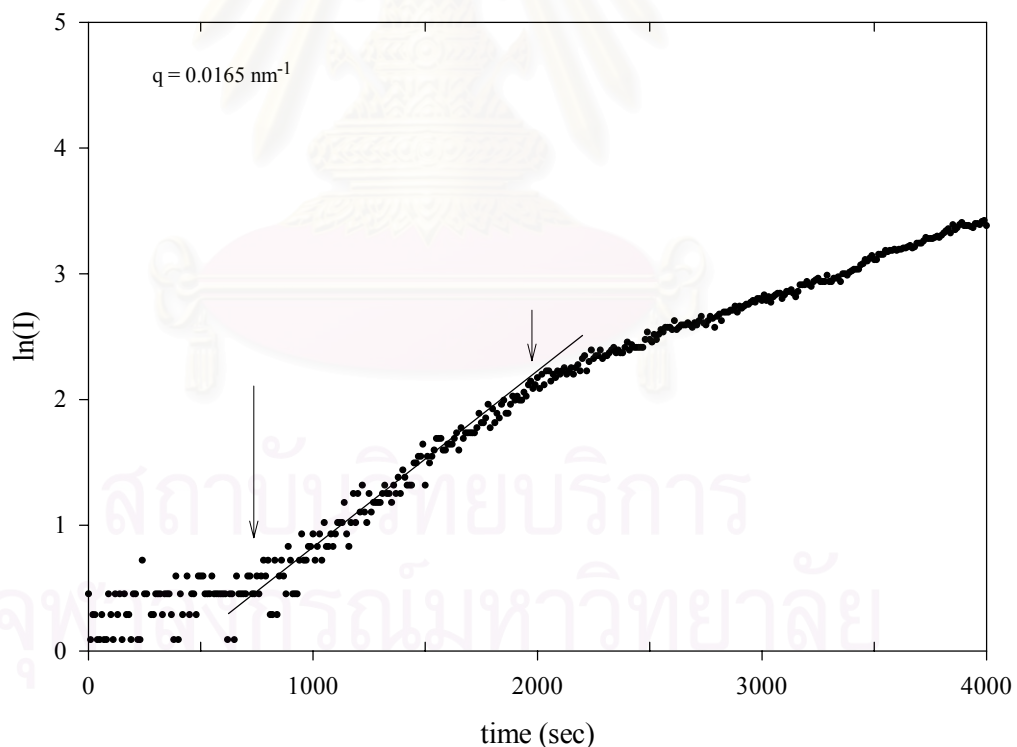


Figure C-1 Plot of $\ln I$ again time for 20/80 phase separated at 210 °C. Two arrows indicate the range of early stage SD.

As shown in figure C-1, it is clear that after the delay, which herein is approximately 700 seconds, the scattering intensity starts to rise, and grows exponentially with time as seen from the linear trend of the plot of $\ln I$ against time. The scattering intensity deviates from the linear characteristic at about 2000 seconds, which can be used as a sign of the beginning of intermediate SD. The boundary between the intermediate SD and the late stage SD can be determined from the time-independence of $F(X)$. As seen in figure C-2, it was found that $F(X)$ is independent of time at approximately 5200 seconds, indicating the beginning of the late stage SD.

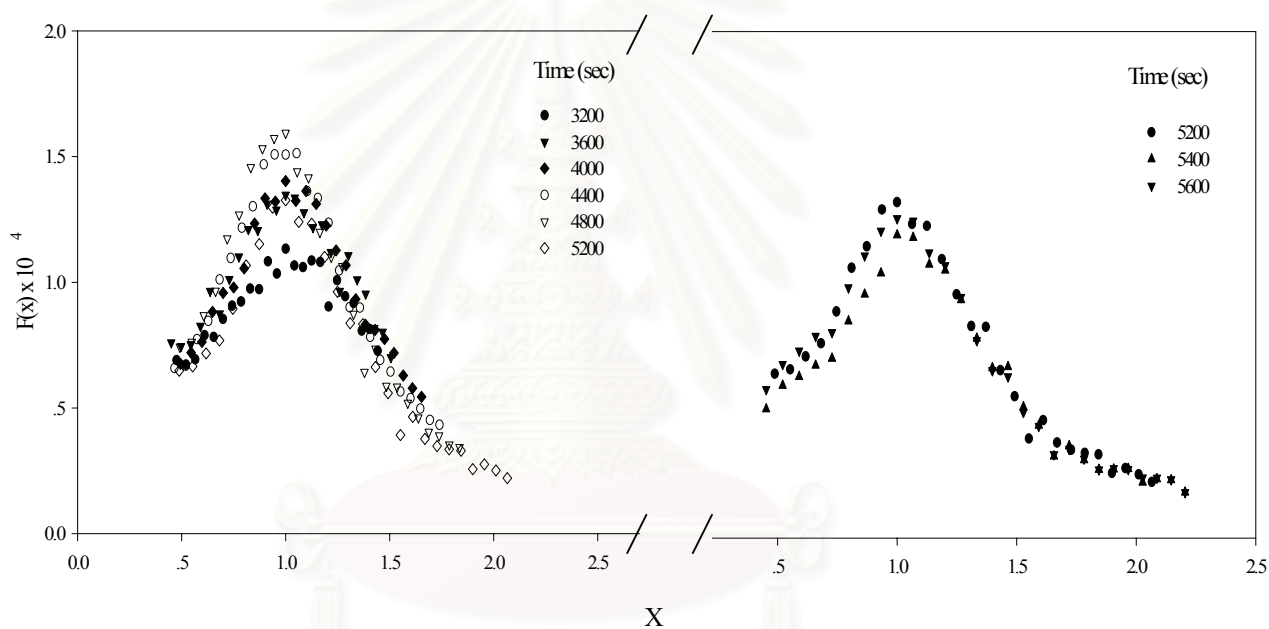


Figure C-2: Time evolution of the scaling function $F(X)$ for a melt mixed 20/80 SMA/PMMAe blends, phase separated at 210 °C

Appendix D

Thermograms from DSC experiments

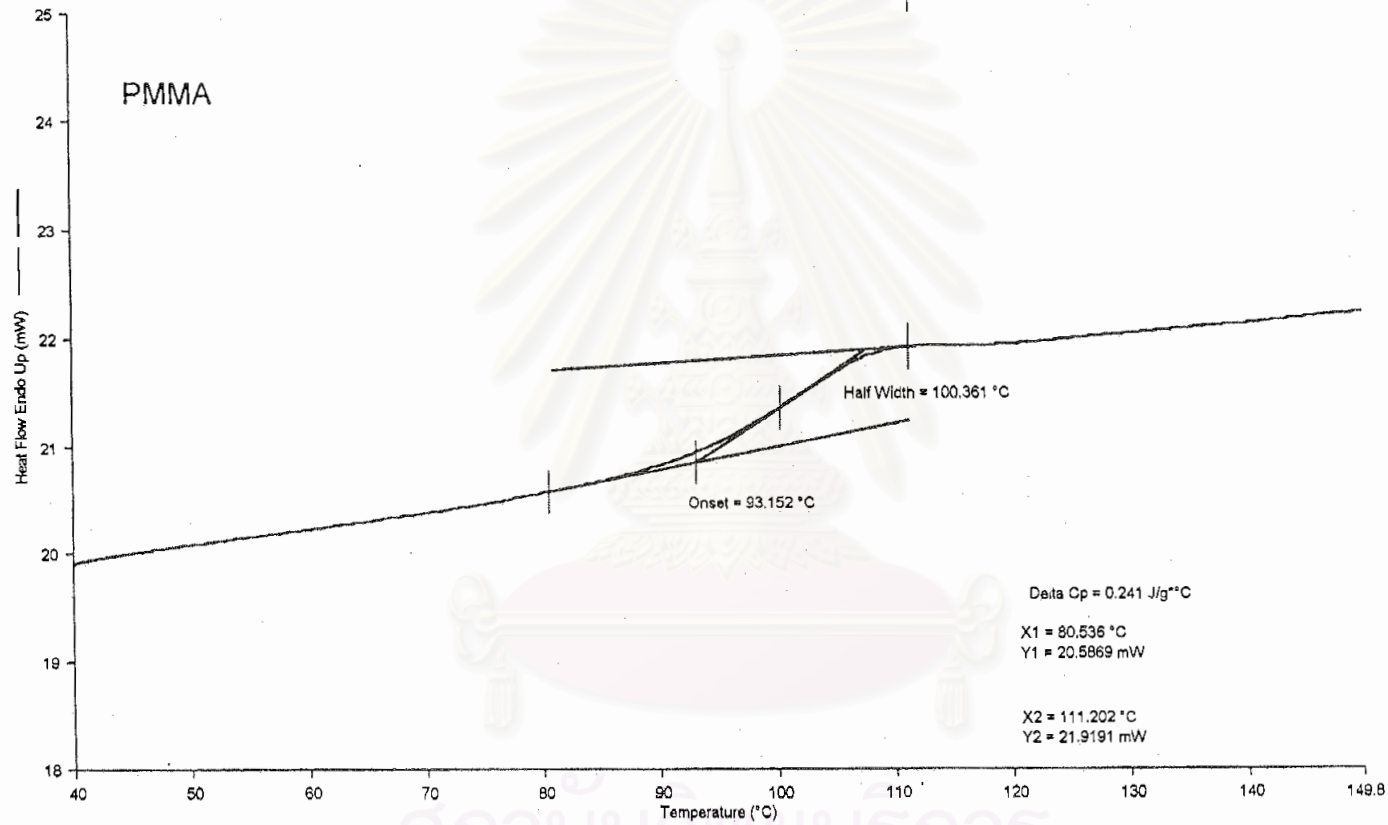
The thermograms of miscible SMA/PMMAe blends are shown in this section. As seen in these figures, the steep and single changes of heat flow were observed for each experiment, indicating a miscible blend with a single glass transition temperature. It should be noted that the mid point of specific heat change was used to indicate each T_g .



สถาบันวิทยบริการ
จุฬาลงกรณ์มหาวิทยาลัย

Filename: c:\dsc\pichet\pmma.dcd - 16/2/98 10:34:58
 Operator ID: pichet
 Sample ID: pmma
 Sample Weight: 10.140 mg
 Comment: pmma kept in desiccator 2 weeks

pmma: pmma.dcd
 Unsubtracted Heat Flow Endo Up (mW) : Step: 4



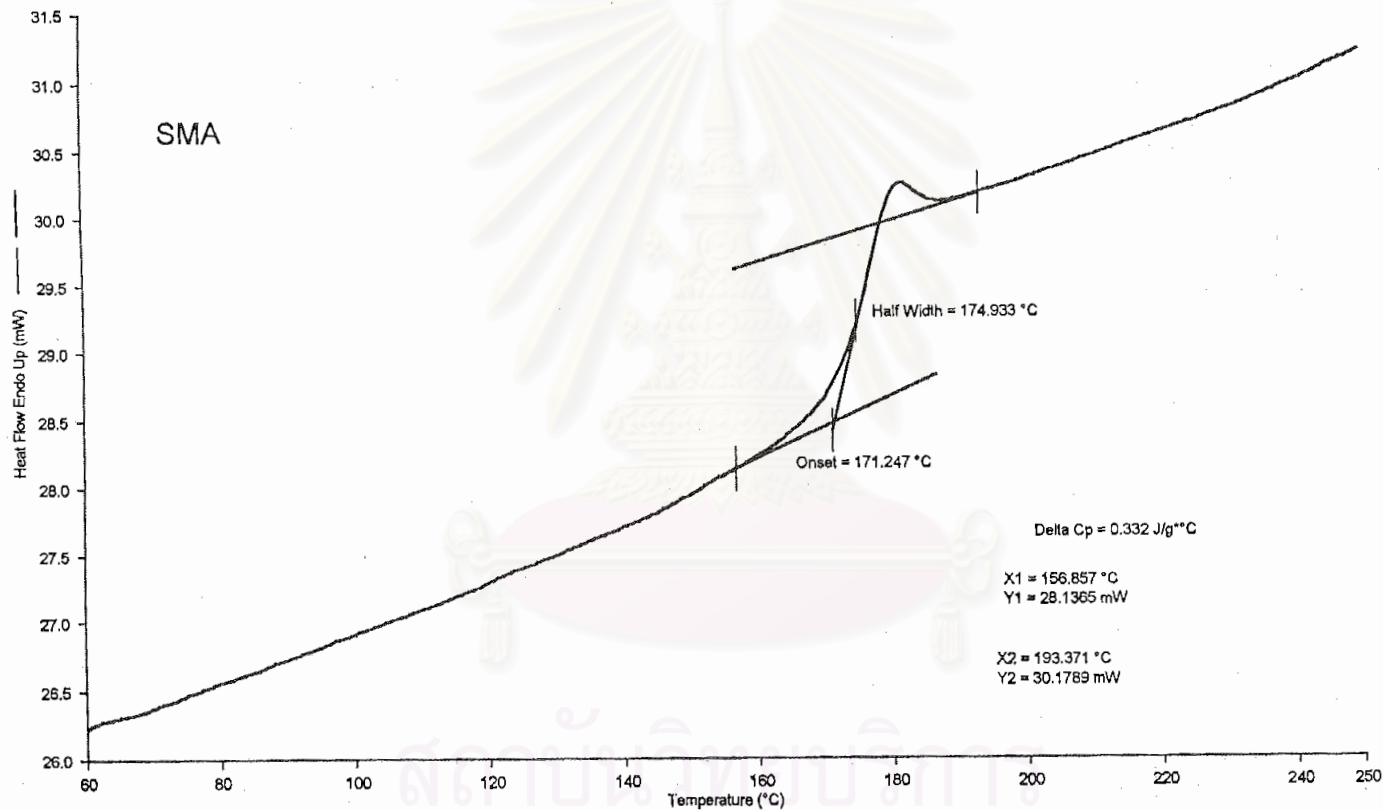
1) Heat from 30.00°C to 150.00°C at 20.00°C/min
 2) Cool from 150.00°C to 30.00°C at 20.00°C/min
 3) Hold for 5.0 min at 30.00°C
 4) Heat from 30.00°C to 150.00°C at 20.00°C/min

16/2/98 10:53:00

จุฬาลงกรณ์มหาวิทยาลัย

Filename: c:\dsc\pichet\sma.dcd - 30/6/98 15:16:04
Operator ID: pichet
Sample ID: PURE SMA
Sample Weight: 12.690 mg
Comment: STYRENE MALEIC ANHYDRIDE

PURE SMA: SMA.dcd
Unsubtracted Heat Flow Endo Up (mW) : Step: 4



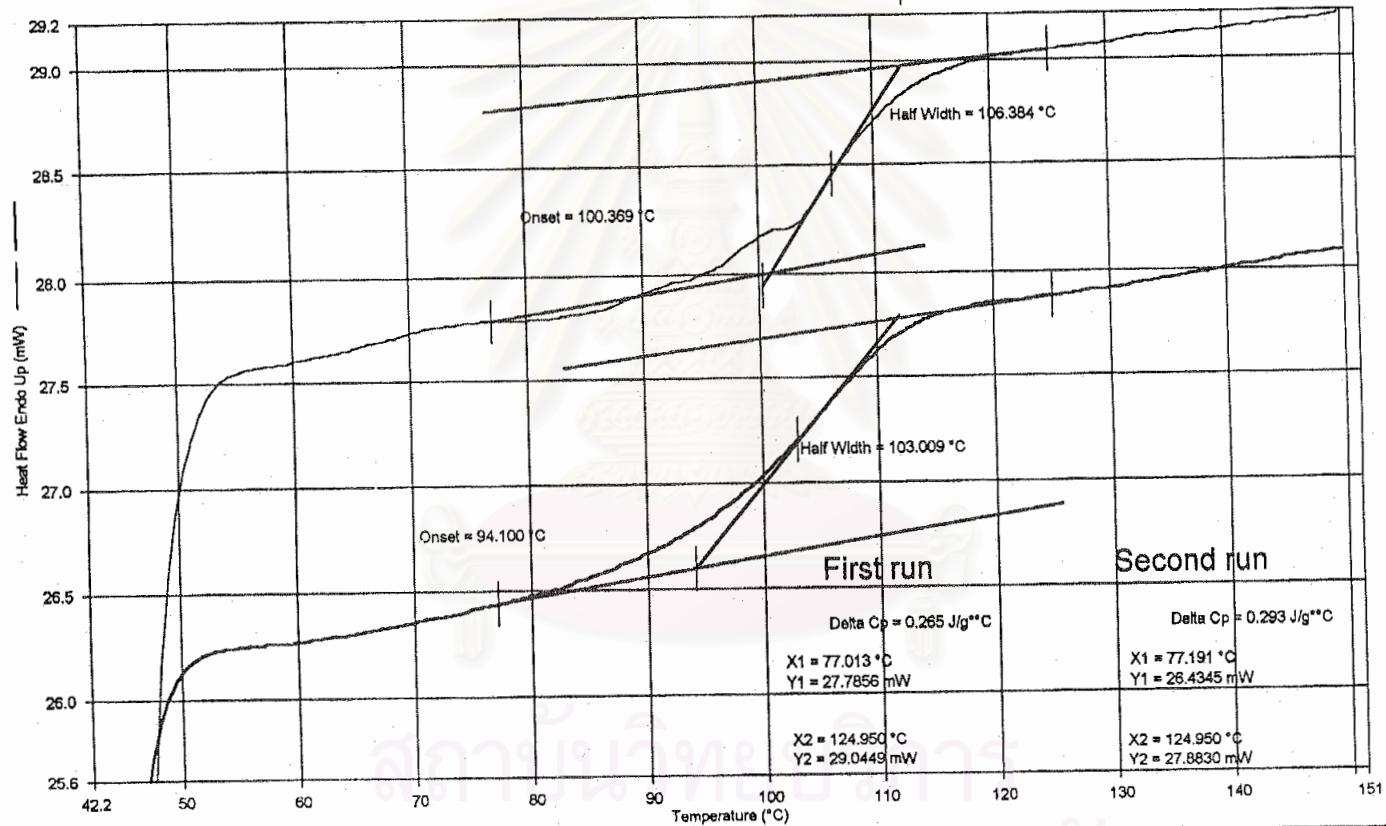
1) Heat from 50.00°C to 250.00°C at 20.00°C/min
2) Cool from 250.00°C to 50.00°C at 20.00°C/min

3) Hold for 3.0 min at 50.00°C
4) Heat from 50.00°C to 250.00°C at 20.00°C/min

30/6/98 16:05:32

Filename: c:\dscpichet\31empmm.dcd - 13/3/98 15:13:30
 Operator ID: pichet
 Sample ID: 3109empmm
 Sample Weight: 10.750 mg
 Comment: melt mixed 10/90 sma/pmma prepared on 4/3/98

3109empmm: 31empmm.dcd
 Unsubtracted Heat Flow Endo Up (mW) : Step: 1
 3109empmm: 31empmm.dcd
 Unsubtracted Heat Flow Endo Up (mW) : Step: 4



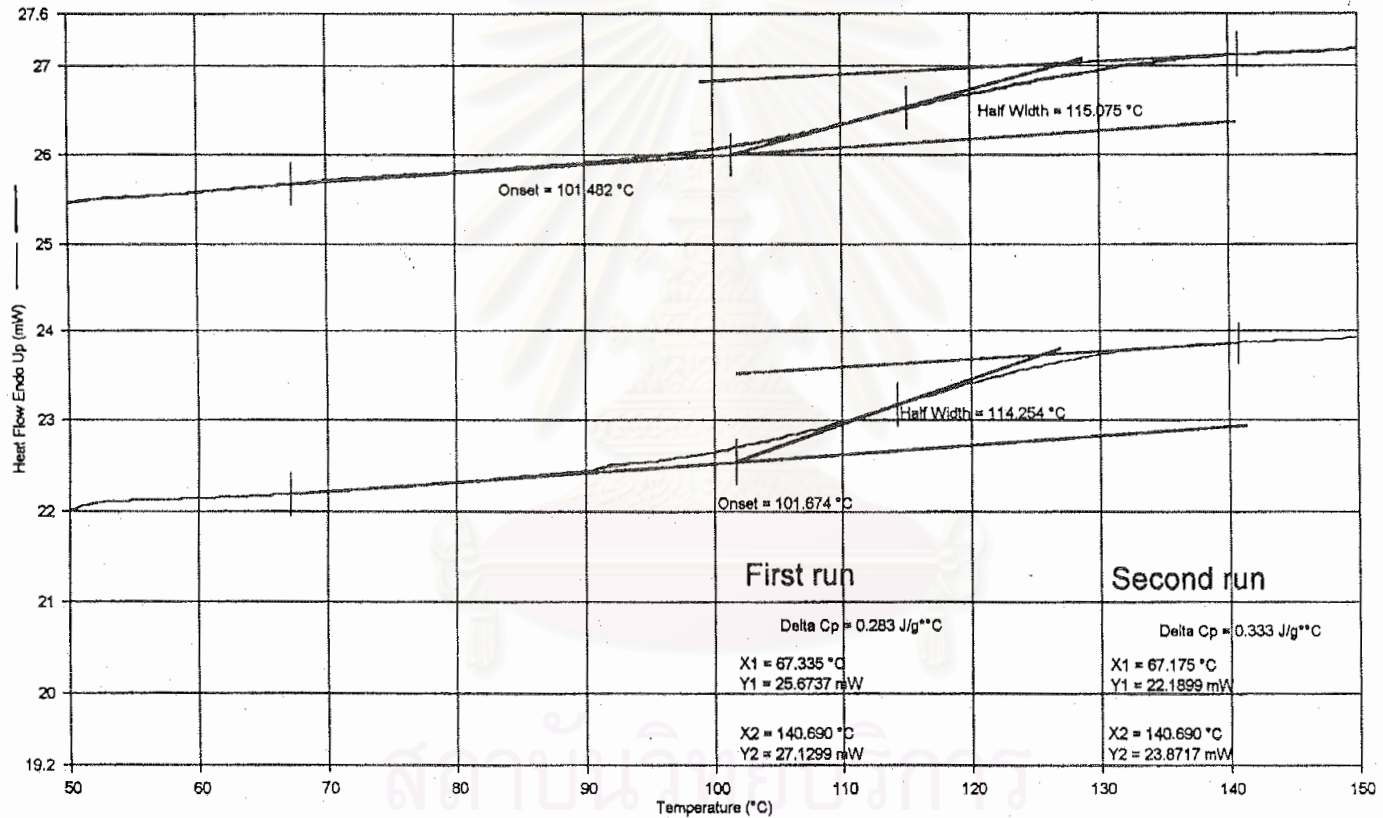
1) Heat from 40.00°C to 150.00°C at 20.00°C/min
 2) Cool from 150.00°C to 40.00°C at 20.00°C/min

3) Hold for 5.0 min at 40.00°C
 4) Heat from 40.00°C to 150.00°C at 20.00°C/min

13/3/98 15:49:16

Filename: c:\dscpichel\32smpmm.dcd - 13/3/98 15:50:05
 Operator ID: pichet
 Sample ID: 3208smpm
 Sample Weight: 9.700 mg
 Comment: melt mixed 20/80 sma/pmma prepared on 3/3/98

3208smpm: 32smpmm.dcd
 Heat Flow Endo Up (mW) : Step: 4
 3208smpm: 32smpmm.dcd
 Heat Flow Endo Up (mW) : Step: 1



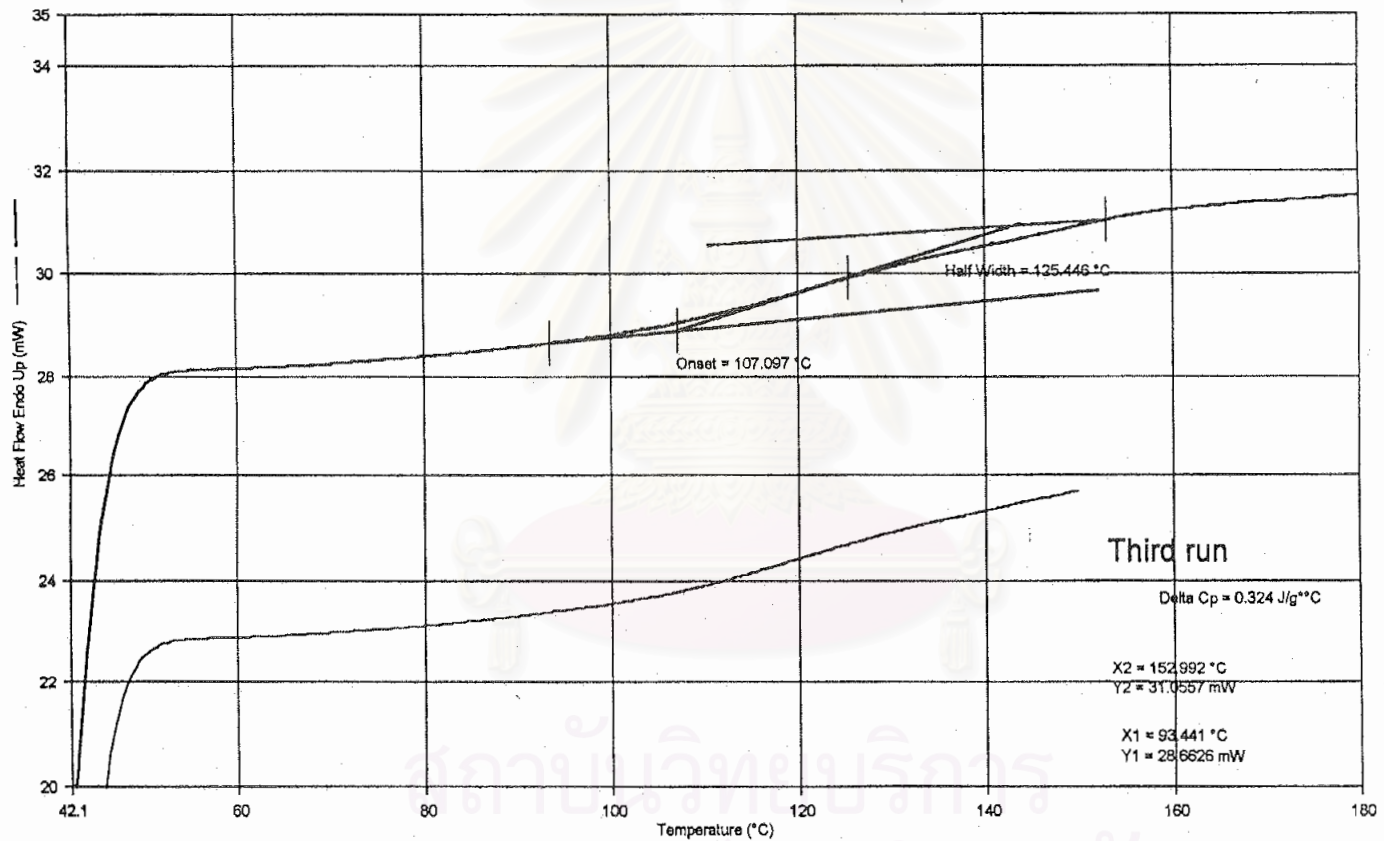
1) Heat from 40.00°C to 150.00°C at 20.00°C/min
 2) Cool from 150.00°C to 40.00°C at 20.00°C/min

3) Hold for 5.0 min at 40.00°C
 4) Heat from 40.00°C to 150.00°C at 20.00°C/min

13/3/98 16:15:01

Filename: c:\dsc\pichel\33smpmm1.dcd - 13/3/98 16:44:30
Operator ID: pichet
Sample ID: 3307smpm
Sample Weight: 15.240 mg
Comment: melt mixed 30/70 sma/pmma prepared on 4/3/98

3307smpm: 33smpmm1.dcd
Heat Flow Endo Up (mW) : Step: 4
3307smpm: 33smpmm1.dcd
Unsubtracted Heat Flow Endo Up (mW) : Step: 1

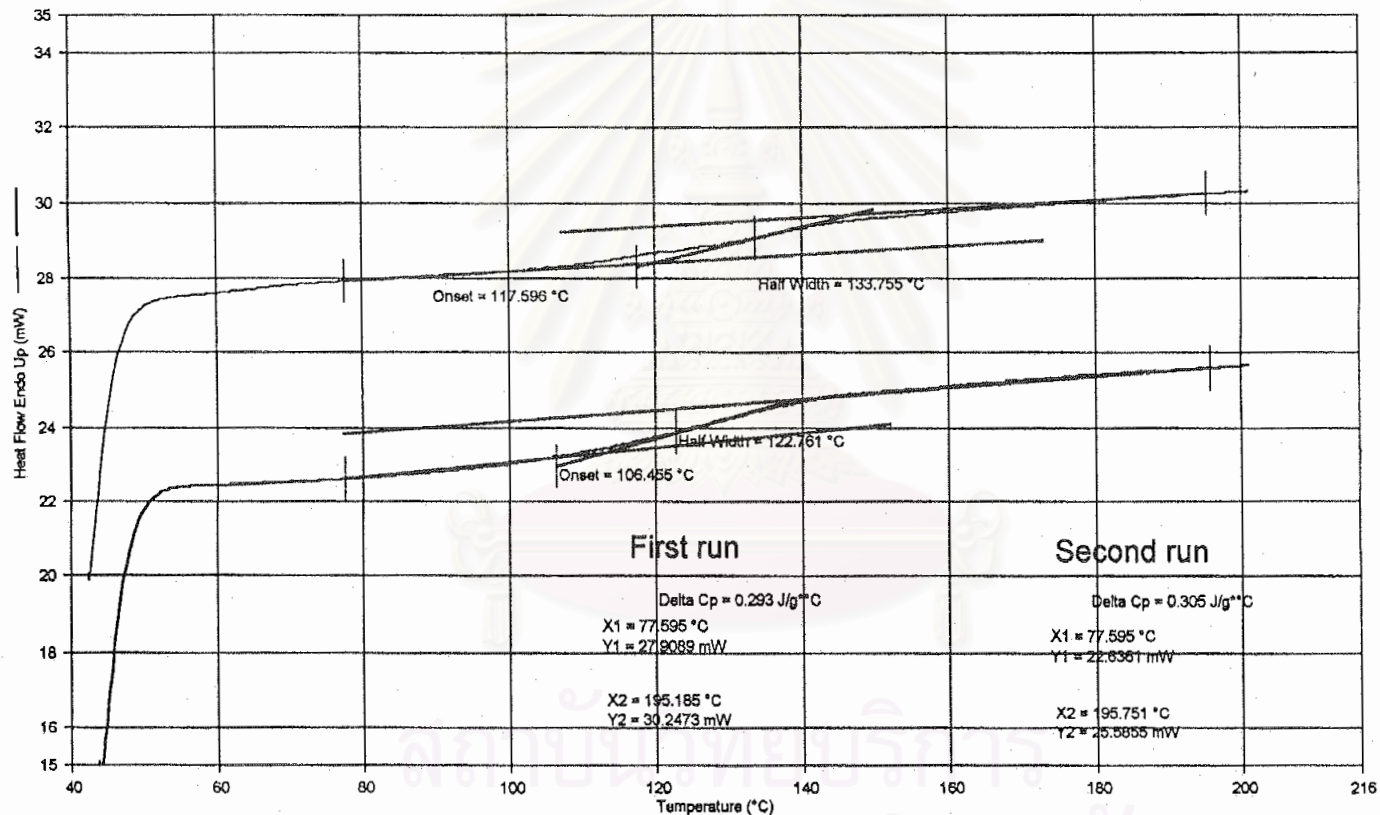


1) Heat from 40.00°C to 180.00°C at 20.00°C/min

13/3/98 16:52:11

Filename: o:\dcpichet\34smpmm.dod - 13/3/98 17:29:08
 Operator ID: plchet
 Sample ID: 3406smpm
 Sample Weight: 13.080 mg
 Comment: malt mixed40/60 sma/pmma prepared on 3/3/98

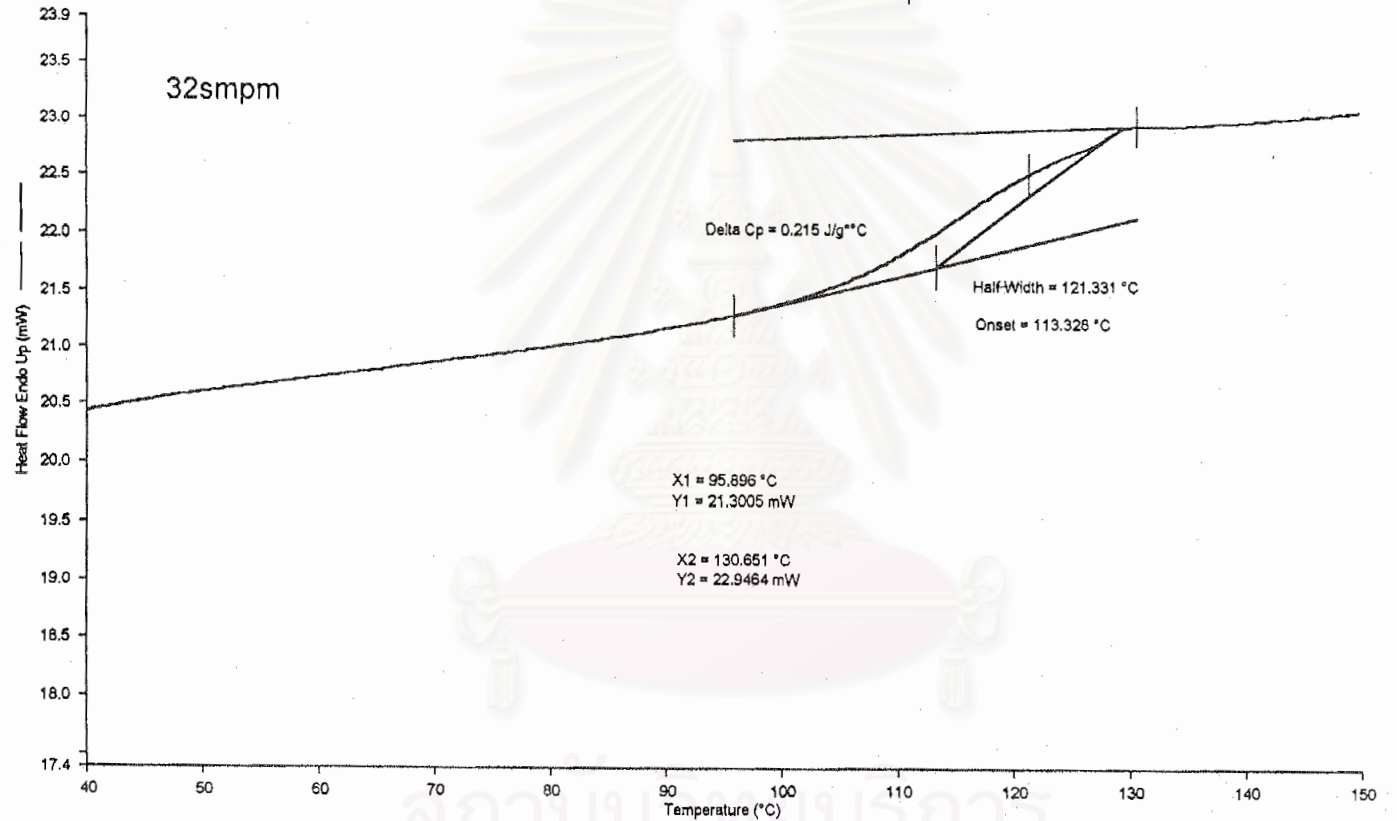
3406smpm: 34smpmm.dod
 Heat Flow Endo Up (mW) : Step: 4
 3406smpm: 34smpmm.dod
 Heat Flow Endo Up (mW) : Step: 1



1) Heat from 40.00°C to 200.00°C at 20.00°C/min
 2) Cool from 200.00°C to 40.00°C at 20.00°C/min
 3) Hold for 5.0 min at 40.00°C
 4) Heat from 40.00°C to 200.00°C at 20.00°C/min
 13/3/98 17:49:30

Filename: c:\dscpichet\32smpm.dcd - 13/2/98 11:11:09
 Operator ID: pichet
 Sample ID: 3208smpm
 Sample Weight: 12.040 mg
 Comment: sma32/pmna12 at 20/80 composition prepared on 31/1/98

3208smpm: 32smpm.dcd
 Unsubtracted Heat Flow Endo Up (mW) : Step: 4

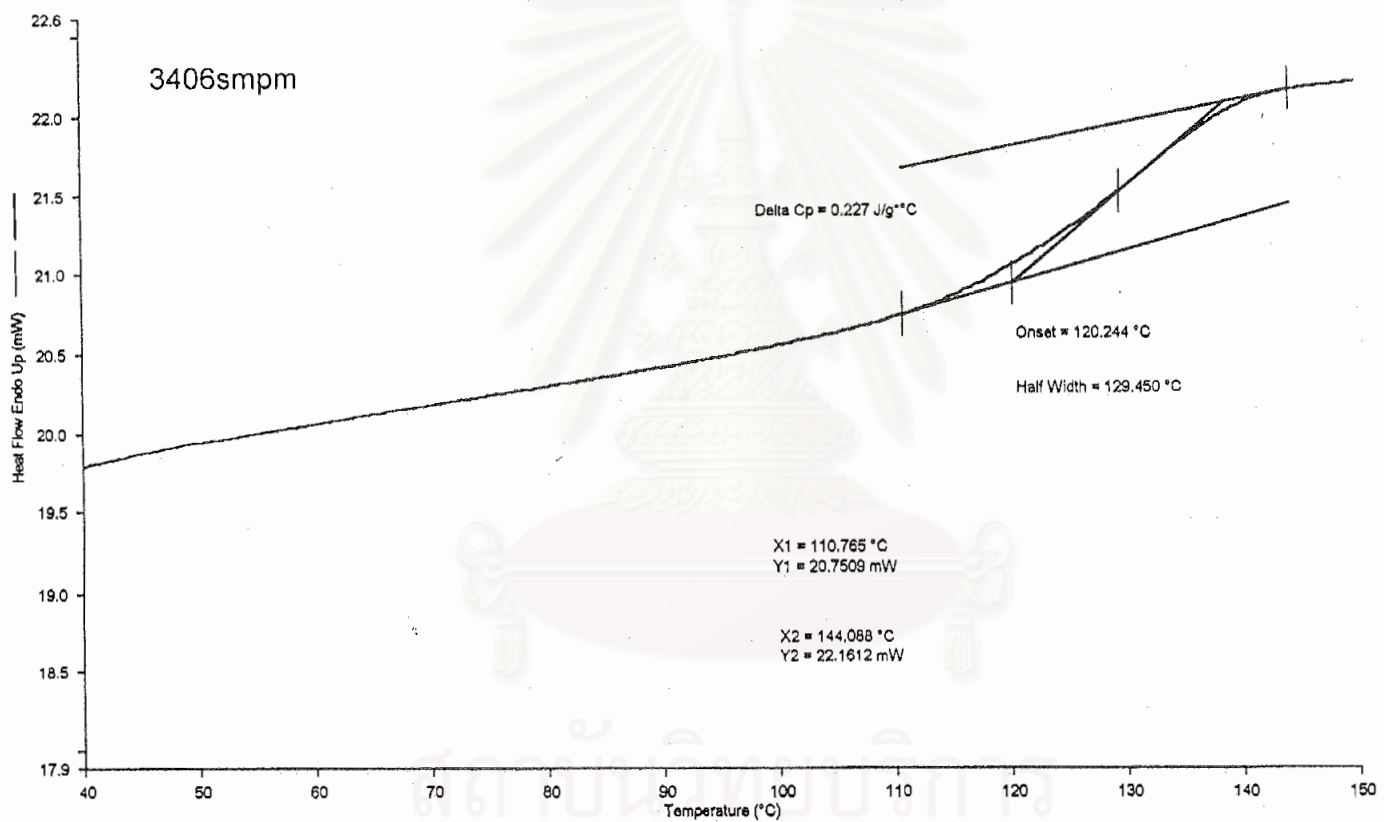


- | | |
|---|---|
| 1) Heat from 30.00°C to 150.00°C at 20.00°C/min | 3) Hold for 5.0 min at 30.00°C |
| 2) Cool from 150.00°C to 30.00°C at 20.00°C/min | 4) Heat from 30.00°C to 150.00°C at 20.00°C/min |
- 13/2/98 12:03:23

จุฬาลงกรณ์มหาวิทยาลัย

Filename: c:\dsc\pichel\3406smpm.dcd - 13/2/98 12:20:01
 Operator ID: pichel
 Sample ID: 3406smpm
 Sample Weight: 10.460 mg
 Comment: sma32/pmme12 at40/60 composition prepared on 31/1/98

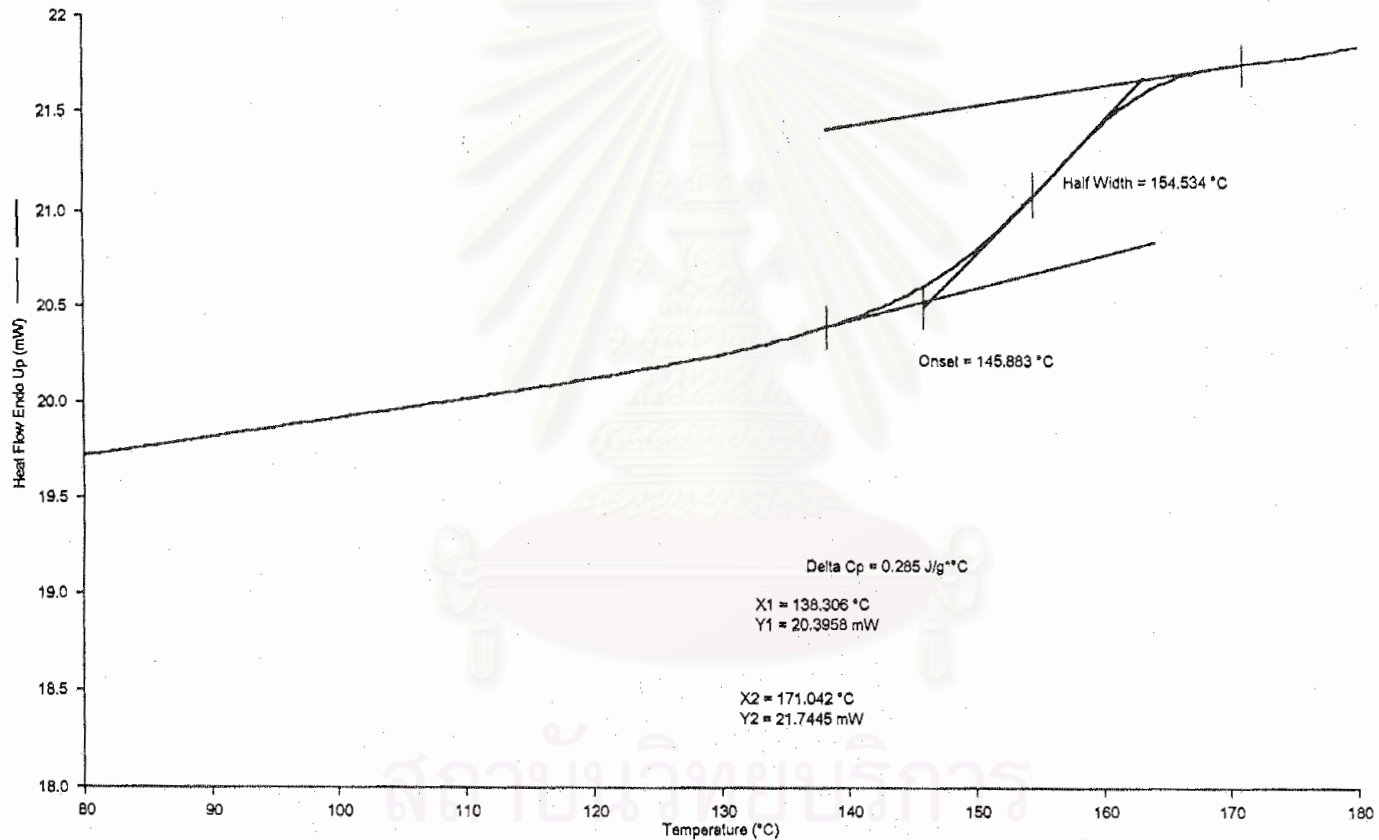
3406smpm: 3406smpm.dcd
 Unsubtracted Heat Flow Endo Up (mW) : Step: 4



1) Heat from 30.00°C to 150.00°C at 20.00°C/min	3) Hold for 5.0 min at 30.00°C	
2) Cool from 150.00°C to 30.00°C at 20.00°C/min	4) Heat from 30.00°C to 150.00°C at 20.00°C/min	13/2/98 12:33:52

Filename: c:\dscpichel\38smpm2.dcd - 13/2/98 13:07:49
Operator ID: pichet
Sample ID: 3802smpm
Sample Weight: 10.010 mg
Comment: sma32/pmma12 at 80/20 composition prepared on 31/1/98

3802smpm: 38smpm2.dcd
Unsubtracted Heat Flow Endo Up (mW) : Step: 1



1) Heat from 30.00°C to 180.00°C at 20.00°C/min

13/2/98 13:40:18

Appendix E

The method of measure the inter-domain distance from the TEM pictures

Following the procedure of determining the inter-domain distance as described by Lauger *et al.* [1995]. A set of equi-distant lines was super-imposed on the TEM picture as shown in figure E-1. The distance between the lines was taken as the estimated thickness of the percolation structure. The inter-domain distance was measured from the centre of a percolation structure to the centre of its neighbour along the equi-distance line. The average of the inter-domain distance was determined from a distribution of all sections in the figure.

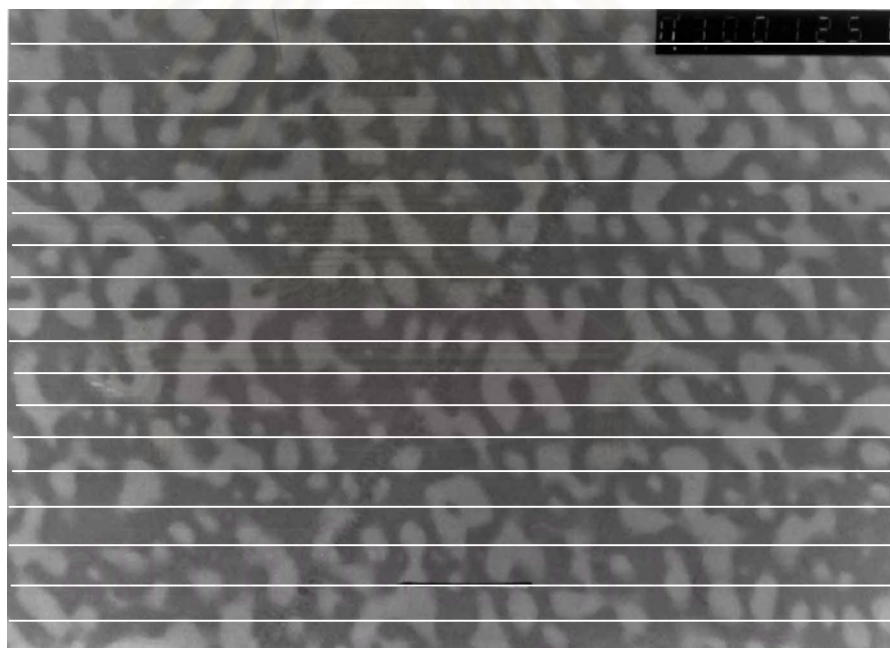


Figure E-1: Example for the determination of the inter-domain distance

CURRICULUM VITAE

NAME: Pichet Rojanapitayakorn

DATE OF BIRTH: May 16, 1973

EDUCATION:

- | | |
|-------------------|---|
| June' 95- present | PhD, candidate, Polymers, G.P.A. 3.88/4.0
Department of Chemical Engineering,
Chulalongkorn university, Bangkok 10330, Thailand |
| June' 91- Apr' 95 | B.Eng., Chemical Engineering, G.P.A. 3.26/4.0 (Second class honour)
Department of Chemical Engineering
Chulalongkorn university, Bangkok 10330, Thailand. |

RECENT PUBLICATIONS AND PRESENTATIONS:

1. Rojanapitayakorn P.; Thongyai S.; Higgins J.S.; Clarke N., *"Effects of Sample Preparation Method on Mixing and Phase Separation in Binary Polymer Blends"*, Polymer, 42, 2001, 3475.
2. Wacharawichanant S; Thongyai S.; Rojanapityakorn P., *"Phase Separation of Poly(methyl methacrylate) and Styrene-Acrylonitrile Copolymer Blends"*, The First Thailand Materials Science and Technology Conference, Bangkok, July 19-20, 2000.
3. Rojanapitayakorn P.; Thongyai S.; Wacharawichanant S., *"Phase Separation, Morphology in Poly(methyl methacrylate)/Poly(styrene-co-maleic anhydride) Blend"*, The Polymer Processing Society Asia/Australia Regional Meeting 1999, Bangkok, Dec 1-3, 1999.
4. Rojanapitayakorn P.;Thongyai S.;Covavisaruch S.*"Kinetics of Phase Separation, Morphology, and Mechanical Properties of Poly(methyl methacrylate) /Poly(styrene-co-maleic anhydride) Blends"*, 23rd Australian Polymer Symposium: Polymer for new Millenium, Geelong, Australia, Nov 28-Dec 2, 1999.
5. Rojanapitayakorn P.; Thongyai S.; Higgins J.S.; Clarke N., *"Kinetics of Phase Separation of Blends of Poly(styrene-co-maleic anhydride) with Poly(methyl methacrylate)"*, The Sixth European Symposium on Polymer Blends, Planck-Institut fur Polymerforschung, Mainz, Germany, May 16-19, 1999.